1995

THE REACTIVITY OF SOME TRANSITION METAL NITRIDES AND CARBIDES

CLARK, JEREMY NEIL

THE REACTIVITY OF SOME TRANSITION METAL NITRIDES AND CARBIDES

by

JEREMY NEIL CLARK

A thesis submitted to the University of Plymouth
in partial fulfilment for the degree of

DOCTOR OF PHILOSOPHY

Department of Environmental Sciences
Faculty of Science

in collaboration with
British Steel, Teesside

April 1995

THE REACTIVITY OF SOME TRANSITION METAL NITRIDES AND CARBIDES

Jeremy Neil Clark

ABSTRACT

The formation and oxidation of transition metal nitrides and carbides is reviewed and the crystal structures and types of bonding are discussed. Types of nitrides and carbides are categorized in terms of physical and chemical properties and type of bonding. The principles of sintering are summarised.

The theory and applications of thermal analytical techniques are reviewed. Surface area determination and estimation of average crystallite size by the BET method utilizing the adsorption of nitrogen gas at -196 °C are explained along with the application of x-ray diffractometry and scanning electron microscopy to work in this area.

In this present research selected transition metal nitrides and carbides have been oxidised in air and carbon dioxide. Activation energies have been determined for these reactions from isothermal oxidations utilizing the Arrhenius equation and from oxidations at different heating rates utilizing the Kissinger equation. Kinetic schemes for the isothermal oxidations have been proposed based on two models of the reactions, that is half order kinetics in which the rate of reaction is determined by the diffusion of oxidising gas through the oxide product and two-thirds order kinetics in which the reaction takes place at the surface of a spherical particle of diminishing size as the reaction proceeds. Surface area measurements and electron microscopy have been utilized to study the ability of the product formed during the oxidations to sinter. X-ray diffractometry has been used to identify the crystal phases present in the initial nitride or carbide and in the oxidation products.

The activation energies of the carbides were found to be lower than that found for the respective nitrides. At low temperatures the carbides oxidised more extensively than the respective nitrides, but at high temperatures the situation was reversed. This is explained in terms of the difference in the pre-exponential term of the Arrhenius equation. The kinetics were found to be dependent on whether the oxide produced was structurally compatible with the remaining reactant and whether the oxide produced was able to sinter at the temperature used in the experiment.

CONTENTS

TABLES

FIGURES

PLATES

ACKNOWLEDGEMENTS

I wish to express my grateful thanks to Dr S.A.A. Jayaweera and the late Dr D.R. Glasson who started my interest in the oxidation of the transition metal nitrides and carbides, and for their help, encouragement and advice during the course of this work.

I also wish to thank Dr R. Lowry and Dr G.P. Matthews who have stepped in as supervisors after the death of Dr D.R. Glasson.

My thanks are due also to Mr B.R. Lakey and Dr R. Moate for their assistance and instruction in the use of the electron microscope. Dr M.O. Boles and Mr P. Davies are also thanked for their help and assistance in the operation of the x-ray diffraction equipment.

The late Dr K.E. Adams is thanked for his help and encouragement during the course of this work. The late Mr K. Pearson, Mr I. Doidge and the technical staff of the Department of Environmental Science are thanked for facilitating this work to be carried out.

AUTHOR'S DECLARATION

At no time during the registration for the degree of Doctor of Philosophy has the author been registered for any other university award.

Relevant scientific conferences were attended at which work was presented, and papers published.

Conferences attended:
Journees d'etudes sur les nitrures VI (JENI 6), Saint-Etienne, France, September 1984.
Journees d'etudes sur les nitrures VII (JENI 7), Rennes, France, September 1986.
23rd International vacuum microbalance techniques conference, Teesside, UK, August 1989.
Journees d'etudes sur les nitrures VIII (JENI 8), Saint-Etienne, France, October 1990.

Results also presented by Dr S.A.A. Jayaweera or Dr D.R. Glasson at:
21st International vacuum microbalance techniques conference, Dijon, France, August 1985.
22nd International vacuum microbalance techniques conference, Rabat, Morocco, April 1987.
24th International vacuum microbalance techniques conference, Hammamet, Tunisia, November 1991.

Publications:
Thermochimica Acta,1986, 103, 193-199.
Revue de Chimie Minérale, 1987, 24, 654-666.

Signed: 

22 March 1996

CHAPTER 1

INTRODUCTORY SURVEY AND REVIEW

1.1 INTRODUCTION

Nitrides and carbides are the compounds formed when nitrogen or carbon react at elevated temperatures with other elements, especially the more electropositive elements (Toth (1971)).

Transition elements such as those of sub groups IVa, Va and VIa of the periodic table form nitrides and carbides. Most of these compounds have high melting points (1700 - 4200 °C) and great hardness that can approach the hardness of diamond (Whittemore (1968)). The hardness and high melting points were appreciated by Moissan in the 1890's (Frad (1968)) and because of this they are often termed refractory materials. Several of the group VIa nitrides are exceptions in that they decompose at relatively low temperatures. Transition metal nitrides and carbides may also possess some of the properties of metals or alloys and hence they may exhibit thermal and electrical conductivities of the same order of magnitude as pure metals. They may also show metallic lustre. The term 'hard metal' is also often applied to these compounds, along with the metal borides and silicides (Schwarzkopf (1950), Schwarzkopf and Kieffer (1953) and Hägg (1953)).

The above mentioned properties of the transition metal nitrides and carbides make them to be of considerable technological importance. Nitrides of sub groups IVa to VIa have been used in high melting point cermets - a heat resistant material made by the sintering of an intimate mixture of ceramic and metallic powders (Shorter Oxford Dictionary (1993)) (Schwarzkopf and Kieffer (1953)). High melting points in combination with good non-scaling properties have resulted in these materials being used in jet and rocket technology where the demands on the materials in respect of thermal shock

resistance are particularly severe, owing to the high rates of temperature change (Kingery (1955)). The refractory nitrides exhibit their refractory properties best in a nitrogen atmosphere (Bradshaw and Matthews (1958)).

The proccess of nitriding is extensively used for the hardening of steel surfaces. During this process, atomic nitrogen is absorbed from either a gaseous or liquid salt carrier and thus into the base metal. The 'case' is quite hard and acquires excellent wear resistance properties. The traditional blacksmith's method of nitriding iron or steel involves heating the metal to red heat before plunging the hot metal object into potassium ferricyanide placed on a carbon block.

Previous work has studied the oxidation of selected transition metals and the properties of the oxides formed (Glasson (1956, 1958 a & b, 1960, 1961 a & b, 1963 a & b, 1967), and Glasson and Sheppard (1968)). Selected nitrides have been studied by Glasson and Jayaweera (1969) and Ali (1970). Selected carbides have been reviewed by Glasson and Jones (1969 a & b). Properties of transition metal carbides and nitrides have been reviewed by Toth (1971), refractory carbides by Storms (1967) and Kosolapova (1971). Oxidation of metals and alloys, including some nitrides and carbides, has been reviewed by Kubaschewski and Hopkins (1962).

Because of the good mechanical, physical and chemical properties of transition metal nitrides and carbides, they are used industrially as coatings to metals and as ceramics. However, the nitrides and carbides of transition metals and metal alloys may be produced as an unwanted byproduct in the production and subsequent treatment of these metals and alloys where the presence of small quantities of nitride or carbide may have unpredictable effects on the properties of the materials.

1.2 SOLID-GAS REACTIONS

Solid-gas reactions are important in many industrial applications e.g. metal extraction, combustion of solid fuels and refuse incineration etc. In many solid/gas reaction systems, the product forms a layer around the remaining unreacted solid. The overall reaction process may involve:

a) diffusion of the gas from the bulk to the external surface of the reacting solid;

b) diffusion of the gas through pores in the partially reacted solid, or through pores in a solid reaction product, to the reaction site;

c) adsorption of gas molecules onto the surface of the solid;

d) desorption of products;

e) diffusion of gaseous products through pores in the remaining solid reactant or through pores in a solid reaction product;

f) diffusion of gaseous products away from the surface of the remaining reactant solid or solid reaction product.

The kinetics of the reaction may thus depend upon the external mass transfer of gas, pore diffusion, adsorption/desorption and the rate of the chemical reaction. Transfer of heat through the solid and structural changes to the solid (e.g. cracking or sintering) may also be involved. The factors affecting the reaction rate may vary in importance as temperature, particle size, gas pressure etc. are changed. Where the transfer of gas to the reaction site is relatively easy (e.g. small particles or large pores) the reaction is likely to be controlled by a chemical step. Where a chemical reaction is energetically favoured the reaction is likely to be controlled by the transport of gas molecules to the reaction site. At conditions between these limits a process may be under "mixed control".

1.2.1 NON-POROUS SOLID-GAS REACTION

If the solid reactant is non-porous, the reaction between the solid and the gas occurs at a well defined interface and the system may be described in terms of simple geometrical models.

Progress of such a reaction is controlled by the contraction of the solid/gas interface. Where diffusion effects are absent, a conversion function for a reaction, $f_F(\alpha)$ may be defined such that

$$f_F(\alpha) = 1 - (1 - \alpha)^{1/F}$$

where α represents the fraction of the reactant solid that has reacted and F is a shape factor with values 1, 2 and 3 for infinite plates, long cylinders and spheres respectively. F may be found empirically as the value that gives a straight line between experimental values of $f_F(\alpha)$ and reaction time t. $f_F(\alpha)$ is also given by

$$f_F(\alpha) = \text{time(t)/time of complete reaction } (t_{\alpha = 1})$$

thus

$$f_F(\alpha) = t/t_{\alpha = 1} = 1 - (1 - \alpha)^{1/F} = 1 - (\text{fraction of solid remaining})^{1/F}.$$

A straight line plot of experimental data need not necessarily indicate that the reaction is controlled by the chemical reaction. The effect of initial particle diameter, d, on the time required to reach a given value of α, t_α, can yield further information. t_α is proportional to d^2 for diffusion control, proportional to d for chemical control of non-porous solids and independent of d for chemical control of porous solids.

Where the rate of reaction is controlled by the diffusion of gas through the solid reactant or product the conversion factor $g_F(\alpha)$ is given by

$$g_F(\alpha) = \alpha^2 \qquad \text{for F = 1}$$

$$g_F(\alpha) = \alpha + (1 - \alpha)\ln(1 - \alpha) \qquad \text{for F = 2}$$

$$g_F(\alpha) = 1 - 3(1 - \alpha)^{2/3} + 2(1 - \alpha) \qquad \text{for F = 3.}$$

These equations are derived and discussed by Szekely et al (1976).

Other equations representing solid-gas reactions include:

a) the Jander equation for a diffusion controlled reaction of a spherical particle

$kt/r^2 = [1 - (1 - \alpha)^{1/3}]^2$

where k is a constant and r is the radius of the particles;

b) for particles where the initial solid reactant and final solid product differ in volume Carter (1961) proposed the following

$k't/r^2 = (\{Z - [1 + (Z - 1)\alpha]^{2/3} - (Z - 1) - (1 - \alpha)\} / 2(Z - 1))^{2/3}$

where r is the initial radius of the particle, k' a constant and Z the ratio of final volume of product to initial volume of reactant. When $Z = 1$ this equation reduces to the Jander equation.

In these equations it is assumed that the shrinking, unreacted core is non-porous and that the product layer around the unreacted core is uniform in thickness.

If the temperature at which the reaction occurs is greater than $T_m/3$, where T_m is the melting point in Kelvin of either the reactant or a solid reaction product then coalescence of the particles may occur by surface diffusion. Above $T_m/2$ sintering of the particles by bulk diffusion is possible (see section 1.2.4).

1.2.2 POROUS SOLID-GAS REACTION

In a porous medium diffusion of gas into the body of the solid can occur. Hence, the reaction occurs in a diffuse zone rather than at a sharply defined reaction boundary. Thus there is a gradual change in the degree of conversion through the reactant particle. As the reaction proceeds a layer of product will

build up on the outside of the partially reacted reactant core, the reaction in this zone occurring simultaneously with diffusion of gas to the zone.

When a chemical reaction is the rate determining step, the concentration of gas will be constant through the particle and the reaction will occur uniformally throughout the volume of the solid. When the diffusion of gas through the solid reactant or solid reaction product is the rate determining step, the reaction will occur in a narrow boundary between the reacted and unreacted zones where the concentration of gaseous reaction becomes zero (or reaches its equilibrium concentration in the case of reversible reactions). When the reaction is controlled solely by the diffusion of gas the model is identical to that given for non-porous particles of diminishing size.

1.2.3 TWO-THIRDS AND HALF ORDER REACTION KINETICS

For a reaction occurring at constant temperature it is assumed that the kinetics can be expressed by a formal equation

$$d\alpha/dt = k(1 - \alpha)^n$$

where α is the fraction of the reactant that has reacted, t the time, k the rate constant and n the order of reaction. When integrated the equation becomes

$$1/n - [1/(1 - \alpha)^{(n - 1)} - 1] = kt$$

or

$$\alpha = 1 - [1 - kt(n - 1)]^{1/(n - 1)}$$

For a solid-gas reaction, if the kinetics are controlled by the movement of a reaction boundary due to spherically shaped particles decreasing in size as the reaction proceeds then the rate of the reaction will be proportional to $v^{2/3}$ where v is the volume of the particle and hence n will have the value 2/3 (Blazak (1973)). However, if the kinetics are controlled by the diffusion of gas through a product layer before reacting at the reaction boundary then the rate is proportional to $1/x^2$ where x is the thickness of product, and hence n

will have the value 1/2 (Blazek (1993)). For other values the mathematical treatment is complicated by the non-linear appearance of n in the rate equation. If the reaction proceeds following two-thirds order kinetics, a plot of $(1-\alpha)^{1/3}$ against time will be linear. If the rate of reaction is determined by the gas diffusing through a layer of product to reach the underlying reactant solid then a plot of α^2 against time will be linear.

1.2.4 SINTERING

Sintering is the process by which small particles of a solid form larger aggregates when the solid is held at an elevated temperature below its melting point. It is of great importance to the ceramic and powder metallurgy industry. In the process of sintering the volume of the solid is reduced, but the density of the solid remains less than that of a single crystal due the presence of remaining voids and pores. Sintering is a complex phenomenon and is thought to occur by grain boundary or volume diffusion, usually considered to proceed in three stages:

1) initially grain boundaries merge at the points where they touch adjoining grains. During this initial stage there is an increase in mechanical strength, and in conducting materials a reduction in resistivity;
2) the intermediate stage involves the further merging of grain boundaries leaving closed pores at the point where several grains come together;
3) during the final stage, the remaining pores close.

This is shown schematically below.

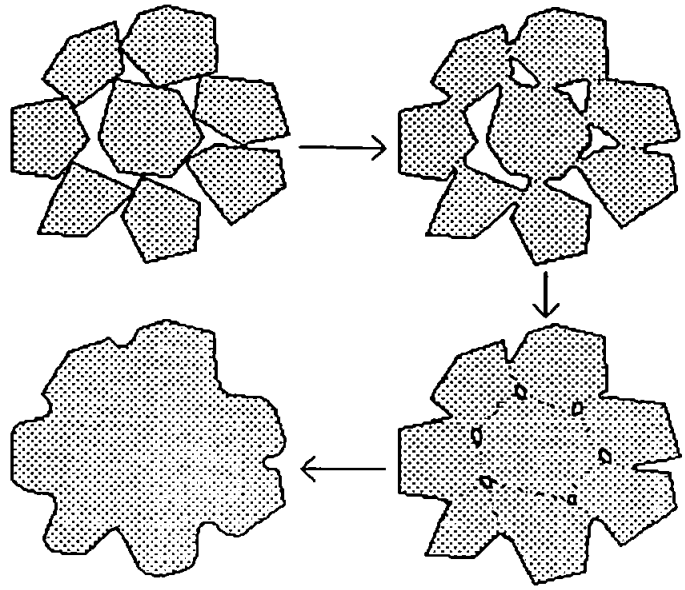

The activation energy for sintering is high. It takes place at an appreciable rate above a temperature in the range of 0.4 - 0.5 of the thermodynamic melting point of the solid (the Tammann temperature). Surface diffusion can occur at lower temperatures (approximately 0.33 of the thermodynamic melting point).

Vacancies at the particle surface diffuse through the bulk and disappear at the grain boundaries. Thus there is a net flow of atoms from the boundary into the pores. Alteration of the vacancy concentration by impurities and additives affects the rate of diffusion (Hannay (1967)). Kinetics of sintering have been studied by Kingery (1960). Since the rate depends on the inverse third power of the particle size, milling of the material has a large effect on the subsequent sintering rate.

The driving force for sintering is the surface energy of the material. The surface area of the unsintered material being large, a considerable reduction in free energy takes place on forming a solid with a smaller surface area. A sintered particle, therefore, has a smoothed, more rounded surface than the

original material. The theory of sintering has been reviewed by Coble (1973) and various models are discussed by Waldron and Daniell (1978).

1.3 CLASSIFICATION OF NITRIDES AND CARBIDES

Nitrides are categorised generally as ionic, covalent or interstitial (or metallic) depending on the nature of their bonding (Brown (1964), Moore (1948)). The atomic number of nitrogen being 7, the electronic configuration in the ground state is $1s^2$, $2s^2$, $2p^3$, the three 2p electrons occupying different space orbitals in accordance with Hund's rules (Cotton and Wilkinson (1976)). There are three ways in which nitrogen may acquire electronic stability,

a) as in ionic compounds, it may form the nitride ion N^{3-};

b) it may form covalent compounds by the overlapping of its singly occupied orbitals with similar orbitals of other atoms;

c) in interstitial nitrides, the small nitrogen atoms occupy some or all of the octahedral interstices in the metallic lattices, which are generally close packed.

In practice, there seems to be little need for a rigorous classification, in view of the fact that their bonding is a combination of metallic, covalent and ionic forces, of which one type may predominate depending on the crystal structure (Ali (1970)).

Jayaweera (1969) and Ali (1970) classified the nitrides according to their properties as follows:

a) readily hydrolysable nitrides that form ammonia are considered ionic. These are typified by metals in group I (M_3N) and the alkaline-earth metals of group II (M_3N_2). The formation of nitrides of other alkaline metals in group I is restricted by crystal structure conditions. Whether elements are capable of forming stable nitrides is indicated by comparing heats of formation of corresponding oxides and fluorides

(van Arkel (1956)) which are more stable than the nitrides, their standard free energies varying with temperature (Glasson and Jayaweera (1968)). Since the radii of F^-, O^{2-} and N^{3-} are similar, variation in heats of formation will depend mainly on the charge on the negative ion. The electron affinities, E, and crystal energies, U, will be affected. E is expected to predominate in compounds with large positive ions of low charge, so that the heat of formation decreases with increasing negative ion charge; e.g. LiF, Li_2O and Li_3N have heats of formation of 611, 297 and 63 kJ mol^{-1} respectively (Ali (1970)). The sharp decrease from NaF (Juza et al. (1959)) to Na_2O (Samsanov (1965)) suggests a very low value for Na_3N, which is evidently unstable at room temperature. The Madelung constant is also significant in that it is unfavourable for Li_3N and high for LiF. The decrease in the heats of formation are greater than in the group III series, AlF_3 (Stadelmaiser and Tong (1961)), Al_2O_3 (Mott (1958)) and AlN (Guilland and Wyart (1947)) where the nitride has a higher Madelung constant compared with Li_3N. Croato et al. (1951) showed that when comparing molecular susceptibilities, the polarising action of the metal ion decreases from Mg to Zn to Cd;

b) elements with high ionic charge and small ionic radius tend to form covalent nitrides e.g. B, Al, Ga, Si and Sn;

c) interstitial nitrides are mainly formed by transition metals. These are often nitrogen deficient, non stoichiometric compounds, retaining many of the properties of the parent metal. Although non-metal vacancies occur in large numbers in these compounds, there is evidence for metal vacancies in TiN (Brager (1939b) and Straumanis et al (1967)) and in NbN (Brauer and Schnell (1964)). Most of these compounds crystallize as either close-packed cubic or hexagonal structures (or in a slight modification of one of these structures). There are variations in

the number of nitrogen occupied sites and their type (octahedral or tetragonal). Hence these compounds have certain homogeneity ranges. The composition of interstitial metal nitrides with a narrow range of homogeneity is not determined by the metal valency, in contrast to some transition metal oxides also having narrow homogeneity ranges.

Meerson (1964) proposed classifying the carbides in the same way as the nitrides. This was modified by Samsanov (1965 a & b) and formed the basis of the classifications used by Kosolapova (1971):

a) Salt-like or ionic carbides formed by alkali and alkaline-earth metals having valence s-electrons with first ionisation energies from 290 to 675 kJ mol^{-1} (3 to 7 eV);

b) Metals of sub-groups Ib and IIb, which as a result of their high ionization energies (723 - 1060 kJ mol^{-1} (7.5 - 11 eV)) making it difficult for the s-electrons to transfer to the bond with the carbon atoms, either do not form carbides at all or form unstable ones. As a result of this they can be put in the first group or into a separate group of covalent-metallic carbides;

c) Covalent (as in boron or silicon) and covalent-ionic (beryllium and magnesium) carbides formed by elements having valence sp-electrons.

d) Metallic carbides formed by the sd-transition metals. To this group belong carbides consisting of the interstitial phase and Fe_3C-type carbides having structures similar to interstitial phases; their properties are the result of a regular and monotonic change on passing from the carbides of metals of subgroup IVa to those of metals of subgroups Va and VIa and group VIII;

e) Salt-like covalent-metallic carbides formed from sdf-transition metals. These are the carbides of scandium, yttrium, the lanthanides and the actinides.

1.3.1 TRANSITION METAL NITRIDES AND CARBIDES

These materials form one of three fundamental classes of refractory compounds:

a) compounds of metals with non-metals, such as borides, carbides, nitrides, oxides, silicides, phosphides and sulphides;

b) compounds of non-metals with other non-metals, such as carbides, nitrides, sulphides and phosphides of boron and silicon and alloys of boron and silicon;

c) compounds of metals with other metals, generally known as intermetallic compounds.

The bonding in transition metal nitrides and carbides is predominantly metallic or covalent with a small proportion of ionic bonding (Toth (1971)). These bonds are established mainly by transition metals with non-metals having ionization energies sufficiently low to avoid exclusive ionic bond formation. The first ionization energy of nitrogen being higher than that of carbon or oxygen (1401, 1086 and 1314 kJ mol^{-1} [14.53, 11.256 and 13.614 eV] respectively (CRC Handbook of Chemistry and Physics (1994))), the nitrides have a greater proportion of ionic bonding than the carbides or oxides. Decreasing the nitrogen or carbon content of the refractory compound within its homogeneity range strengthens the metal-metal bonds and weakens the metal-non-metal bonds (Toth (1971)). Cooper and Hansler (1963), Santoro and Dolloff (1968) and Williams (1964) showed that reducing the carbon content of TaC and TiC from the stoichiometric value increased the electrical resistivity of the carbide. The change in resistivity is greater than that due to the scattering of electrons by vacant carbon sites and Williams (1964) suggested that the effect is due to the small number of conducting electrons, a large effective charge on vacancies and poor screening of that charge. Goodenough (1963) termed nitrides with rock salt structures as "ionic

compounds with metallic conductivity". The bond is partly ionic due to the difference in electro-negativity between nitrogen and the transition metal.

1.3.2 HÄGG RULES

Hägg (1930, 1931 a & b, 1953) formulated a set of empirical rules relating the crystal structure types formed by transition metal carbides and nitrides (and borides and hydrides). According to the rules the structure formed is dependent on the ratio of the radii of the metal and non-metal atoms, $r = r_x/r_m$ where r_x is the radius of the non-metal atom and r_m the radius of the metal atom. If r is less than 0.59 the metal atoms form very simple structures: face-centred cubic, body-centred cubic, hexagonal close packed or simple hexagonal. The light elements (carbon or nitrogen) are accommodated in the interstitial sites of the relatively simple crystalline structure of the metal host. The interstitial site must be smaller than the atom to be accommodated otherwise there will be insufficient bonding between the metal and non-metal and the structure will be unstable (Toth (1971)). If the interstitial site is too small the interstitial atom will expand the host metal to the point where the metal-metal bonds become too weak and the structure loses stability (Rundle (1948)). If r is greater than 0.59 the transition metal and interstitial elements form complicated structures. Hägg observed that the atomic volume occupied by each metal atom is less in the complex structures than in hypothetical simple structures. Schwarzkopf and Kieffer (1953) indicated that the limiting value of $r = 0.59$ is only valid for carbides as nitrides generally have lower radii ratios than carbides.

Usually, the metal atoms in the interstitial compounds are arranged differently from the original metal structure. Non-metal atoms occupy those interstices where they can remain in contact with the metal atoms. Face-centred, close packed hexagonal and body-centred lattices have two types of interstices,

tetragonal and octahedral with co-ordination numbers of 4 and 6 respectively. The octahedral hole is perfectly regular in face-centred cubic (fcc) and close packed hexagonal (hcp) structures, but has tetragonal symmetry in body-centred cubic structures. The simple hexagonal structure has only one octahedral site (6-fold co-ordinated) at the centre of trigonal prisms of metal atoms.

In interstitial compounds not all the interstices of one type are necessarily occupied, so that many homogeneous phases show wide composition ranges. Homogeneity ranges often approximate to a simple stoichiometric composition corresponding to definite proportion of the available interstices being occupied. In the body-centred cubic lattice the carbon and nitrogen atoms are difficult to accommodate, and having a preference for octahedral sites, the metal forms a face-centred cubic or hexagonal close packed structure (Toth (1971)). Many mononitrides and monocarbides have radii ratios in the range 0.41 - 0.59, and crystallise as sodium chloride (fcc) type structures regardless of the parent metal structure. (Rundle (1948)).

1.3.3 PAULING-RUNDLE THEORY

Rundle (1948) noted that the metal-metal bond length is greater in transition metal carbides and nitrides than in the parent metal. He suggested that metal-non-metal bonding is octahedral, with six bonds being directed towards the corners of an octahedron from the non-metal, as exemplified by the rock salt structure. He applied Pauling's concept of resonance of covalent C- or N-bonds between the six positions (Pauling (1938, 1940, 1947, 1948, 1949) and Pauling and Ewing (1948)). Pauling introduced, and Rundle expanded, the concept of half bonds, where an electron pair in an atomic orbital are used to form two bonds. The principal bonding mechanism is between the sp electrons of the carbon or nitrogen and the d^2sp^3 electrons of the transition

metal. Bonding is accomplished by the use of the non-metal p orbitals or alternately by two p and two sp hybrid orbitals. The resulting six orbitals point towards the metal atoms at the corners of an octahedron. The electrons of the metal atoms are also used in these orbitals and so no electrons are in effect transferred between the metal and non-metal atoms (Toth (1971)). Hume-Rothery (1949) made a critical appraisal of Pauling's theory of metals and also criticised Rundle's theory (1953), pointing out that the octahedral arrangement is equally valid in the close packed hexagonal structure. In the face-centred cubic structure, however, the metal has mutually perpendicular bonds directed towards its nearest six neighbours, a situation not present in the hexagonal structure.

1.3.4 BAND THEORY

Bilz (1958) attempted to resolve the relative importance of metal-metal bonds and metal-non-metal bonds. Bilz (1958) and Denker (1968) applied band theory of metals to refractory compounds with a rock salt structure. Bilz's band model consists of a narrow d band (3.5 eV wide) superimposed on a wide s-p conduction band. The result is that the energy of the original p band of the interstitial atom is lowered so that electrons are transferred from the metal to the non-metal 2p bands. The d band is mainly empty for refractory compounds from subgroups IVb to VIb. Hardness, brittleness and other characteristics result from the direction of the metal-non-metal bonds. From their theories the transition metal nitrides and carbides should develop greater metallic characteristics with increasing occupance of the d band in the parent metal from scandium to titanium and vanadium. Nuclear magnetic resonance measurements of ScN and VN support this (Kume and Yamagishi (1964)), but this increase in metallic character is not supported by electrical conductivity (Nemchenko et al. (1962)). According to Goodenough (1960 a & b) the electron distribution between localised and delocalised bonding states in

transition metals and compounds is dependent upon a critical interatomic distance of 2.9 Å. Above this separation the electrons are localised, but below it they are present as "collective" electrons. Electrical conductivity is limited to those materials in which the interatomic distance is less than 2.9 Å. Transition from cubic to orthorhombic symmetry is associated with localisation of the covalent bond (Goodenough (1960b)).

1.3.5 UBBELOHDE-SAMSANOV THEORY

Ubbelohde (1932, 1937) provided evidence for the dissolution of hydrogen in palladium, titanium and tantalum. It was assumed that hydrogen dissolved as atoms which were subsequently ionized, the electrons from the dissolved hydrogen being accepted into vacant level of the d band of the transition metal. The metal is therefore the electron acceptor and hydrogen the donor. As the first ionization energies of nitrogen, carbon and oxygen are of the same order as that of hydrogen (CRC Handbook of Chemistry and Physics (1994)), it was expected that these elements could behave in a similar manner and the theory was extended by Umanskii (1943) to include nitrides and carbides.
Decreasing acceptor ability causes a corresponding decrease in electrical conductivity (Schaffer and Samsanov (1964)), heat of formation, lattice energy and hardness (Sarkisov (1954), Baughan (1959) and Shulishova (1962)). The theory has been further supported by Seith and Kubaschewski (1935) and Prosvirin (1937) who demonstrated the ionic nature of carbon and nitrogen dissolved in iron and Kiessling (1950) who studied the borides. Kiessling (1957) also emphasised the importance of the metal-metal bond length and why only small non-metal atoms may form interstitial compounds with transition metals. The theory that bonding between metals and non-metals in refractory materials is mainly metallic in nature has been developed further by Samsanov (1953, 1956a & b, 1964, and 1965b) and Neshpor (1964) and by Samsanov and Neshpor (1958 and 1959). In their theory, partial filling of the

electron deficit of the metal is achieved by transfer of valance electrons from the non-metal to the electron cloud of the compound. The theory has also been used to explain the structure of nitrides, carbides and carbonitrides of iron, cobalt and nickel by Jack (1948) and Clarke and Jack (1951).

1.4 PRODUCTION OF REFRACTORY NITRIDES AND CARBIDES

The main methods for the production of transition metal nitrides and carbides are given by Toth (1971), Storms (1967) and Kosolapova (1971). Powder metallurgy techniques for the production of polycrystalline carbides and nitrides include:

a) direct action of the metal or metal hydride with either nitrogen, ammonia or carbon;

b) direct reduction of the metal oxide with nitrogen, ammonia or carbon in a reducing environment;

c) reaction of the metal with a carbon containing gas e.g. hydrocarbons or carbon monoxide;

d) reduction of metal halides with ammonia;

e) precipitation from the gas phase by reacting the metal halide with ammonia or a hydrocarbon in a hydrogen reducing atmosphere;

f) precipitation from the gas phase by reducing the metal carbonyl with hydrogen.

Direct reaction of the metal or hydride with carbon or nitrogen is the most common method of producing carbides and nitrides in the laboratory, and is one of the best for producing relatively pure products (Toth (1971)). The production of homogeneous samples of high-purity requires high temperatures, highly purified starting materials and for some techniques high vacuum conditions. The actual conditions required vary depending on the desired product, with many being prepared from molten metal. Preparation techniques for the carbides used as cutting tool components are described by Kieffer et al (1953) and by Kieffer and Benesovsky (1964 a & b). The final composition and homogeneity is dependent on the temperature at which the product is formed and the length of time for which the formation reaction is allowed to occur. One method for the preparation of substoichiometric compounds is to mix the metal with the carbon or nitrogen in the proportions

of the final desired product. Alternatively a non-homogeneous product is formed at lower temperatures than required to form the stoichiometric compound, which is then homogenised by heating the substoichiometric compound under an inert atmosphere. The thermodynamics of nitride (and hydride) formation by the action of ammonia on metals have been investigated by Lakhtin et al (1978) and Katsura (1992) and the kinetics by Jentzsch and Boehmer (1979). The enthalpies of formation of transition metal mononitrides, carbides and oxides have been estimated by Stolten et al (1993). Tungsten carbide with high surface areas have been produced by Ribeiro et al (1991) and using a molecular precursor by Currie and Howard (1992). Hafnium carbide and nitride have been produced by a reduction technique using magnesium (thermite process) by Kobayashi et al (1992 and 1993).

Single crystals of carbides have been produced by the modified Verneuil technique, the floating zone technique and by precipitation from molten metals. Single crystals of nitrides have been produced by vapour deposition techniques. Single crystals of molybdenum, titanium, zirconium and niobium carbides have been produced by the Verneuil technique in which carbide powder is slowly poured through an electric arc furnace, the molten carbide solidifies as a single crystal (Kiffer (1960)). This method is not ideal as only small crystals can be produced (<1 cm) and the boule produced tends to crack on cooling. Crystals of substoichiometric VC and TiC have been produced by the floating zone method in which rods of sintered, isostatically pressed rods of the carbide are passed under a helium atmosphere at 10 atmospheres pressure through a radio frequency (rf) induction furnace in which the carbide melts and forms on cooling a single crystal. Thermal shock on cooling is reduced by after heaters (Precht and Hollox (1968)). Tobin and Fleischer (1967) prepared near stoichiometric ZrC by heating a rod of zirconium metal in a tight fitting graphite tube to above the melting point of zirconium. The

carbide forms at the surface and then progressively throughout the metal by the diffusion of carbon. This technique has also been used to produce vanadium carbide but was unsuitable for the production of hafnium and tantalum carbides (TaC and Ta_2C). Zhao et al (1990) reported the formation of tungsten carbide powders in a vapour phase reaction in a hydrogen/chlorine flame. This method produced powders with particle sizes smaller than 1 μm. Molybdenum nitrides of high surface area have been made by Jaggers et al (1990) by a similar method.

Brager (1939a & b) reported the production of single crystals of titanium nitride by the vapour deposition on copper from titanium tetrachloride and ammonia at 800 °C, and the formation of zirconium and titanium nitride single crystals by the vapour deposition from the metal tetrachloride and ammonia or hydrogen and nitrogen on hot tungsten (Moers (1931)). Nitrides have also been produced by chemical vapour deposition (CVD) by Krysmann and Schroter (1992) and Won and Chun (1993)

Thin films of nitride or carbide can be prepared by the direct nitridation or carbidation of the metal or by the vapour deposition from the metal tetrahalide. If a thin film of nitride or carbide is required on a different metal base, then either a film of the desired metal has to be deposited first or the desired metal nitride or carbide can be deposited directly by the vapour deposition from the tetrahalide.

High quality nitrides have been produced by dc or ac sputtering of metal in the presence of nitrogen (Toth (1971)). Backovic et al (1994) have reported the formation of nitrides of titanium alloys by ion implantation and molybdenum nitride thin films by Choi et al (1992). MacInnes et al (1991) have reported the formation of refractory-metal carbides on carbon fibres.

The preparation of carbides and nitrides and their catalytic properties have been reviewed by Oyama (1992) and Leclercq et al (1989).

1.5 OXIDATION OF CARBIDES AND NITRIDES

Oxidation of hafnium carbide with and without transition metal additions has been studied by Courtright et al (1991), Bargeron et al (1993 a & b) and Shimada et al (1992) and the oxidation of indium nitride films by Sawada and Hashimoto (1994). Padilla (1991) studied the high temperature oxidation of tungsten carbide and Bronoel et al (1991) studied the action of hydrogen on carbides of tungsten and molybdenum.

1.5.1 TITANIUM NITRIDE AND CARBIDE SYSTEMS

The methods of producing titanium nitride have been reviewed by Glasson and Jayaweera (1968). More recently Sugimoto et al (1994) have produced titanium nitride fibres by the action of nitrogen gas on titanium oxide at 1000 °C. The titanium oxide was produced by the decomposition of titanium alginate. Titanium nitride layers have been produced by the action of ammonia on titanium metal at high pressures (Hara et al (1990)). Other methods of production include alloying techniques (Calka (1991)), ion implantation or plating (Matsumura et al (1993), Omura (1991) and Ignatev et al (1992)), chemical vapour deposition (CVD) (Kaizuka et al (1994), Elger et al (1989), Michalski and Wierzchon (1989) and Hedge et al (1993)), ion-beam mixing (Kiuchi et al (1989) and Nakagawa et al (1993)). Pilyankevich et al (1977) studied the conditions required to obtain as near perfect crystals as possible by CVD. Mechanisms of formation by dc magnetron sputtering have been investigated by Richter et al (1992).

Titanium nitride whiskers have been formed by the reaction between sodium/titanium bronze and molten sodium cyanide (Bamberger et al (1989)). Titanium nitride and gold multilayer films have been produced by rf sputtering by Yoshida et al (1979) and investigated by Banerjee et al (1991) and using microwave (magnetron) radiation by Moon et al (1991).

Arbuzov et al (1977) studied by x-ray analysis the cubic δ-TiN and the lower nitride phase ε-TiN_x which is normally tetragonal and confirmed a δ'-TiN_x phase under certain conditions of thermal treatment. Friction and wear characteristics of titanium nitride in air has been studied by Singer et al (1991). The effect of concentrated solar-energy on titanium nitride coatings has been studied by many researchers (Georgson et al (1991), Oberlander et al (1994) and Franck et al (1993)). The properties of colloidal suspensions of titanium nitride on silica has been investigated by Partch et al (1993) and the growth of anodic oxides by Montero et al (1993).

Oxidation and degradation of ultrafine powdered titanium nitride has been studied by Sakka et al (1992). The effect of oxidation on the friction and wear characteristics of titanium nitrided steel has been investigated by Stott and Mitchell (1991) and Sun and Bell (1993) and in carbon dioxide by Mitchell and Stott (1992). The action of steam on nitride coated dental surgical tools has been reported by Louw et al (1991). Tompkins (1991 and 1992) and Saha and Tompkins (1992) studied the oxidation of reactive thin films, formed by sputtering, in air and oxygen, Massiani et al (1992) studied the photochemical properties of sputtered oxide and nitride films. Oxidation kinetics have been studied by Wittmer et al (1979) in the temperature range 500 - 650 °C. They studied the oxidation of films in oxygen and determined the activation energy to be 198 ±5 kJ mol^{-1} (2.05 ±0.05 eV) and found the rate limiting process to be the diffusion of oxygen through the oxide layer. The films formed were found to be semi-conductors with resistivities of the order 10^6 Ωcm. Lefort et al (1978 and 1979a & b) found the activation energy to be 154 ±21 and 180 kJ mol^{-1} for titanium nitride plates of different nitride content (TiN_x where x = 0.79 and 0.91), the kinetics were pseudo-linear with the diffusion of oxygen being the rate limiting factor. Voitovich and Golovko (1980) studied the oxidation of titanium nitride at reduced pressures. Mass

loss was observed during the initial stage of oxidation due to the loss of nitrogen from the oxide/nitride system. This effect was more noticeable at higher oxygen pressures.

The titanium carbide system has been reviewed by Storms (1967) and Kosolapova (1971). Titanium carbide has a wide homogeneity range. The homogeneity range has been reported as $TiC_{0.48 \pm 0.01}$ (Rudy et al (1965) and Cadoff and Nielson (1953)) to $TiC_{0.95}$ (Norton and Lewis (1963)) above this upper value free carbon has been reported as being present with the carbide (Rudy et al (1965)). The earliest techniques for the preparation of titanium carbide included its isolation from cast iron containing titanium (Shimer (1887)) and the reduction of the dioxide with carbon (Moissan (1985 and 1987) and Lyubimov (1992)). Samsanov (1956c) proposed the following reduction steps

$$TiO_2 \rightarrow Ti_3O_5 \rightarrow Ti_2O_3 \rightarrow TiO \rightarrow TiC \text{ or } Ti$$

the final product being dependent on the heating rate and final temperature attained. Titanium carbide coatings have been formed on steels from molten titanium/lead mixtures (Wakamatsu et al (1993)). Chemical vapour deposition has been used to form carbided plates by Jiang et al (1990) and Thorne et al (1992) and mixed layers by Colombier and Lux (1989). Dual ion beam implantation has been used to form thin films (Min et al (1991)) and has been found to be induced by ion bombardment in titanium/iron mixes (Selvam et al (1990)). Steinmann and Hintermann (1985) studied the adhesion of titanium carbide and cyanide coatings on steels.

Golovko et al (1990) and Pugach et al (1990) studied the oxidation of the carbides of titanium based alloys. Oxidation of ultra-dispersed powders of titanium nitride and carbide have been studied by Kochergina and Fedoseev (1990). Voitovich and Laverenco (1991) studied the effect of purity of the

carbide on the oxidation of the material and Askarova and Zhilyaev (1994) investigated the oxidation at low air pressures. As with the nitride, the further oxidation of carbide plates and films are hindered by the oxide formed.

1.5.2 ZIRCONIUM NITRIDE AND CARBIDE SYSTEMS

Ali (1970) reviewed the techniques and kinetics of nitriding zirconium. The main methods are similar to those of titanium (Mellor (1927)). The reaction between zirconium and ammonia is slower than between zirconium and nitrogen (Samsanov et al (1961)). The kinetics of formation of zirconium nitride composite ceramics by the reaction of zirconium with boron nitride has been studied by Johnson et al (1991). The nitride has also been produced by a cryochemical technique by Egorova et al (1992), by the reduction of the oxide by Okada and Atoda (1980) and in a rf discharge by Konuma and Matsumoto (1977). The phase diagram for the zirconium-nitrogen system is given by Toth (1971) and shows that zirconium nitride has a homogeneity range from $ZrN_{0.7}$ to ZrN_1 and possibly beyond. Fridlender et al (1977) studied the change in thermal diffusivity with temperature using nitrides of varying nitrogen content, ZrN_x (where x = 0.74 - 0.99). From these studies it was shown that on increasing the concentration of metalloid vacancies (x), the thermal diffusivity decreased, and the coefficient of thermal diffusivity changed sign. Bolgar et al (1976) determined the standard enthalpy at various temperatures in the range 955 - 2114 °C for ZrN_x where x = 0.76 to 0.96. Desmaison et al (1977) studied the effect of oxygen pressure on the oxidation of zirconium nitride plates and spheres. For both of these geometries the oxidation curves followed a sigmoidal shape, and this was retained when different oxygen pressures were used. They concluded that the activation energy was constant over the temperature range 600 - 800 °C and that the oxidation was controlled by an external phase boundary reaction. Caillet et al (1977) also studied the effect of oxygen pressure on the oxidation of zirconium

nitride. At low oxidation temperatures (below 600 °C) an initial weight loss occurred. Between 600 and 650 °C the oxidation curves were approximately linear after an initial period of curvature. They concluded that the mechanism of oxidation involves the formation of zirconium-oxygen solid solutions before forming zirconium dioxide (zirconia).

Storms (1967) gives the phase diagram for the zirconium carbon system, showing that the homogeneity range extends from $ZrC_{0.6}$ to $ZrC_{0.99}$. Kosolapova (1971) states that the main commercial method of producing zirconium carbide is by the reduction of zirconium sand (containing 67% ZrO_2). Other methods of production are similar to those of titanium carbide. Rao and Venugopal (1994) studied the oxidation of sintered carbide powder under varying temperature and oxygen pressure regimes and concluded that the oxidation kinetics were controlled by the diffusion of oxygen into the remaining carbide.

1.5.3 VANADIUM NITRIDE AND CARBIDE SYSTEMS

The Va subgroup nitrides and carbides are complicated by their ability to form more than one nitride or carbide phase (Toth (1971)). Thus vanadium can form VN and V_2N and VC and V_2C. According to Toth the exact homogeneity ranges are uncertain. Mellor (1927) gives a summary of the production methods of the nitrides. Below 1200 °C it is difficult to produce the nitride by the reduction of the pentoxide with nitrogen in the presence of carbon due to the formation of the carbide, but has been produced by the reaction of ammonium vanadate with ammonia at 900 - 1100 °C (Epelbaum and Ormont (1946 and 1947). Hahn (1949) produced the nitride by the direct action of nitrogen on vanadium metal, and by sintering a mixture of VN and vanadium metal reported the formation of V_3N. Ali (1970) oxidised milled vanadium nitride at 500 and 600 °C. At these temperatures, the first half of

the sample oxidised rapidly, whilst the remaining material oxidised more slowly as the oxide formed during the initial stage of the reaction sintered causing the rate of further reaction to be controlled by the diffusion of oxygen through the oxide layer. Lefort et al (1979) studied the oxidation of nitrogen deficient vanadium nitride ($VN_{0.95}$) and found similar reaction kinetics. Litvinenko et al (1980) investigated the thermodynamic properties in the homogeneity range.

The vanadium carbide system are described by Kosolapova (1971) and Storms (1967) where they list the main methods of manufacture and properties.

1.5.4 NIOBIUM NITRIDE AND CARBIDE SYSTEMS

An account of the methods of production of niobium nitride is given by Mellor (1927). The nitride can be produced by the action of nitrogen on niobium metal at 1200 °C (Duwez and Odell (1950)). Miki et al (1992) have produced nanocrystalline niobium nitride by mechanically alloying niobium in an nitrogen atmosphere and superconducting niobium nitride has been produced by molecular beam epitaxy techniques (Kawaguchi and Sohma (1991)). Hennessey and Morral (1992) studied the oxidation of the nitride at temperatures above 1150 °C. At these temperatures the oxide produced in the initial stages of oxidation sinters and the oxidation is controlled by the diffusion of oxygen through the oxide layer.

Niobium forms three carbide phases (Kosolapova (1971)):

1) α-phase consisting of a solution of carbon in niobium, the solubility increasing with temperature (to a maximum of 0.8 wt% at 2200 °C);
2) β-NbC_x where x ranges from 0.48 to 0.500 (hexagonal);
2) γ-NbC_x where x ranges from 0.71 to 0.99 (cubic).

Between these homogeneity ranges mixtures of phases occur. Kosolapova (1971) and Storms (1967) review commercial and historical methods of production of the carbide. Huang (1991) produced niobium carbide and

tantalum carbide by carbon ion implantation methods. When heated in oxygen the carbide will burn and in air corrosion becomes severe above 1000 °C (Storms (1967)).

1.5.5 TANTALUM NITRIDE AND CARBIDE SYSTEMS

Mellor (1927) and Brown (1964) summarise the commercial production methods for producing the carbide and nitride of tantalum. The nitride can be produced by the action of nitrogen on the metal at 900 °C, although this does not give the stoichiometric composition. The nitride has been produced by sputtering techniques (Coyne and Tauber (1967)), chemical vapour deposition (Gaydon (1967)) and by direct ion implantation (Zhou et al (1990)). Toth (1967) reports the possible occurrence of several phases:

a) nitrogen is soluble in β-Ta to produce $TaN_{0.05}$;

b) hexagonal close packed TaN_x where x is between 0.41 and 0.5;

c) TaN which has a very narrow homogeneity range;

d) Ta_3N_5;

e) the phase δ-TaN_x where x is between 0.80 and 0.90 is uncertain.

The oxidation of reactively-sputtered, tantalum nitride thin films has been studied by Ibidunni (1993) and Ibidunni et al (1993). They measured the change in electrical resistance of the films against time at temperatures within the range 200 to 500 °C. The oxidation kinetics could be expressed as $\Delta R/R = k't$ where $\Delta R/R$ was the change in resistance expressed as %, k' the rate constant and t was time. For the thickest films the reaction curves were parabolic in shape above 325 °C but for the thinner films the reaction curves were parabolic at all temperatures studied. The rate constants obeyed the Arrhenius relation and the activation energy was calculated to be 147 kJ mol^{-1} (1.52 eV).

Mellor (1927) and Brown (1964) summarise the methods for producing tantalum carbide. Several phases of tantalum carbide are given by Kosolapova (1971).

1.5.6 MANGANESE NITRIDE AND CARBIDE SYSTEMS

Mellor (1927) and Brown (1964) review the methods of producing the nitride and carbide. Zhang and Schleich (1994) produced mixed iron-manganese carbide by the reduction of the oxides with carbon in nitrogen.

1.5.7 CHROMIUM NITRIDE AND CARBIDE SYSTEMS

Metals with up to five electrons in the outer d-shell form less stable d^0 and more stable d^5 configurations (Cotton and Wilkinson (1976)). Where the stable d^0 and d^5 configurations vary widely, as in titanium or zirconium, only one or two interstitial nitride or carbide phases are formed, but with a wide homogeneity range. When the d^5 configuration becomes the more stable, as in chromium with five electrons in the 3d-shell, more discrete phases are formed, but with narrower homogeneity ranges; thus chromium forms two nitrides (Cr_2N and CrN) and three carbides ($Cr_{23}C_6$, Cr_7C_3 and Cr_3C_2) (Toth (1971)).

The nitrides can be produced by the direct action of nitrogen on the metal or by the action of ammonia on the boride (Mellor (1927) and Brown (1964)). The carbides can be produced by the reduction of the oxide with carbon (Storms (1967)). A metastable face centred cubic structure for chromium carbide has been reported by Liu and Cheng (1992) when produced by carbon ion implantation techniques.

1.5.8 IRON NITRIDE AND CARBIDE SYSTEMS

The traditional method of nitriding iron involves heating iron metal to red heat then plunging the hot metal into potassium ferricyanide on a graphite block.

Nitrides and carbides can form during the processing of iron in the blast furnace (Adams (1988)). Other methods of producing the nitrides and carbides are given by Mellor (1927) and Brown (1964). Gorbach et al (1991) observed several nitride phases formed by nitriding porous iron. Funakubo et al (1993) prepared iron nitride and iron nitride/titanium nitride films by chemical vapour deposition techniques. Iron carbide has been produced by a chemical vapour technique using laser energy to create the ions (Jervis and Zocco (1990)).

1.6 AIMS OF THIS RESEARCH

This work forms part of a continued study of the formation and oxidation of the borides, carbides and nitrides of transition metals. Previous workers in these laboratories have investigated the formation of the nitrides of titanium and zirconium (along with the nitrides of calcium, magnesium, cadmium, zinc and boron) and the formation of, and the effect of milling on, the nitrides of titanium, zirconium, vanadium, niobium, tantalum, chromium and molybdenum. Other workers have studied the formation and properties of some transition metal borides and carbon boride with metal additives.

In this work it was hoped to gain an insight in to some aspects of the oxidation of the nitrides of titanium, zirconium, vanadium, chromium and iron and the carbides of titanium, zirconium, vanadium, niobium, chromium, tantalum and manganese in air. It was also hoped to investigate the possibility of oxidising the nitrides of iron, titanium and chromium in carbon dioxide. The above named metals are all additives commonly used (in greater or lesser proportions) in the production of steel.

Oxidations were to be studied thermogravimetrically and mathematical models applied to rate studies. Where possible, surface area studies and electron microscopy studies were to be correlated with the results obtained from thermogravimetric studies. Crystallite phases present during the oxidations were to be identified by x-ray diffractometry.

CHAPTER 2

EXPERIMENTAL TECHNIQUES

2.1 THERMAL ANALYSIS

2.1.1 REVIEW AND INTRODUCTION

Thermal analysis is defined as a group of techniques in which a chemical or physical property of a substance is measured as a function of temperature during which the sample is subjected to a controlled temperature program (Wendlandt, 1986). This program may be isothermal, where the sample is maintained at a constant temperature and the selected property is measured as a function of time, or may be dynamic, where the sample temperature is altered at a predetermined rate. The principal thermoanalytical techniques have been described by Wendlandt (1986), Keattch and Dollimore (1975) and Pope and Judd (1977).

Thermogravimetry (TG) involves the measurement of the weight of the selected sample whilst the predetermined temperature programme is executed. The sample may be heated, cooled, held at constant temperature or cycled between temperatures.

The isothermal TG method is suitable for slower reactions and is considered by some authors to be more accurate than dynamic methods. From the TG curve, the dimensionless "degree of transformation" α (the fraction of reactant that has reacted) is used to evaluate data, based on the assumption that the kinetics can be expressed by the formal equation

$$d\alpha/dt = k(1 - \alpha)^n$$

where t is time, k the rate constant and n the order of reaction. Values of $n = 2/3$ and $1/2$ correspond to the movement of a reaction boundary due to spherically shaped particles decreasing in size and gas diffusing through product to the reaction boundary respectively (see section 1.2.3). In a solid-

gas reaction, if the reaction is controlled by the reaction proceeding at the surface of a sphere whose diameter is decreasing as the reaction proceeds then a plot of $(1-\alpha)^{1/3}$ against time should be linear. If the rate of reaction is determined by the gas diffusing through a layer of product to reach the underlying reactant solid then a half order reaction mechanism is expected and a plot of α^2 against time should be linear. The application of numerical methods in the determination of n and k has been discussed by Norris et al (1974). Keattch and Dollimore (1975) also discuss the use of reduced time plots ($t/t_{0.5}$) applied to diffusion controlled reactions.

The temperature dependence of the rate constant, k, is given by the Arrhenius equation

$$k = A \exp(-E_a/RT)$$

where A is the frequency factor, E_a the activation energy, R the gas constant and T the temperature. The combination of the rate equation

$$d\alpha/dt = k(1 - \alpha)^n$$

and the Arrhenius equation leads to the equation

$$d\alpha/dt = f(\alpha) \exp(-E_a/RT)$$

where $f(\alpha) = A(1 - \alpha)^n$. From a plot of log $d\alpha/dt$ versus 1/T obtained from a series of isothermal reactions at a series of temperatures, the value of E_a can be deduced from the slope. In this work initial rate (da/dt) values were measured either within $\alpha = 0.05$ to 0.4 or within t = 5 to 15 minutes depending on the nature of the reaction, i.e. measurements were taken during the initial linear part of the reaction curve.

Dynamic TG curves are mathematically more complex. The kinetic equation and Arrhenius equation are combined and expressions evaluated by differential, integral and approximation methods. Wendlandt (1986) and Blazek (1973) give comparison and criticism of the various methods.

Derivative thermogravimetry (DTG) yields the first derivative of the TG curve. Whilst giving no further information than the TG curve, the DTG curve is useful in resolving overlapping TG curves.

Differential Thermal Analysis (DTA) is a technique that measures the difference in temperature between the sample being studied and an inert reference material whilst both are subjected to the same controlled thermal regime. In this technique all changes in enthalpy, physical or chemical, are recorded. The obtained results are more dependant on experimental conditions than they are in TG.

Kinetic information may be obtained from DTA and many equations have been derived for determining E_a and n from peak maxima (or minima) and heating rate. During the reaction it is assumed that the reactants and products have constant thermal capacity and lack temperature gradients within the sample or reference. From the weight change α can be calculated and the corresponding DTA peak is proportional to the enthalpy of the reaction. The actual DTA peak height, and thus the temperature difference between the sample and reference is dependant on the individual masses, their thermal capacities and the energy change involved. Kissinger (1956) combined the kinetic equation and the Arrhenius equation and applied it to dynamic conditions, deriving the equation

$$-E_a/R = d\ln(\Phi/T^2_m)/d(1/T_m)$$

for first order reactions where Φ is the heating rate (dT/dt), and T_m is the temperature at which the reaction proceeds at its maximum rate. A plot of $\ln(\Phi/T^2_m)$ against 1/T should give a straight line of slope $-E_a/R$. Kissinger assumed that T_m occurs at the temperature at which the rate of energy change

of the reaction system is greatest. Kissinger (1957) later modified the equation to account for reactions of other orders. ASTM Standard E698-79(1984) gives two equations for the determination of activation energies. The first takes the form

$$E_a = (-R/D)d\ln\Phi/d(1/T_m)$$

or

$$E_a = (-2.303R/D)d\log_{10}\Phi/d(1/T_m).$$

Initially D takes the value 1.0516. Once E_a has been calculated, the value is refined by substituting a revised value of D as given in the standard. The alternative equation given in the standard is the Kissinger equation above. The ASTM Standard states that the method is not valid for reactions that are inhibited, or where two or more reactions overlap. Reed et al (1965) showed mathematically that the DTA peak does not coincide with the maximum rate of reaction. Sharp (1972) reviewed the theoretical and experimental aspects of obtaining meaningful kinetic parameters from DTA studies of solid state reactions.

Benoit et al (1985) compared kinetic data obtained from isothermal and dynamic studies of the thermal decomposition of several organic compounds. From their studies they showed that it is necessary to determine from isothermal studies that the reaction order is the same at the lower and higher ends of the temperature range that is to be studied under dynamic conditions if useful data is to be obtained.

Thus it can be seen that TG and DTA are useful tools for the study of reaction kinetics.

2.1.2 THE MASSFLOW THERMOBALANCE

The Stanton-Redcroft Massflow Thermobalance model MF-H5 was originally purchased in 1974 and has since been subject to modification. The original electromechanical furnace control was disconnected and the furnace controlled by a Stanton-Redcroft / Eurotherm linear temperature controller model LVP-C, with programmed heating rates up to 20 °C min^{-1}. Sample temperature and DTA signal were recorded on a Leeds and Northrup "Speedomax W" chart recorder. A schematic diagram of the balance and ancillary equipment is shown in figure 1.

The thermobalance design incorporated two beams, one inside the chamber and one outside. The inner beam was coupled to the outer beam by a magnetic link that ensured that any movement of the inner beam due to a change in weight of the sample was followed by the outer beam. Mounted on the outer beam was a metal plate which forms one plate of an air spaced capacitor, the position of the second plate of the capacitor was adjusted electro-mechanically so that the capacitance between the two plates remained constant and thus any movement of the inner beam was detected and recorded by a pen on the chart recorder connected to the plate adjustment mechanism by a mechanical link. The full beam deflection was 20 mg with a sensitivity of 0.2 mg. Once the beam had travelled to its maximum deflection counterweights were automatically added or removed, to a maximum of 200 mg, to bring the beam back onto scale. Every five minutes the balance was arrested and released to ensure that the beam did not stick.

A schematic diagram of the balance chamber is shown in figure 2. The balance chamber consisted of a 178 mm internal diameter, 10 gauge copper tube, which was coated internally with epoxy resin. Removable end plates, also of 10 gauge epoxy coated copper, allowed access to the inner balance

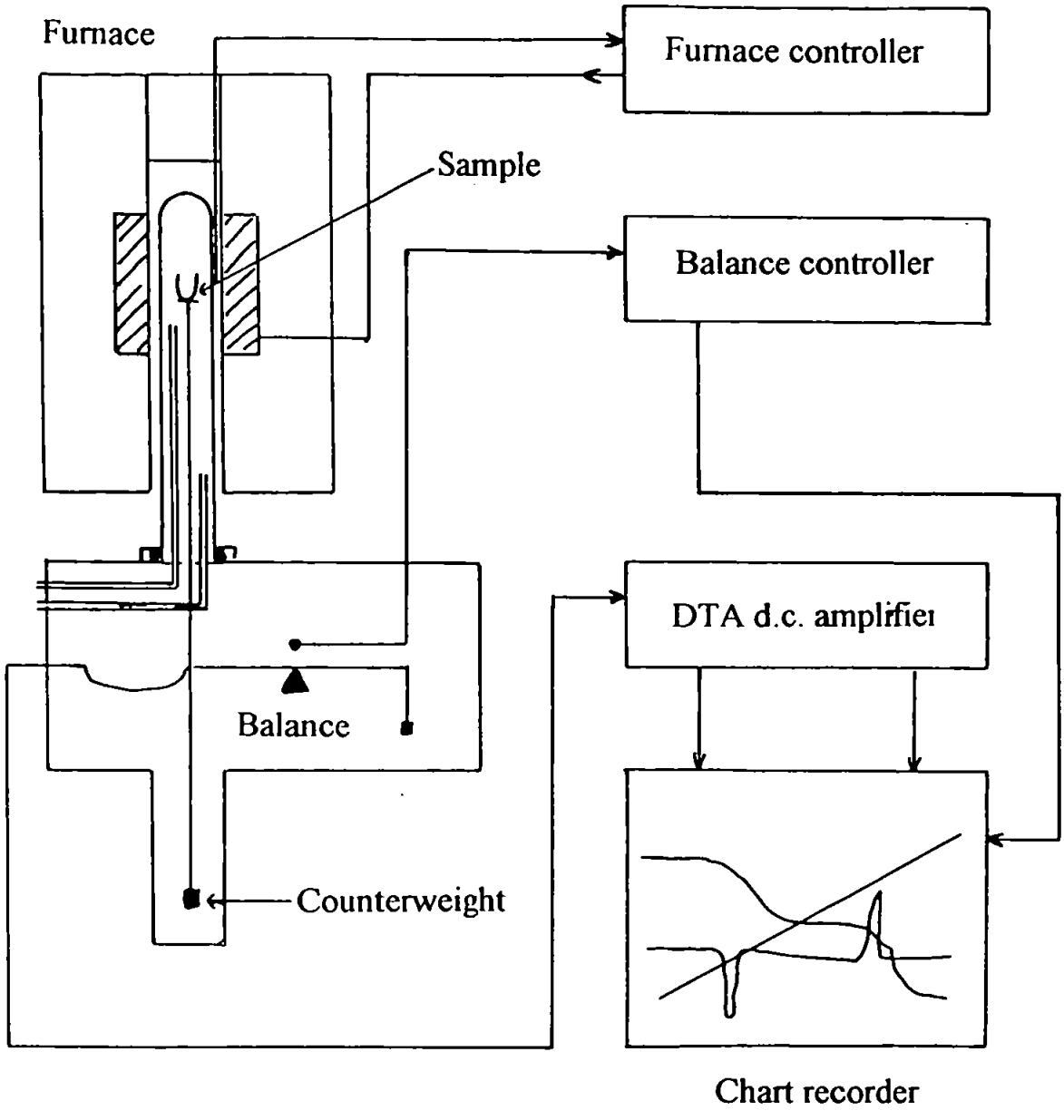

Figure 1
Schematic diagram of Massflow thermobalance.

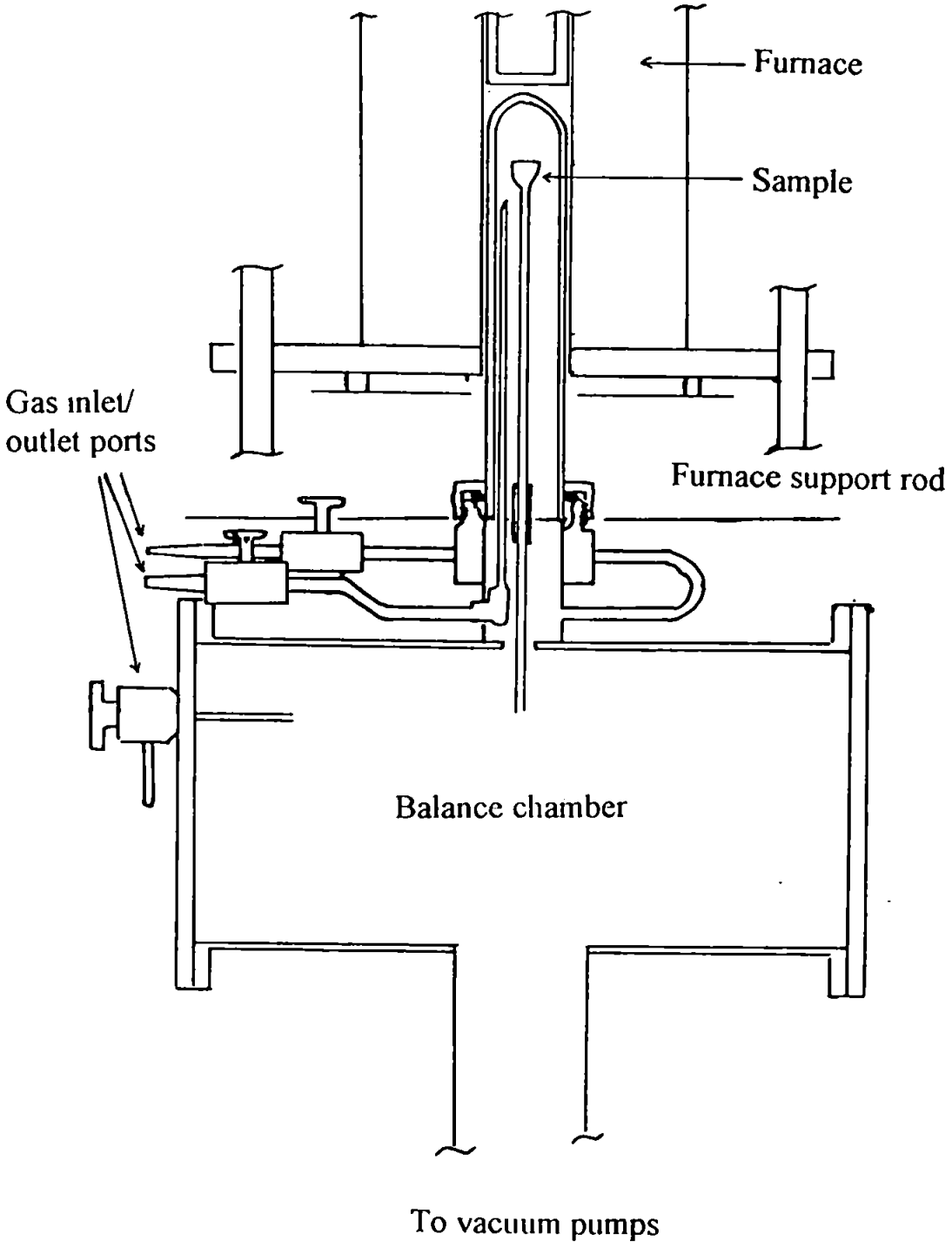

Figure 2
Schematic diagram of Massflow reaction chamber and gas inlet/outlet ports.

beam. Rubber "O" rings are used to seal the plates to the main body. A mullite reaction chamber was mounted above the balance chamber and sealed with a water cooled rubber "O" ring. Four ports allowed gas into or out of the system, two ports into or out of the reaction chamber, one gas port into the balance chamber and a vacuum port, thus it was possible to flush the balance chamber with an inert gas whilst corrosive gases are present within the reaction chamber.

The sample holder (figure 3a) consisted of a block of alumina, 20 mm in diameter and 13 mm deep, into which were machined two wells each 6.5 mm in diameter and 10 mm deep to take the sample and reference crucibles. A depression in the base of each of the matched platinum crucibles allowed a thermocouple to be inserted and the temperature of the relevant crucible and its contents to be measured. Calcined alumina of a mass equal to the sample was used as the reference material. Other reference materials can be used but should have similar physical characteristics, e.g. density, thermal capacity etc., as the sample. The alumina block was mounted onto the inner balance beam by alumina and silica rods. The thermocouple leads were threaded through the rods and brought out to a junction panel mounted on the beam. 0.026 mm diameter platinum wires were used to connect the junction panel to ceramic insulated pins mounted through the balance chamber end plate to which were connected the leads to the DTA dc amplifier, constant temperature junction and temperature chart recorder. Pt/13%Rh Pt thermocouples were used to monitor the sample and reference temperatures. Movement of the 0.026 mm wires as the balance beam moved had negligible effect on the beam. A cold reference junction consisting of a thermocouple placed in, but electrically isolated from, an ice/water slush bath contained in a dewar flask was used in conjunction with the temperature measuring thermocouple.

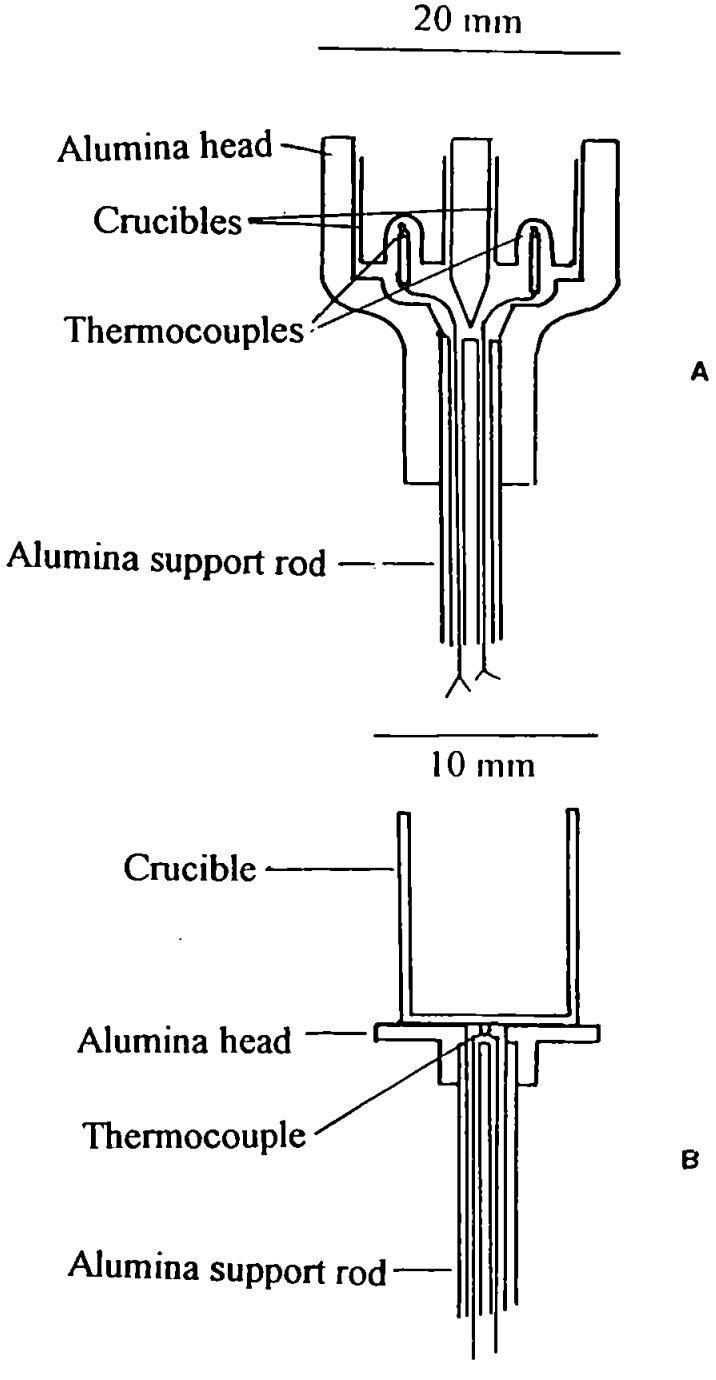

Figure 3

A) Schematic diagram of DTA sample head showing positioning of thermocouples.

B) Schematic diagram of TG sample head showing position of thermocouple.

The dc DTA amplifier had seven ranges from 0.02 to 1.0 mV full scale deflection (fsd). The single channel chart recorder was connected via a switching unit that allowed the DTA output to be recorded for 4 min 55 s followed by the temperature output for 5 s. Figure 4 shows a schematic diagram of the thermocouple connections.

An alternative head (figure 3b) consisted of a 10 mm diameter alumina disc mounted on the beam as before. This arrangement had only one thermocouple to record temperature but allowed crucibles of larger capacity to be used for TG only studies, the amplifier and switching unit not being used.

The furnace consisted of a bifilar platinum-rhodium winding, capable of a maximum temperature of 1500 °C, wound around an alumina former of 50 mm internal diameter. The top of the furnace was stoppered with an 100 mm deep alumina plug filled with calcined alumina. The furnace was lowered vertically over the reaction tube so that the sample crucible, or alumina block, is in the centre of the furnace.

The furnace was controlled by a Stanton-Redcroft / Eurotherm LVP-C linear temperature programmer with a Pt/13%Rh Pt thermocouple placed between the furnace tube and the mullite reaction chamber sensing the furnace temperature. The controller was capable of heating rates up to 20 °C min^{-1}, up to a predetermined maximum temperature which could then be held indefinitely thus creating isothermal conditions.

Calibration of the instrument was carried out monthly (or if calibration error was suspected) according to the manufacturer's instructions using traceable standards. Calibration curves in both static and flowing gas, different gases and different heating rates to determine any buoyancy effects in TG and

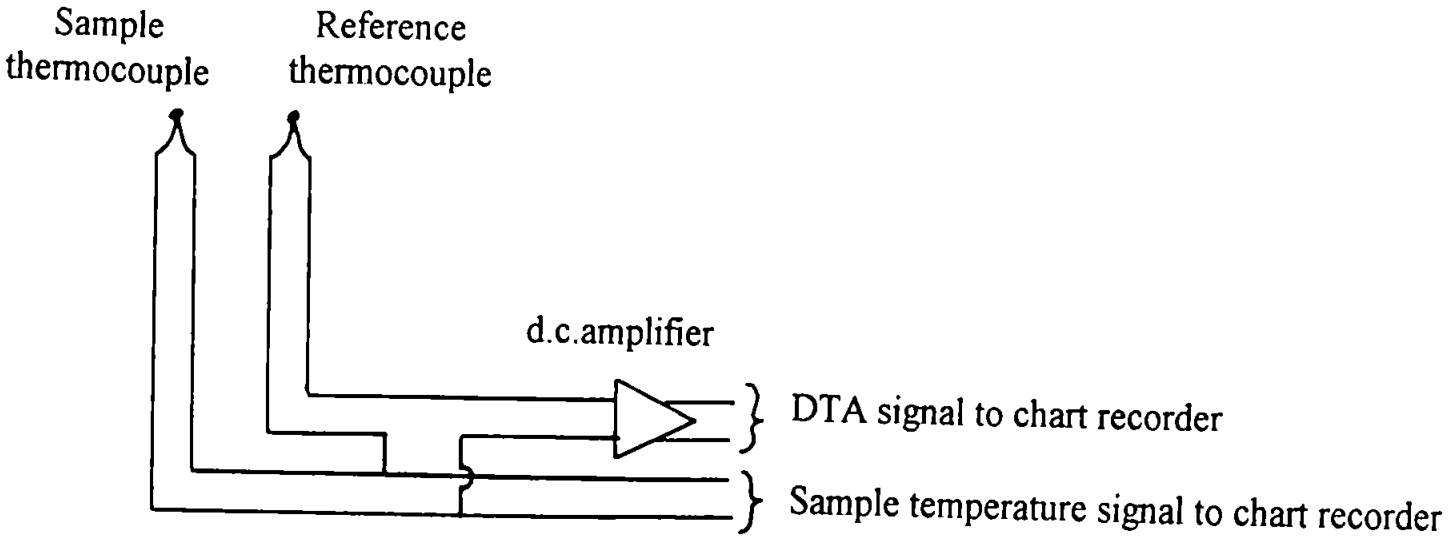

Figure 4
Schematic diagram of the thermocouple electrical connections.

baseline drift in DTA, using alumina in both crucibles was carried out. The apparent weight gain was 2 mg as the temperature was raised to 200 °C, after which there was negligible change in weight. Isothermal curves showed no effect above 200 °C. All TG work was corrected for buoyancy effects. Positioning of the sample within the furnace had greater effect on DTA baseline drift than gas flow or heating rate.

Gas was supplied to the instrument from bottled gas supplied by South West Industrial Gases, via a manifold that allows switching between compressed air, nitrogen, argon, carbon dioxide or mixtures of these gases without breaking the supply lines. The gases as supplied were of at least 99.9% purity. The gas then passed through a drying tube (self-indicating) and molecular sieve trap to reduce water and hydrocarbon content to less than 0.1 ppm. Gases, other than air, were also passed through a molecular sieve trap to reduce oxygen content to less than 0.1 ppm. The manifold also supplied gases to the tube furnace and the STA 781 thermal analyzer. Gas flow rate was measured by an inline "Rotameter" calibrated for air at atmospheric pressure and room temperature. If other gases were used a correction factor had to be taken in to account. The flow rate for other gases is given by

$$\text{Flow rate} = \text{Indicated rate} \times (\rho_{air}/\rho_{gas})^{1/2}$$

where ρ_{air} is the density of air at room temperature and pressure, and ρ_{gas} is the density of the gas being used at room temperature and pressure.

2.1.3 PROCEDURE

For DTA analysis, a suitable weight of sample was weighed out into a crucible, normally 100 - 200 mg (platinum crucible). For TG analysis a sample of 100 mg (platinum crucible) or 1 g (alumina crucible) was used. In the case of DTA analysis calcined alumina was used as a reference material, the same mass of reference material being utilised as that of the sample. The

crucible/s were then positioned on the sample head and counterweights added to the balance beam to bring the balance to the equilibrium position. The balance was released and checked to ensure that it was free to move before being arrested. The mullite sheath was lowered around the sample and secured in position and cooling water turned on before the furnace was lowered. Once the sheath was in position the required gas flow was set up, usually 300 cm^3 min^{-1}, and the system purged for five minutes to remove air from the system, unless air was the desired atmosphere. The desired heating regime was then initiated, the balance released and the chart recorders started. In the case of isothermal oxidations, once the sample had equilibrated at the desired temperature the flow of inert gas was stopped and the desired reactant gas allowed into the system and the point at which gases were changed over noted. Once the experiment was complete the furnace was switched off and the system allowed to cool to room temperature before the samples could be recovered. There was no provision for forced cooling of the system.

2.1.4 THE STA 781 THERMAL ANALYZER

At the heart of the system was a 5 g capacity microbalance and its associated microprocessor controller. Full scale deflection could be set to any desired weight change between 2 and 20 mg with a resolution of 1 μg, and between 20 and 200 mg with a resolution of 10 μg. Electronic taring over the full range, multiple inject and DTG facilities were incorporated within the controller. A schematic diagram of the system is shown in figure 5.

Suspended from the balance was an alumina hangdown with platforms formed at the bottom for sample and reference crucibles. Fused to the platforms were the Pt/13%Rh Pt thermocouples used to sense the sample and reference temperatures. An alumina washer placed between the platforms and crucibles

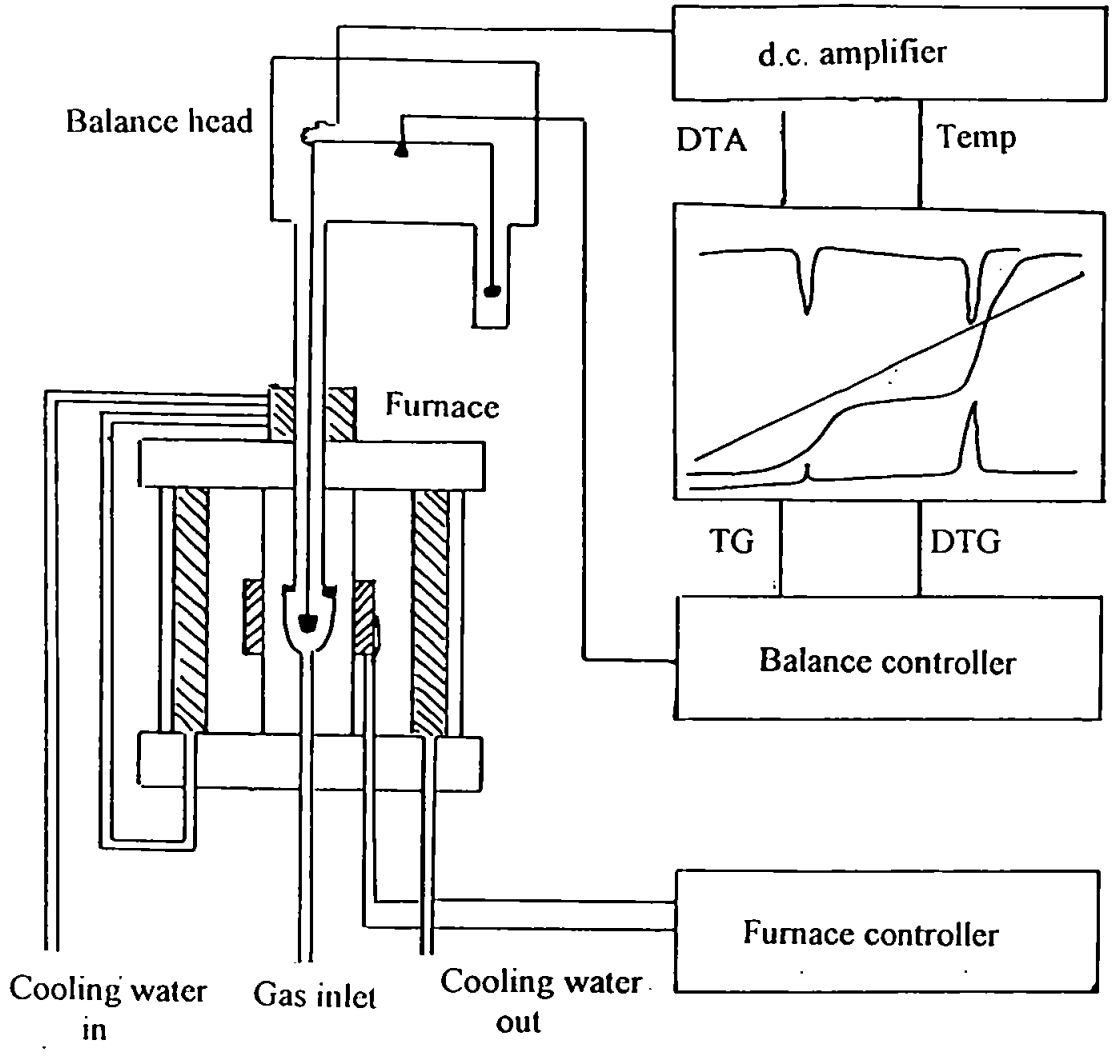

Figure 5
Schematic diagram of STA 781 thermal analyser.

prevented fusion of the crucibles to the thermocouples at high temperatures, whilst still allowing the thermocouples to sense the crucible temperature accurately. Crucibles of 5 mm diameter and 4 mm deep were used, made of quartz, alumina or platinum rhodium alloy depending on maximum temperature being used. The hangdown assembly is shown in figure 6.

Thermocouple connections were taken from the hangdown assembly using 0.026 mm diameter Pt or 13%Rh Pt wires to the external measuring circuits. The DTA signal was amplified by a low noise dc amplifier with a maximum sensitivity of 10 μV full scale. A cold reference junction consisting of a thermocouple mounted in, but electrically isolated from, an ice/water slush bath contained in a dewar flask was used in conjunction with the temperature measuring thermocouple.

The hangdown assembly was surrounded by a water cooled jacket for about two-thirds of its length. This and the design of the reaction chamber resulted in negligible buoyancy effects. The arrangement of crucibles within the furnace is shown in figures 5 and 6. Gases were admitted through a needle valve and rotameter from beneath the crucibles. Usual flow rates were between 25 and 75 $cm^3\ min^{-1}$. The gas flow rate was measured using a rotameter calibrated for air at atmospheric pressure, and a correction factor had be used for other gases as given in section 2.1.2. Calibration curves using alumina as sample and reference showed a buoyancy error of less than 0.1 mg over the range 20 to 1400 °C.

The furnace consisted of a platinum rhodium alloy bifilar winding on an alumina former. The reaction chamber was mounted within the furnace and the whole assembly was raised and lowered automatically to ensure constant

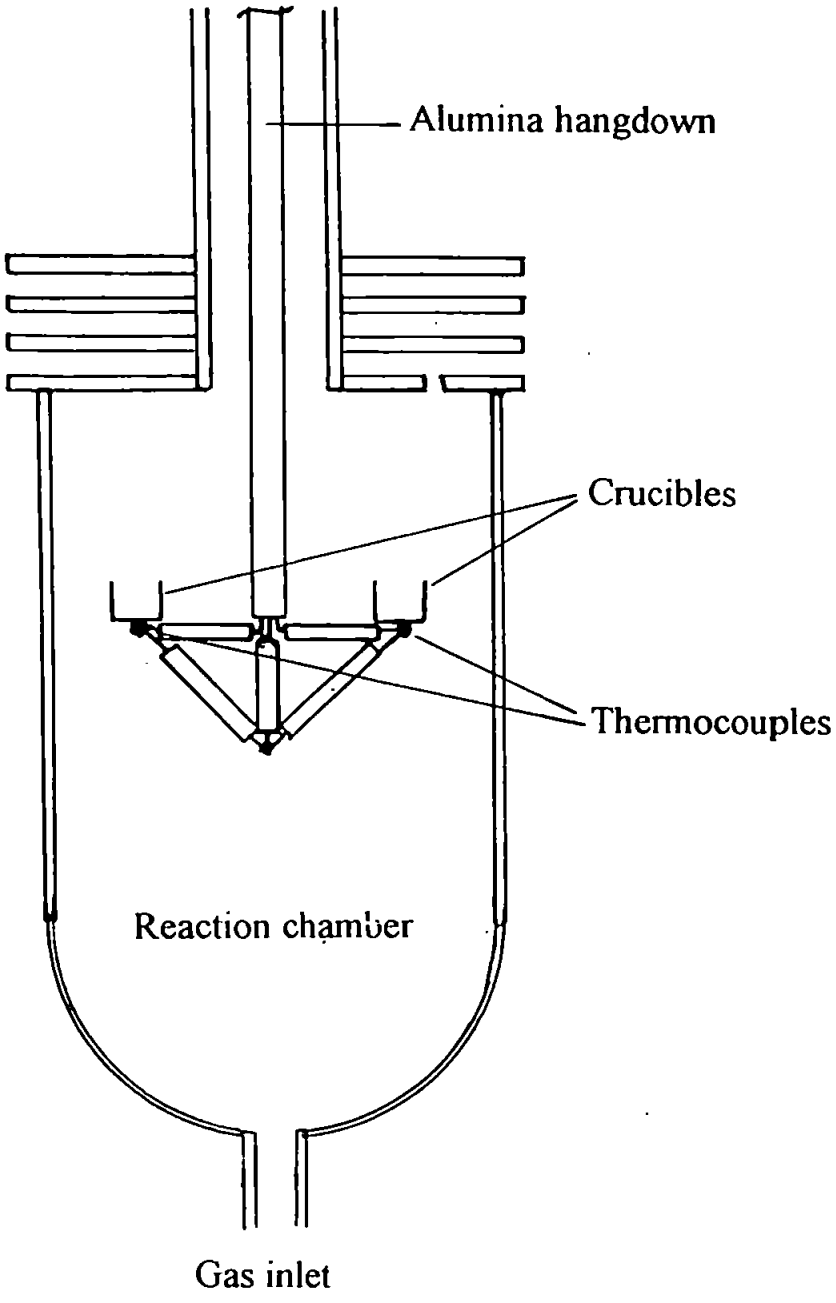

Figure 6
Schematic diagram of DTA hangdown assembly and reaction chamber.

positioning of the crucibles within the reaction chamber. The outer surface of the furnace was water cooled.

The calibration of the balance was checked, and adjusted if necessary, monthly (or if calibration error was suspected) against traceable standards according to the manufacturers instructions.

The furnace temperature was controlled by a temperature controller capable of heating rates of between 0.1 and 50.0 °C min^{-1}, although rates above 20 °C min^{-1} were not recommended as fast heating rates shorten the life of the furnace winding.

2.1.5 PROCEDURE

A suitable weight (normally 15 mg) of sample and alumina was weighed out into platinum crucibles. These crucibles were then positioned on the hangdown, the control unit was adjusted to display the sample weight and the span altered to give the desired weight change as full scale deflection on the chart recorder. The furnace was raised up around the sample hangdown and the cooling water switched on Once the furnace was in position the required gas flow was set up, usually 50 cm^3 min^{-1}, and the system purged for five minutes to displace air from the system, unless air was the desired atmosphere. The required heating regime was then initiated and the chart recorder started. In the case of isothermal oxidations, once the sample had equilibrated at the desired temperature, the flow of inert gas was stopped and the desired reactant gas allowed into the system, the point at which the gases were changed over being noted. Once the experiment was complete the furnace was switched off or programmed cooling was initiated and the system allowed to cool to room temperature before recovery of the samples.

2.1.6 TUBE FURNACE

A Griffin and George tube furnace capable of a maximum temperature of 1450 °C was modified by the removal of the original controller and temperature indicating circuits and the addition of a Stanton Redcroft Linear Temperature Programmer, model LVP-C, which had a maximum heating rate of 40 °C min^{-1}. The original auto-transformer was retained to step the output voltage of the programmer from 240 to the 270 V required for the furnace to reach its maximum temperature. This allowed the tube furnace temperature to be controlled with the same programs as the thermobalance. The furnace consisted of a firebrick lined box of internal dimensions 15 x 15 x 15 cm through which is passed a mullite or alumina tube of external diameter 30 mm. Positioned approximately 30 mm away from the tube and running parallel to it were four equally spaced silicon carbide heating elements which were connected electrically in series. The tube, 83 cm long, through the furnace extends some way either side of the furnace so that only the middle 15 cm of the tube is heated. Suitable amounts of sample in alumina boats were positioned within the hot zone of the tube before the heating program was started, or the boat was positioned in the hot zone once the tube had reached the desired temperature. Carbon dioxide, argon, nitrogen, air, oxygen or gas mixtures could be passed over the sample.

2.1.7 PROCEDURE

A suitable amount of sample was weighed out into an alumina boat, usually 1 g. Depending on the reactant gas, the sample would then either be placed into the preheated furnace or into the cold furnace and heated in an inert atmosphere before changing to the desired atmosphere once the required temperature had been reached. Once the sample had been heated for the desired length of time, the atmosphere was changed to an inert atmosphere such as nitrogen or argon. Gas flow rates of 1 dm^3 min^{-1} were normally used.

2.2 SURFACE AREA DETERMINATION

2.2.1 REVIEW AND INTRODUCTION

The reactivity of a solid towards gases is governed, inter alia, by its active surface area. Thus measurement of the specific surface area at different stages of the reaction may provide useful information concerning the reactivity of the solid.

When a finely dispersed solid is exposed to a gas or vapour at a defined pressure and temperature, the sample will begin to adsorb the gas or vapour until an equilibrium is established between the adsorbed gas or vapour and the surrounding non-adsorbed gas or vapour at the equilibrium pressure.

Adsorption takes place as a consequence of the force of attraction emanating from the solid. Because the atoms at the surface of the solid have no like atoms above the surface plane with which to form chemical bonds but are capable of forming a similar number of bonds as atoms in the bulk of the solid, they may attract fluid molecules in order to satisfy their bonding capacity. The two main types of adsorption forces are termed physical and chemical. In physical adsorption or "van der Waal's" adsorption the molecules are held by short-range, weak forces arising from permanent and induced dipoles, hence this process is reversible. In chemical adsorption or chemisorption the adsorbed molecules are held by covalent bonds. Electrostatic adsorption can also exist due to electrovalent forces. All these types of adsorption are exothermic and the mass adsorbed decreases with increased temperature as the increased energy in the system can overcome the adsorbent\adsorbate interaction.

The amount of gas adsorbed is a function of the solid adsorbent, the gas or vapour adsorbate, the temperature, T, of the system and the pressure, p, of the system.

i.e $X = f[p, T, \text{adsorbent, adsorbate}]$

where X is the amount of adsorbate adsorbed, usually expressed as grams of adsorbate per gram of adsorbent. When the adsorbate is below its critical temperature the form

$$X = f[(p/p_0), T, \text{adsorbent, adsorbate}]$$

is more useful, where p_0 is the saturated vapour pressure of the adsorbate at temperature T.

Freundlich (1909) proposed the following empirical equation to account for the adsorption isotherm

$$X = kc^n$$

where c is the concentration of adsorbate, k and n are constants (n>1). This equation does not take into account any saturation of the adsorbent surface. If the equation applies to a system, a plot of log X against log c gives a straight line of slope n and an intercept of log k.

Langmuir (1916) suggested that at a pressure p, an equilibrium exists between condensation and evaporation of gas molecules at the surface. The equation he proposed can be expressed as

$$\Theta = kp/(V + kp)$$

where Θ is the fraction of the surface covered with a unimolecular layer, k is a constant and V is a constant for the system.

There are two special situations that can arise:

a) when at high pressures the surface is completely covered, the amount of gas adsorbed is independant of pressure;

b) when Θ is small, the surface is partially covered and the amount of gas absorbed is proportional to pressure.
Between these limits the expression simplifies to the Freundlich equation.

Langmuir made the assumption that all sites on the surface of the adsorbent are the same and that interaction between adsorbed gas molecules does not occur. Systems in which these conditions apply are described as exhibiting "ideal adsorption" or "Langmuir adsorption". However, in reality there is often deviation from the ideal Langmuir isotherm. Deviations may arise due to the surface not being uniform or interactions between adsorbed gas molecules (i.e. a molecule already adsorbed may hinder or help the adsorption of a gas molecule at an adjoining site).

Adsorption of a gas onto a porous material often gives rise to hysteresis, i.e. the adsorption branch and the desorption branch of the isotherm differ. Observation of reproducible isotherm hysteresis can be associated with the type of porosity in the adsorbent.

The majority of adsorption isotherms resulting from physical adsorption may, for convenience, be grouped into one of five classes, illustrated in figure 7. These classes were originally proposed by Brunauer, Demming, Demming and Teller (BDDT) (1940) (now commonly known, incorrectly, as the Brunauer, Emmett and Teller (BET) (1938) classification). Type 4 shows a hysteresis loop where the solid lower line is the adsorption branch and the dotted upper line is the desorption branch. Types 2 and 4 are the most common types found in real systems, types 3 and 5 are relatively rare. Type 1 is typical of microporous materials. De Boer (1956) classified the relationship between hysteresis shape and pore geometry, distinguishing between fifteen idealised pore geometries.

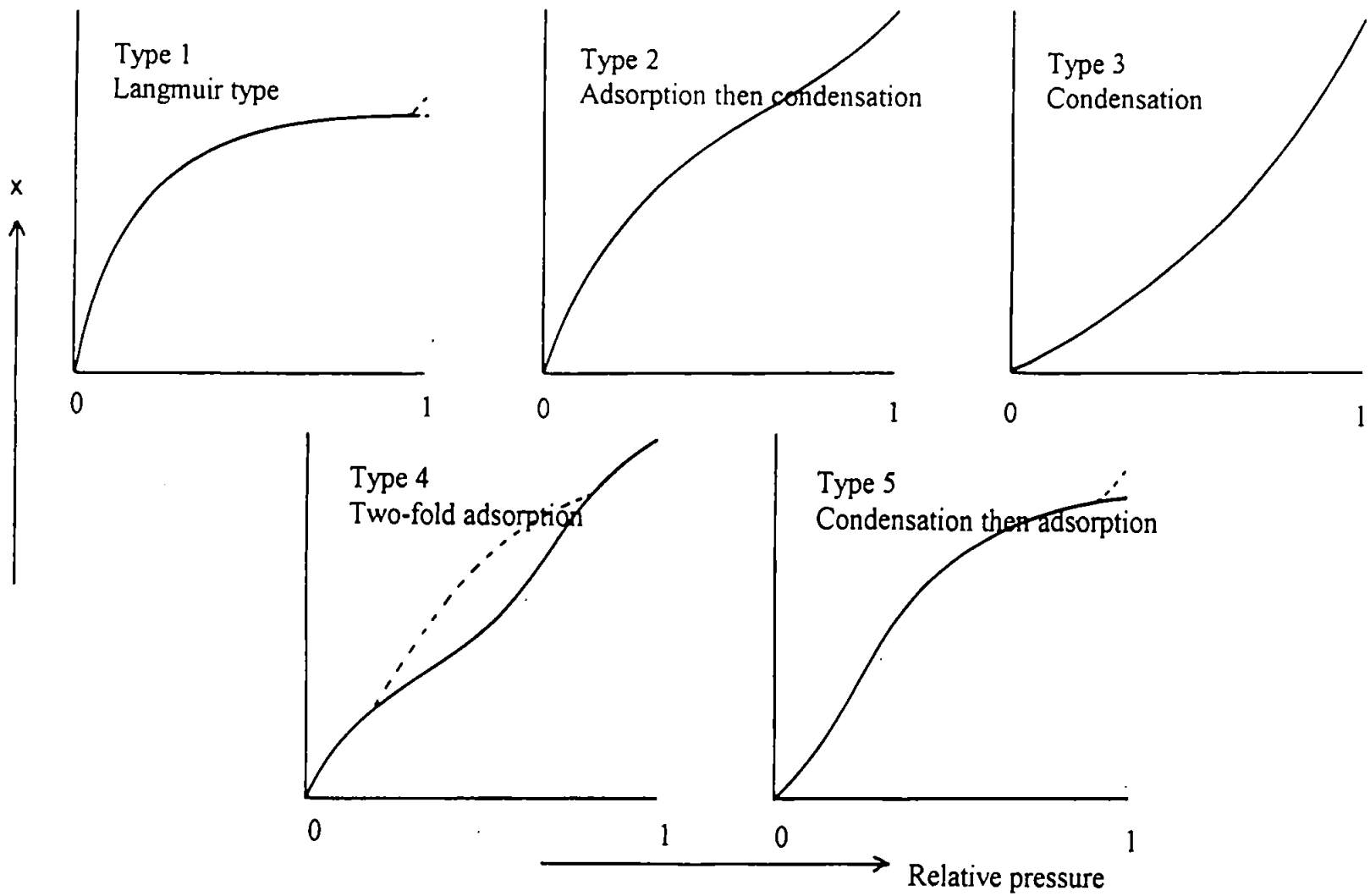

Figure 7
The five types of adsorption isotherm in the B.E.T. classification.

It is from these isotherms that the monolayer capacity of the adsorbent may be calculated by mathematical models based on physical models. The monolayer capacity, X_m, is defined as the quantity of adsorbate that will completely cover the adsorbent with a unimolecular layer. The specific surface, S (m^2g^{-1}), is directly proportional to the monolayer capacity, assuming that the molecules are close packed, and is given by the equation

$$S = (X_m N A_m / M) \times 10^{-20}$$

where N is Avogadro's constant, M is the relative molecular mass of the adsorbate and A_m is the area occupied by one molecule of the adsorbate (in square Angstroms) at the isotherm temperature. For this work A_m was taken to be 16.2 $Å^2$ for nitrogen at -196 °C. Gregg and Sing (1967) and Sutherland (1967) discuss the calculation of adsorbate cross-sectional areas from liquid density, critical constant data and other methods.

In characterising a solid by physical adsorption measurements, a mathematical model of the adsorption process has to be applied. Langmuir's original equation, which can be expressed as

$$X = X_m bp/(1+bp)$$

where b is an adsorption coefficient, X is the amount of adsorbate adsorbed per g of adsorbent at equilibrium pressure p, was based on a kinetic approach and a graph of p/X against p gives a linear graph of slope $1/X_m$. Langmuir's equation is only valid for type 1 isotherms and cannot be used successfully on non-porous or wide pore adsorbents due to multilayer formation and/or capillary condensation.

Brunauer, Emmett and Teller (1938) applied a statistical approach to localised multilayer adsorption (which, with some simplifying assumptions) allows for multilayer adsorption and condensation in pores. This has been widely and

successfully applied to isotherms of type 2 and 4. Their equation is a modification of Langmuir's equation. It takes the form

$$p/(V(p_o-p)) = 1/(V_m c) + ((c-1)/(V_m c)) \times p/p_o$$

where p_o is the saturated vapour pressure of the adsorbate at the temperature of the isotherm and V is the volume of gas adsorbed at pressure p, V_m is the volume of gas required to completely cover the surface of the adsorbent with a unimolecular layer of adsorbate and c is a constant equal to $\exp((E_1-E_2)/RT)$ where E_1 and E_2 are the heats of adsorption of the first and subsequent layers. In this work it is used in its modified form and utilizes weights of gas adsorbed rather than volume of gas adsorbed and takes the form

$$p/(X(p_o-p)) = 1/(X_m c) + ((c-1)/(X_m c)) \times p/p_o$$

A plot of $p/(X(p_o-p))$ against p/p_o gives a straight line graph of slope $(c-1)/(X_m c)$ and intercept of $1/(X_m c)$. The addition of these two values gives $1/X_m$ from which X_m and hence S can be calculated. The graph is, however, only linear over the range p/p_o from 0.0 to 0.3. Above this upper limit the formation of multilayers causes the plot to deviate. Deviation and discussion of the BET equation is given by Gregg (1961) and Lowell (1979).

Adsorption into wide pores can be treated by assuming that bulk condensation occurs in the pores, and is thus governed by the Kelvin equation. Hence the saturated vapour pressure, p, above a curved surface of a liquid in a capillary will be less than that of the open surface, p_o, and

$$\ln(p/p_o) = -(2\gamma v/rRT)\cos\theta$$

where γ is the surface tension of the liquid, v the molar volume, r the radius of the capillary and θ is the angle of contact between the solid and the liquid, which is often taken as zero (i.e. $\cos\theta = 1$).

In practice, a finite desorption step is considered, giving a method of calculating pore size distribution. For non-intersecting cylindrical pores the mean pore radius, r, is given by

$$r = 2V_p/S$$

where V_p is the total pore volume and S the surface area of the pores. This equation, however, fails to give a true value of r below a certain minimum as V_p approaches V_m. Pores are divided into three classes:

a) micro (pore radius less than 1 nm);

b) meso (pore radius in the range 1 to 25 nm);

c) macro (pore radius greater than 25 nm).

Cranston and Inkley (1957) proposed a method for the determination of pore structures and surface area using data determined from isothermal adsorption/desorption studies of materials with type 4 isotherms.

Dubinin (1960) suggested that with micro-porous adsorbents, adsorption results in volume filling of pores due to an adsorption force field in the entire volume of the pores rather than by layers as implied by the Langmuir and BET treatment. This is based on the approach of Polanyi (1914) which considered the force of adsorption as an intermolecular potential gradient. The adsorption potential at a point at or near the surface of the adsorbent is defined as the isothermal work done in bringing a molecule from the bulk gas to that point. Micropores are commensurate with the size of the adsorbate molecules and the adsorption must depend on the nature of the system as a whole. Dubinin's fundamental equation is defined as

$$X = X_o \exp(-A/E)^n$$

where $A = RT\ln(p_o/p)$, X_o is the mass of absorbed gas when all micropores are filled and X is the mass of gas adsorbed at a particular relative pressure, E is a characteristic free energy depending on the system and n is a small integer

with no physical meaning ascribed to it. When n = 2, the equation takes the form of the Dubinin-Radushkevich (D-R) equation

$$X = X_o \exp\{-B(T/\beta)^2 \log^2(p_o/p)\}$$

where B is a structural constant and β is an affinity constant that is dependant on the nature of the adsorbate and adsorbent.

If the adsorbent is considered to be composed of non-porous, non-aggregating spheres, from surface area determinations it is possible to make an estimate of the mean particle size. If 1 g of sample contains n spherical particles of radius r and density ρ then the surface area is given by

$$S = 4\pi r^2 n$$

and occupies a volume V given by

$$V = 1/\rho = 4\pi r^3 n/3$$

which when rearranged and substituted into the above equation gives

$$r = 3/(S\rho)$$

or the diameter, d, is given by

$$d = f/(S\rho)$$

where f = 6 for cubes or spheres, 4 for rods or cylinders and 2 for plates.

2.2.2 THE NITROGEN SORPTION BALANCE

The nitrogen sorption balance, constructed in 1974, is shown in plate 1. The balance is capable of determining surface areas within the range 0.2 to 1000 m^2g^{-1} using samples of approximately 0.25 g. At the heart of the system is a mark 2 micro-force balance manufactured by C.I. Electronics. This consists of a balance head of 1 g capacity enclosed within a glass housing connected to a control and display unit by an eight-way cable. Mounted on the balance arm (figure 8) is a shutter that is positioned between a light bulb and a pair of matched silicon photodetectors which form two arms of a Wheatstone Bridge. When the balance beam is at its equilibrium position, the

Plate 1
The nitrogen sorption balance.

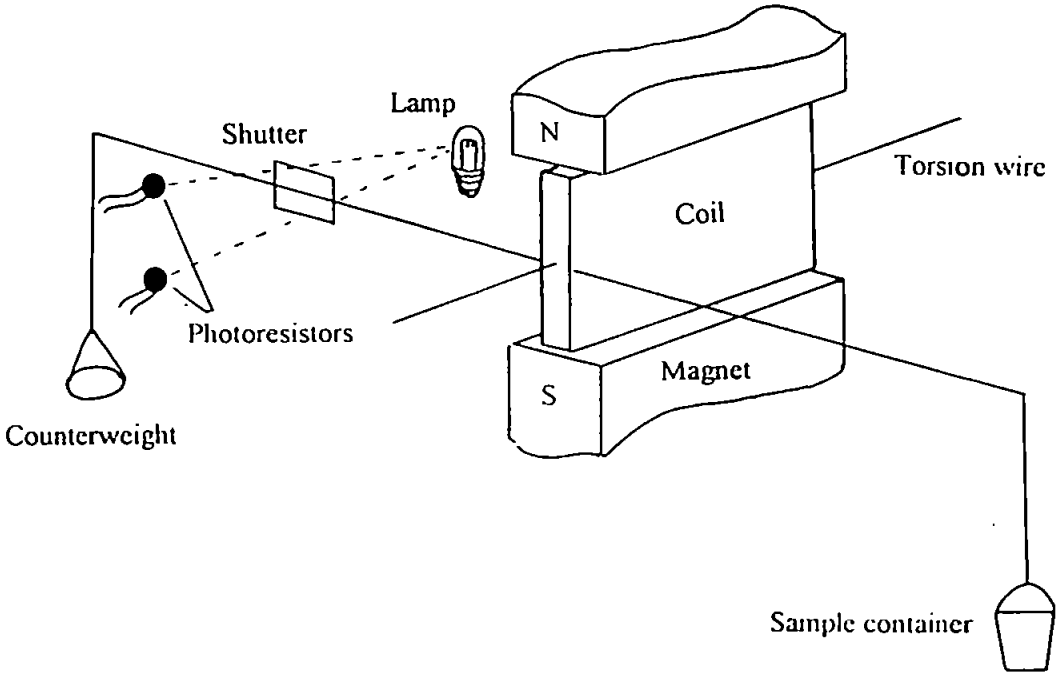

Figure 8
Schematic diagram of C.I. Electronics Microforce balance.

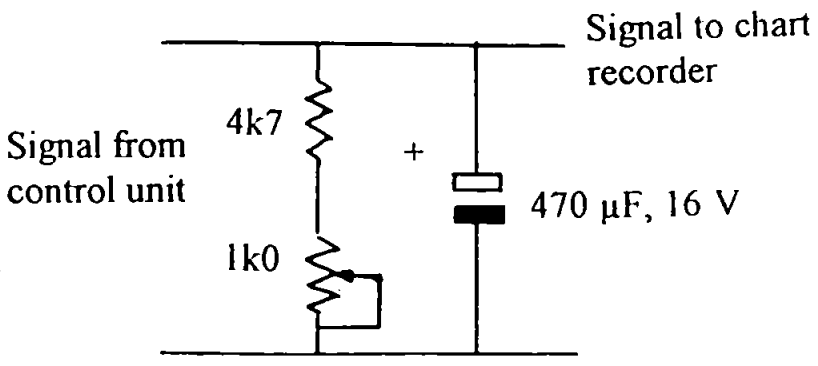

Figure 9
Chart recorder interface circuit.

photodetectors are obscured equally and the bridge circuit is balanced. When the balance beam is not at its equilibrium position one of the photodetectors is illuminated more than the other and thus the bridge circuit is not balanced causing a current to flow between the two arms. This current is amplified to drive a servo that brings the beam back to the equilibrium position. The electromagnetic force balances the torque produced by the sample. The current required to bring the balance beam back to the equilibrium position is proportional to the torque produced by the sample weight applied to the beam and is displayed on an analogue meter. For convenience the meter signal is also fed to a chart recorder using the circuit shown in figure 9. This ensures that the control unit is matched into a 5 kΩ load and the capacitor is included to reduce chart recorder noise without damping the signal unduly. The vacuum head has B34 glass fittings through which the sample and any counterweight may be suspended whilst maintaining an enclosed environment. A metal B24 fitting connects to the two stage rotary vacuum pump and the rest of the system. The vacuum head is designed to work down to pressures of 10^{-6} Torr (1.33×10^{-4} Pa). A two way tap allows the vacuum balance unit to be isolated, connected to either the cold trap and two stage rotary vacuum pump or connected to the doser. The doser, with a capacity of approximately 40 cm^3, is connected via taps to the vacuum head, the vacuum pump (for purging the system if it has been opened to atmosphere or if the adsorbant gas is to be changed) or to the nitrogen reservoir and nitrogen cylinder. Mercury manometers are used to determine the pressures of the vacuum line, vacuum head and nitrogen reservoir.

The control unit used with the balance head was a model 2C with ranges of 0-1 mg, 0-2.5 mg, 0-10 mg, 0-25 mg and 0-100 mg, the ranges being selected manually. Manual tare of up to 11 mg is possible on all ranges.

A second sorption balance was constructed in 1982, the design is similar to the older sorption balance except that a model 2B control unit is used with ranges 0-25 μg, 0-250 μg, 0-2.5 mg, 0-10 mg and 0-100 mg and a smaller doser of approximately 15 cm^3 was used. The lower ranges of this balance allowed surface areas to be determined within the range 0.05 to 1000 m^2g^{-1}. The model 2B and 2C control units are interchangeable. The use of the smaller doser allows CO_2 to be used as the adsorbate at -77 °C as well as nitrogen at -196 °C.

Due to the difference in densities of nitrogen gas at room temperature (20 °C) and -196 °C (1.165 and 4.430 mg cm^{-3} respectively),the Pyrex hangdown, Pyrex counterweights, sample container and sample, a buoyancy correction has to be applied to the weight readings. The buoyancy correction factor (BCF) that has to be subtracted from the weight indicated by the meter is given by

$$BCF = (p/p_{atmos}) \times \{C - [\rho_{N\text{-}196\,°C}((M_c/\rho_c) + (M_s/\rho_s))]\}$$

where p is the pressure of nitrogen at which the weight reading is noted, p_{atmos} is the atmospheric pressure, $\rho_{N\text{-}196\,°C}$ is the density of gaseous nitrogen at -196 °C, M_c is the mass of the sample container, ρ_c is the density of the sample container (2.7 gcm^{-3} for Al), M_s is the mass of sample, ρ_s is the density of the sample and C is a constant for the system given by

$$C = \{(M_{cw} \times \rho_{N\text{-}196\,°C}) + 0.5(M_h \times \rho_{N\text{-}196\,°C}) + 0.5(M_h \times \rho_{N20\,°C})\}/\rho_{py}$$

where M_{cw} is the mass of the counterweight, M_h is the mass of the hangdown, $\rho_{N20\,°C}$ is the density of nitrogen at 20 °C and ρ_{py} is the density of Pyrex (2.23 g cm^{-3}).

The balance was checked and calibrated weekly or as necessary according to the manufacturers instructions using certified weight traceable to national standards.

2.2.3 PROCEDURE

0.25 g of the sample was placed in an aluminium foil bucket and suspended from the balance beam by a fine Pyrex fibre 27 cm long. This ensured that the sample was suspended at least 15 cm below the level of the coolant liquid. The coolant used was liquid nitrogen in a dewar flask which, as previously determined by Glasson (1956) maintains the liquid temperature within ± 0.1 °C. It has been found in practice that the sample temperature is about 1 °C warmer, as determined by Glasson and Linstead-Smith (1973) using separate thermocouples. For CO_2 adsorption isotherms a solid CO_2/ether slush bath is used as the coolant.

A Pyrex limb is placed around the sample and the system evacuated using a two stage rotary pump capable of reducing the pressure to 10^{-3} Torr (0.2 Pa). A cold trap is used to aid the outgassing of the sample and to prevent any corrosive vapours or moisture entering the pump. A small oven could be used to aid the outgassing by gently warming the sample. Once the sample had outgassed and reached a constant weight the true sample weight was noted, i.e. less the adsorbed water and volatiles, and the balance tared to a convenient starting point. The dewar containing the coolant was raised around the sample limb and a pressure of 30 - 50 Torr (4 - 6.7 kPa) of nitrogen was introduced into the system and allowed to attain equilibrium after which the sample pressure and weight gain were noted before a second dose of nitrogen was admitted to the system. Six or seven readings were taken in the BET range i.e. up to a relative pressure of 0.3, thereafter pressures of 70 - 80 Torr (9.3 - 10.7 kPa) were admitted until a relative pressure (p/p_o) of 0.95 had been attained.

Desorption points were determined by pumping out the system in similar pressure steps.

Weight readings were corrected for buoyancy effects of the sample, container and Pyrex hangdown and counterweight.

2.3 X-RAY DIFFRACTION

2.3.1 INTRODUCTION

Most crystalline solids consist of a three-dimensional array of atoms forming regularly repeating units. The individual crystallites may be very small. Points within the structure that have identical surroundings are known as lattice points, and a collection of lattice points form a crystal lattice. The unit cell is formed by the joining of a lattice point with its adjacent points. The unit cell is the smallest convenient repeating unit of the structure and may be defined in a number of ways, characterised by three vectors, not in one plane, that are the edges of a parallelepiped of length a, b and c and at angles α, β and γ from each other. Some cells have more complex structures with lattice points at the centre of the cell (body centred) or on the cell face (face centred).

Crystal lattices may be grouped in to seven systems as indicated by Kelly and Groves (1973) and shown in table 1. Symmetry operations of reflection, rotation and inversion gives rise to 32 point groups and when all symmetry elements are taken into account, e.g. screw axes, glide planes etc., 230 space groups are obtained in three dimensions.

Sets of parallel planes may be drawn through the lattice points. Each set of planes can be completely described by three integers ($\underline{h}$, $\underline{k}$, $\underline{l}$), known as the Miller indices, corresponding to the three axes ($\underline{a}$, $\underline{b}$, $\underline{c}$) respectively. Index $\underline{h}$ is the reciprocal of the fractional value of the intercept made by the set of planes on the $\underline{a}$ axis etc. The lattice type can be deduced from observation of sets of h, k, l reflections that are systematically absent.

As the dimensions of the crystal lattice are of the same order of magnitude as the wavelength of x-rays, the lattice can behave as a three dimensional diffraction grating, and diffraction is observed governed by Bragg's law:

Crystal Class	Conditions limiting cell dimensions		Minimum symmetry
Cubic	$a = b = c$	$\alpha = \beta = \gamma = 90^o$	Four three-fold axes
Trigonal	$a = b = c$	$\alpha = \beta = \gamma \neq 90^o$	One three-fold axis
Tetragonal	$a = b \neq c$	$\alpha = \beta = \gamma = 90^o$	One four-fold axis
Hexagonal	$a = b \neq c$	$\alpha = \beta = 90^o, \gamma = 120^o$	One six-fold axis
Orthorhombic	$a \neq b \neq c$	$\alpha = \beta = \gamma = 90^o$	Two perpendicular two-fold axes or two perpendicular planes of symmetry
Monoclinic	$a \neq b \neq c$	$\alpha = \beta = 90^o, \gamma \neq 90^o$	One two-fold axis or one plane of symmetry
Triclinic	$a \neq b \neq c$	$\alpha \neq \beta \neq \gamma \neq 90^o$	None

Table 1

Classification of crystal systems, based on characteristic symmetry

$$n\lambda = 2d \sin\theta$$

where λ is the wavelength of the x-rays, n is the diffraction order (usually 1), d is the interplanar spacing and θ is the angle of diffraction. d is related to the cell dimension by the Miller indices.

With powder diffractometry the small crystalline particles are in random orientation and produce reflections from those planes that happen to be at the correct angle θ to the incident x-ray beam.

The intensity and distribution of the diffracted beams with respect to the Bragg angle is characteristic of a particular crystalline structure and may be used to identify the component phases present.

Amorphous samples, which do not have a regular repeating structure, do not produce a diffraction pattern and therefore x-ray diffraction cannot be used to identify these types of materials.

Diffraction patterns for most compounds are listed in the Joint Committee for Powder Diffraction Standards file, JCPDS 1967 et seq., which incorporates the older American Society for Testing and Materials (ASTM) file and gives d-spacings, intensities and other data on the crystalline material.

The width of a peak in a diffraction pattern is affected by a number of factors including the finite width of the entrance slit of the detector, the wavelength spectrum of the x-rays, distribution of particle sizes and lattice strain within the crystallites. If the dimensions of the crystallites in a specimen fall below about 100 nm, appreciable broadening of the diffraction lines will result. The mean crystallite dimension, D, normal to the diffraction planes is related to the broadening, β, by the Scherrer equation,

$$D = K\lambda/(\beta\cos\theta)$$

where K is the Scherrer constant. The value of K is dependant on the method by which β is measured (integral breadth or breadth at half-maximum intensity). The size and shape distribution of the crystallites also affects the value of K. Klug and Alexander (1954) recommended that K should always take the value of 1, to provide an easy comparison between published results. The mean lattice distortion or strain, η, will also give rise to broadening of the diffraction pattern due to variations in the dimensions of the unit cell. The mean lattice strain is related to line broadening by the equation

$$\eta = \beta\cot\theta.$$

The strain distribution will affect the shape of the diffraction pattern. Because the size and shape distribution and lattice strain are not always known, this method cannot be used to accurately determine the crystallite size but may be used to compare a series of related samples.

Further theory is given by Stout and Jensen (1968) and Lipson and Steeple (1970).

2.3.2 X-RAY GENERATOR

A Philips PW1729 x-ray generator was used fitted with a Philips X-ray tube with a copper target. Other targets may be used. The x-rays produced were filtered with a nickel filter to remove the K_β component before entering, via a collimator and slits, a Philips PW1771/00 powder diffractometer.

The signal output was recorded using a Philips PM8203A chart recorder and also processed by a BBC microcomputer.

2.3.3 PROCEDURE

A sample holder was prepared by sticking self adhesive tape (Sellotape) across the back of the frame. Powdered sample was spread across the exposed adhesive surface of the tape, any surplus sample being gently shaken off before the sample holder was positioned inside the diffractometer and the covers positioned on the diffractometer. The anode accelerating voltage and current were set according to the manufacturers instructions for the target employed.

Under microprocessor control the x-ray shutter was opened and the diffractometer and chart recorder started.

2.4 ELECTRON MICROSCOPY

2.4.1 INTRODUCTION

The resolving power of a microscope depends largely on the wavelength of the radiation employed, which for an optical microscope limits the resolution to between 200-300 nm. Optical microscopy can reveal surface defects, grain boundaries and gross morphology of solids, but with the advent of electron microscopy greater detail became possible.

The three different arrangements employed in optical microscopy, transmission electron microscopy (TEM) and scanning electron microscopy (SEM) are shown in figure 10.

The basis of electron microscopy rests on the wave-particle duality of electrons, as expressed by the de Broglie equation

$$\lambda = h/(m_e v)$$

where m_e is the mass of the electron, v its velocity, h is Planck's constant and λ is the associated wavelength of the electron.

An electron accelerated through a potential difference V volts gains eV energy, where e is the charge on the electron. This is equivalent to a gain in kinetic energy of $(m_e v^2)/2$ thus

$$m_e v = (2eV)^{1/2}$$

and hence the wavelength associated with the accelerated voltage can be calculated. Due to the high electron velocities attained a relativistic correction has to be made when accelerating voltages in excess of 100 kV are used. Under these conditions the mass of the electron, m_e, should be replaced by the value $m_e((1-v^2)/c^2)^{-1/2}$ where c is the speed of light, and hence

$$\lambda = h/\{[(2m_e((1-(Ve/m_e))/c^2)^{-1/2})Ve]^{1/2}\}.$$

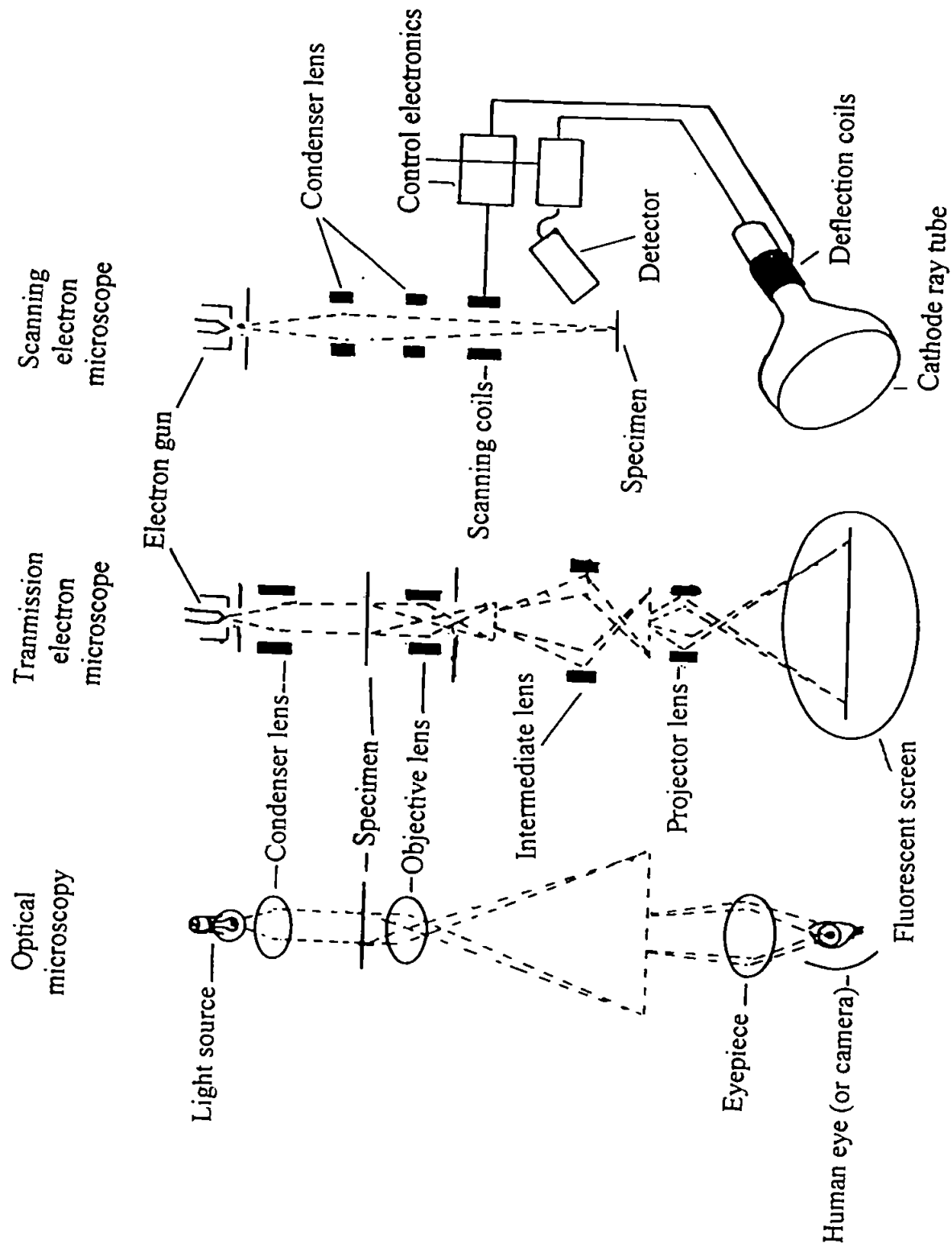

Figure 10
Schematic diagram of light microscope, transmission electron microscope and scanning electron microscope.

This equation may be simplified by the insertion of appropriate constants to yield the equation

$$\lambda = 1.5/(V(1 + 10^{-6}V))^{1/2}$$

The wavelength of electrons accelerated through 80 kV is 0.0043 nm or 4.3 pm, so that by the use of such a beam of electrons and a thin sample the theoretical resolving power of the transmission electron microscope is 1 pm. In practice the theoretical resolving limit is not attained due to aberrations caused by limitations of the lens design and manufacture, material impurity and contamination in the microscope column.

Unavoidable interactions between the electron beam and the sample limit the thickness of the sample to about 200 nm if internal detail is to be observed. The size of the sample chamber is the only limitation on the size of sample that can be observed with the scanning electron microscope. The range of magnifications overlap those of the optical microscope and the transmission electron microscope with a maximum resolution of about 20 nm. Further principles and applications are described by Goldstein et al (1981).

In scanning electron microscopy the area of the sample to be examined is irradiated with a fine beam of electrons which may be kept static or swept over an area of the sample. The electrons striking the surface of the specimen cause secondary electrons, back scattered electrons, Auger electrons, x-rays and photons of various energies to be emitted. The secondary and back scattered electrons vary as the beam is swept across the surface of the specimen as a result of the surface topography. The secondary electrons are detected and electronically processed to form an image on a cathode ray tube. As the microscope has a large depth of field the image has a three dimensional appearance with detailed surface relief. Because the secondary electrons originate from a small volume near the electron beam, the use of a very finely

focused beam results in high resolution. The depth to which the electron beam penetrates the sample is dependant on the accelerating voltage and the density of the sample. For samples with densities in the range 5 to 10 g cm^{-3} and an accelerating voltage of 20 kV, the electron beam penetrates between 1 and 2 μm. The diameter of the electron beam is dependant on the magnification selected and the accelerating voltage.

2.4.2 THE JOEL JSM-T20 SCANNING ELECTRON MICROSCOPE

The JSM-T20 scanning electron microscope was developed as an easy to use and maintain instrument with a resolution of 20 nm, and magnifications of 35x to 10,000x in 16 selectable steps. Both secondary electron image and backscattered electron images can be selected. A joystick is used to select the area irradiated by the electron beam, and hence the area observed, by small amounts, larger shifts can be obtained by mechanically altering the position of the sample within the microscope chamber. The image is observed on a 22.8 cm (9 inch) cathode ray tube. A camera can be positioned over the screen and the image photographed, during which the image is made up of more rasters than during the normal viewing mode so that a higher resolution is obtained on film.

The electron "optic" system consists of an electron gun with an accelerating voltage of 19 kV and a three stage lens system comprising two condensers and one objective.

The three modes of operation are controlled from the console which are wave-form for focusing and filament adjustment, Y modulated image or secondary electron image. Scanning speed, picture size, astigmatism, contrast and brightness are also controlled from the console.

A schematic diagram of the system is shown in figure 10. The beam of electrons is focused into a fine beam by the three lenses which is then made to scan the image by being electromagnetically deflected by the double deflection coils which scan at the same rate as the deflection coils of the cathode ray tube. The whole system is evacuated by a rotary pump and an oil diffusion pump until a pressure of 10^{-5} Torr (1.3 mPa) or lower is achieved. The secondary electrons are detected by a scintillation detector and photomultiplier, amplified and displayed as an image. Magnification is determined by the ratio of image size to scanned area and the resolution of the instrument can not be less than the diameter of the electron beam.

2.4.3 PROCEDURE

Samples were attached to aluminium or brass stubs with double sided adhesive tape, any surplus material being gently shaken off. The sample and mounting stub were then coated with gold to a thickness of 12 nm in a Polaron E5100 SEM coating unit, this ensured that when in the microscope the sample would conduct electricity and prevent the build up of charge on the sample that would otherwise repel the electron beam. The prepared stubs were then placed on the microscope stage and a grub screw tightened to prevent the stub moving within the stage or falling out. The stage was then positioned within the sample chamber, ensuring that the "O" rings made a good seal against the vacuum chamber, and the system evacuated. Interlocks prevented the filament being switched on until the pressure had been pumped to a sufficiently low pressure. The desired magnification and area of sample were selected, the sample moved within the chamber by a mechanical link. The image was focused, and the brightness and contrast adjusted to give the optimum image which if desired was then photographed. A scale bar was superimposed on the screen for determination of final magnification once the prints were made from the photograph negative.

The system had to be vented to atmosphere before the sample could be removed from the microscope.

2.5 PRODUCTS USED

In this work all nitrides and carbides were commercially available products of manufacturer's stated purity as listed below:

Manufactured and supplied by Alfa Inorganics:

titanium nitride	99 % (metal basis)

Manufactured by Ventron and supplied by Alfa Inoganics:

titanium carbide	99 %
zirconium carbide	88.2 % Zr, 11.3 % C
vanadium carbide	81.5 % V, 18.3 % C
niobium carbide	99+ %
iron nitride	mixed Fe_2N and Fe_4N
tantalum carbide	6.3 % C

Manufactured and supplied by Johnson Matthey:

zirconium nitride	99 %
vanadium nitride	98.5 %
chromium nitride	99.8 % (metal basis)
manganese carbide	mixed Mn_3C and Mn_5C_2

Supplied by Aldrich:

chromium carbide	no stated purity

All compounds were used as received.

Gases (Ar, N_2, CO_2 and air) were supplied by Air Products (South West Industrial Gases) and stated as being 99.9 % purity. All gases were passed through self-indicating molecular sieves to reduce hydrocarbon content to less

than 0.1 ppm and water to less than 0.1 ppm. Gases, other than air, were also passed through a molecular sieve to reduce oxygen to less than 0.1 ppm.

CHAPTER 3

RESULTS OF OXIDATIONS IN AIR

3.1 INTRODUCTION

Isothermal and dynamic thermogravimetric studies were made using either a Stanton Redcroft STA 781 Thermal Analyzer with 15 mg samples and gas flow rates of 50 cm^3 min^{-1} or a Stanton Redcroft Massflow Balance with samples of between 100 and 200 mg and gas flow rates of 300 cm^3 min^{-1}. Samples to be studied isothermally were heated to the required temperature under an inert atmosphere of either argon or nitrogen. Once the sample temperature had stabilized the reactant gas was admitted to the system.

From the TG curves, initial rate ($d\alpha/dt$) values were measured either within $\alpha = 0.05$ to 0.4 or within t = 5 to 15 minutes depending on the nature of the reaction, i.e. measurements were taken during the initial linear part of the reaction curve. For both Arrhenius plots and Kissinger plots, slope values and error limits were determined using the "Maths Powergraph" program running on a BBC microcomputer.

Larger samples for x-ray studies, BET studies and electron microscopy were heated and oxidised under similar conditions in a tube furnace or in an open furnace preheated to the required temperature.

All melting point temperatures and sample densities are quoted from Alfa (Johnson Matthey) Catalogue (1993), CRC Handbook of Chemistry and Physics 75th edition (1994), or from the appropriate JCPDS file card.

3.2 OXIDATION OF TITANIUM NITRIDE AND CARBIDE IN AIR

Figure 11 shows the results of dynamic oxidation of 15 mg samples of titanium nitride, in flowing air (50 cm^3 min^{-1}) at atmospheric pressure, at various heating rates. This shows that oxidation began at 500 °C at low heating rates. The final weight gain (29.1 wt-%) was consistent with that expected for TiN being oxidised to the dioxide TiO_2.

X-ray diffraction studies confirmed the starting material as cubic TiN (a = 4.24 Å, JCPDS card 6-0642) and the dioxide TiO_2 (rutile) as the product (tetragonal, a = 4.5933, c = 2.9592 Å, JCPDS card 21-1276). There was no evidence from the x-ray studies of the lower nitride Ti_2N being present in the starting material. The x-ray diffraction patterns were determined for the nitride as supplied and oxidation products prepared by oxidising 1 g samples of the nitride for various times at a heating rate of 10 °C min^{-1}. From these x-ray studies there was no evidence of the lower oxides TiO or Ti_2O_3 being formed at any stage of the oxidations.

Isothermal studies (figure 12) for the oxidation of TiN showed that at 475 °C only 8 % of the starting material had been oxidised after 2 hours ($\alpha = 0.08$) but at 755 °C the reaction was complete within 2 hours ($\alpha = 1$) and at 900 °C the reaction was complete within 30 minutes. From the Arrhenius plot (figure 13) derived from these isothermal TG curves (table 2) the activation energy was calculated to be 62.7 ± 3 kJ mol^{-1}. Further isothermal studies showed that alteration of the gas flow rate had no noticeable effect on the reaction except at very low flow rates (< 5 cm^3 min^{-1}). During isothermal oxidation studies performed with a static atmosphere, the reaction was impeded due to the localised starvation of oxygen used in the reaction and a build up of gaseous products in the reaction chamber.

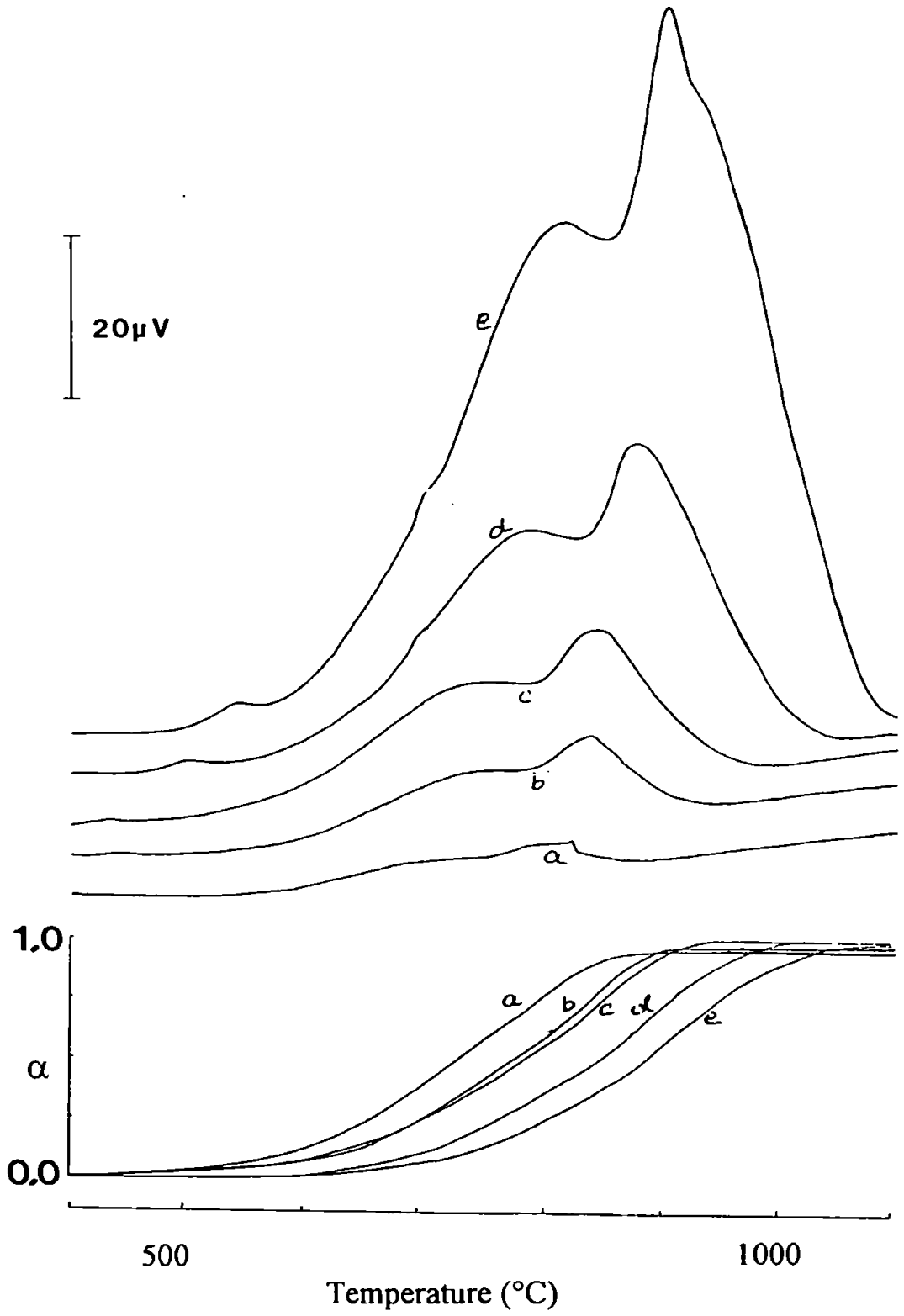

Figure 11

DTA curves (upper) and TG curves (lower) for oxidation of titanium nitride in flowing air (50 ml min^{-1}) heated at a) 1 °C min^{-1}, b) 2.5 °C min^{-1}, c) 5 °C min^{-1}, d) 10 °C min^{-1}, e) 25 °C min^{-1} to 1100 °C.

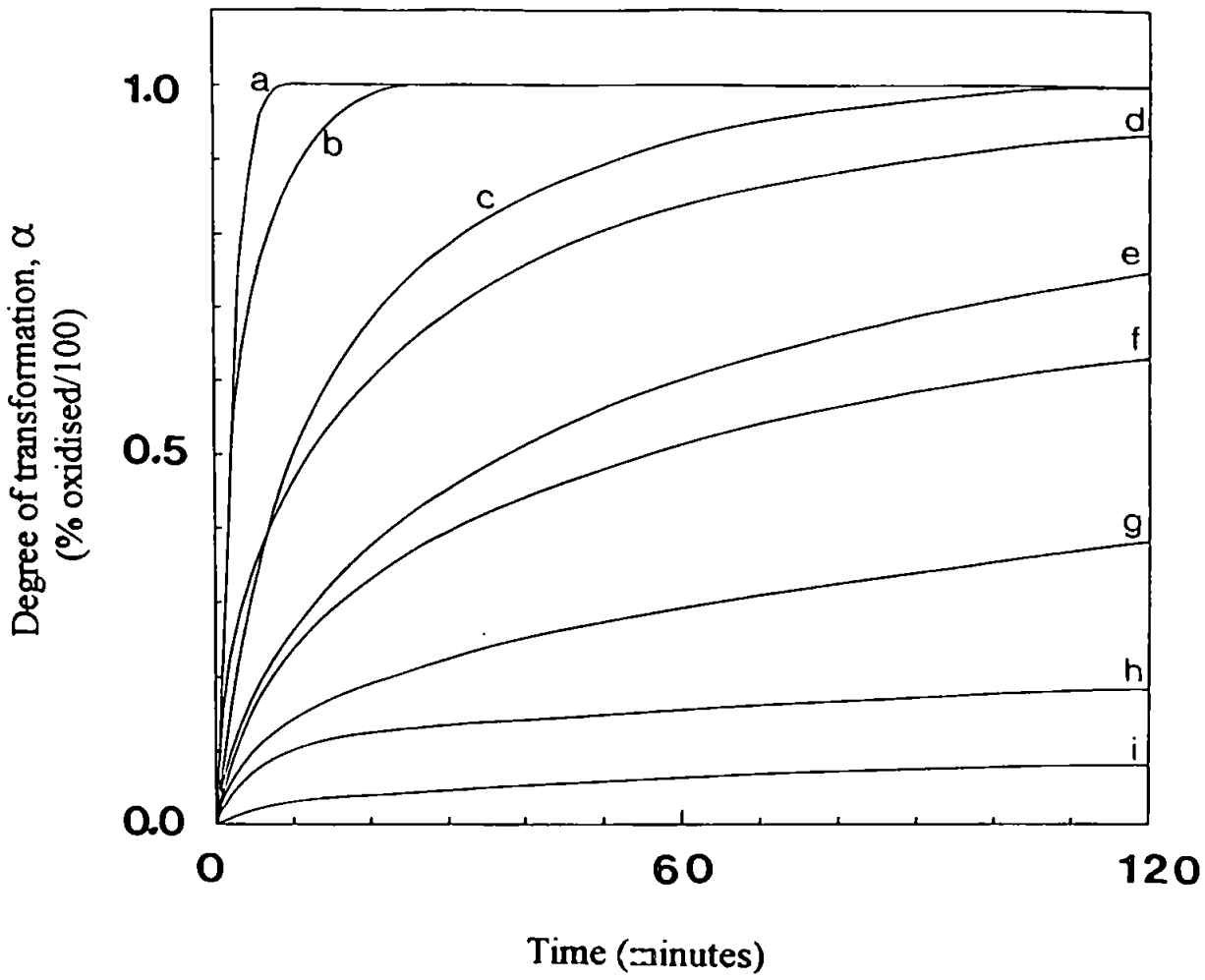

Figure 12
Isothermal TG curves for the oxidation of titanium nitride in static air (*) and flowing air (50 ml min^{-1}) at a) 1000 °C*, b) 900 °C*, c) 755 °C, d) 800 °C*, e) 718 °C*, f) 650 °C, g) 615 °C, h) 512 °C, i) 475 °C.

Temperature, T		dα/dt	ln(dα/dt)	1/T
°C	K	x 10^{-3} sec^{-1}		x 10^{-4} K^{-1}
1000	1273	3.750	-5.59	7.85
900	1173	2.500	-5.99	8.52
800	1073	1.667	-6.40	9.32
755	1028	1.000	-6.91	9.73
718	991	0.556	-7.50	10.09
650	923	0.467	-7.67	10.83
615	888	0.500	-7.60	11.26
525	791	0.067	-9.61	12.53

Arrhenius plot
Gradient of slope = -80800 K
Correlation coefficient = -0.96

Table 2
Isothermal oxidation of titanium nitride in air

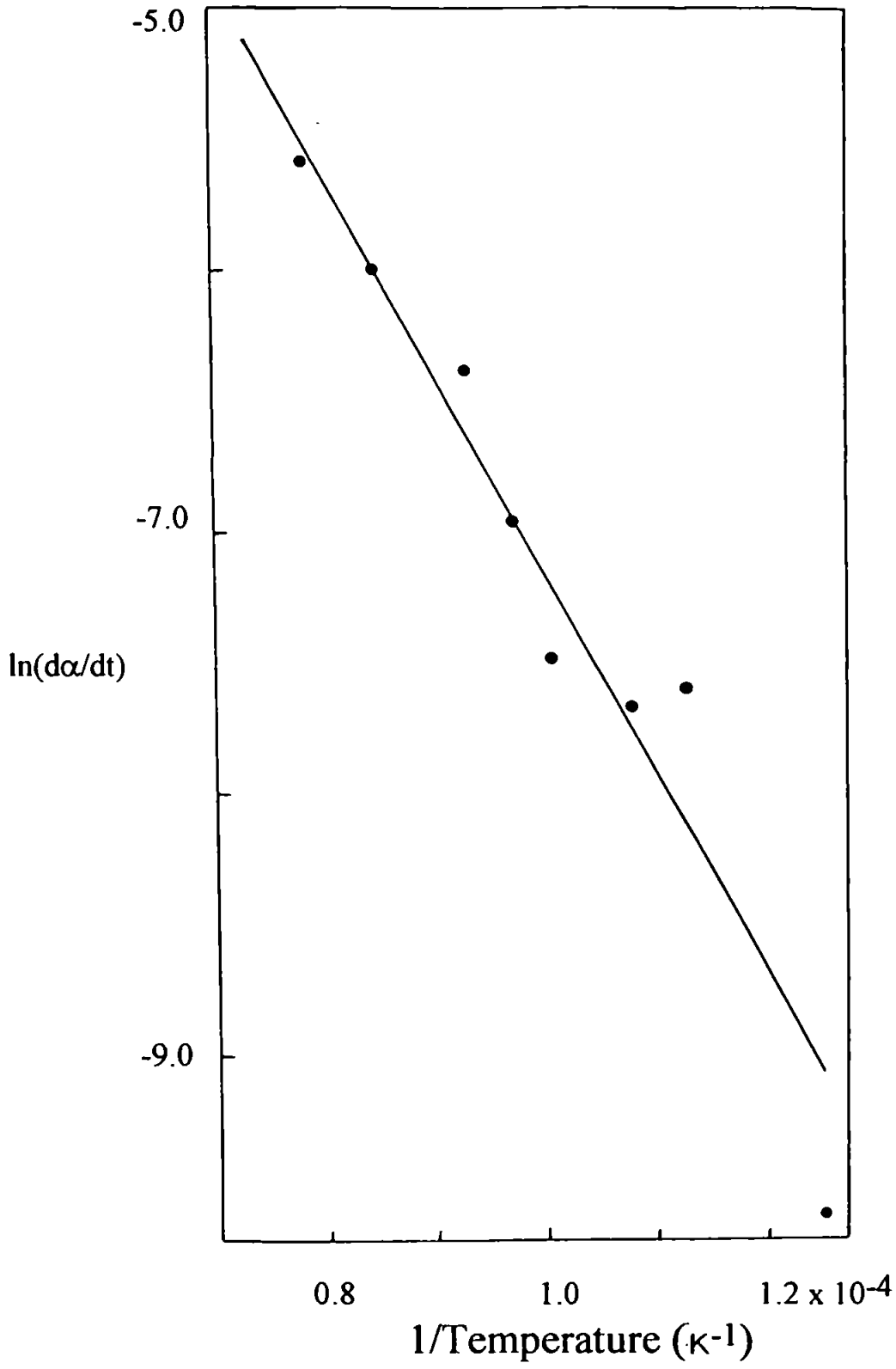

Figure 13
Arrhenius plot for the oxidation of titanium nitride in air.

The kinetic plots for this reaction (figure 14) show that the kinetics are indeterminate. Above 650 °C, the two-thirds order plots are initially linear indicating that the reaction occurred at the surface of a sphere of diminishing size. Since the melting point of titanium nitride is 2930 °C, sintering of the initial material by surface diffusion may occur at temperatures above 790 °C. Similarly as the melting point of the oxide is 1840 °C, sintering of the product may occur at temperatures above 430 °C by surface diffusion and above 780 °C by crystal lattice diffusion. As the reaction proceeds, the two-thirds order plots deviate from the expected straight line indicating that the oxide product hindered further oxidation. However, the half order kinetic plots are not linear, indicating that the further reaction was not controlled purely by the diffusion of gas through the oxide product. The kinetic plots for 650 °C indicate that the reaction followed half order kinetics indicating that the reaction is controlled by the diffusion of gas to the reaction site.

Increasing the heating rate had the expected effect of raising the onset temperature, and moving the associated exothermal DTA peak to higher temperatures (figure 11). At higher heating rates (>10 °C min^{-1}) the exothermic DTA peak became asymmetrical in shape with a shoulder forming on the high temperature side of the main peak. From the DTA peak position a Kissinger plot was obtained (table 3 and figure 15). This Kissinger plot shows two distinct regions. At lower heating rates the plot is linear but at higher heating rates the data points deviate (indicated by the broken line) from the initial slope. When the DTA maxima temperature was extrapolated to take account of the shoulder, the data points deduced continued the linear line. The activation energy determined by the Kissinger method was calculated to be 330 ± 12 kJ mol^{-1}. This value is considerably higher than that obtained from the isothermal studies already presented in this work and those obtained by Lefort et al (1977) of 180 kJ mol^{-1} for powdered $TiN_{0.95}$, Lefort et al (1978)

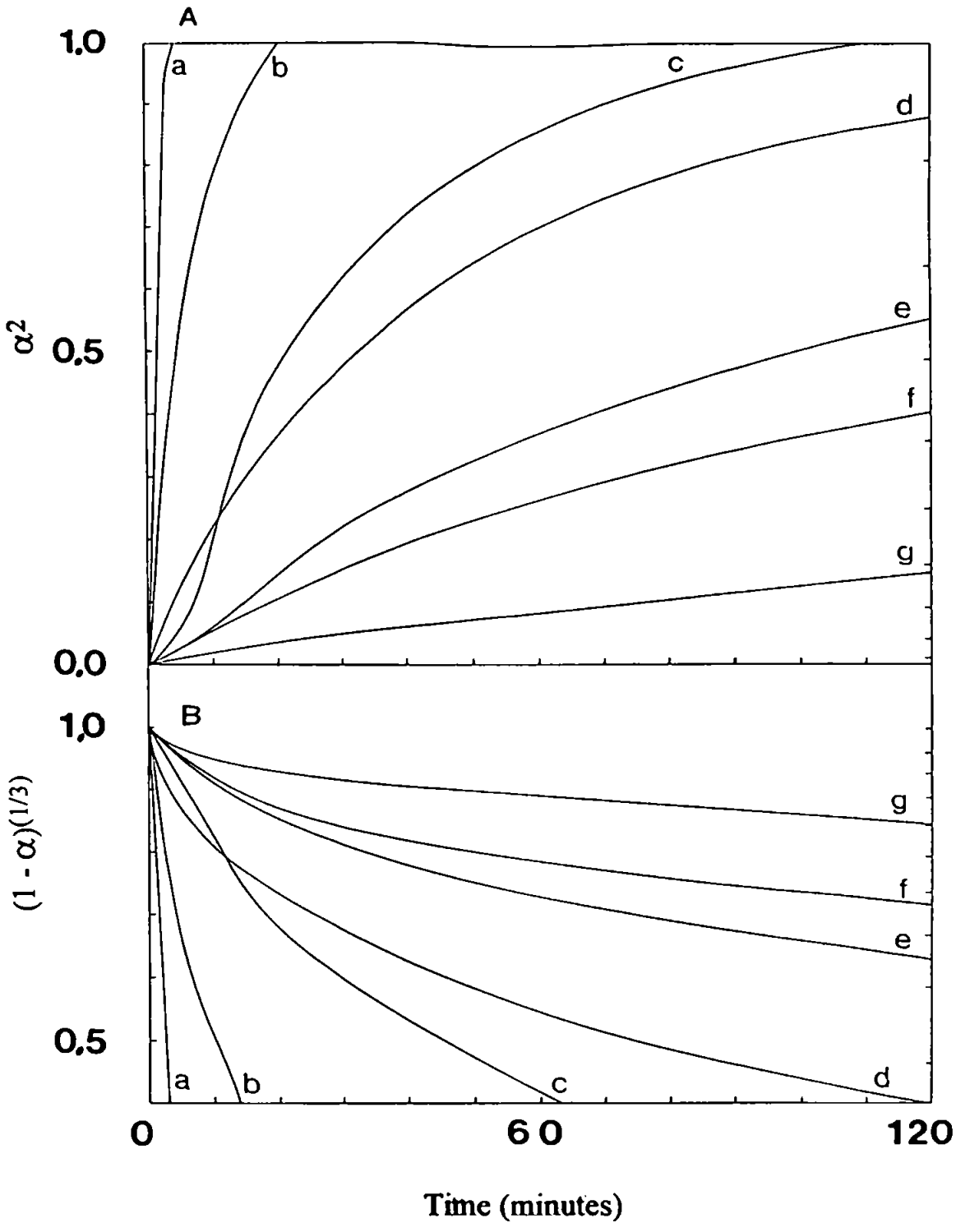

Figure 14
Half order (A) and two-thirds order (B) kinetic plots for the isothermal oxidation of titanium nitride in air at a) 1000 °C*, b) 900 °C*, c) 755 °C, d) 800 °C*, e) 700 °C, f) 718 °C*, g) 650 °C. (* static air)

Heating rate, Φ K min^{-1}	DTA peak, T K	$\ln(\Phi/T^2)$	1/T x 10^{-4} K^{-1}
1	1077	-13.96	9.28
2	1101	-13.32	9.08
2.5	1101 (a)	-13.09	9.08
	1105 (b)	-13.10	9.05
4	1117	-12.65	8.95
5	1130	-12.45	8.85
6	1133	-12.27	8.83
8	1135	-11.99	8.81
10	1133 (a)	-11.76	8.83
	1133 (a)	-11.58	8.83
	1149 (b)	-11.61	8.70
15	1149 (a)	-11.39	8.70
	1153 (b)	-11.39	8.67
20	1157 (a)	-11.11	8.64
	1162 (b)	-11.12	8.61
25	1178 (a)	-10.92	8.49
	1186 (b)	-10.94	8.43

(a) actual DTA maxima
(b) extrapolated peak maxima

Kissinger plot
Gradient of slope = -39500 K
Correlation coefficient = -0.99

Table 3
Effect of heating rate on the oxidation of titanium nitride in air

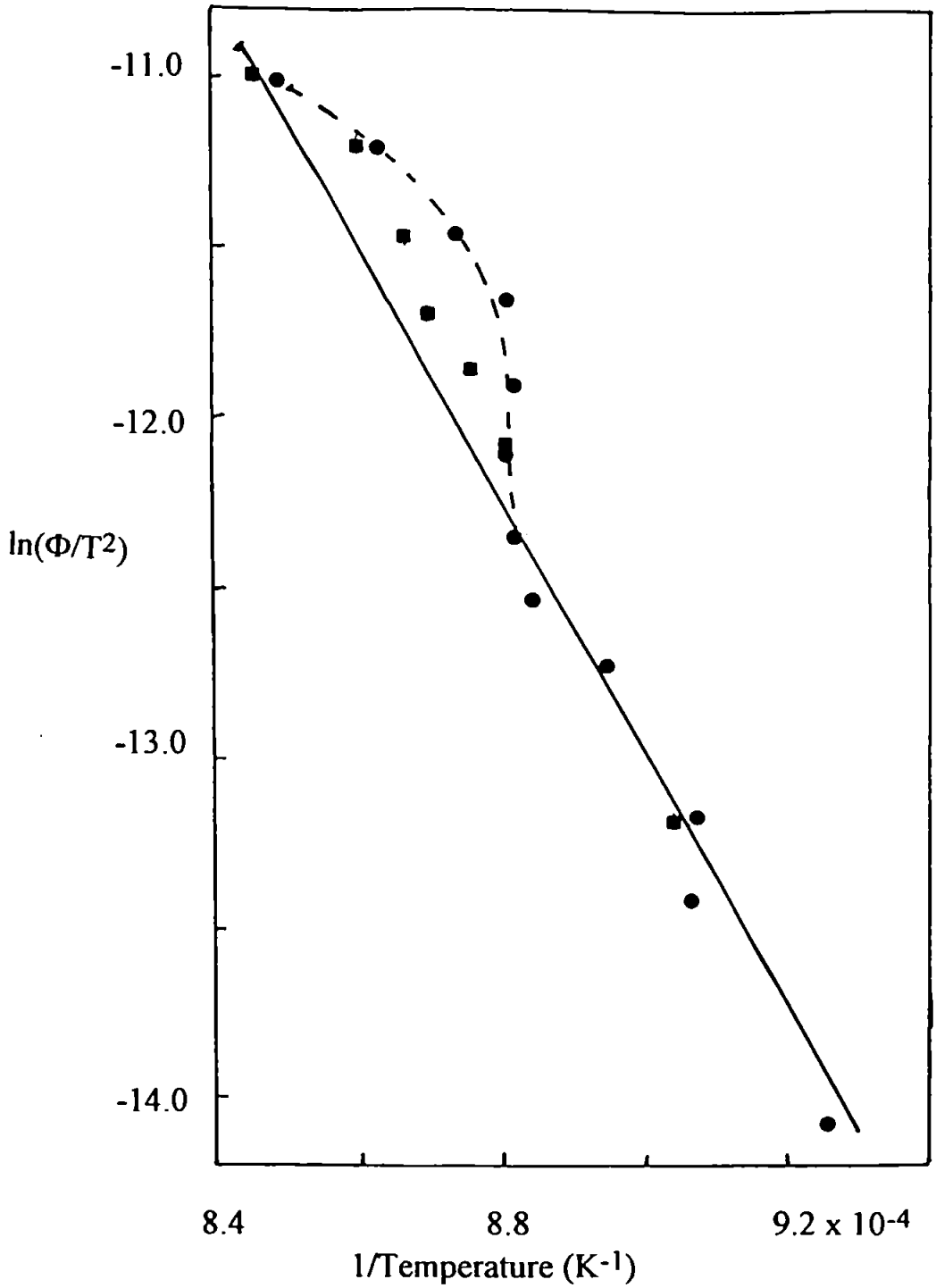

Figure 15
Kissinger plot for the oxidation of titanium nitride in air.

of 154 kJ mol^{-1} for nitrided titanium plates and Wittmer et al (1981) of 197 kJ mol^{-1} for thin nitride films.

Previous research by Glasson and Jayaweera (1969) indicated that the rutile TiO_2 formed (which has a tetragonal structure) splits away from the remaining nitride (which has a cubic-F structure) thus leaving the nitride vulnerable to further oxidation. Figure 16 shows the x-ray diffraction patterns for the nitride and some of the oxidation products. The pattern due to a cubic-F structure can be seen in the original nitride and that due to a tetragonal crystal in the products produced at temperatures above 800 °C. Glasson and Jayaweera (1969) showed that at 600 °C the surface area increases during the first half of the reaction and the number of crystallites increases approximately 20-fold. The splitting of the crystallites occurs due to the change in crystal structure and the increase in volume as the nitride is converted to the less dense oxide, with the release of nitrogen.

When observed by electron microscopy the original nitride and oxide products produced at low temperatures were angular in appearance ranging from 1 to 10 μm in size, whereas the oxides produced at high temperature were more rounded (plates 2 to 5). As 600 °C is above one-third of the melting point of the oxide (1700 °C), sintering by surface diffusion is possible and at 800 °C the oxide is above the Tammann temperature (half melting point) and lattice diffusion is possible. However, titanium oxide produced from the oxidation of the nitride at 800 °C for two hours showed extensive splitting of the crystallites indicating that the product could not have sintered extensively at this temperature but at 900 °C and above the oxide was sintered into larger, relatively smooth lumps.

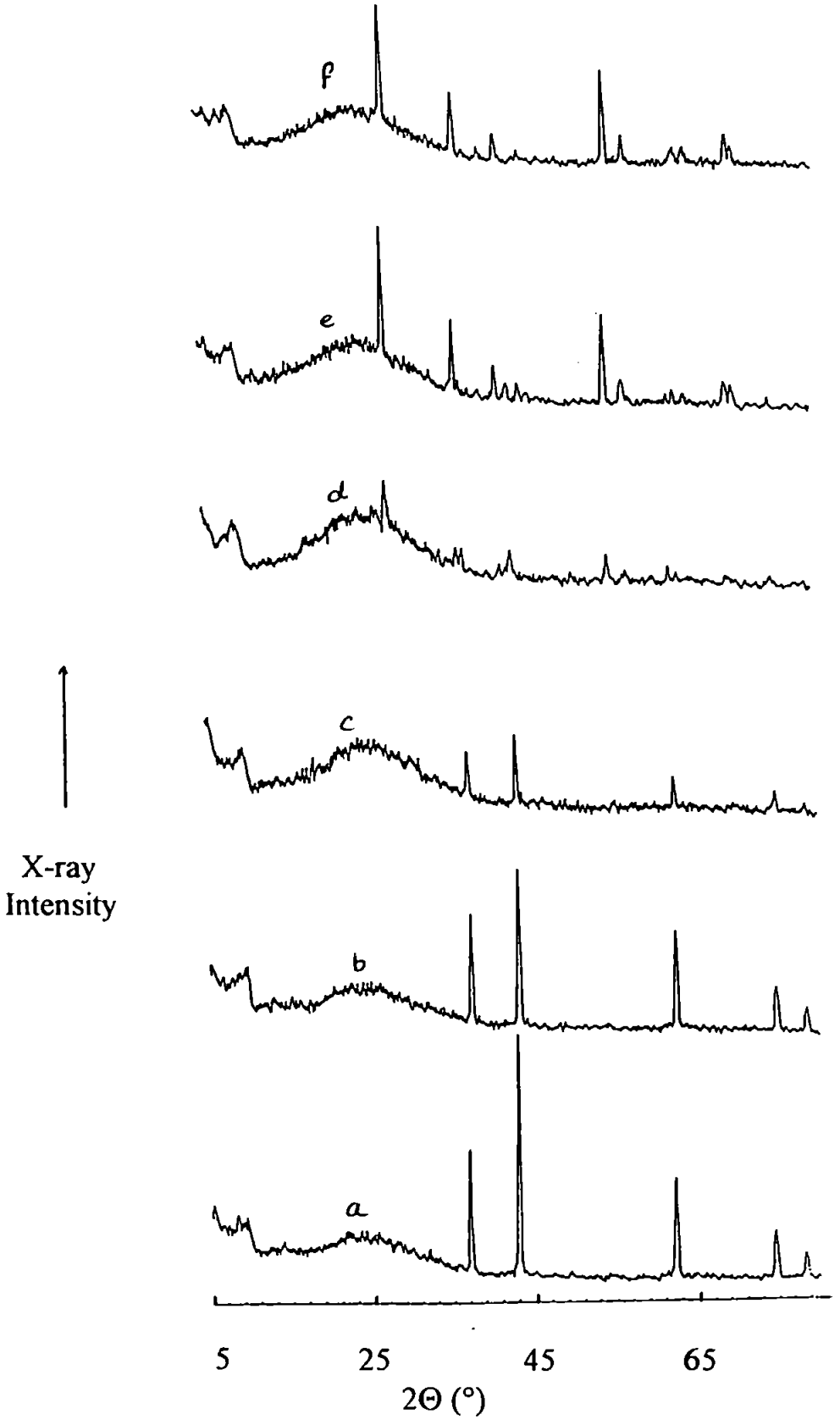

Figure 16

X-ray diffraction traces for titanium nitride (a) and its oxidation products on heating in air at 10 °C min^{-1} to b) 518 °C, c) 690 °C, d) 800 °C, e) 900 °C, f) 1000 °C.

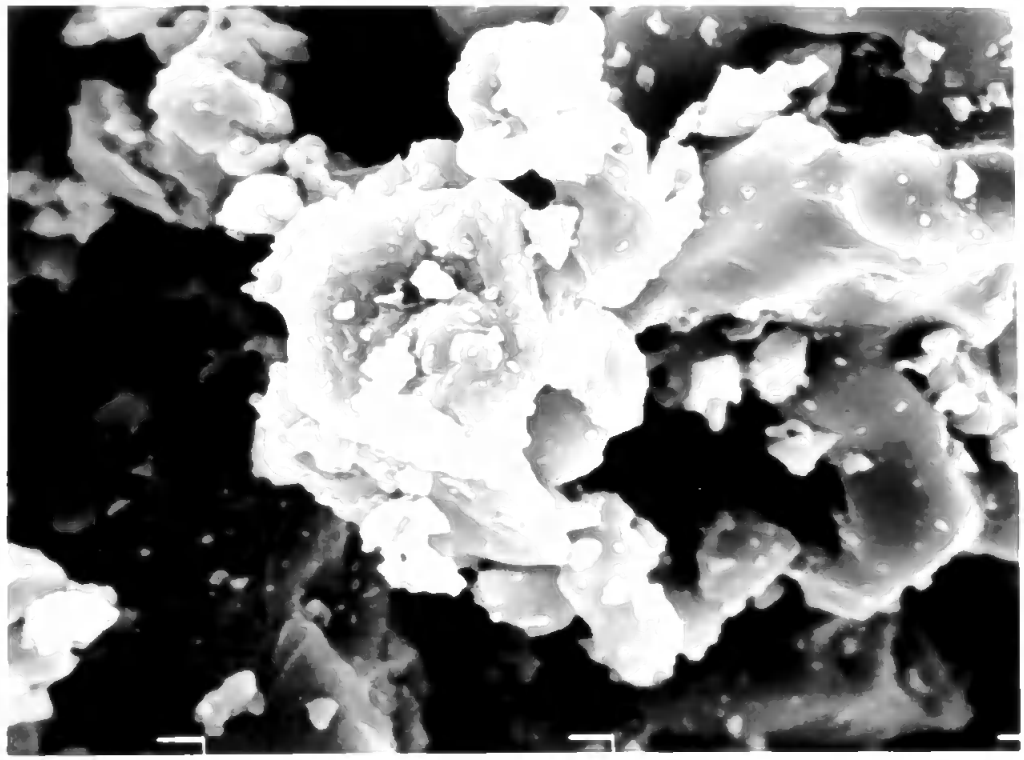

Plate 2
Titanium nitride heated at 10 °C min^{-1} to 518 °C in air

10 µm

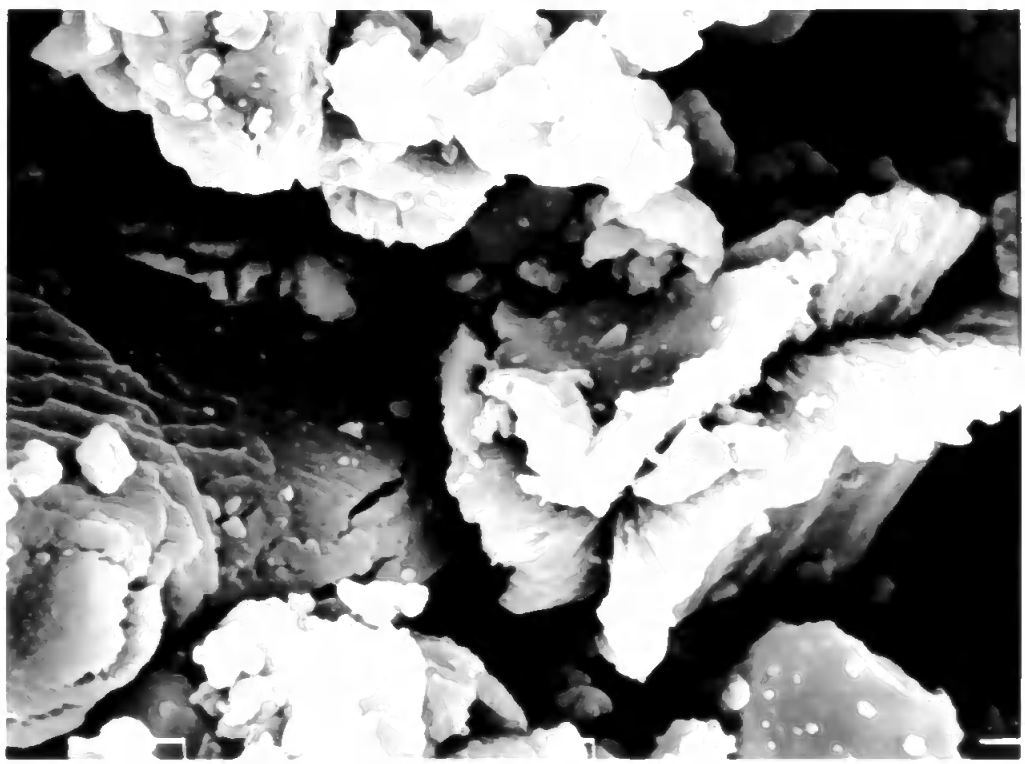

Plate 3
Titanium nitride heated at 10 °C min^{-1} to 800 °C in air

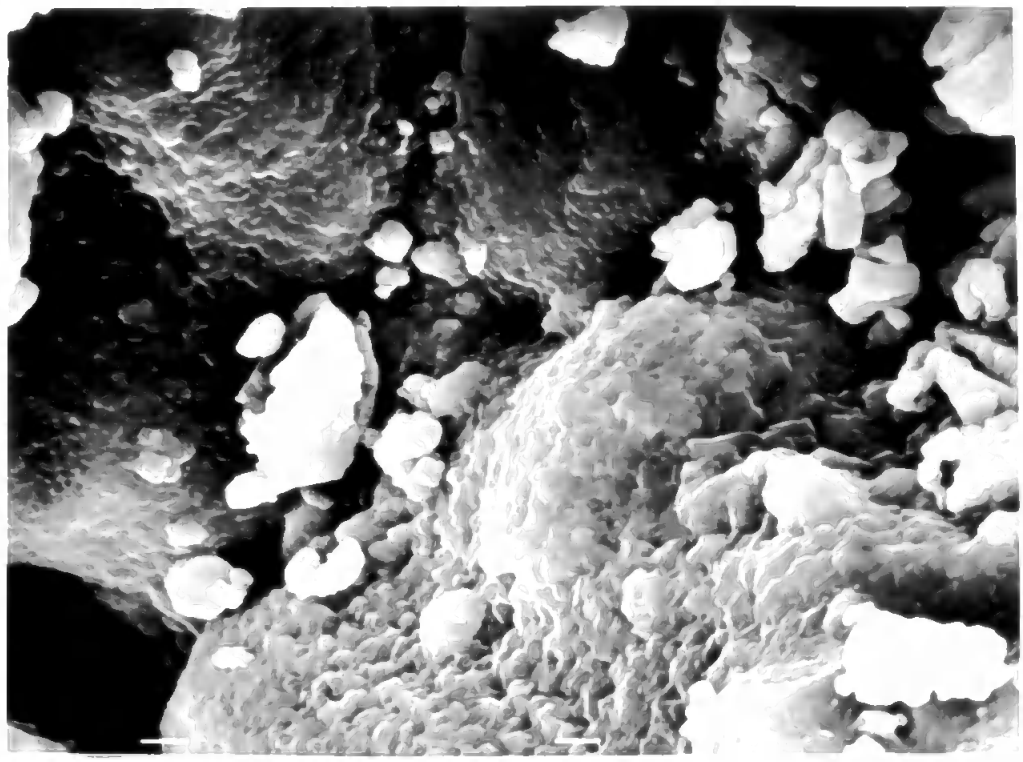

Plate 4
Titanium nitride heated at 10 °C min^{-1} to 900 °C in air

10 μm

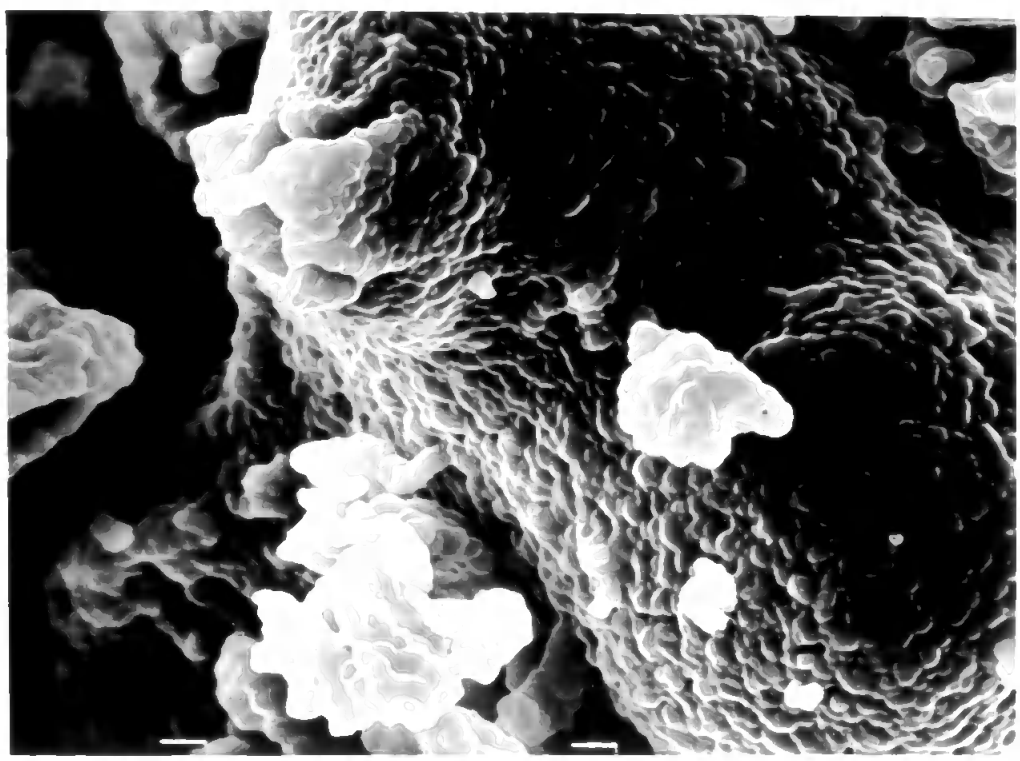

Plate 5
Titanium nitride heated at 10 °C min^{-1} to 1100 °C in air

Dynamic oxidation of 15 mg samples of titanium carbide, TiC, in flowing air (50 cm^3 min^{-1}) at atmospheric pressure and at a heating rate of 10 °C min^{-1} indicated that oxidation began at 400 °C . The weight gain was consistent with that expected for TiC being oxidised to the dioxide TiO_2. X-ray analysis of the initial carbide showed it to be cubic TiC (a = 4.3285 Å, JCPDS card 6-0614). X-ray diffraction showed no evidence of any other phases present in the initial material.

The isothermal curves obtained from the oxidation of titanium carbide (figure 17) show that although the reaction started at a lower temperature than the nitride, the reaction occurred at a slower rate. Thus, at 1000 °C the reaction took 2 hours to complete and at lower temperatures the reaction was even slower. The kinetic plots (figure 18) show that at 1000 °C the half order plot is initially linear, indicating that the reaction was controlled by the diffusion of gas to or from the reaction site, before deviating from the expected line. At 800 and 900 °C the two-thirds order plots are initially linear, indicating that the reaction occurred at the surface of a diminishing sphere. After this initial linear region the plots deviate from the expected straight line indicating that the reaction is partially inhibited by the product. At lower temperatures neither the two-thirds nor the half order plots are linear and thus neither of the models used in this study describe the rate determining step. Since the melting point of the oxide is 1840 °C, the product may sinter at temperatures above 430 °C by surface diffusion and above 780 °C by lattice diffusion. The melting point of titanium carbide being 3140 °C, the carbide may sinter by surface diffusion at temperatures above 860 °C and by lattice diffusion above 1430 °C. Therefore, sintering of the product and limited sintering of the initial carbide may account for the observed deviation from the expected two-thirds and half order kinetic plots.

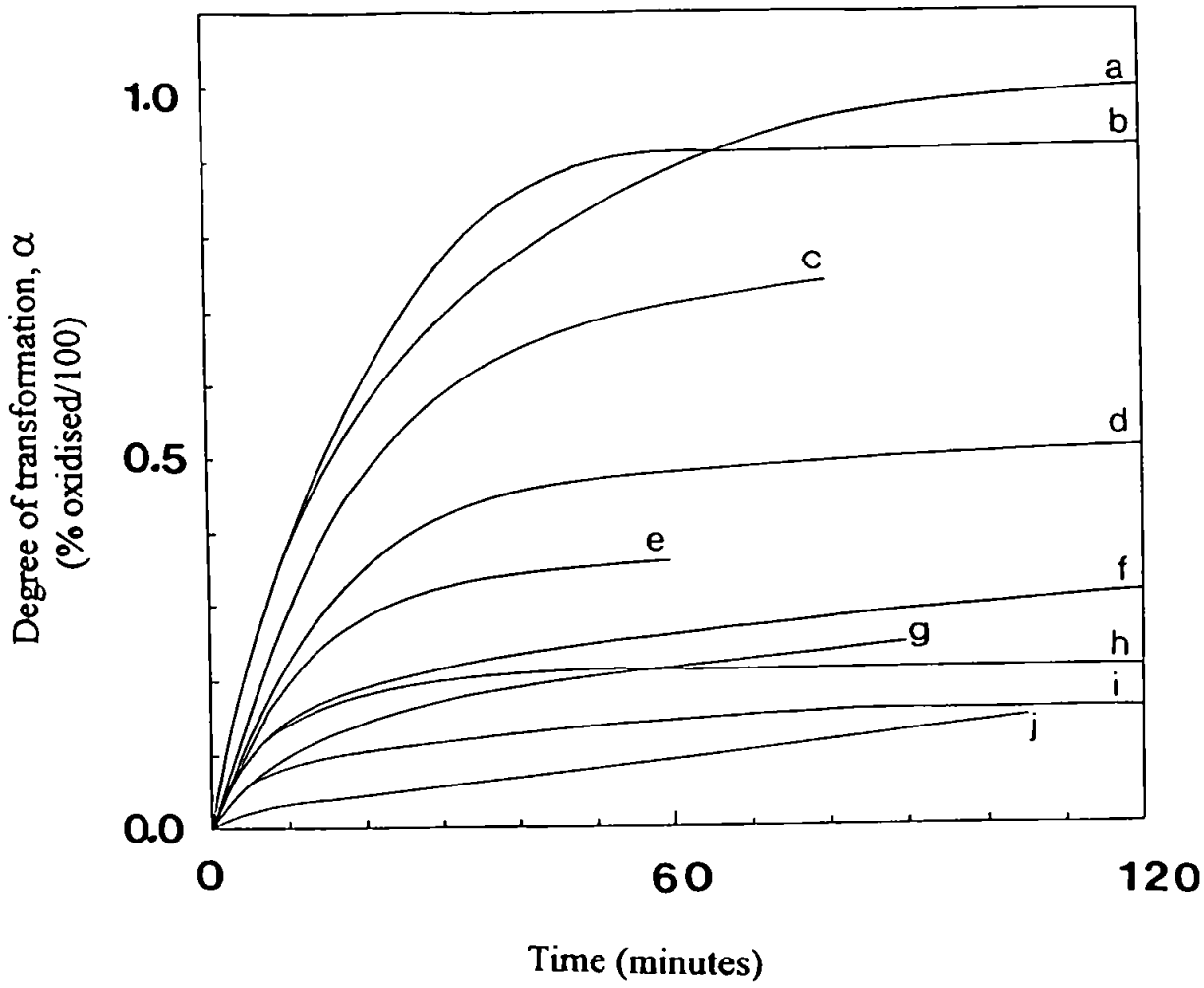

Figure 17
Isothermal TG curves for the oxidation of titanium carbide in flowing air (300 ml min^{-1}) at a) 1000 °C, b) 900 °C, c) 800 °C, d) 700 °C, e) 650 °C, f) 600 °C, g) 450 °C, h) 550 °C, i) 500 °C, j) 500 °C.

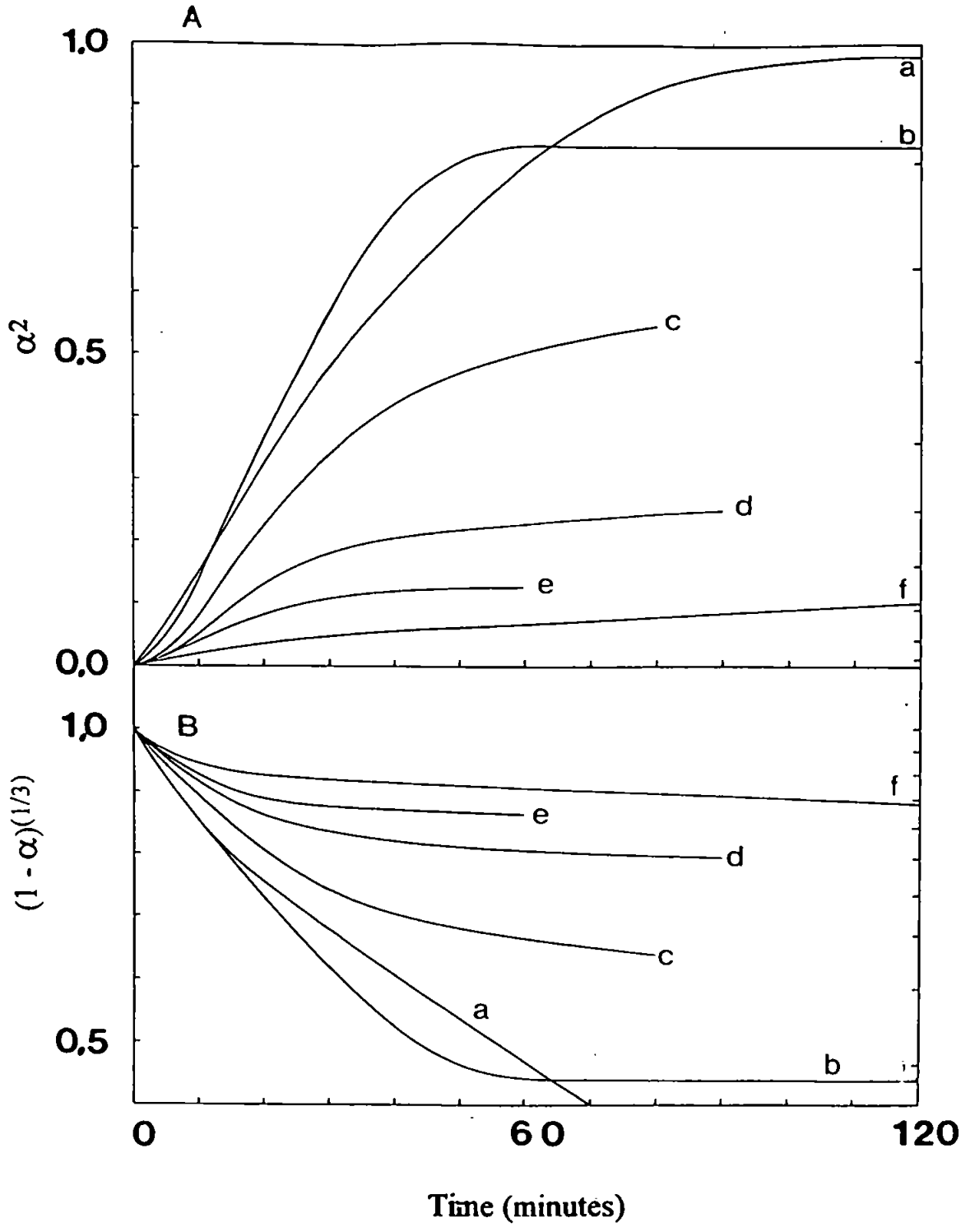

Figure 18
Half order (A) and two-thirds order (B) kinetic plots for the isothermal oxidation of titanium carbide in air at a) 1000 °C, b) 900 °C, c) 800 °C, d) 700 °C, e) 650 °C, f) 600 °C.

From the Arrhenius plot (table 4 and figure 19) derived from these isothermal studies the activation energy of this reaction was calculated to be 22.5 ± 0.5 kJ mol^{-1}.

The initial titanium carbide was found to have a specific surface area of 0.8 m^2g^{-1}, corresponding to an average crystallite size of 1.52 μm (table 5). After 1 hour at 600 °C, 25 % of the carbide had been oxidised ($\alpha = 0.25$) and the total surface area had increased from 0.8 to 1.8 m^2g^{-1}. This corresponds to the formation of an oxide of surface area 4.0 m^2g^{-1}. In comparison, after 1 hour at 800 °C the total surface area increased to 1.0 m^2g^{-1} which corresponds to the formation of oxide of surface area 0.7 m^2g^{-1} (figure 20). Theoretically, when 1 g of TiC (density 4.90 g cm^{-3}) oxidises to 1.33 g of oxide (density 4.26 g cm^{-3}) there is an increase in volume from 0.204 to 0.312 cm^3, or a 0.530-fold increase. Thus the surface area change is given by $S'/S = (1 + 0.530\alpha)^{2/3}$ where S' is the actual surface area produced when 1 g of carbide is oxidised. As the value of α at 600 °C after 1 hour is 0.25, the theoretical surface area should be 0.86 m^2g^{-1}. As the experimental value is greater than this the sample must have split to create a larger surface. At 800 °C after 1 hour $\alpha = 0.76$ and hence the theoretical surface area is 1.0 m^2g^{-1} indicating that the oxide had begun to sinter. At 1000 °C the sintering impedes the reaction so much that it proceeds at about the same rate as at 900 °C.

As with the nitride, the initial carbide and the oxide produced at low temperatures (600 °C) appeared angular (plate 6). At higher temperatures (800 °C) the product was more rounded (plate 7). This indicates sintering of the product at elevated temperatures and hence agrees with the surface area determinations and data from the isothermal studies.

Temperature, T		dα/dt	ln(dα/dt)	1/T
°C	K	x 10^{-4} sec^{-1}		x 10^{-4} K^{-1}
1000	1273	7.833	-7.15	7.86
900	1173	7.833	-7.15	8.52
800	1073	6.500	-7.64	9.32
700	973	4.000	-7.82	10.28
650	923	3.667	-7.91	10.83
600	873	3.333	-8.01	11.46
550	823	2.632	-8.24	12.15
500	773	1.754	-8.65	12.94
400	673	1.282	-8.96	14.86

Arrhenius plot
Gradient of slope = -2720 K
Correlation coefficient = -0.99

Table 4
Isothermal oxidation of titanium carbide in air

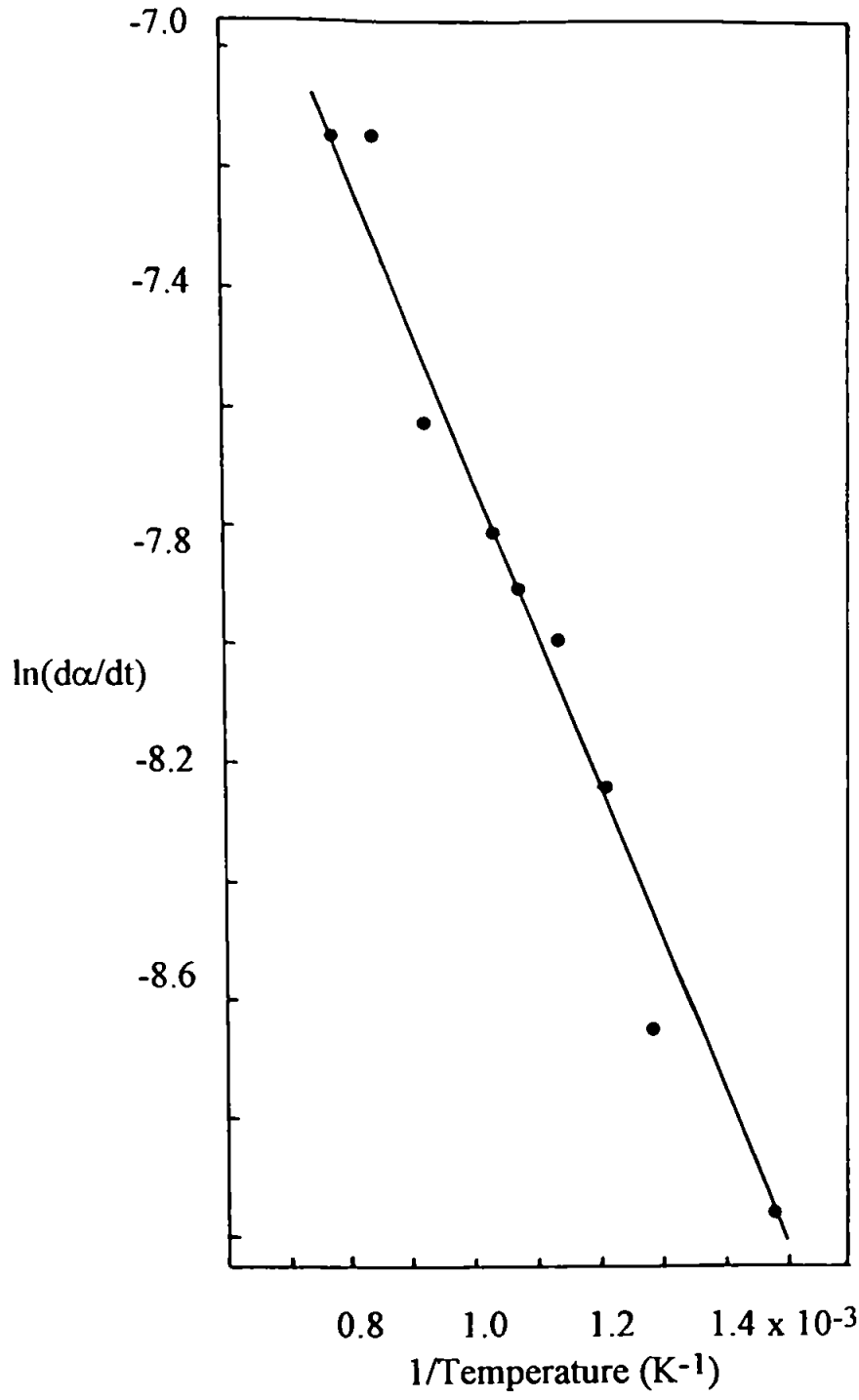

Figure 19
Arrhenius plot for the oxidation of titanium carbide in air.

Temperature °C	Calcining period hours	α	Specific Surface area m^2g^{-1}	Surface area of oxide m^2g^{-1}
Original material		0.00	0.81	
400	1	0.09	0.80	0.73
600	1	0.26	1.84	4.01
700	1	0.47	1.15	1.43
800	1	0.71	1.01	1.05
900	1	0.91	0.72	0.71

Table 5

Variation of surface area during oxidation of titanium carbide in air

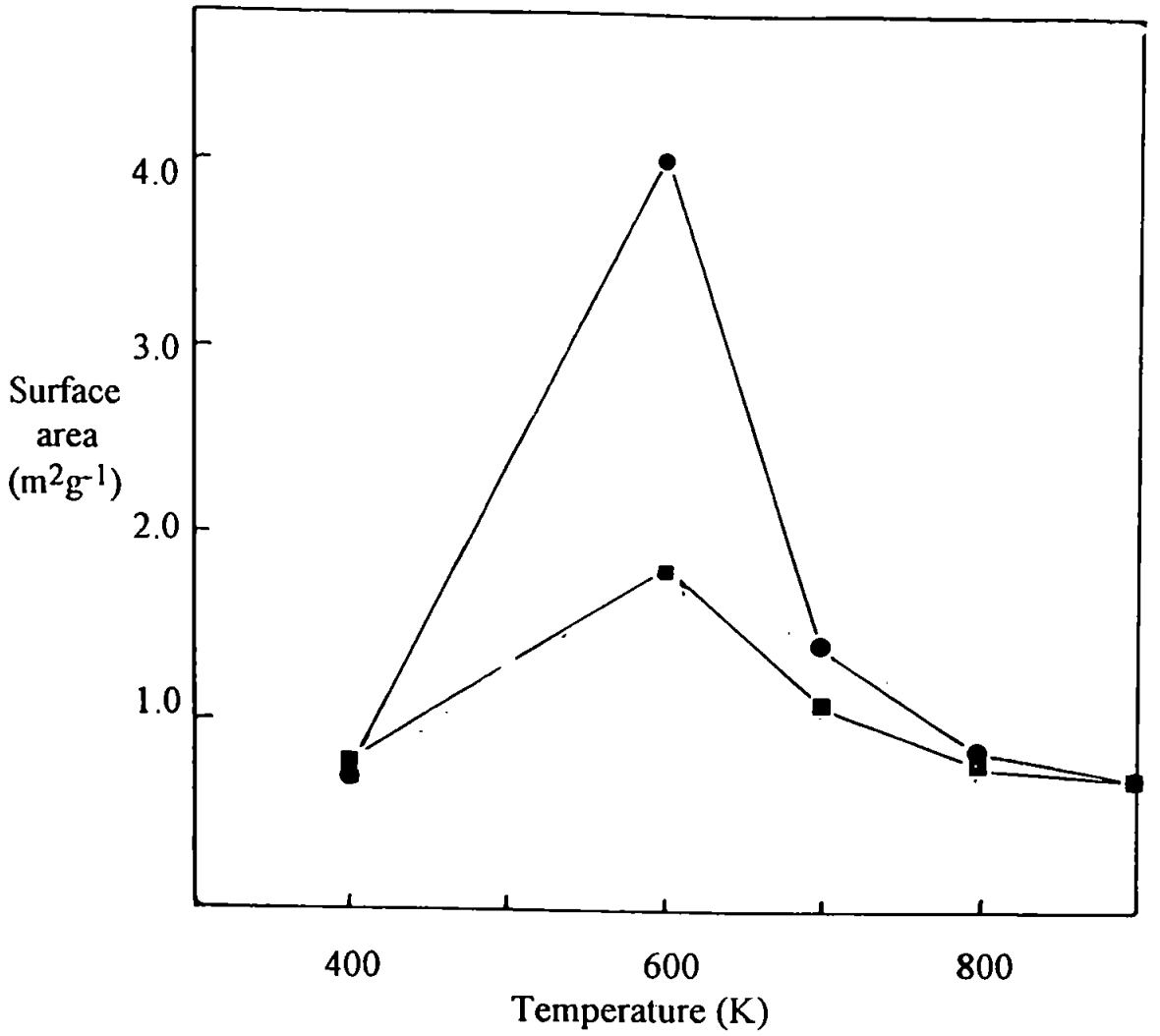

Figure 20

Surface area changes for 1 hour oxidations of titanium carbide in air.

- ■ Total surface area.
- ● Surface area of oxide.

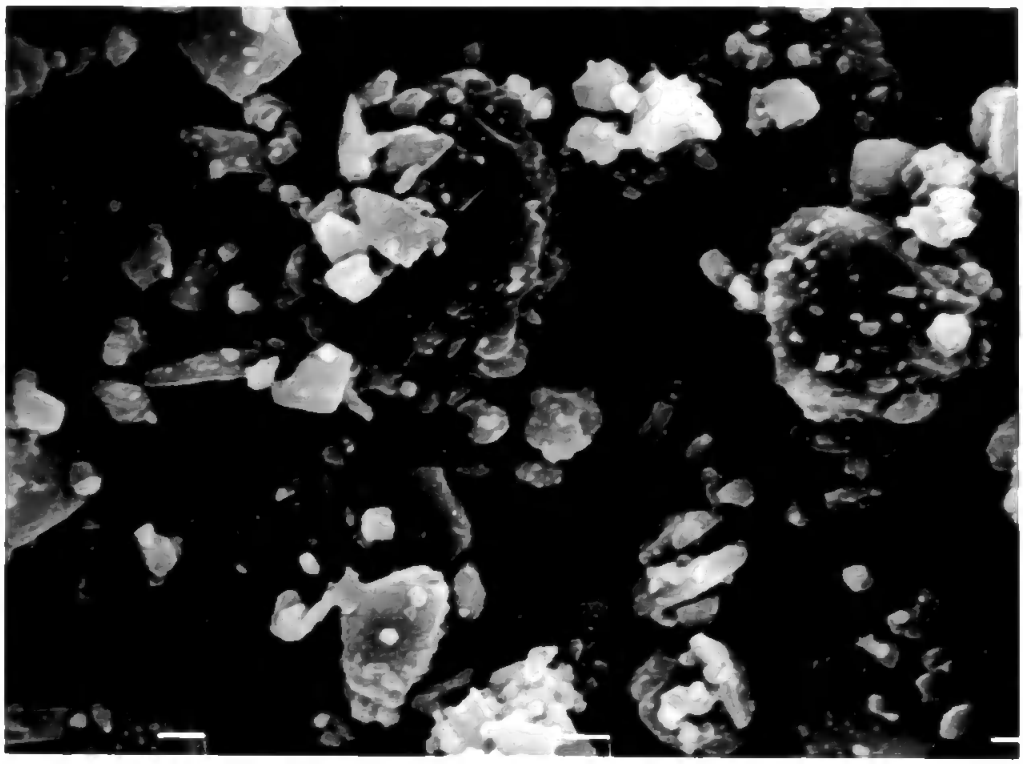

Plate 6
Titanium carbide oxidised for 1 hour at 600 °C in air

10 μm

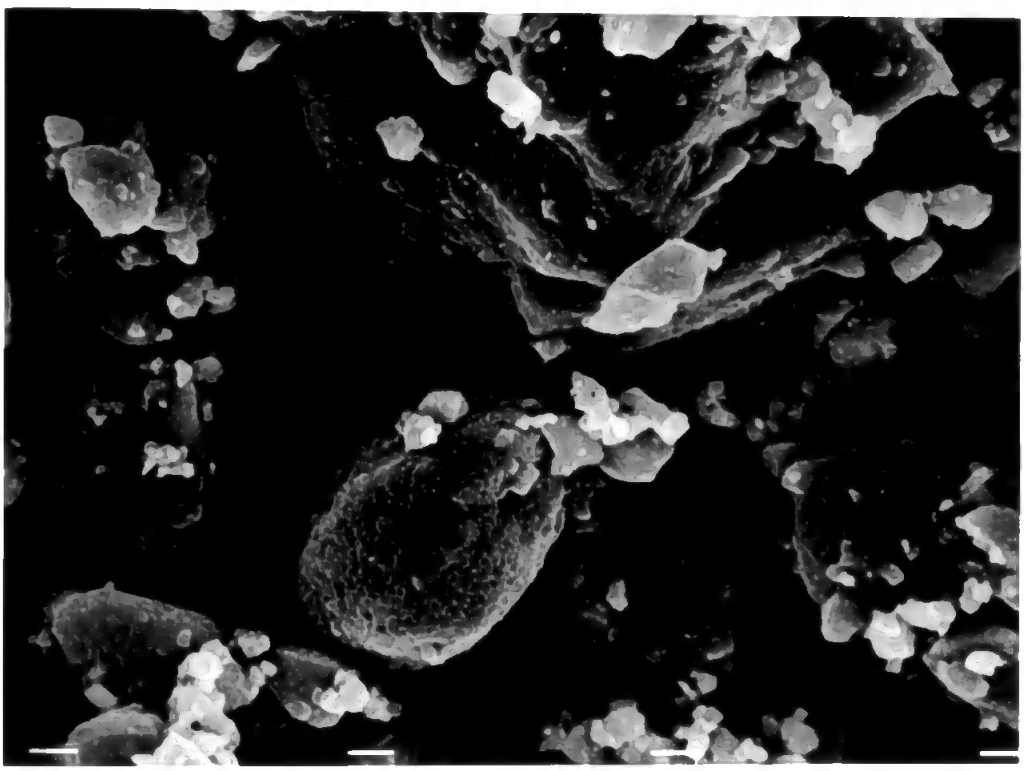

Plate 7
Titanium carbide oxidised for 1 hour at 800 °C in air

X-ray diffraction patterns for the nitride and carbide showed that both are of the cubic-F lattice types and both form the dioxide, TiO_2 (rutile). The rutile pattern was detected in the x-ray diffraction trace of a sample of titanium nitride oxidised at 500 °C for 2 hours, $\alpha = 0.07$, indicating that the oxide could crystallise at low temperatures. At higher temperatures the lower oxide, TiO, is partially soluble in the nitride (Glasson and Jayaweera (1968)), however, no evidence for this intermediate was found. TiO_2 also has limited solubility in TiN (Glasson and jayaweera (1968)). The lattice constants remain unchanged from TiN to $TiN_{0.6}O_{0.4}$ when the binary compounds are sintered at 1700 °C (Samsonov and Golubeva (1956)). No evidence for the formation of oxynitride or oxycarbide was found from the x-ray analyses or thermodynamic data presented in this work.

3.3 OXIDATION OF ZIRCONIUM NITRIDE AND CARBIDE IN AIR

Dynamic oxidation of 15 mg samples of zirconium nitride, ZrN, in flowing air (50 cm^3 min^{-1}) indicated that the oxidation began at approximately 500 °C. The weight gain (17.1 %) was consistent with ZrN being oxidised to the dioxide ZrO_2.

X-ray diffraction studies showed that the initial nitride was cubic ZrN (a = 4.56 Å, JCPDS card 2-956). Analyses of the oxides produced at 600 °C showed that the cubic nitride was oxidised to a cubic form of zirconia, ZrO_2 (a = 5.07 Å, JCPDS card 7-337). At this temperature the height of peaks due to the unoxidised zirconium nitride are greatly reduced, indicating that the crystal structure has broken down significantly. Similarly the peaks due to the product are relatively small indicating that the product is mainly amorphous. Above 600 °C the monoclinic form of zirconia (baddeleyite, a = 5.1477, b = 5.2030, c = 5.3156 Å, β = 99°23', JCPDS card 13-307) was found in increasing proportions (figure 21). It is probable that the 1.80 Å and the 1.53 Å spacings of the cubic structure became the 1.81 Å and 1.54 Å spacings of the monoclinic form. At higher temperatures the x-ray peaks became higher and better defined in shape indicating that the product became increasingly more crystalline. Above 1200 °C the tetragonal form can also be formed (Garvie (1970)).

Isothermal studies (figure 22) showed that at 525 °C the reaction was 15% complete (α = 0.15) after 2 hours, 65% complete after 2 hours at 600 °C and complete within 2 hours at 640 °C. Above 650 °C the reaction was complete within 40 minutes. Figure 23 shows that at 650 and 700 °C the two-thirds order kinetic plots are initially linear indicating that the reaction was occurring at the surface of a diminishing sphere. At 650 °C the plot deviates from the

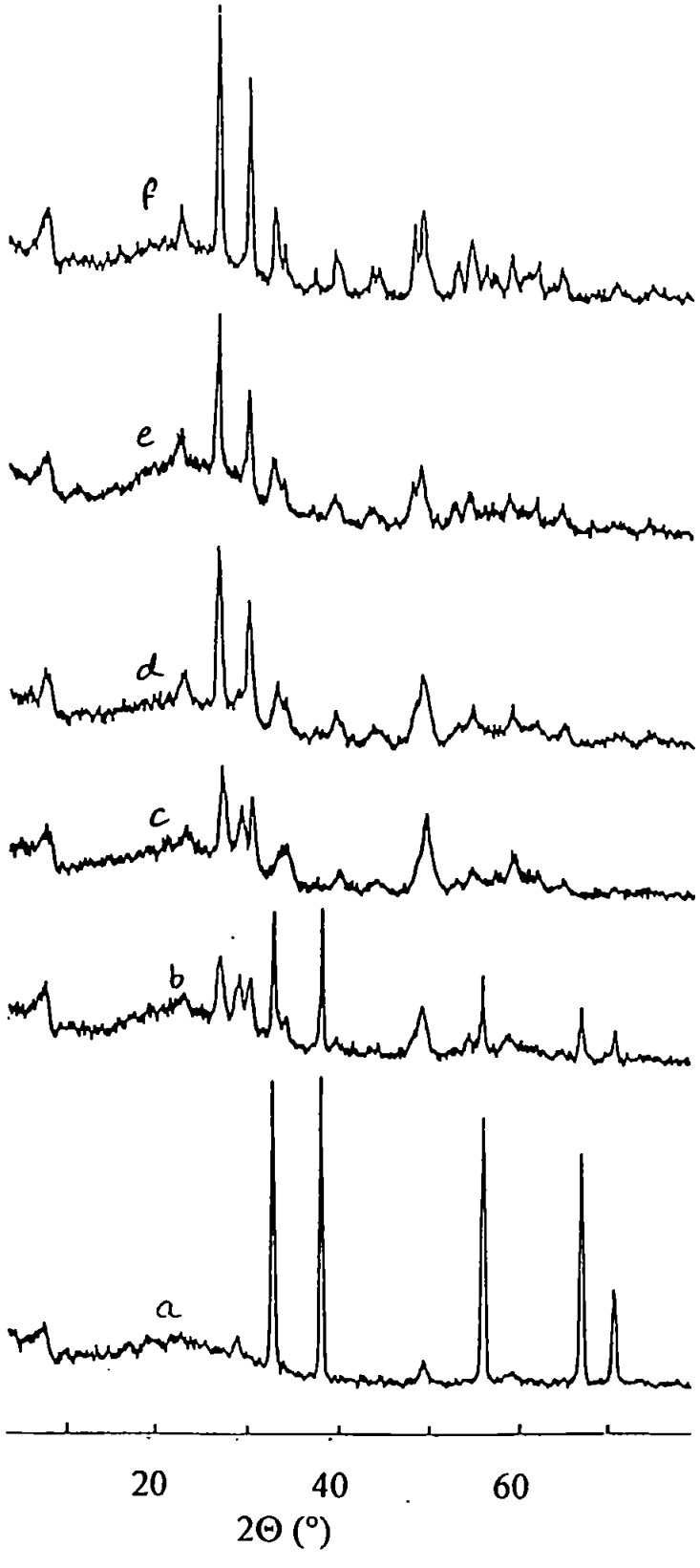

Figure 21
X-ray diffraction traces of the oxidation products of zirconium nitride heated for two hours at a) 500 °C, b) 600 °C, c) 700 °C, d) 800 °C, e) 1000 °C, f) 1200 °C.

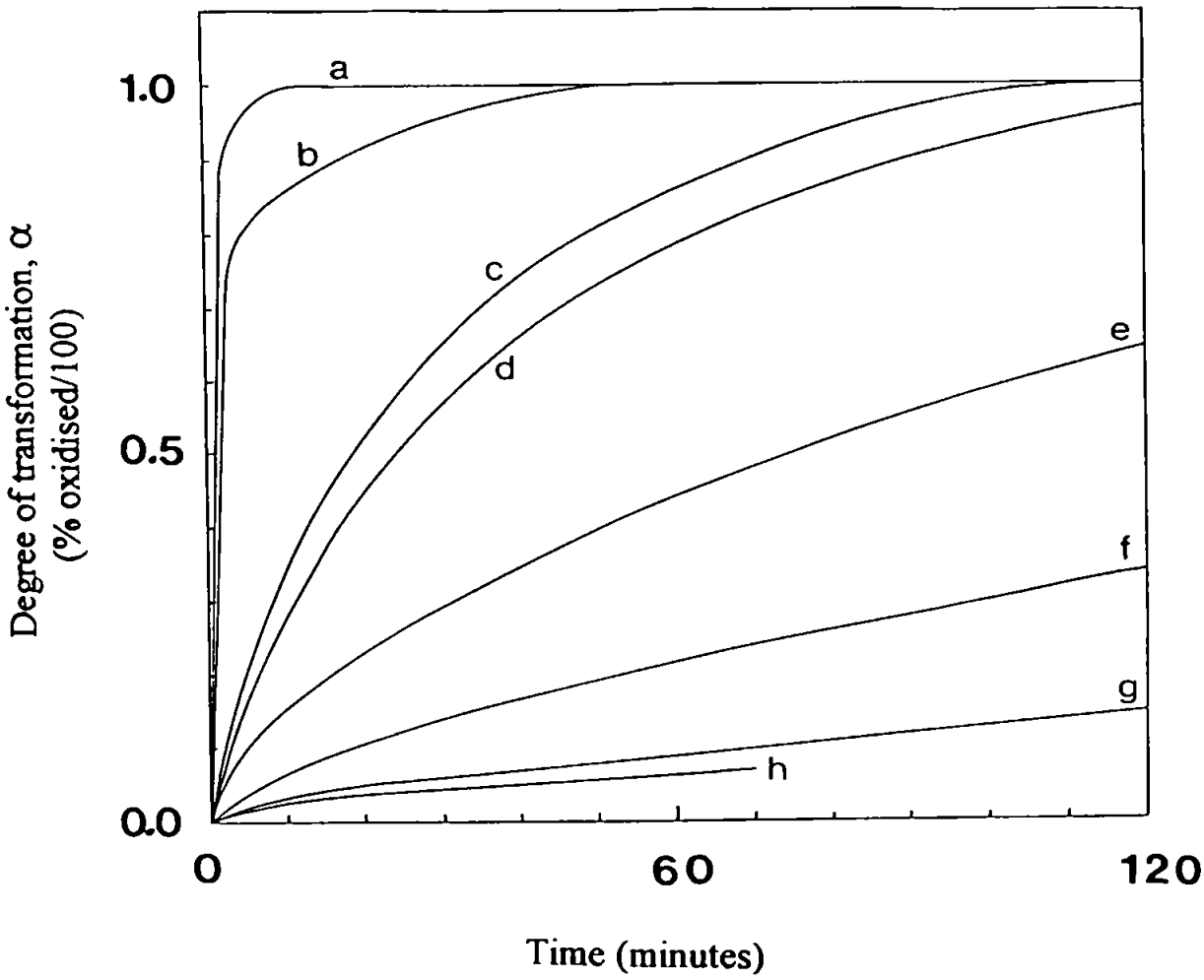

Figure 22
Isothermal TG curves for the oxidation of zirconium nitride in flowing air (50 ml min^{-1}) at a) 700 °C, b) 650 °C, c) 640 °C, d) 630 °C, e) 600 °C, f) 575 °C, g) 525 °C, h) 500 °C.

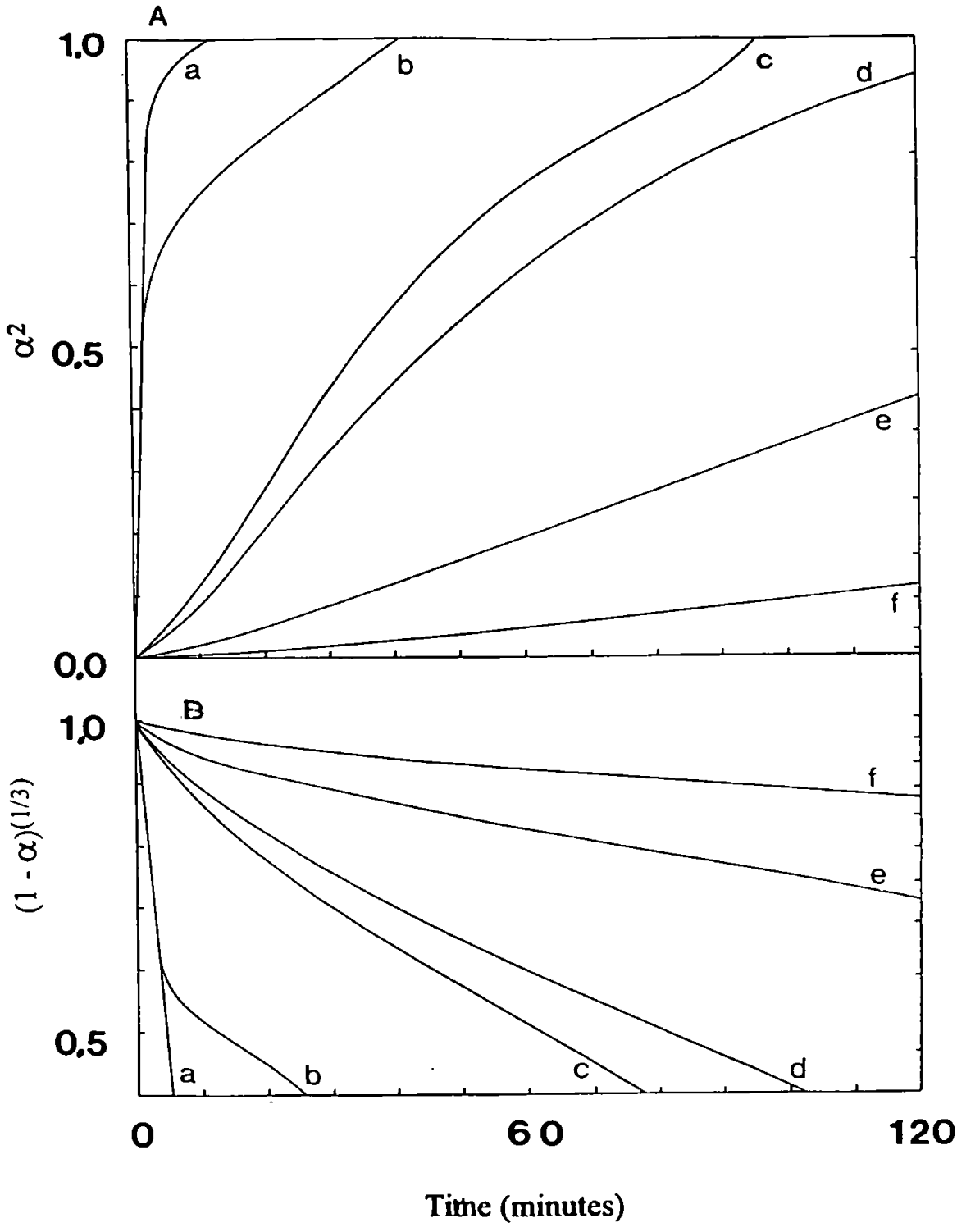

Figure 23
Half order (A) and two-thirds order (B) kinetic plots for the isothermal oxidation of zirconium nitride in air at a) 700 °C, b) 650 °C, c) 640 °C, d) 630 °C, e) 600 °C, f) 575 °C.

expected straight line at $(1-\alpha)^{1/3} \approx 0.6$ and the half order plot becomes linear indicating that the reaction becomes controlled by the diffusion of gas through the product layer. At lower temperatures the kinetic plots are inconclusive. Since the melting point of zirconium oxide is 2715 °C, above 700 °C limited sintering of the oxide by surface diffusion is possible and at temperatures above 1200 °C sintering by crystal lattice diffusion. However, due to the large difference in density between the nitride and the oxide (7.09 and 5.6 g cm^{-3} respectively) and the change in crystal structure it would be expected that the oxide would split away from the nitride. From the Arrhenius plot (table 6 and figure 24) derived from these isothermal studies the activation energy was calculated to be 130 ± 4 kJ mol^{-1}.

Electron micrographs (plates 8 to 11) show that the original nitride particles were angular in shape and ranged in size from 10 to 100 μm. At 600 °C the particles are seen to break up, and at 1300 °C the oxide forms spherical particles of 1 μm diameter, which have sintered into larger lumps.

DTA studies showed that oxidation was exothermic and above 650 °C the reaction was self sustaining. This was confirmed by heating some of the nitride in an open alumina boat with a Bunsen burner until the sample was seen to glow dull red at one end of the boat. On removal of the heat source the remaining nitride was observed to continue oxidising, producing white zirconia as the reaction zone proceeded along the vessel.

As expected the temperature of DTA maxima increased with increasing heating rate (figure 25 and table 7). Heating rates above 10 °C min^{-1} were not used as the exothermic reaction released sufficient heat to alter the true heating rate of the sample and made the accurate determination of the peak temperature impossible. From the Kissinger plot (figure 26) the activation energy was

Temperature, T		dα/dt	ln(dα/dt)	1/T
°C	K	x 10^{-4} sec^{-1}		x 10^{-3} K^{-1}
700	973	75.0	-4.89	1.028
650	923	50.0	-5.30	1.083
645	918	117	-4.45	1.089
640	913	7.67	-7.17	1.095
640	913	12.2	-6.71	1.095
630	903	8.33	-7.44	1.107
619	892	9.47	-6.96	1.121
602	875	5.77	-7.46	1.142
600	873	4.50	-7.71	1.145
575	848	1.50	-8.80	1.179
569	842	2.20	-8.42	1.188
545	818	1.54	-8.78	1.222
525	798	0.67	-9.61	1.253
506	779	0.48	-9.94	1.284
500	773	0.50	-9.90	1.294

Arrhenius plot
Gradient of slope = -15700 K
Correlation coefficient = -0.97

Table 6
Isothermal air oxidation of zirconium nitride

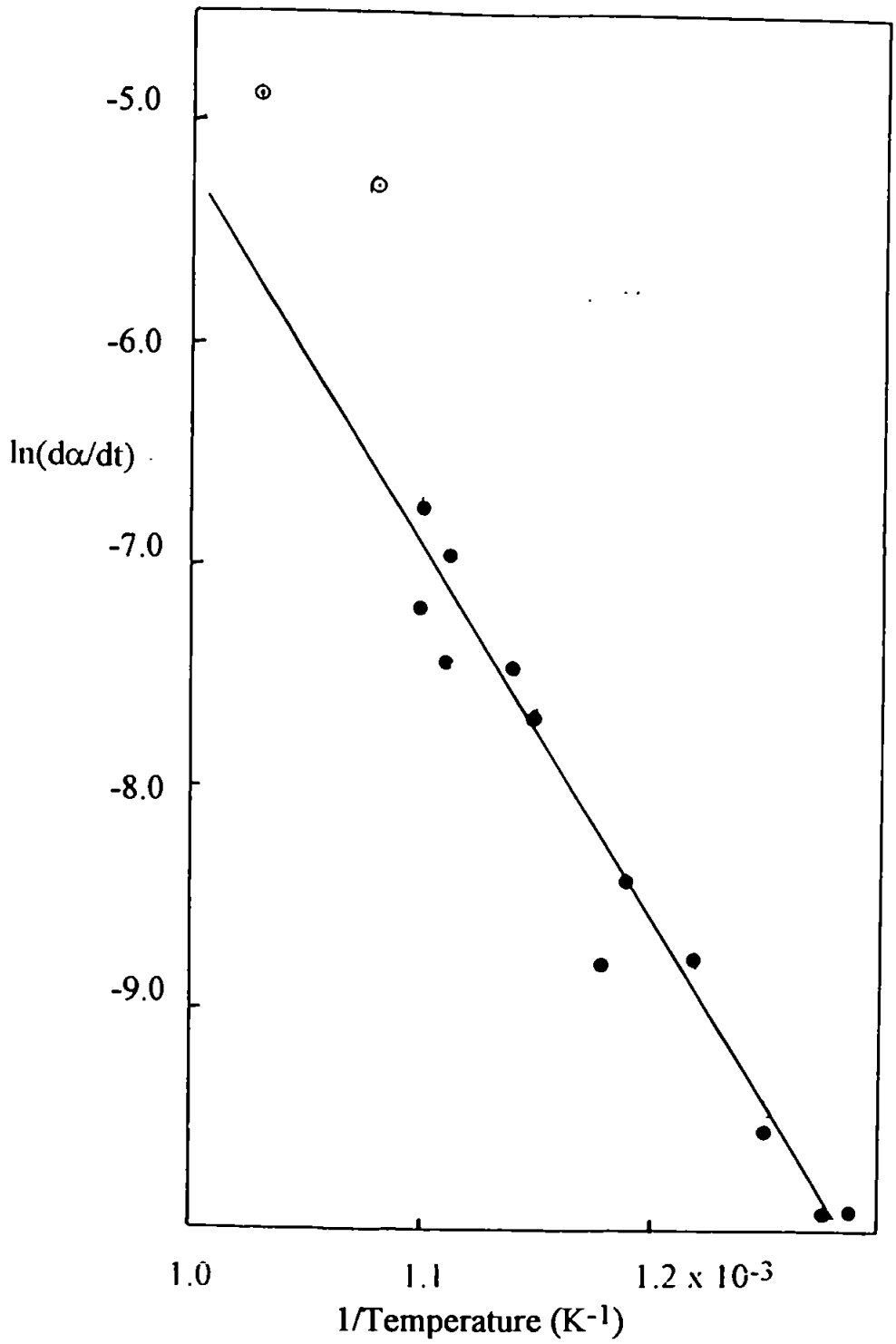

Figure 24
Arrhenius plot for the oxidation of zirconium nitride in air.

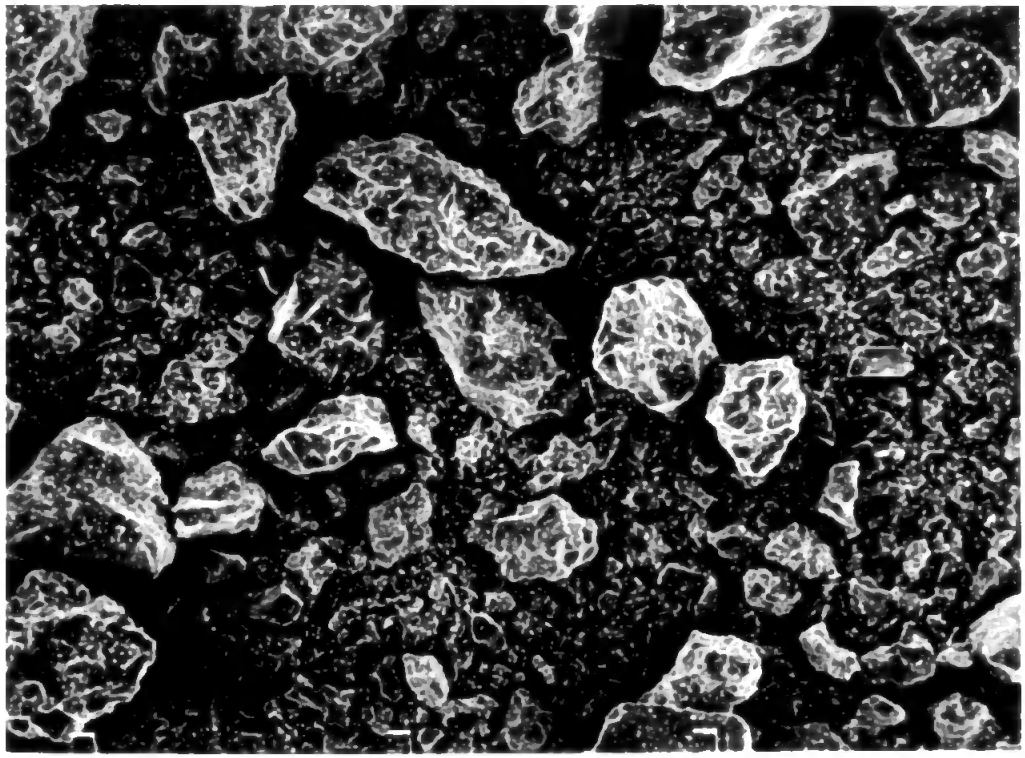

Plate 8
Zirconium nitride — 100 μm

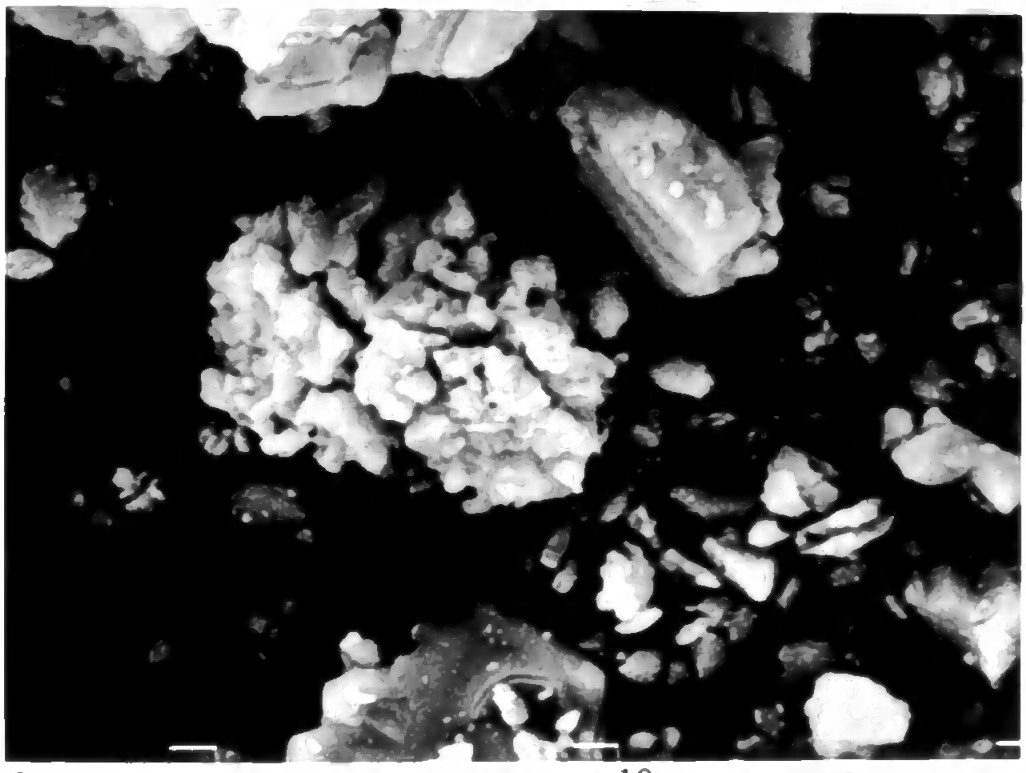

Plate 9 — 10 μm
Zirconium nitride oxidised for 1 hour at 600 °C in air

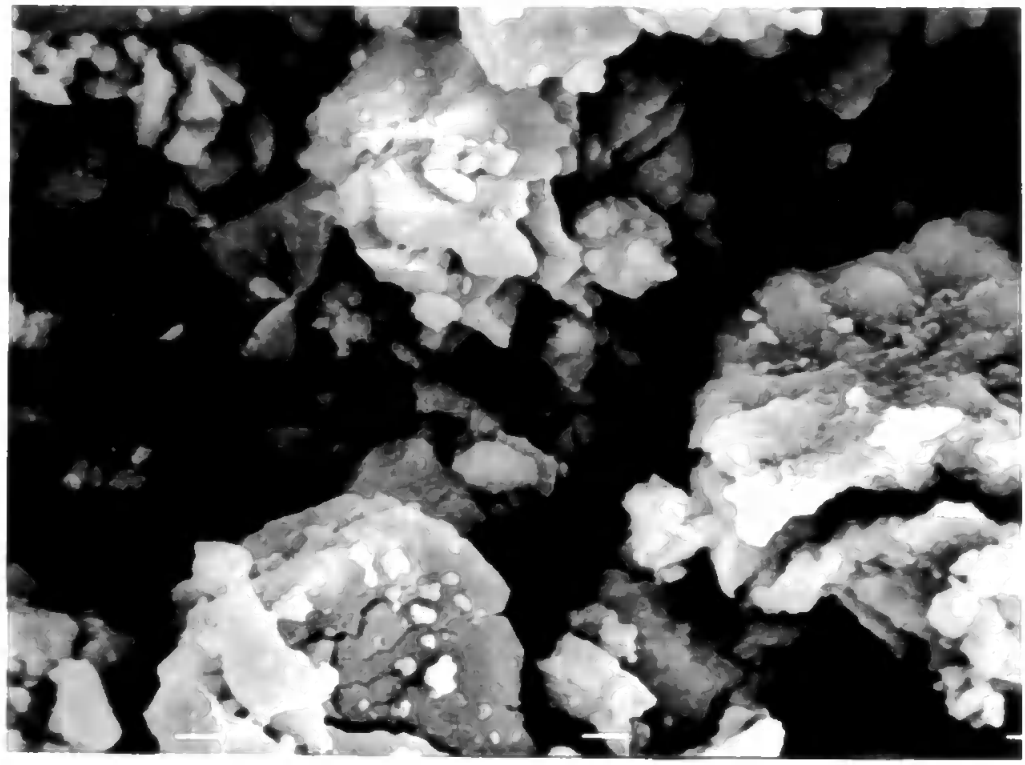

Plate 10
Zirconium nitride oxidised for 1 hour at 1000 °C in air

10 μm

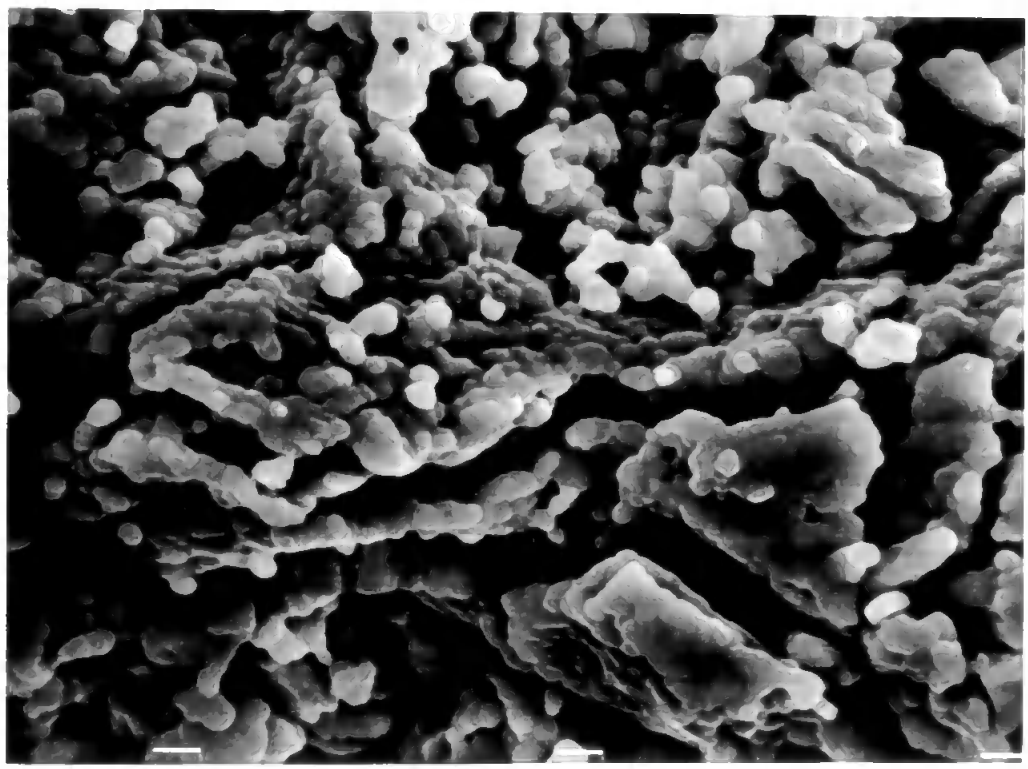

Plate 11
Zirconium nitride oxidised for 1 hour at 1300 °C in air

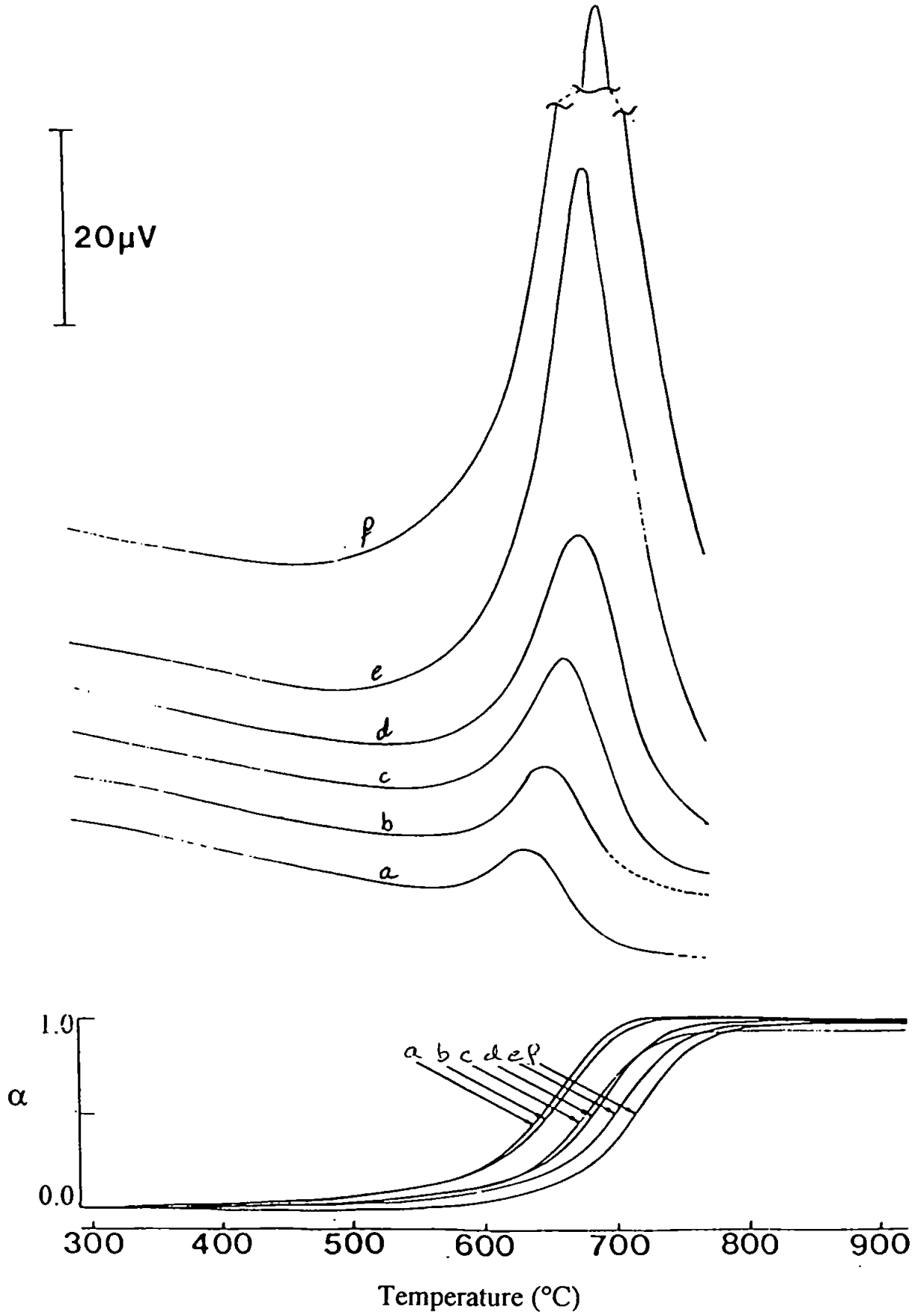

Figure 25

DTA curves (upper) and TG curves (lower) for oxidation of zirconium nitride in flowing air (50 ml min^{-1}) heated at a) 1 °C min^{-1}, b) 1.5 °C min^{-1}, c) 2.5 °C min^{-1}, d) 4 °C min^{-1}, e) 7 °C min^{-1}, f) 10 °C min^{-1} to 900 °C.

Heating rate, Φ K min^{-1}	DTA peak, T K	$\ln(\Phi/T^2)$	1/T x 10^{-4} K^{-1}
1.0	913	-13.63	10.95
	917	-13.64	10.91
1.5	930	-13.27	10.75
2.0	934	-12.99	10.70
2.5	937	-12.79	10.67
3.0	948	-12.61	10.55
4.0	953	-12.33	10.49
5.0	951	-12.11	10.52
	950	-12.10	10.53
7.5	956	-11.71	10.46
10.0	966	-11.44	10.35

Kissinger plot
Gradient of slope = -29000 K
Correlation coefficient = -0.98

Table 7
Effect of heating rate on the oxidation of zirconium nitride in air

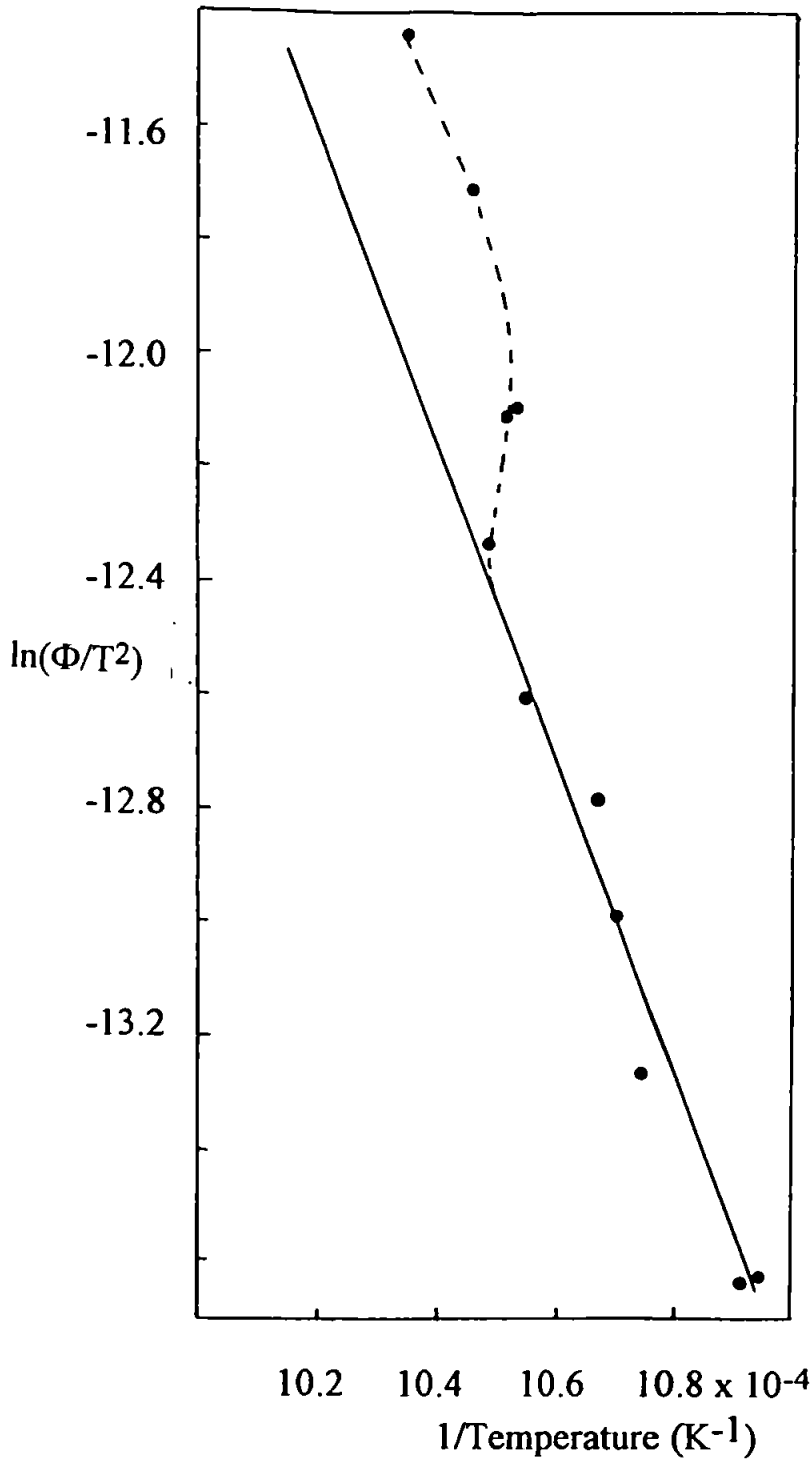

Figure 26
Kissinger plot for the oxidation of zirconium nitride in air.

determined to be 241 ± 4 kJ mol^{-1}, compared with 130 kJ mol^{-1} from isothermal studies. The Kissinger data points form two linear regions. The upper region corresponds to heating rates above 5 °C min^{-1} where the exothermic nature of the reaction significantly affected the heating of the sample and were therefore excluded from data used to calculate the slope of the line, and hence the activation energy.

Isothermal studies (figure 27) showed that the carbide oxidised more readily than the nitride, being 90 % oxidised at 500 °C after 1 hour compared with the nitride which was only 10% oxidised at that temperature after 1 hour. Isothermal oxidations at temperatures above 600 °C showed an initial weight gain greater than that expected for the oxidation of ZrC to the dioxide ZrO_2, the excess weight gain is then lost and the expected weight gain of 19.4 % is achieved. At 700 °C a weight gain maxima of 21.3 % was achieved after 20 minutes, the weight gain then declined to 18.7 %. At 800 °C the weight gain reached a maximum of 24.6 % after 19 minutes and then declined to the expected 19.4 % after a further 100 minutes. At 900 °C the weight gain reached a maximum of 20.3 % after 20 minutes and then declined to the expected 19.4 % after a further 5 minutes. It is assumed that the excess weight is due to the formation of dioxide and free carbon which is then slowly oxidised to carbon dioxide, or to the formation of an oxycarbonate, $ZrO(CO_3)$, which then decomposes to the dioxide and carbon dioxide. It proved impossible to reproduce the oxidation observed in the Massflow balance in the tube furnace and isolate the products at that stage of the reaction. From the Arrhenius plot (table 8 and figure 28) the activation energy for the reaction was calculated to be 14.6 ± 0.3 kJ mol^{-1}. The kinetic plots (figure 29) for isothermal oxidations below 475 °C are inconclusive with neither the half order nor the two-thirds order plots displaying linearity. The half order kinetic plot for the oxidations at 475 and 510 °C shows an initial linear region before the

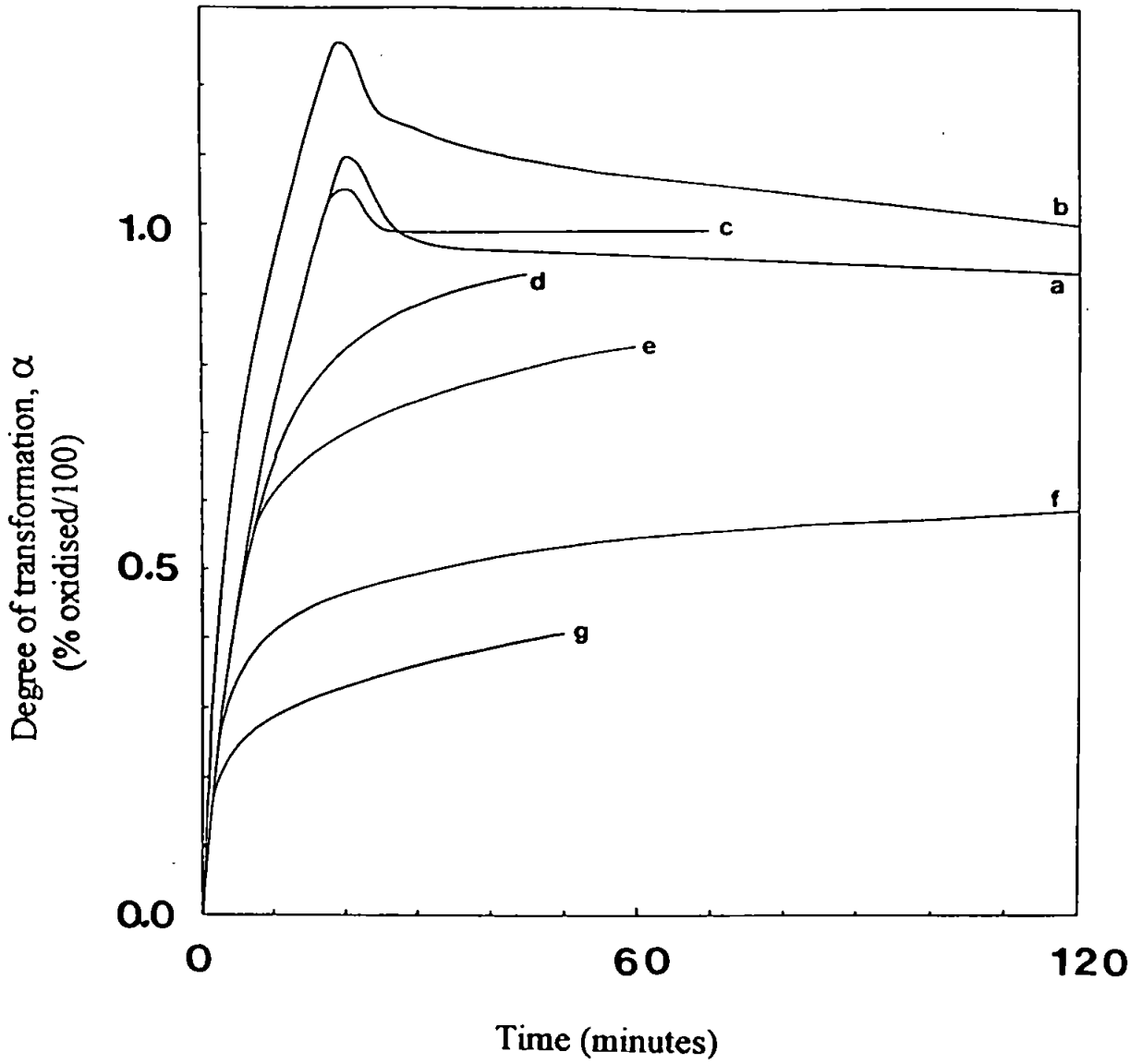

Figure 27
Isothermal TG curves for the oxidation of zirconium carbide in flowing air (300 ml min^{-1}) at a) 900 °C, b) 800 °C, c) 700 °C, d) 510 °C, e) 475 °C, f) 450 °C, g) 425 °C.

Temperature, T		$d\alpha/dt$	$\ln(d\alpha/dt)$	$1/T$
°C	K	x 10^{-3} sec^{-1}		x 10^{-3} K^{-1}
900	1173	5.83	-5.14	0.852
800	1073	2.78	-5.89	0.931
700	973	2.22	-6.11	1.027
510	783	1.67	-6.40	1.277
475	748	1.25	-6.69	1.336
450	723	1.25	-6.69	1.383
425	689	1.11	-6.80	1.432

Arrhenius plot
Gradient of slope = -1760 K
Correlation coefficient = -0.98

Table 8
Isothermal oxidation of zirconium carbide in air

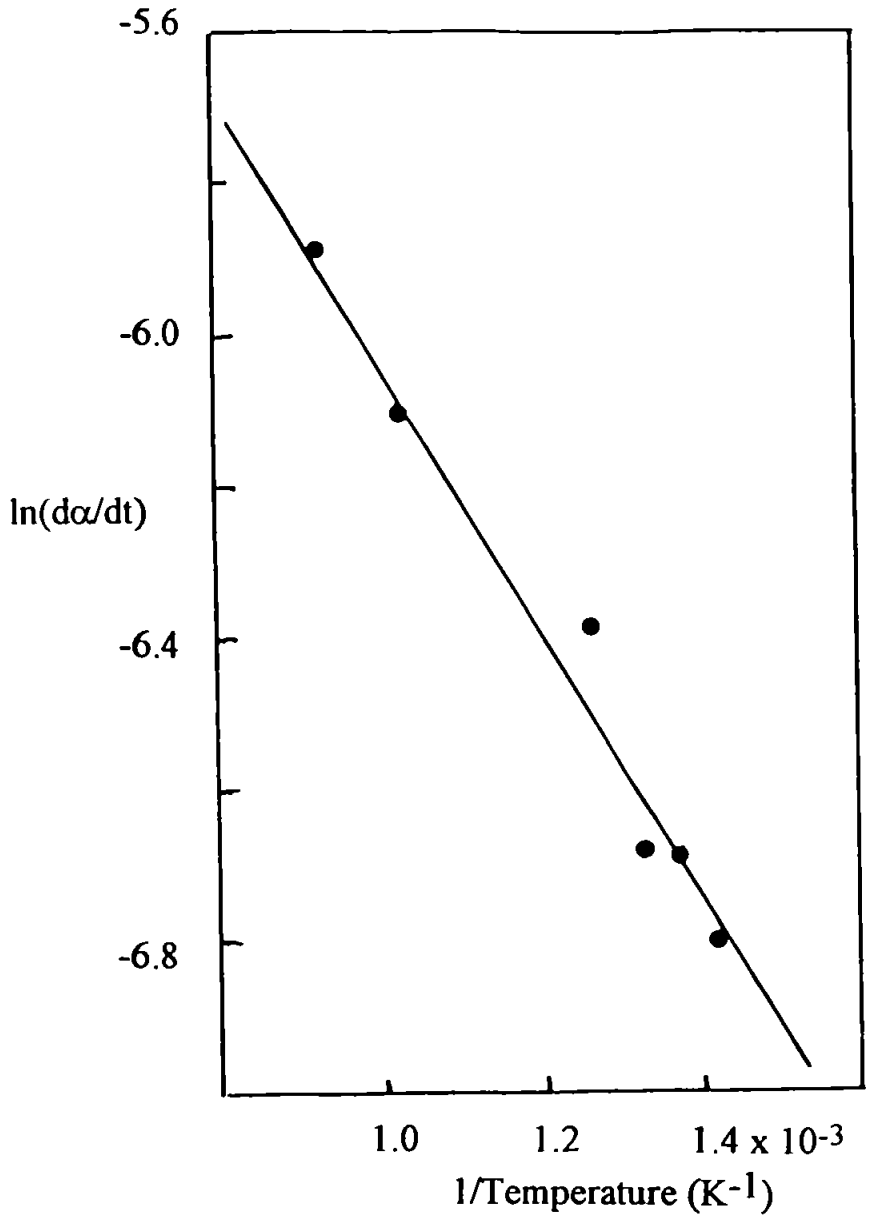

Figure 28
Arrhenius plot for the oxidation of zirconium carbide in air.

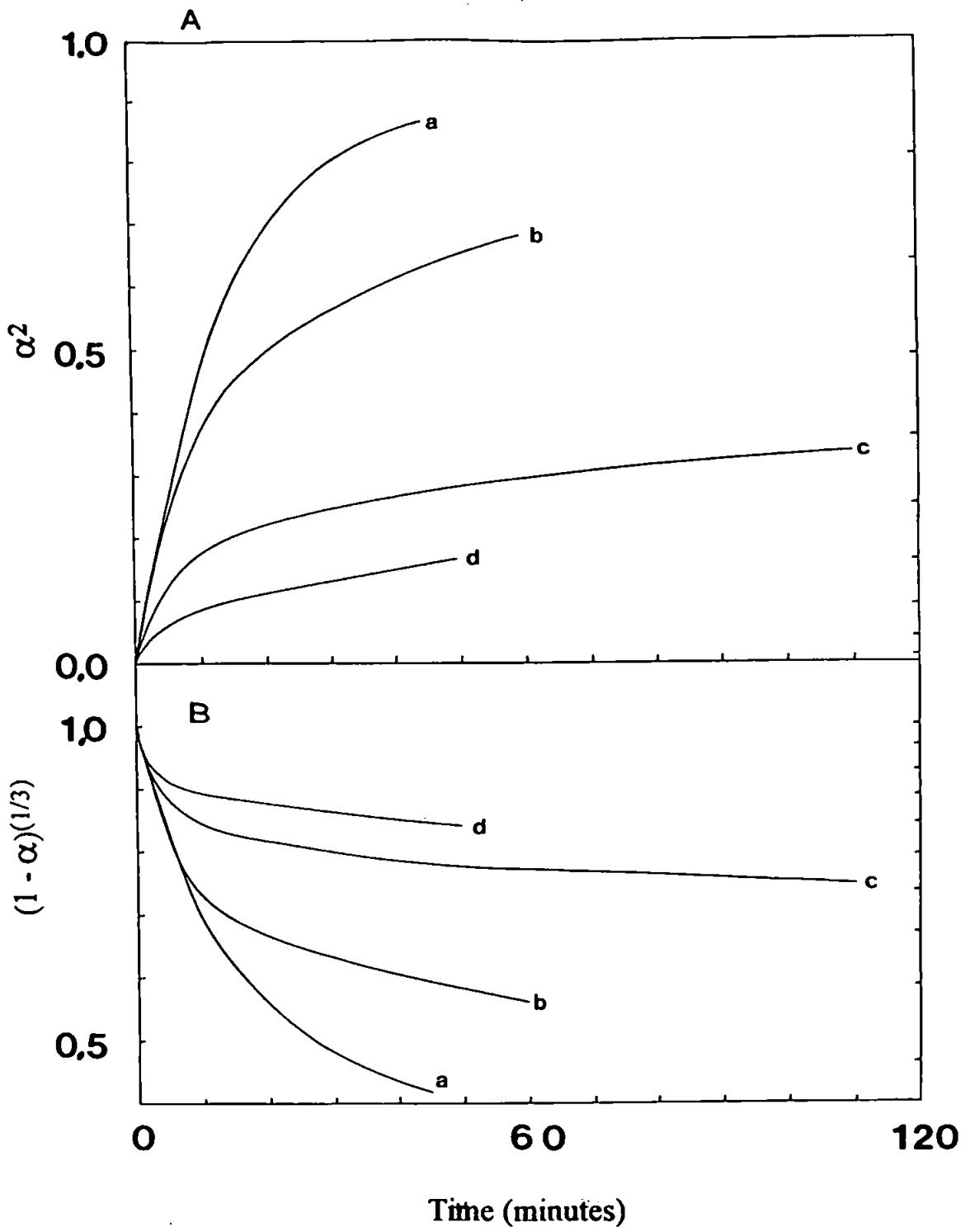

Figure 29
Half order (A) and two-thirds order (B) kinetic plots for the isothermal oxidation of zirconium carbide in air at a) 510 °C, b) 475 °C, c) 450 °C, d) 425 °C.

plot deviates from the expected straight line, indicating that the reaction was initially controlled by the diffusion of gas to or from the reaction site before the reaction was hindered by the presence of oxidation products around the remaining carbide particles. If the oxide is incompatible with the remaining carbide then two-thirds order kinetics, hindered by possible sintering of the oxide, would be expected. From dynamic TG studies, Rao and Venugopal (1994) found the reaction to follow half order kinetics and therefore diffusion controlled, the mechanism being determined by the diffusion of oxygen through the product layer. Zirconium oxide having a melting point of 2715 °C, limited sintering by surface diffusion is possible above 720 °C, and by crystal lattice diffusion above its Tammann temperature of 1220 °C. Thus, sintering of the product could not account for the observed behaviour in the temperature range studied.

X-ray diffraction studies showed the initial carbide to be face centred ZrC (a = 4.6980 Å, JCPDS card 19-1487). X-ray analyses (figure 30) showed that the carbide oxidised for two hours at 400 °C had formed a product with a cubic-F structure not listed in the JCPDS index. This product was dark blue in colour and gave an x-ray diffraction trace with peaks of equal size as the original carbide indicating that the product could crystallise at 400 °C. The (200) spacings of the carbide became the (111) spacing of an intermediate, which could be a sub-oxide or an oxycarbide. It is possible that this intermediate compound is the same as that formed at higher temperatures giving the increased weight gain seen in the mass flow experiments within the first 30 minutes, but at higher temperatures it decomposes before it can be recovered from the furnace and identified. The x-ray trace of the product produced after two hours at 500 °C showed a small amount of this intermediate indicated by the small peak at $2\Theta = 44.6$ °, the remaining oxide being cubic zirconia. At 600 °C and above no intermediate was detected. Oxide

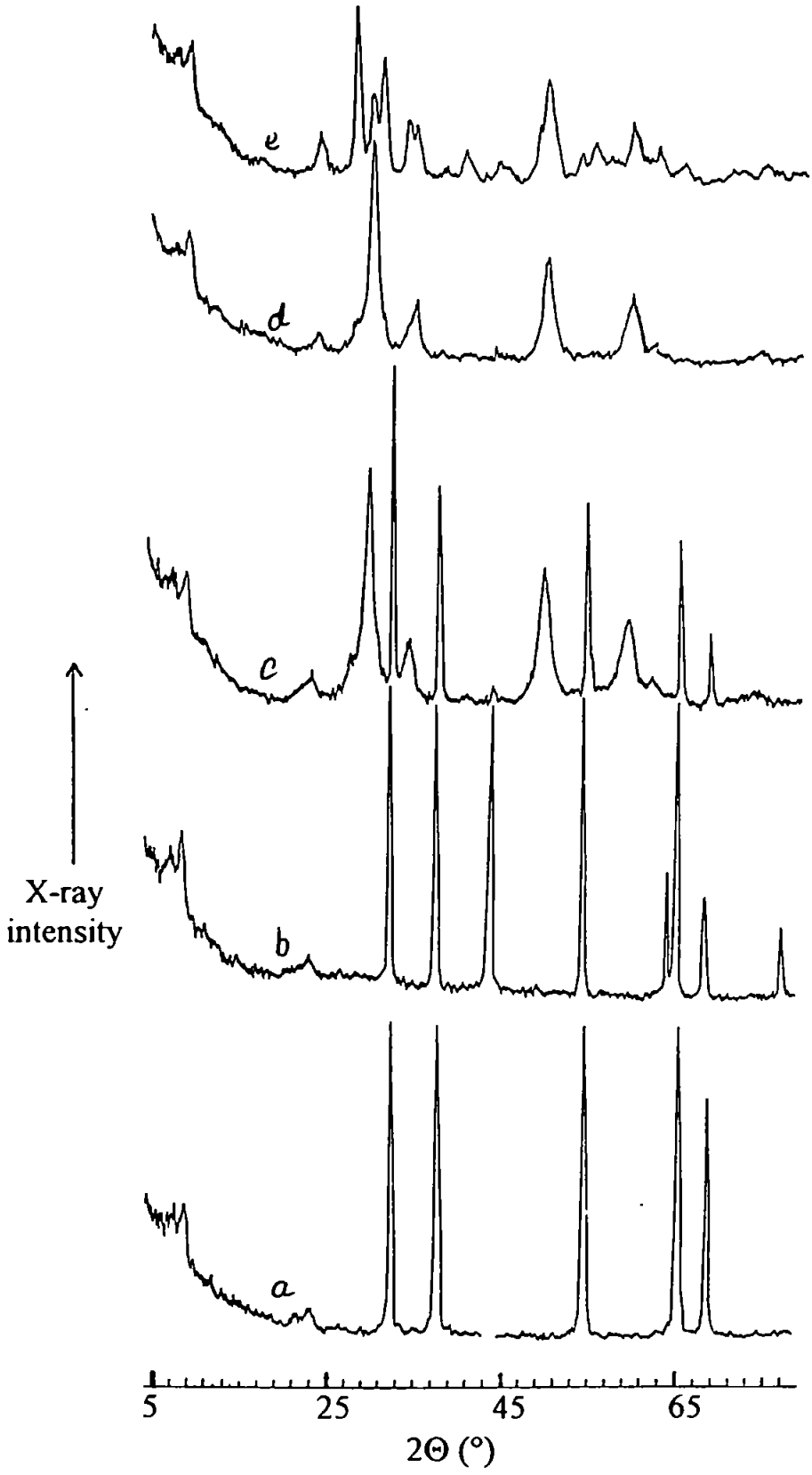

Figure 30
X-ray diffraction traces for zirconium carbide (a) and its oxidation products after two hours in air at b) 400 °C, c) 500 °C, d) 600 °C, e) 700 °C.

produced at 700 °C formed a mixture of cubic and monoclinic zirconia. Rao and Venugopal (1994) found that cubic zirconia was formed below 800 °C and the monoclinic form above 800 °C.

The initial carbide had as specific surface area of 0.59 m^2g^{-1} corresponding to an average crystallite size of 1.51 μm. At 500 °C, the oxide formed after 15 minutes had a surface area of 16.7 m^2g^{-1}, which declined to a surface area of 3.2 m^2g^{-1} after 20 hours. This indicated that sintering of the product occurred at temperatures lower than 723 °C (1/3rd melting point in K). This is illustrated in table 9 and figure 31. Figure 32 shows that the surface area of the oxidation products obtained after 1 hour's oxidation at various temperatures reached a maximum at 500 °C and declined at higher temperatures. This indicates that sintering of the oxide occurred at 500 °C and above.

The electron micrographs (plates 12 to 14) show that the original material consisted of angular particles ranging in size from 1 to 10 μm, whilst the products which resulted from exposure to temperatures of 1000 °C and above consisted of rounded particles of 1 μm that sintered into larger agglomerates.

Temperature °C	Calcining period hours	α	Specific Surface area m^2g^{-1}	Surface area of oxide m^2g^{-1}
Original material		0.00	0.59	
400	1	0.22	0.57	0.51
500	1/4	0.77	13.5	16.7
500	1/2	0.83	13.6	15.8
500	1	0.95	15.2	15.8
500	2	1.00	11.6	11.6
500	20	1.00	3.2	3.2
600	1	1.00	9.9	9.9
600	19	1.00	2.2	2.2
700	1	1.00	5.3	5.3

Table 9

Vaiation of specific surface area of zirconium carbide and oxide products with temperature and oxidation period.

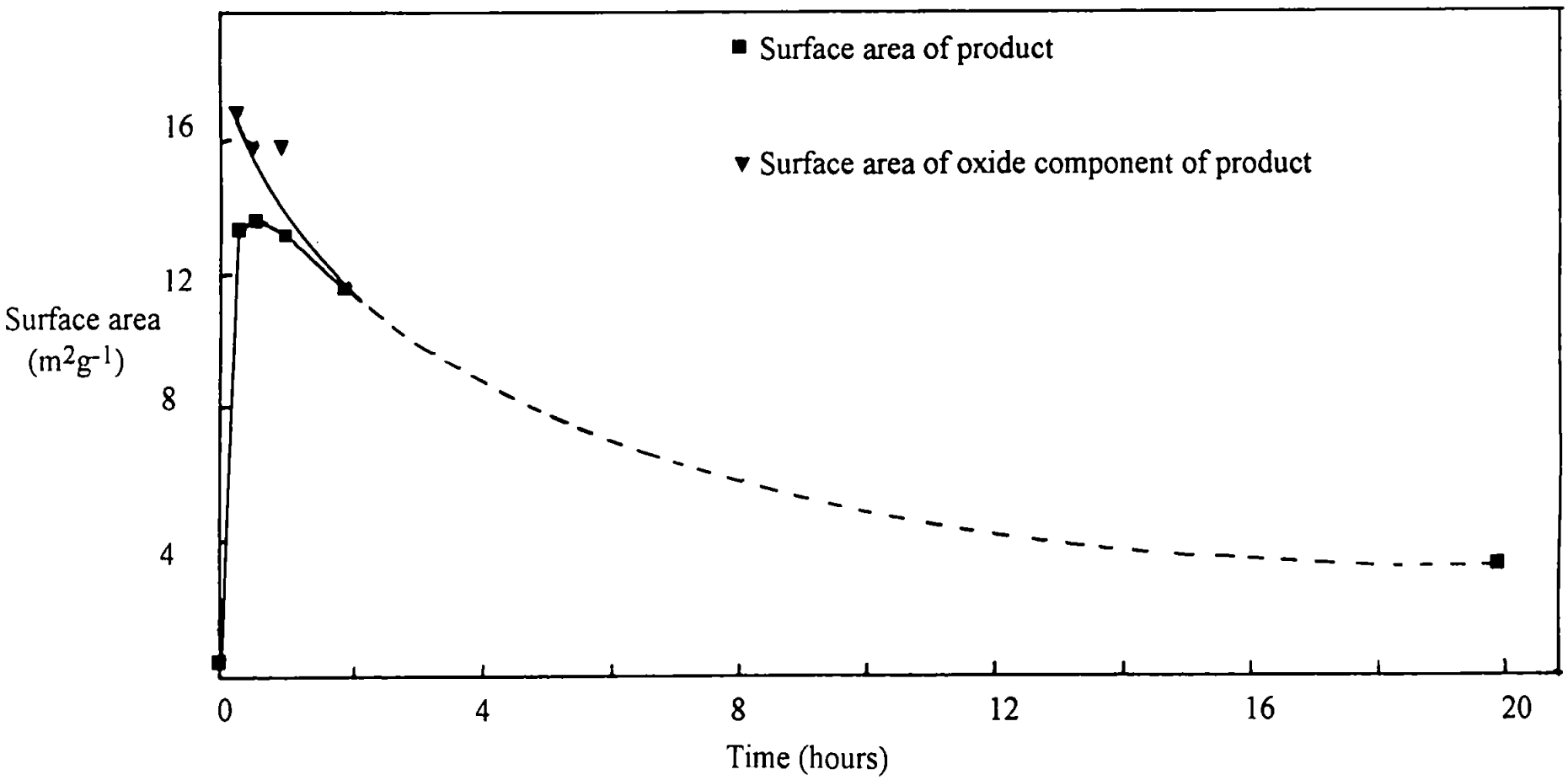

Figure 31
Surface area change for zirconium carbide and its oxidation products at 500 °C.

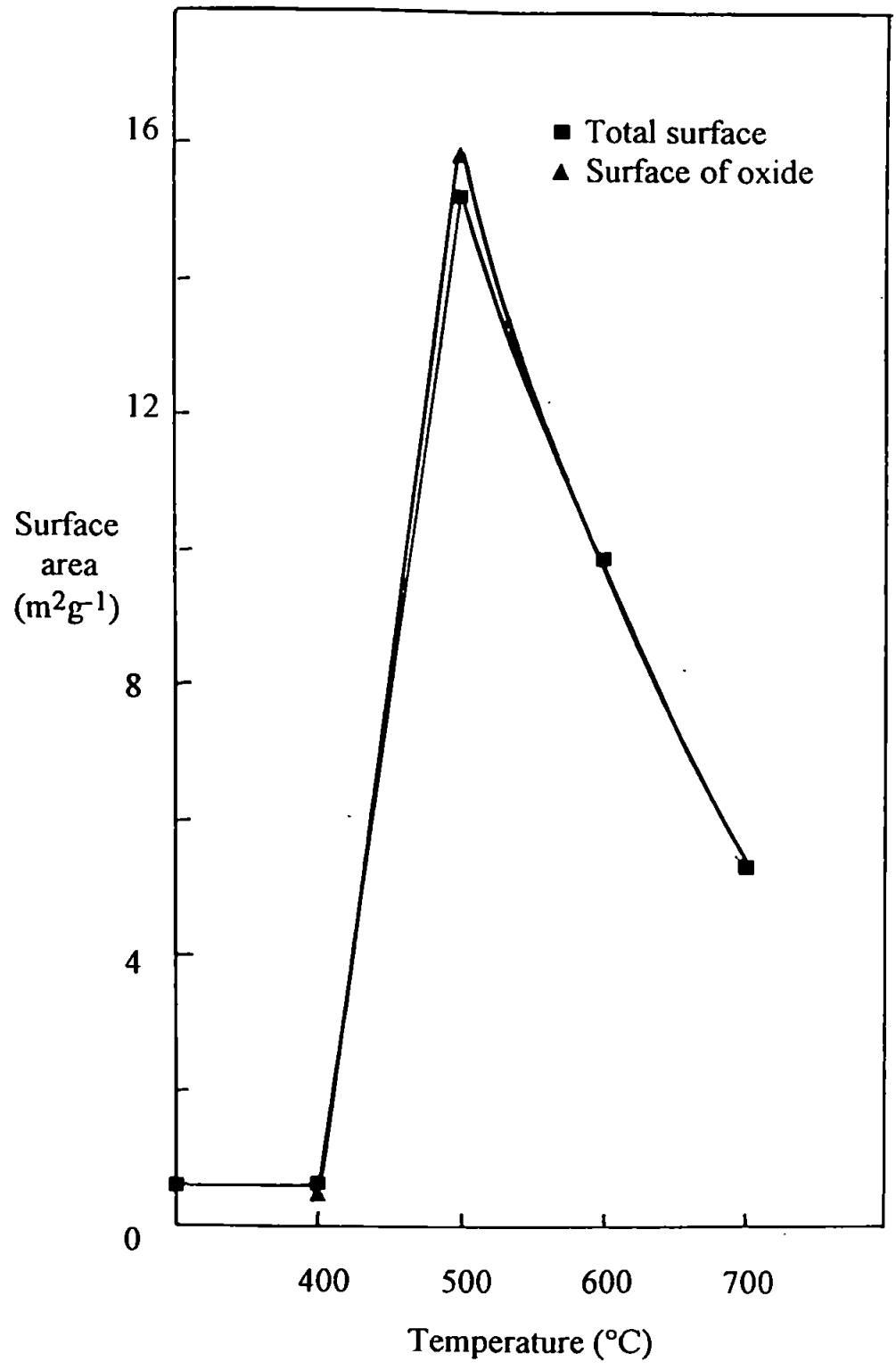

Figure 32
Surface area changes for zirconium carbide and its oxidation products after one hour in air.

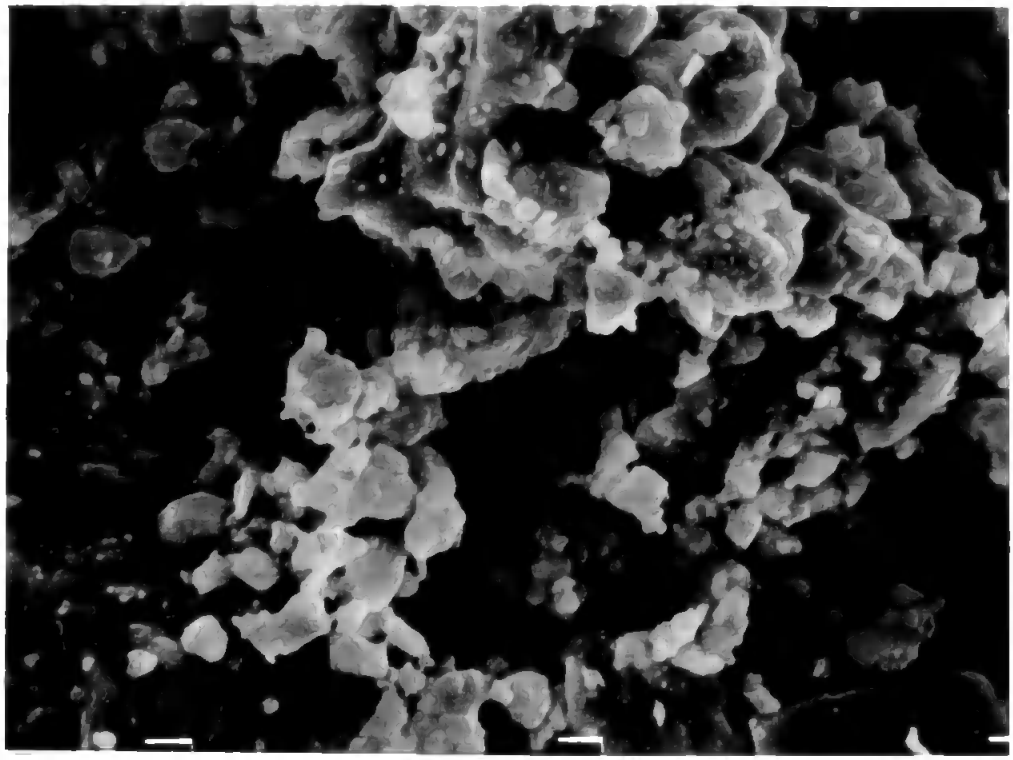

Plate 12
Zirconium carbide

10 μm

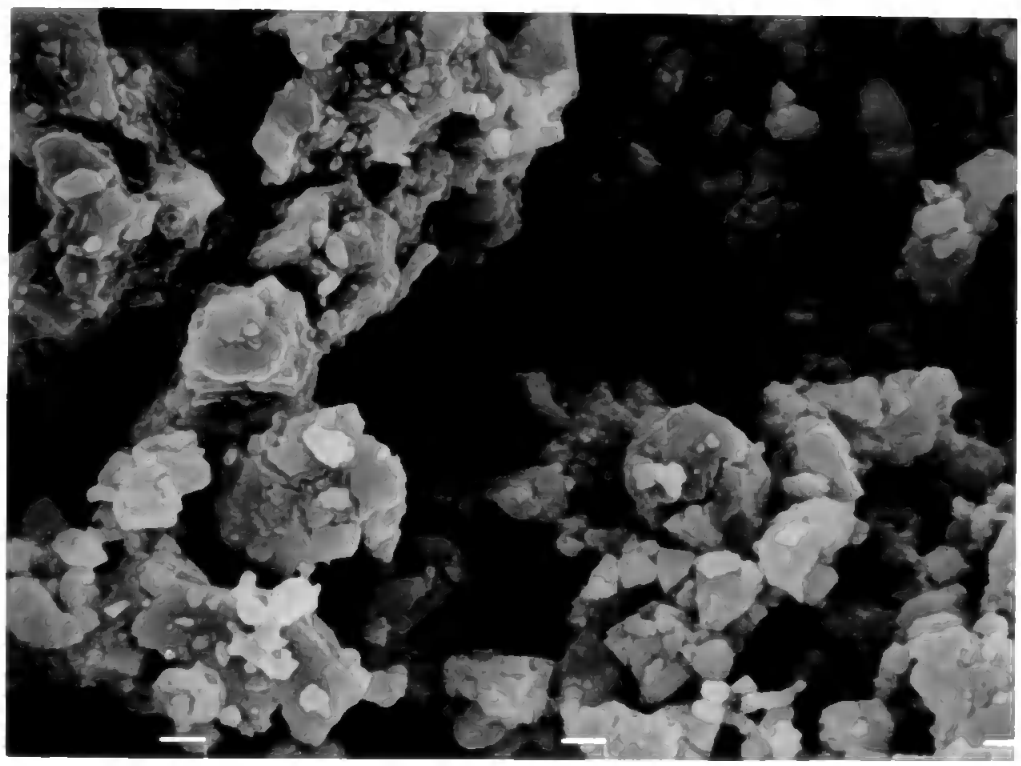

Plate 13
Zirconium carbide oxidised for 1 hour at 650 °C in air

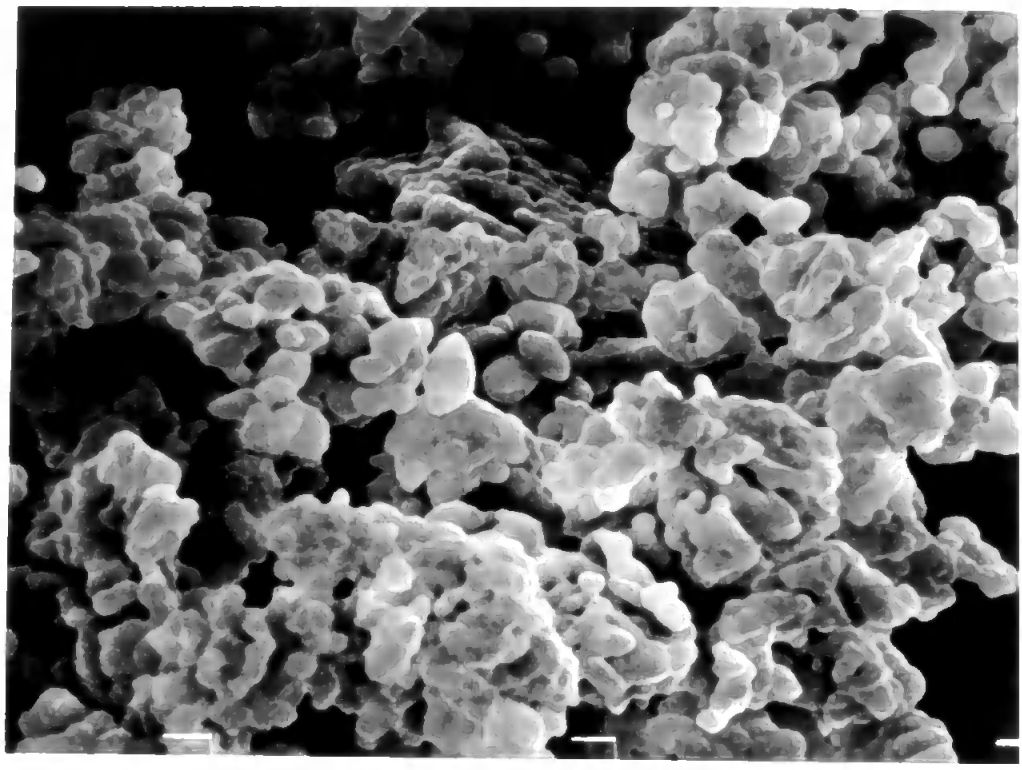

Plate 14
Zirconium carbide oxidised for 1 hour at 1300 °C in air

10 μm

3.4 OXIDATION OF VANADIUM NITRIDE AND CARBIDE IN AIR

X-ray diffraction analyses identified the carbide as the being cubic V_4C_3 (a = 4.16 Å, JCPDS card 1-1159), which on oxidation formed the orthorhombic pentoxide, V_2O_5 (shcherbinaite, a = 11.51 Å, b = 3.559 Å, c = 4.371 Å, JCPDS card 9-387). There was no pattern due to the sub-carbides V_2C and its carbon deficient carbides. V_4C_3 is cubic VC with a carbon composition near the low carbon phase boundary (Storms (1967)).

Vanadium can form many oxides (Kubaschewski and Hopkins (1962)). Of these oxides the pentoxide, V_2O_5, has a very low melting point (690 °C) therefore oxidations were performed below this temperature. It was found that above 600 °C there was significant sublimation of the oxide product, resulting in erroneous weight change measurements.

Preliminary dynamic oxidation of the carbide at 10 °C min^{-1} indicated that the reaction began at 390 °C, however, due to the sublimation of the brown pentoxide onto the surfaces of the reaction chamber the reaction could not be followed to completion on the thermobalance.

Isothermal oxidation at 400 °C (figure 33) showed that after an induction period of 10 minutes, the reaction proceeded at an almost constant rate, and after two hours had reached a value of $\alpha = 0.07$. At 500 °C a value of $\alpha = 0.33$ was achieved after two hours. At 600 °C and above the sublimation of the oxide produced resulted in the TG trace recording a smaller weight change than that expected if sublimation had not occurred.

The kinetic plots (figure 34) showed that at 600 and 650 °C the two-thirds order plots are linear for approximately the first 40 minutes, after which the loss of oxide by sublimation resulted in erroneous weight change

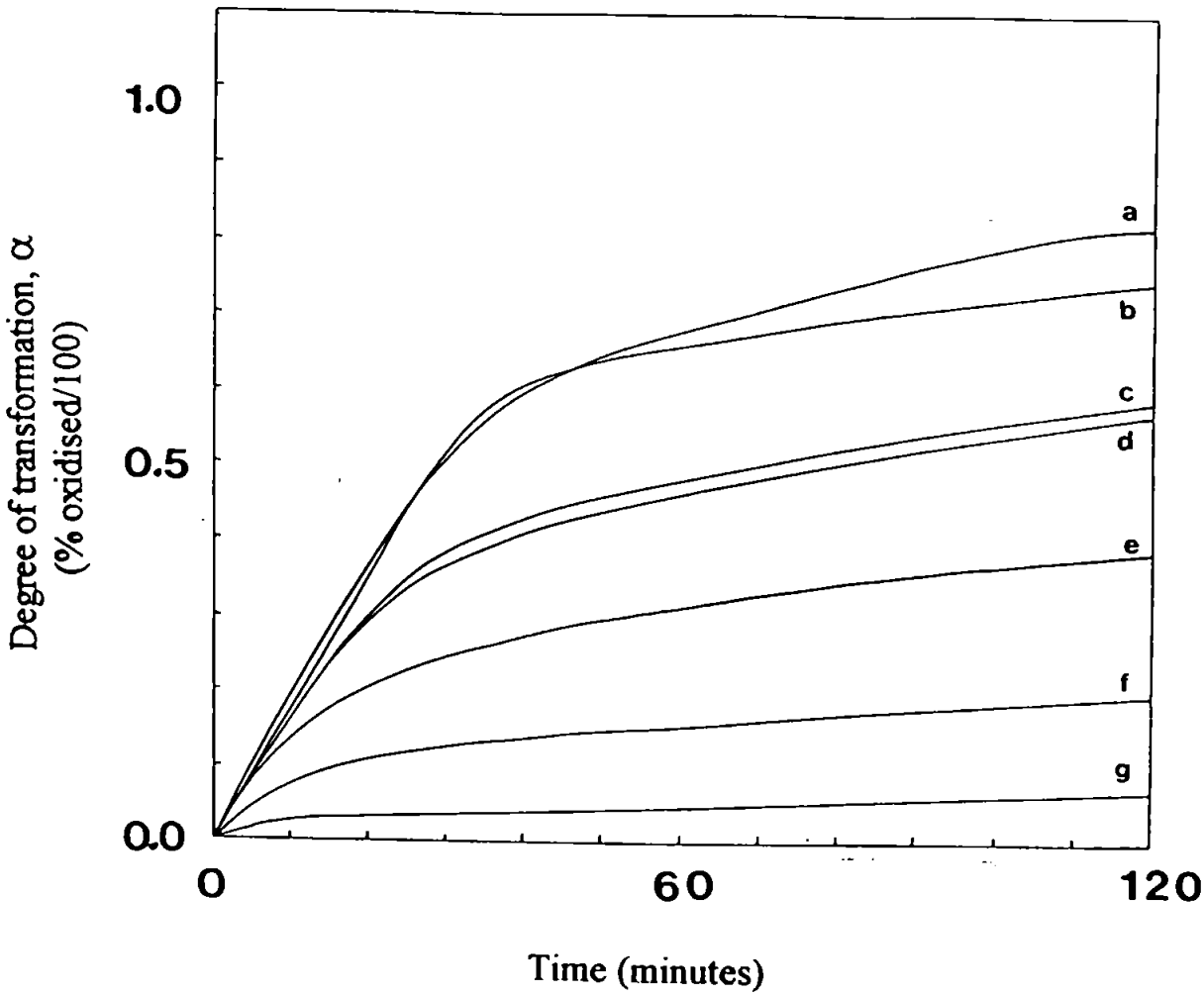

Figure 33
Isothermal TG curves for the oxidation of vanadium carbide in flowing air (300 ml min^{-1}) at a) 650 °C, b) 600 °C, c) 550 °C, d) 550 °C, e) 500 °C, f) 450 °C, g) 400 °C.

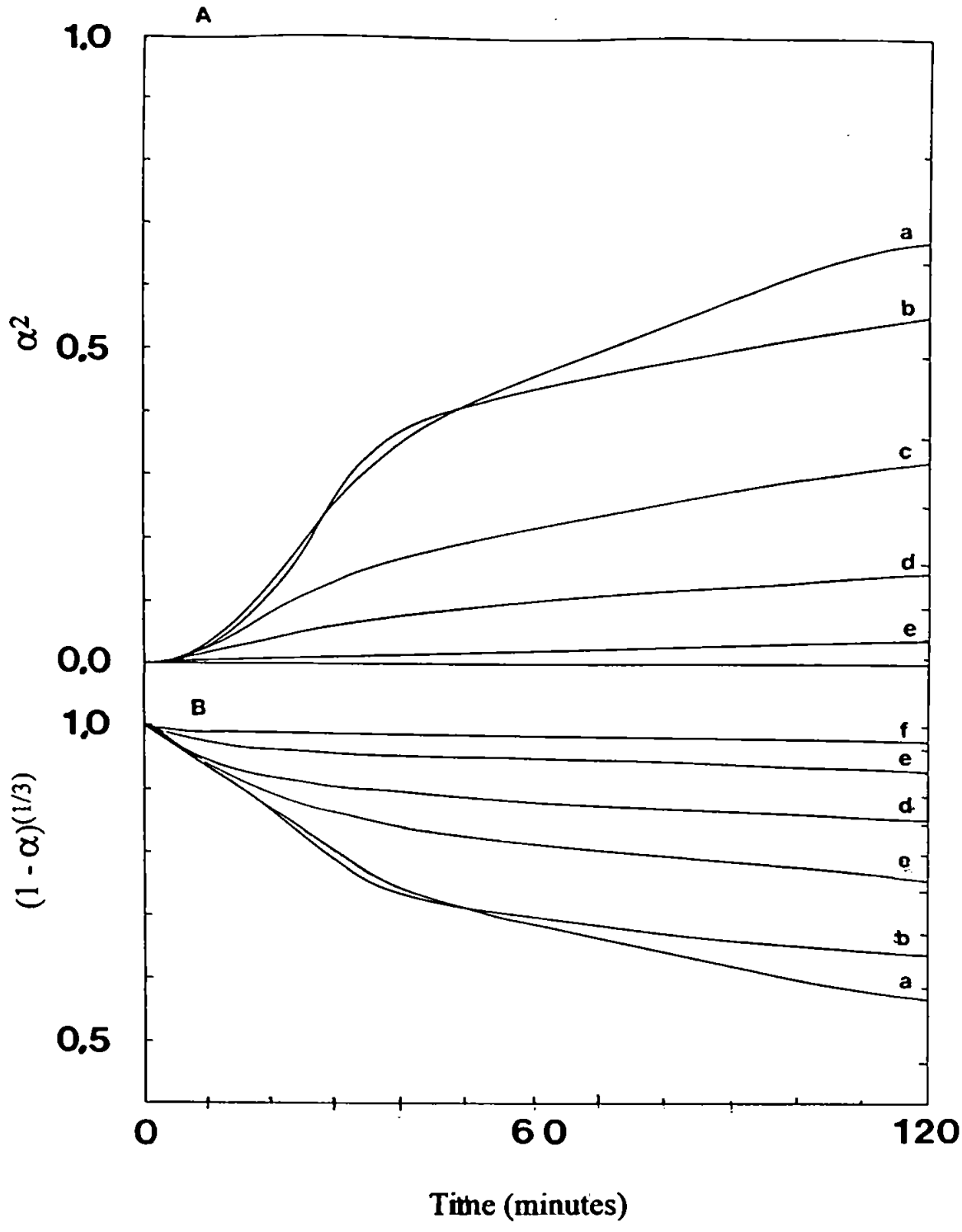

Figure 34
Half order (A) and two-thirds order (B) kinetic plots for the isothermal oxidation of vanadium carbide in air at a) 650 °C, b) 600 °C, c) 550 °C, d) 500 °C, e) 450 °C, f) 400 °C.

measurements. This indicates that at these temperatures the reaction initially occured at the surface of a diminishing sphere. At 400 °C the half order kinetic plot is linear for 2 hours, indicating that the diffusion of gas to the reaction site was the rate limiting step. In between these temperatures neither the half order nor two-thirds order kinetic plots are linear. The low melting point of the pentoxide (690 °C) results in extensive sintering of the product, which may sinter by surface diffusion at temperatures above 48 °C and by crystal lattice diffusion above its Tammann temperature of 208 °C. Whilst it is expected that the oxide layer would be incompatible with the underlying carbide due to the large change in density (5.77 to 3.36 g cm^{-3}) and the change in crystal structure (cubic to orthorhombic), the ability of the oxide to sinter at low temperatures will stabilize the oxide layer and hinder the reaction. Thus it would be expected that the rate of reaction would be determined by the diffusion of oxygen through the product layer, giving rise to half order kinetics. This is what is observed at 400 °C.

The Arrhenius plot for the reaction (table 10 and figure 35) does not give a straight line over the temperature range 400 to 650 °C. It is assumed that at the higher temperatures the loss of oxide due to sublimation gives rise to deviation from a straight line. If data from the lower temperatures only is used the activation energy is calculated to be 76.8 ± 20 kJ mol^{-1}. The large uncertainty is due to only three points on the graph being used.

Due to the very low melting point of the oxide, the products at all temperatures were extensively sintered.

It proved impossible to successfully oxidise the nitride without the oxide formed subliming, leading to gross contamination of the reaction chamber and balance and inconsistent TG curves.

Temperature, T		dα/dt	ln(dα/dt)	1/T
°C	K	x 10^{-4} sec^{-1}		x 10^{-3} K^{-1}
650	923	2.98	-8.12	1.08
600	823	3.09	-8.08	1.15
580	853	2.67	-8.23	1.17
550	823	2.67	-8.23	1.22
500	773	2.70	-8.22	1.29
450	723	1.56	-8.76	1.38
400	673	0.46	-9.98	1.49

Arrhenius plot
Gradient of slope = -9240 K
Correlation coefficient = -0.98

Table 10
Isothermal oxidation of vanadium carbide in air

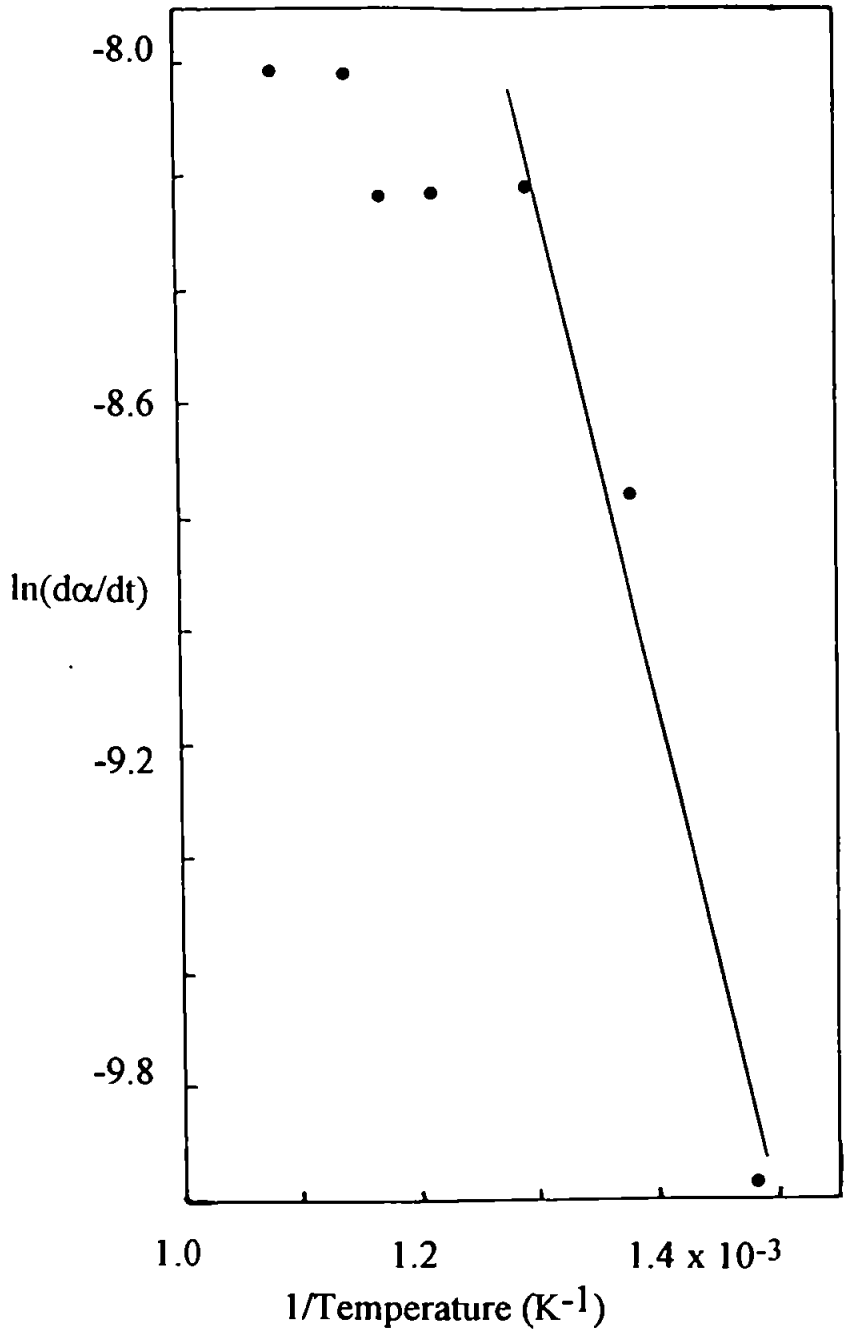

Figure 35
Arrhenius plot for the oxidation of vanadium carbide in air.

3.5 OXIDATION OF NIOBIUM CARBIDE IN AIR

X-ray analysis of the carbide showed that the initial material was cubic niobium carbide, NbC (a = 4.4702, JCPDS card 10-181), without any indication of the sub-carbide, Nb_2C, or any other contaminant. Dynamic oxidation of niobium carbide at 10 °C min^{-1} indicated that the reaction started at about 350 °C, and the weight change (26.7 %) was consistent with the carbide NbC being oxidised to Nb_2O_5 without any of the sub-carbide being present.

Isothermal oxidation of the carbide (figure 36 - for clarity not all curves are shown but initial gradients are given in table 11) indicates that at temperatures below 450 °C the reaction occurs relatively slowly, being only 12.5 % ($\alpha = 0.125$) oxidised at 375 °C after two hours, 13.5 % ($\alpha = 0.135$) at 400 °C, and 50 % ($\alpha = 0.5$) at 450 °C. Above 450 °C the reaction proceeded more vigorously. The reaction is exothermic and therefore the sample was heated by the energy liberated by the reaction. This was illustrated by a sample heated to 500 °C in a nitrogen atmosphere. On admitting air into the reaction chamber the sample was heated by the liberated energy up to 520 °C as the reaction proceeded, leading to 96 % oxidation ($\alpha = 0.96$) after 40 minutes. At 800 °C the reaction was complete within 20 minutes. Between 400 and 500 °C the TG curves became very difficult to reproduce due to the liberated heat causing the sample temperature to vary during the reaction. Figure 37 shows the sample thermocouple trace during heating of the sample and subsequent oxidation, deviation from the selected temperature caused by the reaction is clearly seen.

The kinetic plots (figure 38) show that at low temperature (450 °C and below) an initial induction period occurs after which the two-thirds order plots are linear. Niobium pentoxide has a relatively low melting point of 1520 °C and

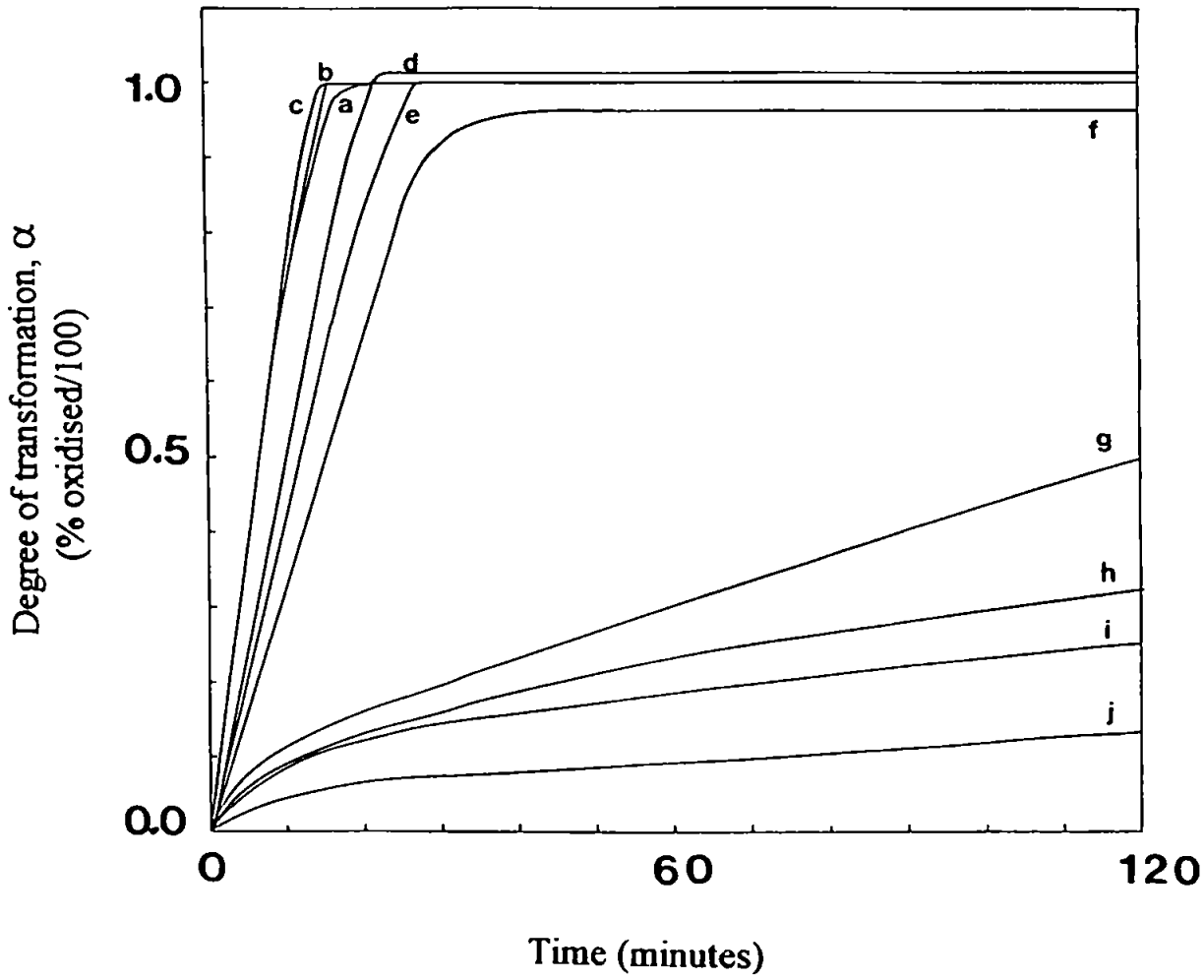

Figure 36
Isothermal TG curves for the oxidation of niobium carbide in flowing air (300 ml min^{-1}) at a) 900 °C, b) 800 °C, c) 700 °C, d) 600 °C, e) 550 °C, f) 500 °C, g) 450 °C, h) 425 °C, i) 400 °C, j) 375 °C.

Temperature, T		dα/dt	ln(dα/dt)	1/T
°C	K	x 10^{-4} sec^{-1}		x 10^{-3} K^{-1}
900	1173	12.32	-6.70	0.83*
800	1073	12.06	-6.72	0.93*
700	973	12.12	-6.71	1.03
600	873	7.90	-7.14	1.15
550	823	7.18	-7.24	1.22
500	773	5.09	-7.58	1.29
475	748	9.55	-6.95	1.34*
		9.23	-6.99	1.34*
460	733	9.42	-6.96	1.36*
456	728	9.30	-6.98	1.37*
450	723	4.45	-7.71	1.38
		6.24	-7.38	1.38*
		4.86	-7.63	1.38*
440	713	9.43	-6.97	1.40*
430	703	4.99	-7.60	1.42
425	698	3.74	-7.89	1.43
400	673	5.41	-7.52	1.48*
		2.99	-8.11	1.48
375	648	2.37	-8.34	1.54

Arrhenius plot
Data points marked * are not used for calculation of activation energy.
Gradient of slope = -3020 K
Correlation coefficient = -0.99

Table 11
Isothermal oxidation of niobium carbide in air

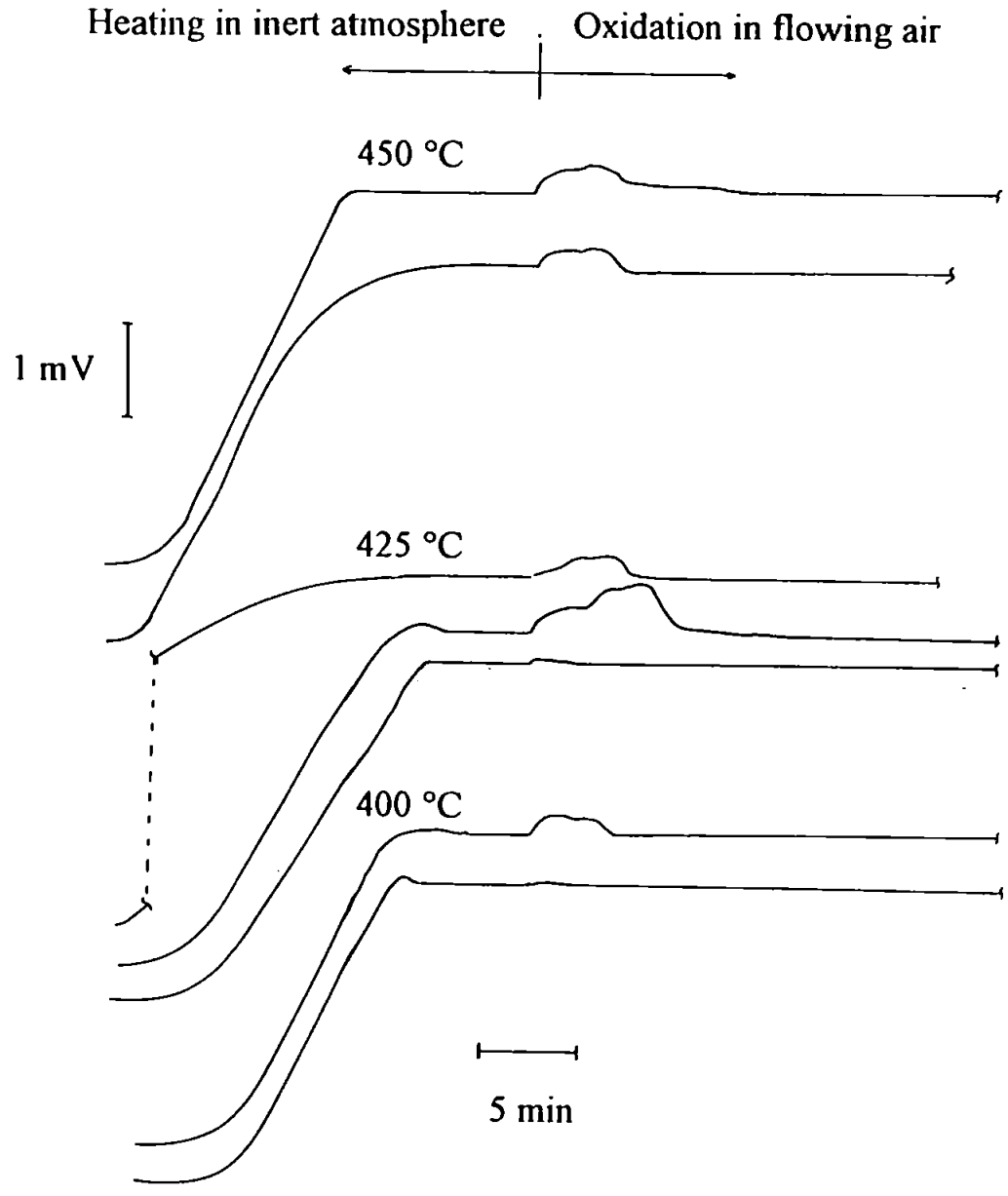

Figure 37
mV output from thermocouple monitoring sample temperature during oxidation in air of niobium carbide heated to indicated temperature.

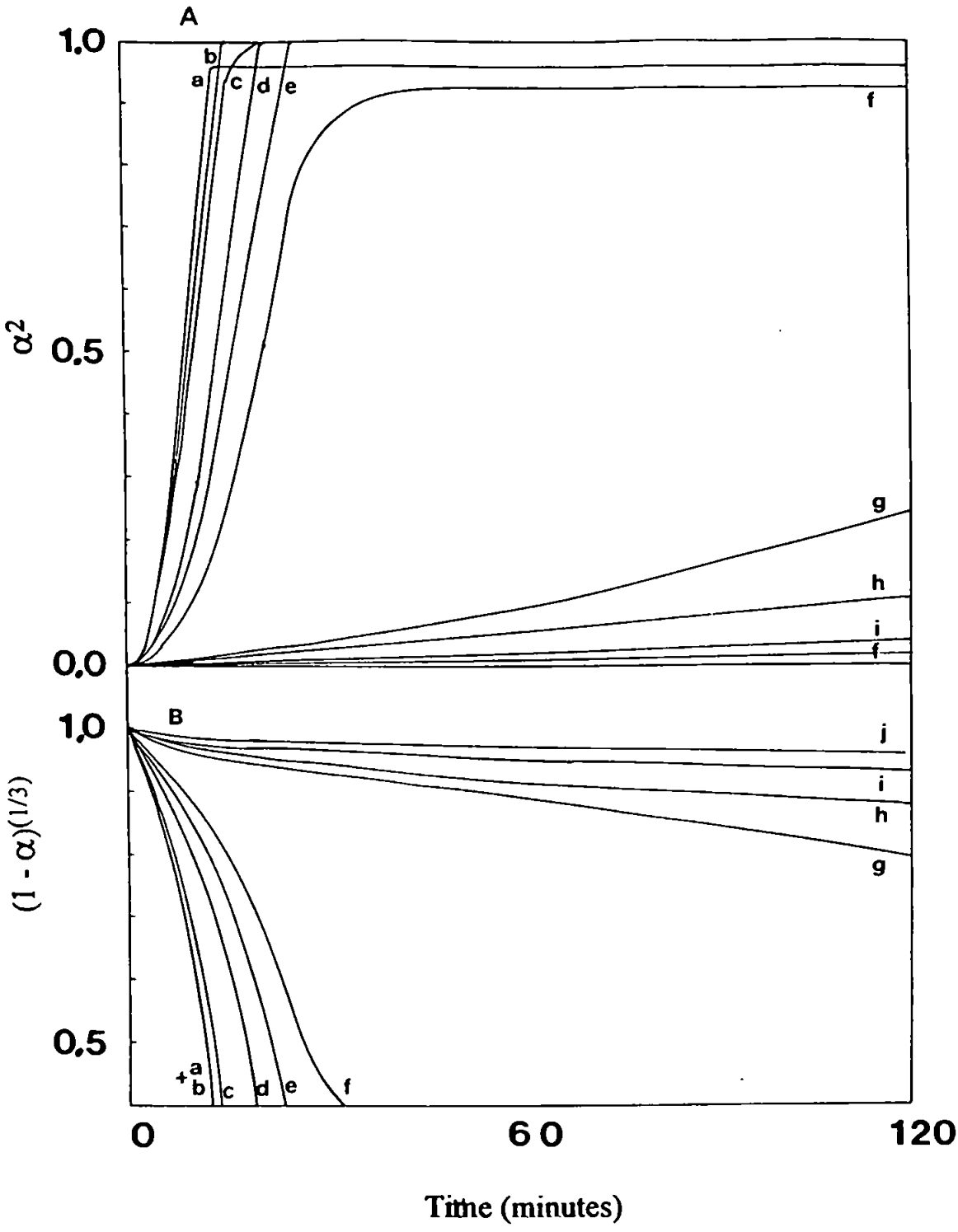

Figure 38.
Half order (A) and two-thirds order (B) kinetic plots for the isothermal oxidation of niobium carbide in air at a) 900 °C, b) 800 °C, c) 700 °C, d) 600 °C, e) 550 °C, f) 500 °C, g) 450 °C, h) 425 °C, i) 400 °C, j) 375 °C.

thus the oxide may sinter by surface diffusion above 324 °C and by crystal lattice diffusion above its Tammann temperature of 623 °C. The carbide having a melting point of 3500 °C, can sinter by surface diffusion above 940 °C, thus prolonged heating at these temperatures before oxidation commences may affect the subsequent reaction. This indicates that the reaction occurred at the surface of a diminishing sphere, without any hinderance due to gas having to diffuse through a product layer. At higher temperatures the half order kinetic plots are linear after an initial period indicating that after $\alpha \approx 0.3$ the rate of reaction is controlled by the diffusion of oxygen through the oxide layer. It would be expected that the variation in density of the carbide compared to the oxide (7.82 and 4.47 g cm^{-3} respectively), and the change in crystal structure from cubic to monoclinic (at 800 °C) would make the oxide layer incompatible with the underlying carbide particle resulting in a lack of adhesion. This would cause the oxide to spall and thus provide little protection to further oxidation of the carbide. However, at temperatures between 550 and 900 °C, the diffusion of oxygen through the oxide product does control the kinetics of the reaction. At temperatures around 450 °C the exothermic nature of the reaction also affects the kinetics of the reaction. Whilst the diffusion of oxygen through an oxide layer determines the rate of the reaction at temperatures between 550 and 900 °C, sintering of the oxide layer does not appear to proceed fast enough to hinder the reaction significantly.

The Arrhenius plot (table 11 and figure 39) indicates that, except at higher temperatures (700 to 900 °C), those samples that were able to dissipate the energy released by the reaction form a straight line. Those samples that could not dissipate the energy sufficiently quickly, and were therefore heated by the energy liberated by the reaction, lie to the right of the line and have not been used in the calculation of the gradient of the graph and hence the activation

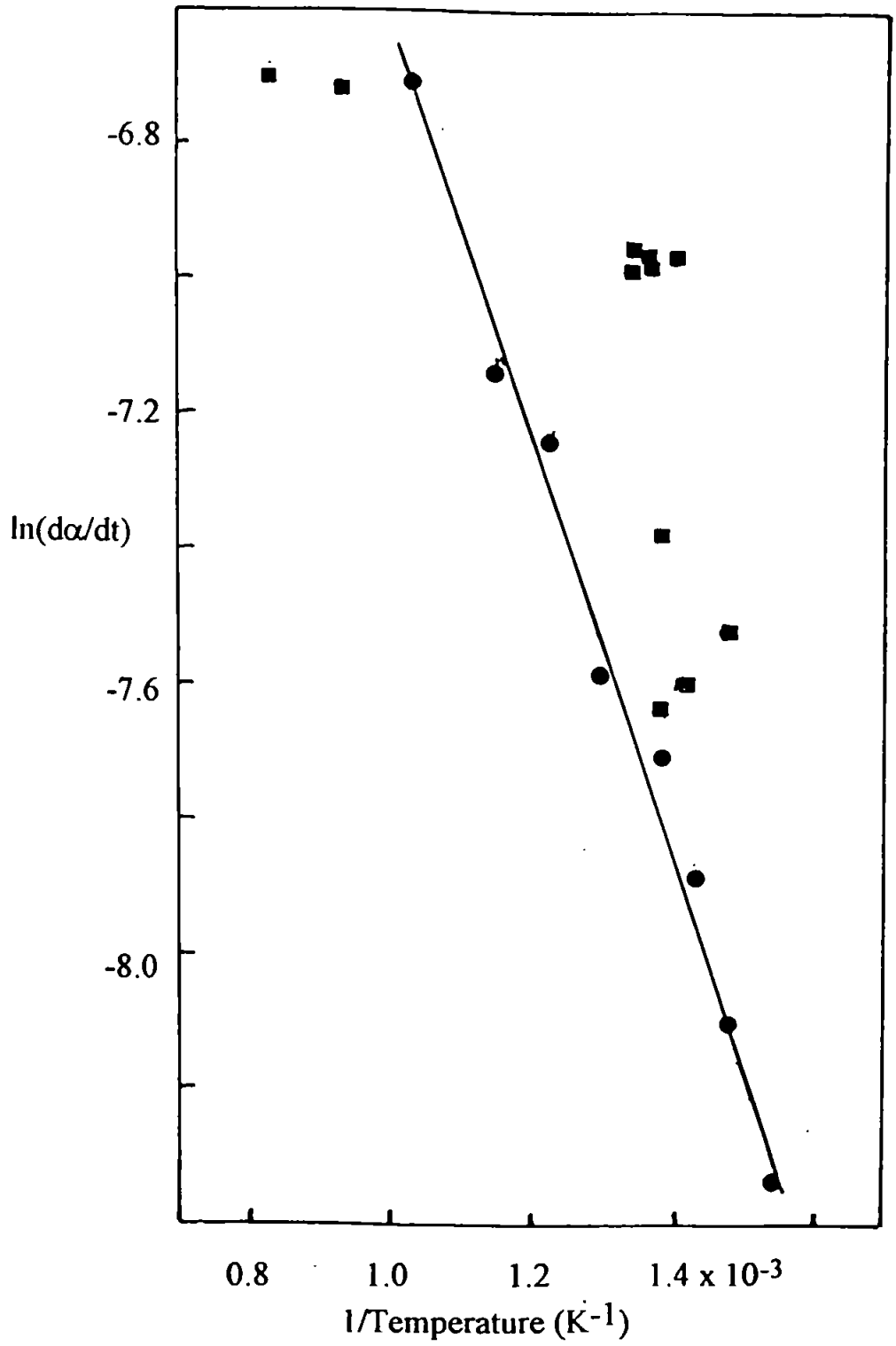

Figure 39
Arrhenius plot for oxidation of niobium carbide in air.

energy. From the data points used, the activation energy was calculated to be 25.1 ± 0.3 kJ mol^{-1}.

After 2 hour oxidation at 400 °C, x-ray analysis of the products indicated that the only material detectable was the original cubic carbide. Thus although the carbide is 26 % oxidised, the oxide does not crystallize in detectable quantities. At 450 °C the diffraction pattern produced by Nb_2O_5 was detected (JCPDS card 5-0352). At 800 °C the oxide formed had a different x-ray pattern. Possible products are β-Nb_2O_5 (monoclinic), α-$Nb_{12}O_{29}$ (monoclinic), β-$Nb_{12}O_{29}$ (orthorhombic), 2($Nb_{47}O_{116}$) (monoclinic) and NbO_2 all of which have very similar x-ray patterns. The weight gain (26.7 %) indicated that the product was not NbO_2. The other oxides have niobium to oxygen ratios of approximately 2:5 and are therefore probably oxygen deficient forms of β-Nb_2O_5. As the reaction took place in an oxygen rich environment the product is probably β-Nb_2O_5 (monoclinic, a = 22.10 Å, b = 7.638 Å, c = 19.52 Å, β = 118°15', JCPDS card 19-862). This is in agreement with Ali (1970) who found that milled niobium nitride oxidised between 300 and 800 °C formed β-Nb_2O_5.

3.6 OXIDATION OF CHROMIUM NITRIDE AND CARBIDE IN AIR

X-ray diffraction analysis of the nitride as supplied, indicated that both nitrides were present, cubic CrN (carlsbergite, a = 4.140 Å, JCPDS card 11-65) being the main constituent with small quantities of hexagonal Cr_2N (a = 4.78, c = 4.44 Å, JCPDS cards 1-1232 and 27-127). During dynamic oxidation of the nitride at 10 °C min^{-1}, the weight increase was 16.73 % compared with the expected 15.15 % for pure CrN. This experimental weight gain corresponds to an initial composition of 88.4 wt-% CrN and 11.6 wt-% Cr_2N. X-ray analysis of the product after heating to 1200 °C showed that the only phase present was hexagonal (rhombohedral) Cr_2O_3 (eskolaite, a = 4.954, c = 13.584 Å, JCPDS card 6-504).

Dynamic heating of chromium nitride at 10 °C min^{-1} to 1250 °C in an inert atmosphere (argon) indicated that at temperatures above 900 °C the nitride began to decompose (figure 40). The decomposition occurred as two overlapping reactions, the final weight loss being 18.75 % after heating to 1256 °C. This temperature was then maintained for 30 minutes. The expected weight loss for total decomposition of the mixed nitride to the metal is 20.14 %. The two decompositions, although overlapping, are of approximately equal magnitude and therefore indicate that the cubic CrN initially decomposed to the hexagonal Cr_2N which then decomposed further to the metal. Had the Cr_2N decomposed before CrN then the decomposition curve would have shown a small weight loss as the minor constituent decomposed followed by the larger weight loss of CrN decomposing directly to the metal. Due to the significant decomposition of the nitride at temperatures above 1000 °C, oxidations were not performed above this temperature.

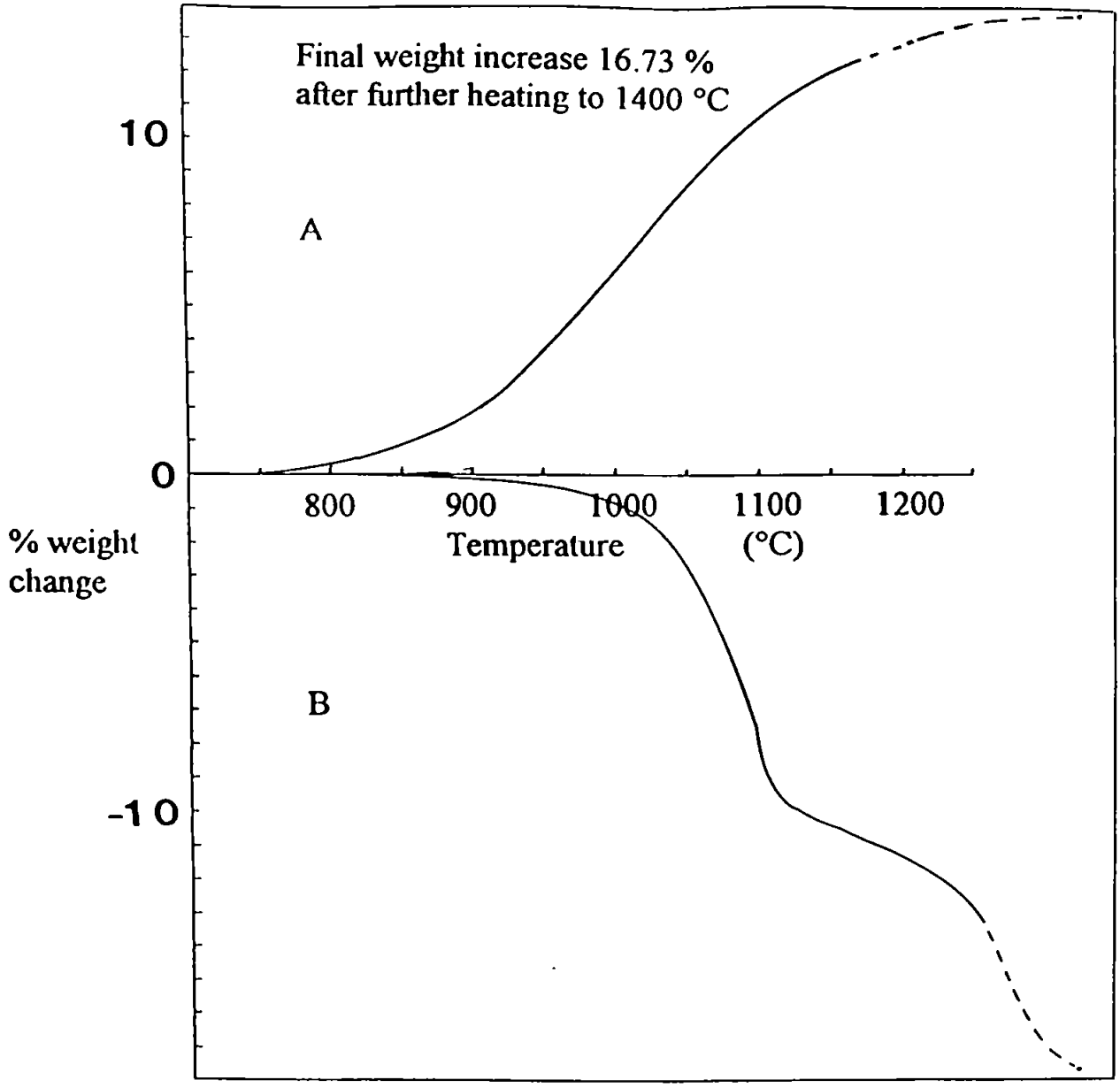

Figure 40
Chromium nitride heated at 10 °C min-1 in (A) air showing oxidation, and (B) argon showing decomposition.

The results of isothermal oxidations of the nitride are shown in figure 41. At 800 °C the nitride was only 18.5 % oxidised after 20 hours. The specific surface area of the nitride was found to be 1.6 m^2g^{-1} corresponding to an average crystallite size of 0.62 μm which on oxidation at 800 °C for 20 hours was reduced to 0.35 m^2g^{-1} (figure 42a). Allowing for the weight increase from 1.00 g to 1.03 g (3.1 %) during the oxidation, this corresponds to a decrease of the surface area of 1 g of nitride from 1.6 to 0.36 m^2. Theoretically the change in volume of 1 g of nitride to 1.152 g of oxide should be from 0.164 to 0.221 cm^3 (densities for these compounds are 6.1 and 5.23 g cm^{-3} respectively) representing a 0.346-fold increase in volume. If the oxide forms a stable film around the nitride, the surface area change should be given by $S'/S = (1 + 0.346\alpha)^{2/3}$ (figure 42b) thus for 18.5 % oxidation the surface area should increase from 1.6 to 1.68 m^2g^{-1}. As the experimental value is less than the theoretical, the oxide layer must be stable and extensively sintered. Figure 42c shows the increase in average crystallite size from 0.62 to 2.9 μm and figure 42d the decrease in surface area. Chromium oxide, having a melting point of 2400 °C, can sinter at temperatures above 650 °C by surface diffusion and by crystal lattice diffusion above its Tammann temperature of 1050 °C. Therefore during oxidation at 1000 °C, where oxidation was 82 % complete within 5 hours, there was considerable sintering and the reaction was hindered by the sintered oxide. The reaction took a further 10 hours before reaching completion. Plates 15 to 18 shows the original nitride and some of its oxidation products. At 800 °C the oxidation products are smaller and more angular than those at 1000 °C which are larger and rounded.

The stable oxide film around the remaining nitride inhibits further oxidation. At 800 °C the reaction curve was parabolic in shape for the first 5 hours (figure 43b), after 10 hours the reaction rate became constant (figure 43a). The

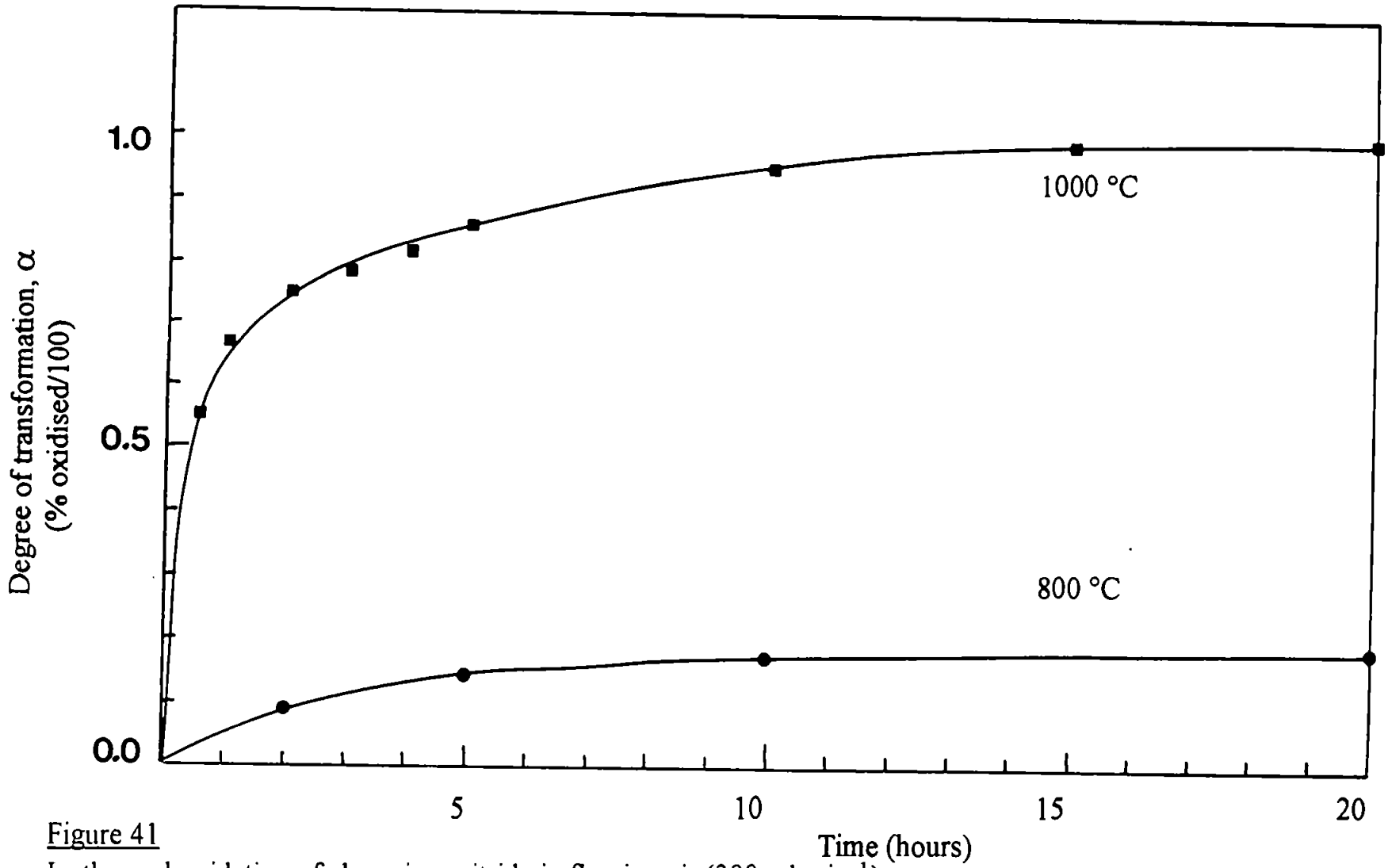

Figure 41
Isothermal oxidation of chromium nitride in flowing air (300 ml min^{-1}).

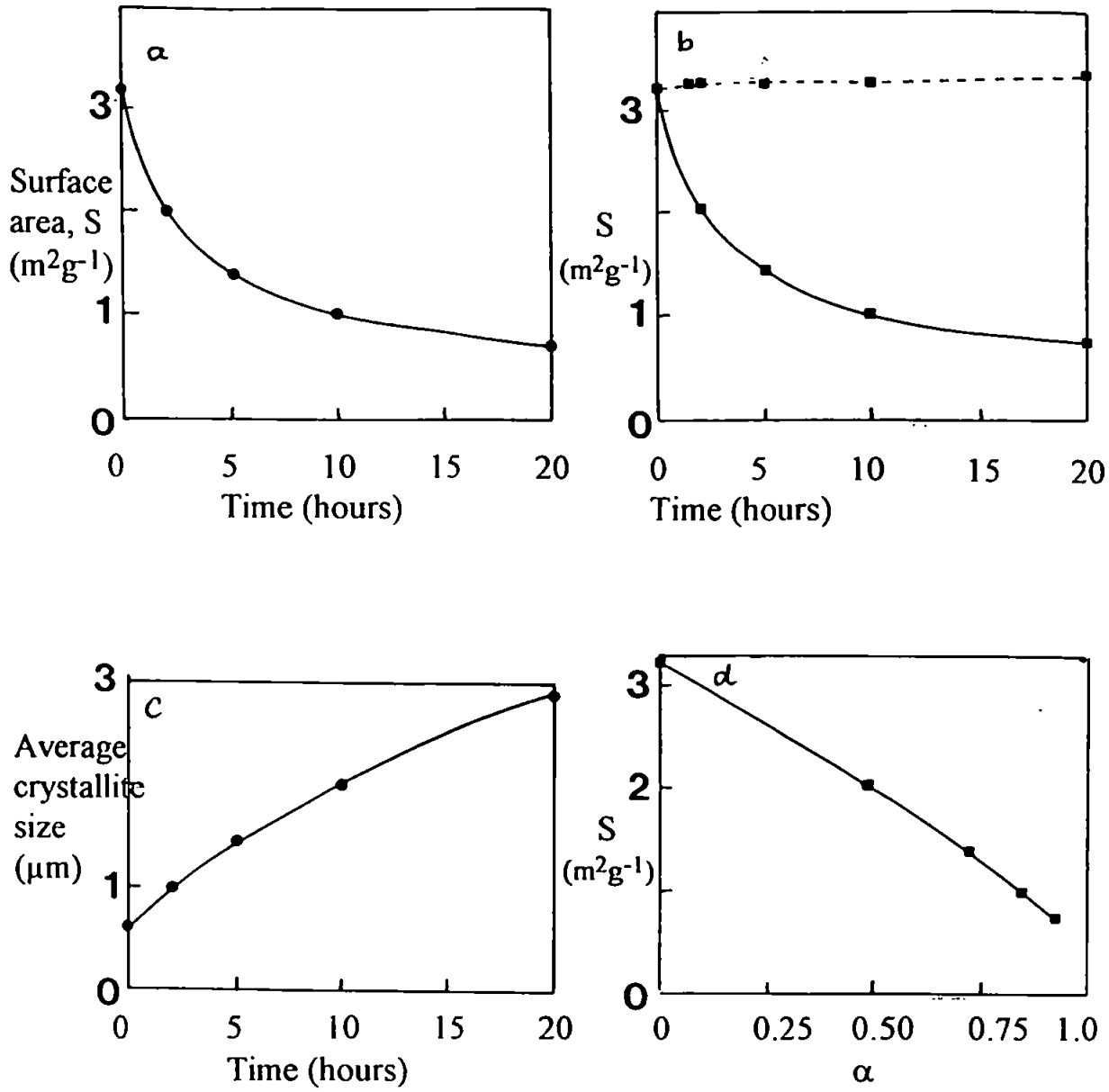

Figure 42

Surface area and average crystallite size change during oxidation in air of chromium nitride at 800 °C.

a) Total surface area change with time.
b) Surface area change of oxide produced with time.
c) Change in average crystallite size with time.
d) Decrease in surface area with α.

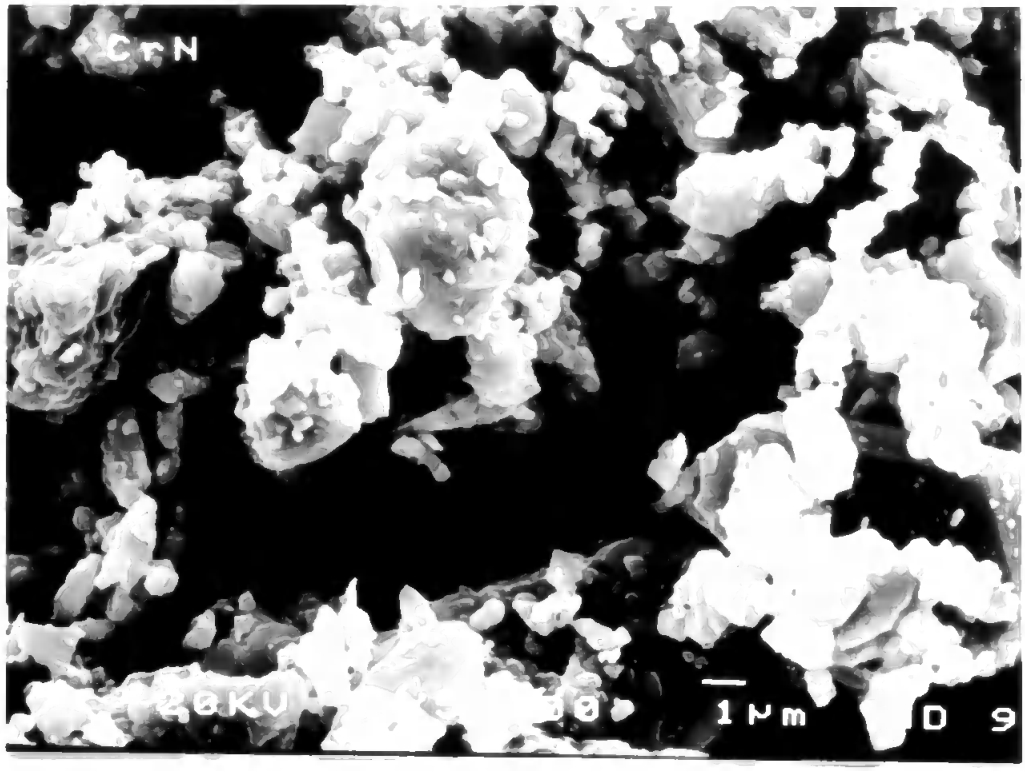

Plate 15
Chromium nitride

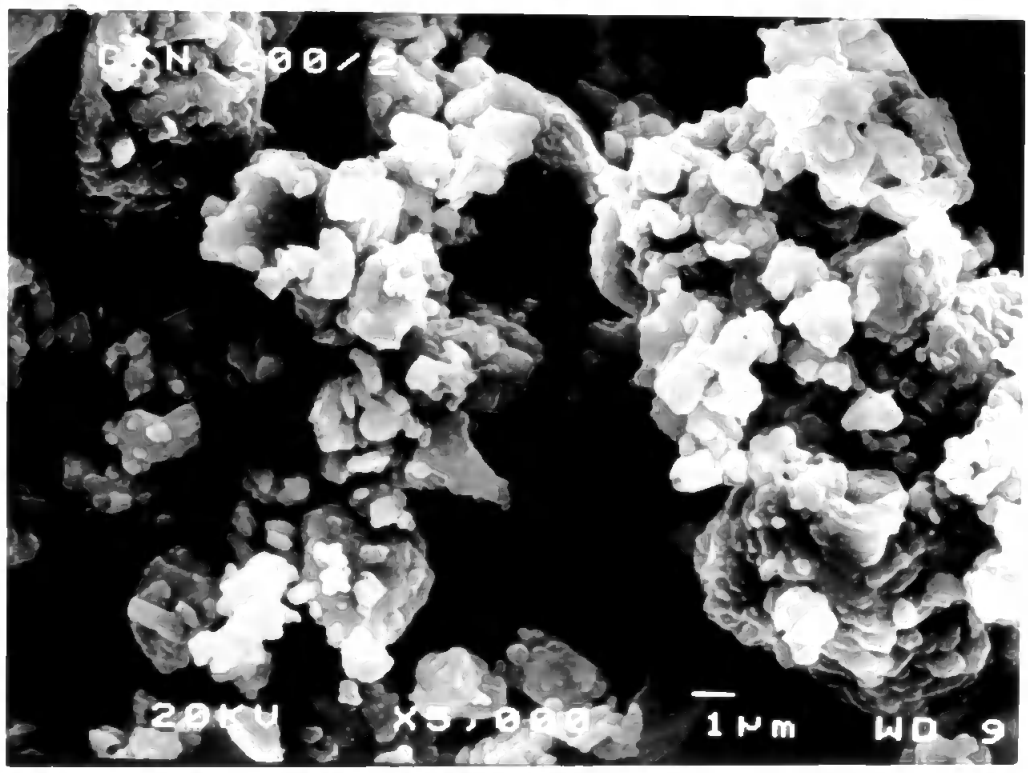

Plate 16
Chromium nitride oxidised for 2 hours at 800 °C in air

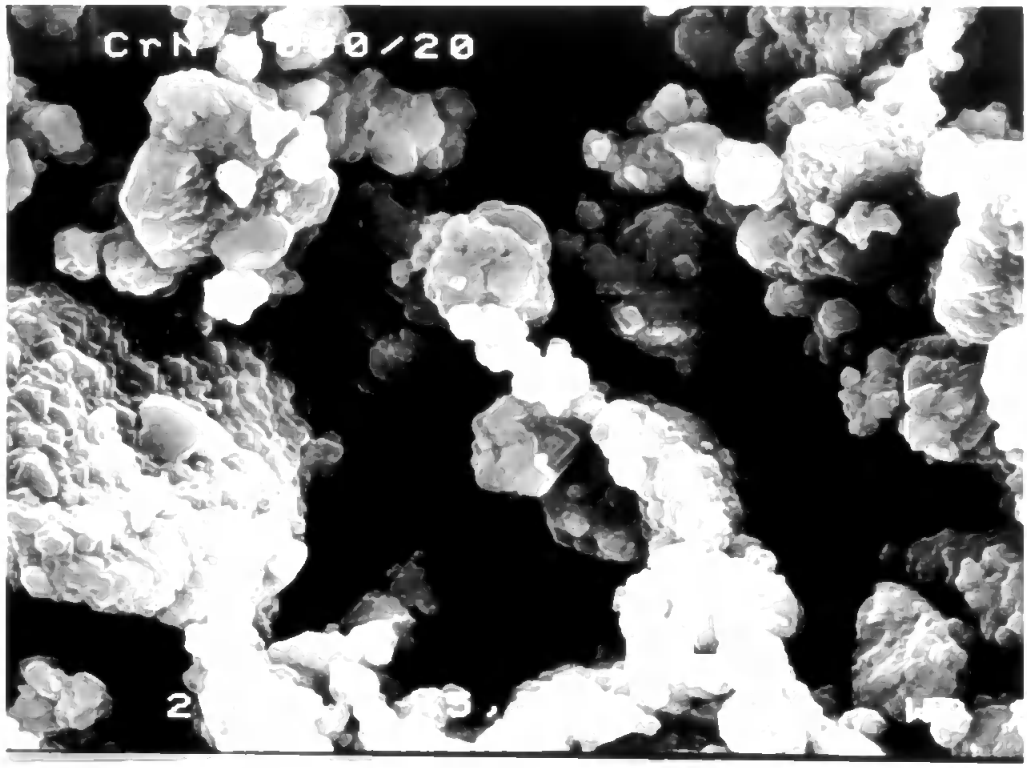

Plate 17
Chromium nitride oxidised for 20 hours at 800 °C in air

10 µm

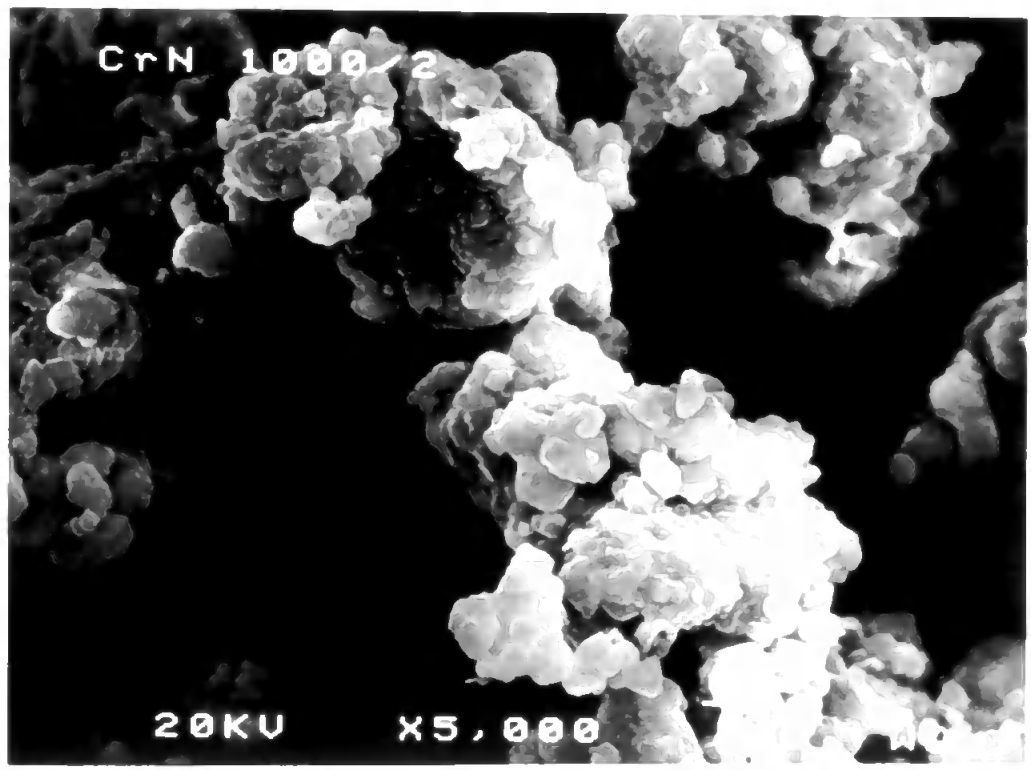

Plate 18
Chromium nitride oxidised for 2 hours at 1000 °C in air

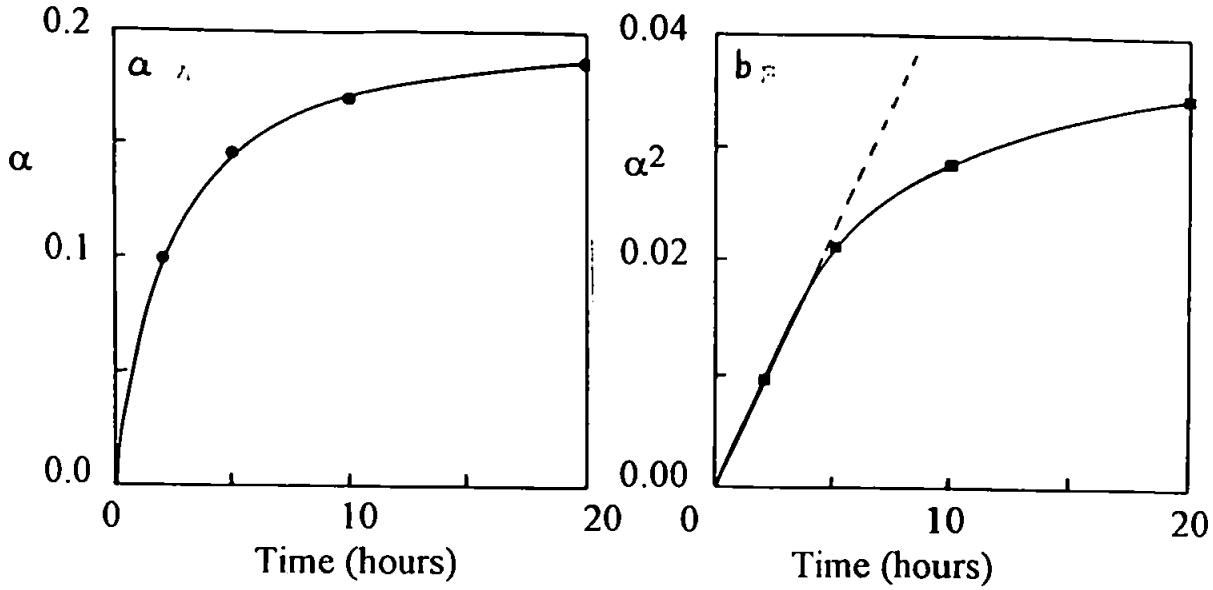

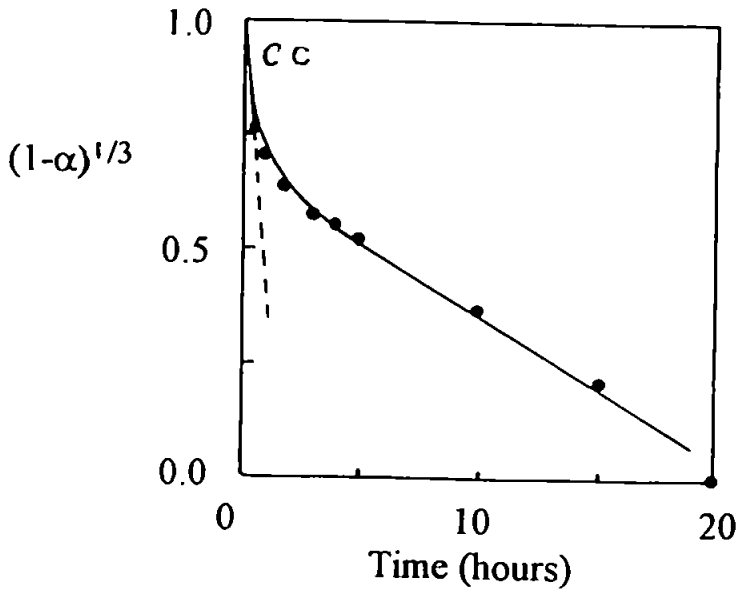

Figure 43
TG curve (A) and half order (B) kinetic plots for the isothermal oxidation of chromium nitride in air at 800 °C, and two-thirds order (C) kinetic plot for the isothrmal oxidation of chromium nitride in air at 1000 °C.

intervening period demonstrates the change in kinetics. At 1000 °C the reaction followed impeded two thirds-order kinetics, restricted by the extensive sintering (figure 43c).

When heated in a nitrogen free atmosphere, the nitride decomposes at temperatures above 900 °C but thermodynamic data (Glasson et al. 1968) shows the nitride to be stable in 0.8 bar nitrogen (as present in air) up to 1200 °C thus the oxidation was not complicated by the simultaneous decomposition of the nitride. Chromium nitride was therefore directly oxidised to the oxide in air at 800 and at 1000 °C.

X-ray diffraction studies showed that the initial carbide phase present was orthorhombic Cr_3C_2 (a = 11.46, b = 5.52, c = 2.821 Å, JCPDS card 14-406) which on oxidation formed the hexagonal (rhombohedral) oxide Cr_2O_3 (eskolaite). There was no evidence of any other carbide or oxide phases.

Dynamic oxidation of the carbide at 10 °C min^{-1} indicated that oxidation began at approximately 600 °C, although most of the reaction occurred at temperatures above 800 °C. From DTA studies, exothermic maximum peak temperatures were determined at various heating rates (table 12 and figure 44), from which the activation energy was calculated to be 269 ± 3 kJ mol^{-1}.

Isothermal studies of the oxidation of chromium carbide (figure 45) showed that at temperatures below 900 °C the reaction occurred very slowly being only 19 % oxidised at 600 °C after 42 hours and 48 % oxidised at 800 °C after 24 hours. At 900 °C the reaction is 94 % complete after 24 hours but at 1020 °C is complete within 10 hours. From the Arrhenius data and plot (table 13 and figure 46) the activation energy was calculated to be 83.1 ± 3 kJ mol^{-1}.

Heating rate, Φ K min^{-1}	DTA peak, T K	$\ln(\Phi/T^2)$	1/T x 10^{-4} K^{-1}
2.5	1220	-13.29	8.20
5.0	1251	-12.65	7.99
7.5	1277	-12.29	7.83
10.0	1282	-12.01	7.80
25.0	1331	-11.14	7.51
30.0	1333	-10.98	7.50

Kissinger plot
Gradient of slope = -32400 K
Correlation coefficient = -0.99

Table 12
Effect of heating rate on the oxidation of chromium carbide in air

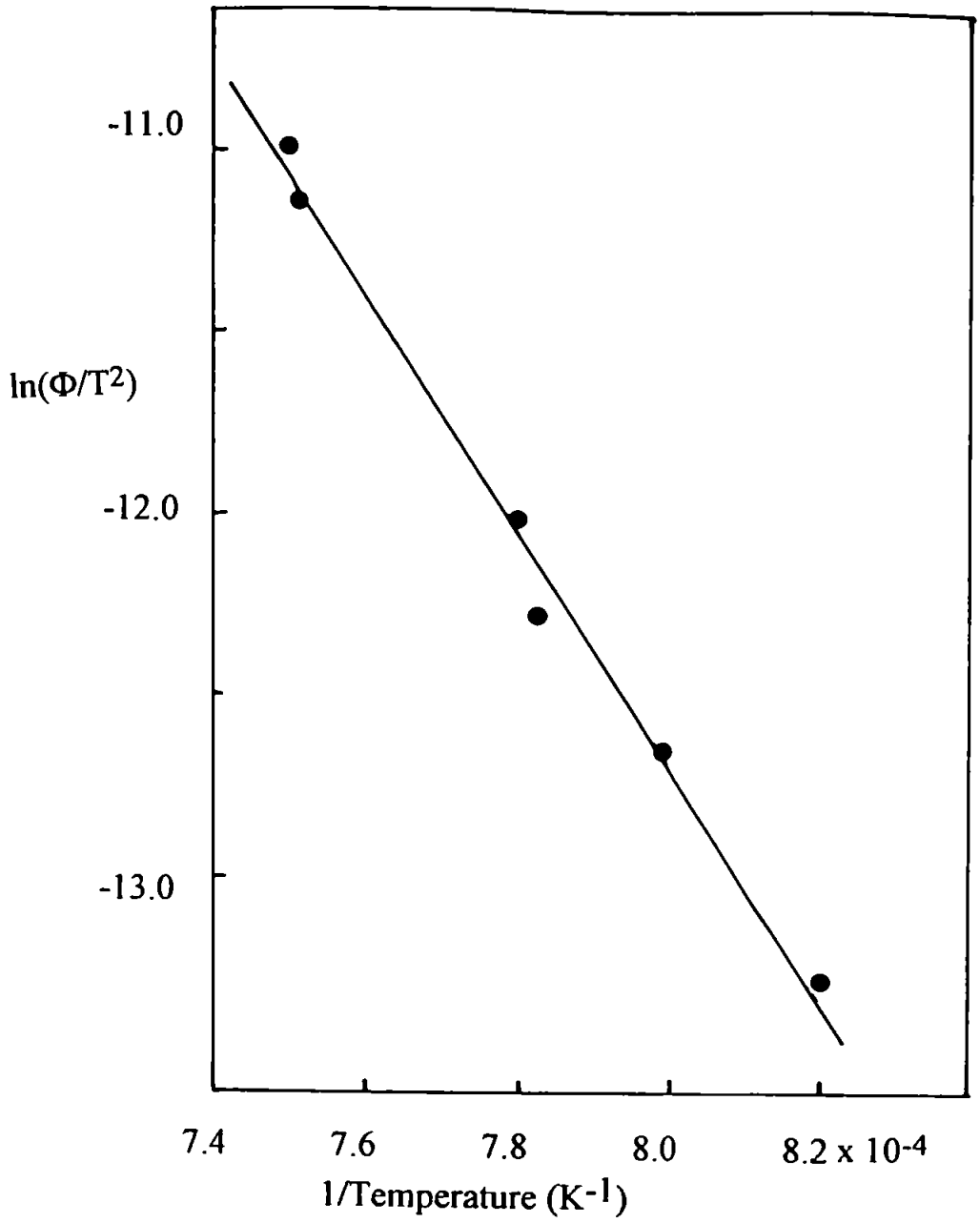

Figure 44
Kissinger plot for oxidation of chromium carbide in air.

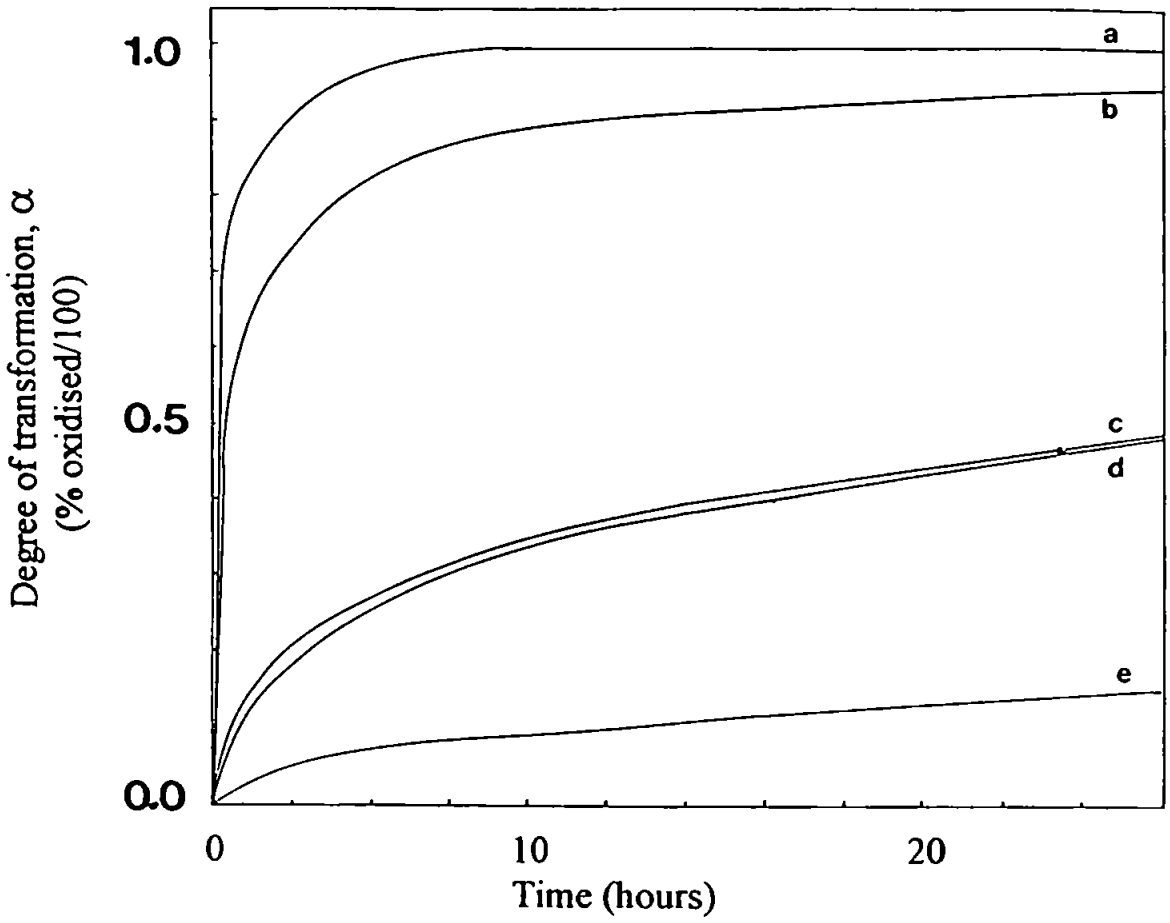

Figure 45

Isothermal TG curves for the oxidation of chromium carbide in flowing air (300 ml min^{-1}) at a) 1020 °C, b) 900 °C, c) 800 °C, d) 700 °C, e) 600 °C.

Temperature, T		dα/dt	ln(dα/dt)	1/T
°C	K	h^{-1}		x 10^{-3} K^{-1}
600	873	0.063	-2.773	1.15
700	973	0.411	-0.916	1.03
800	1073	0.535	-0.625	0.93
900	1173	2.175	+0.777	0.85
1020	1293	2.857	+1.049	0.77

Arrhenius plot
Gradient of slope = -10000 K
Correlation coefficient = -0.97

Table 13
Isothermal oxidation of chromium carbide in air

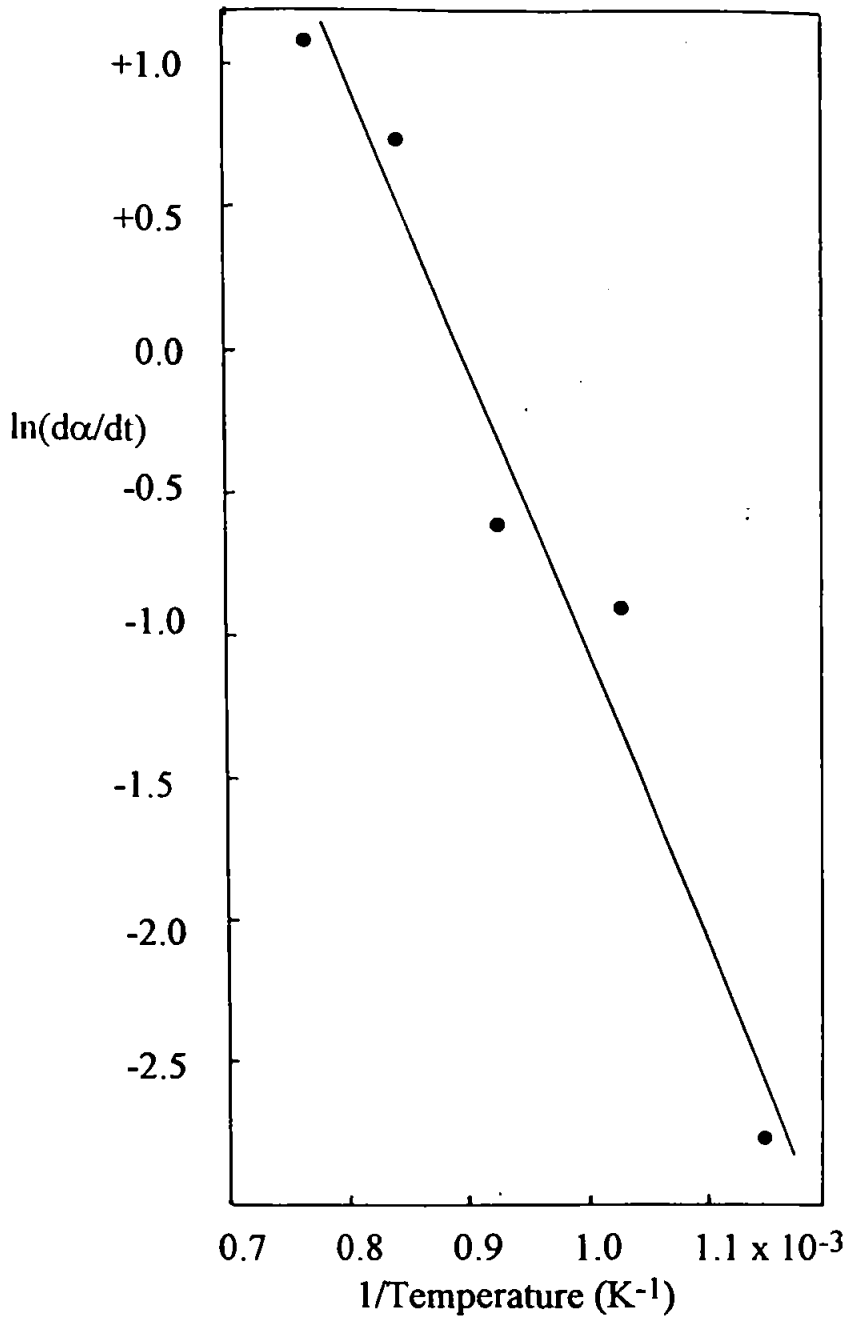

Figure 46
Arrhenius plot for oxidation of chromium carbide in air.

The ability of chromium carbide (melting point 1890 °C) to sinter by surface diffusion at temperatures above 450 °C and by crystal lattice diffusion above its Tammann temperature of 810 °C and chromium oxide to sinter by surface diffusion at temperatures above 650 °C greatly hinders the reaction. Despite the difference in crystal structure and density of the carbide and oxide (orthorhombic, 6.68 g cm^{-3}, and hexagonal, 5.21 g cm^{-3} respectively) the sintering of the carbide and the oxide results in a stable layer of oxide remaining around the carbide at these temperatures.

The specific surface area of the initial carbide was 0.42 m^2g^{-1}, (average crystallite size 2.1 μm). When oxidised for 79 hours at 600 °C (22 % oxidised) the specific surface area was 0.39 m^2g^{-1}. Allowing for the 5.9 % weight increase during the oxidation the surface area change is from 0.42 to 0.41 m^2g^{-1}. Theoretically the change in volume on oxidation of 1 g of Cr_3C_2 to Cr_2O_3 (x-ray densities 6.68 and 5.23 g cm^{-3} respectively) should be from 0.150 to 0.242 cm^3 representing a 0.615-fold increase. Thus if the oxide forms a stable layer around the carbide the surface area change should be given by $S'/S = (1 + 0.615\alpha)^{2/3}$. For 22 % oxidation of chromium carbide at 600 °C the surface area should change from 0.42 to 0.46 m^2g^{-1}. The experimental value is 0.41 m^2g^{-1} indicating that as the specific surface area had not increased the oxide layer cannot have spalled off from the carbide beneath and therefore must have undergone sintering.

3.7 OXIDATION OF IRON NITRIDE IN AIR

Iron forms four nitrides of composition Fe_2N, Fe_3N-Fe_2N, Fe_3N and Fe_4N. Due to the fluorescence of iron compounds when exposed to Cuk_α radiation, x-ray studies were performed utilizing Mok_α radiation. X-ray diffraction studies of the nitride indicated that the main constituent was cubic Fe_4N (a = 3.765 Å, JCPDS card 6-0627) with small quantities of the orthorhombic Fe_2N (a = 5.523, b = 4.830, c = 4.425 Å, JCPDS card 6-0656) present. There was no evidence of either of the other two possible nitrides.

Dynamic heating of the nitride in a flowing inert (argon) atmosphere showed that at temperatures above 525 °C the iron nitride decomposed to iron metal (confirmed by x-ray analysis) and nitrogen gas (figure 47). The weight loss (6.4%) was consistent with a starting composition of 90 wt-% Fe_4N and 10 wt-% Fe_2N or an empirical formula of $FeN_{0.2737}$. Oxidation of this mixed nitride to Fe_2O_3 should give a weight gain of 33.75 %. The weight gain during dynamic oxidation in air at 10 °C min^{-1} to 1200 °C was 32.63 %. This weight gain was achieved by 600 °C and maintained without further loss or gain. X-ray analysis of the oxide indicated the presence of both Fe_3O_4 (cubic magnetite, a = 8.3967 Å, JCPDS card 19-629) and Fe_2O_3 (hexagonal hæmatite, a = 5.038 Å, c = 13.772 Å, JCPDS card 24-72) and the experimental weight gain corresponds to a composition of 75 wt-% Fe_2O_3 and 25 wt-% Fe_3O_4. The oxidation began at 200 °C, but mainly occurred above 400 °C.

Isothermal oxidations (figure 48) showed that at 300 °C the nitride was 8 % oxidised after 5 minutes but after that no further oxidation took place. At 400 °C the nitride was 75 % oxidised after 2 hours and 95 % oxidised at 500 °C within 1 hour (assuming Fe_2O_3 as 100 %). In this work peaks due to Fe_3O_4 and Fe_2O_3 were detected in the x-ray patterns of products produced at all temperatures studied. At temperatures above 525 °C the nitride can

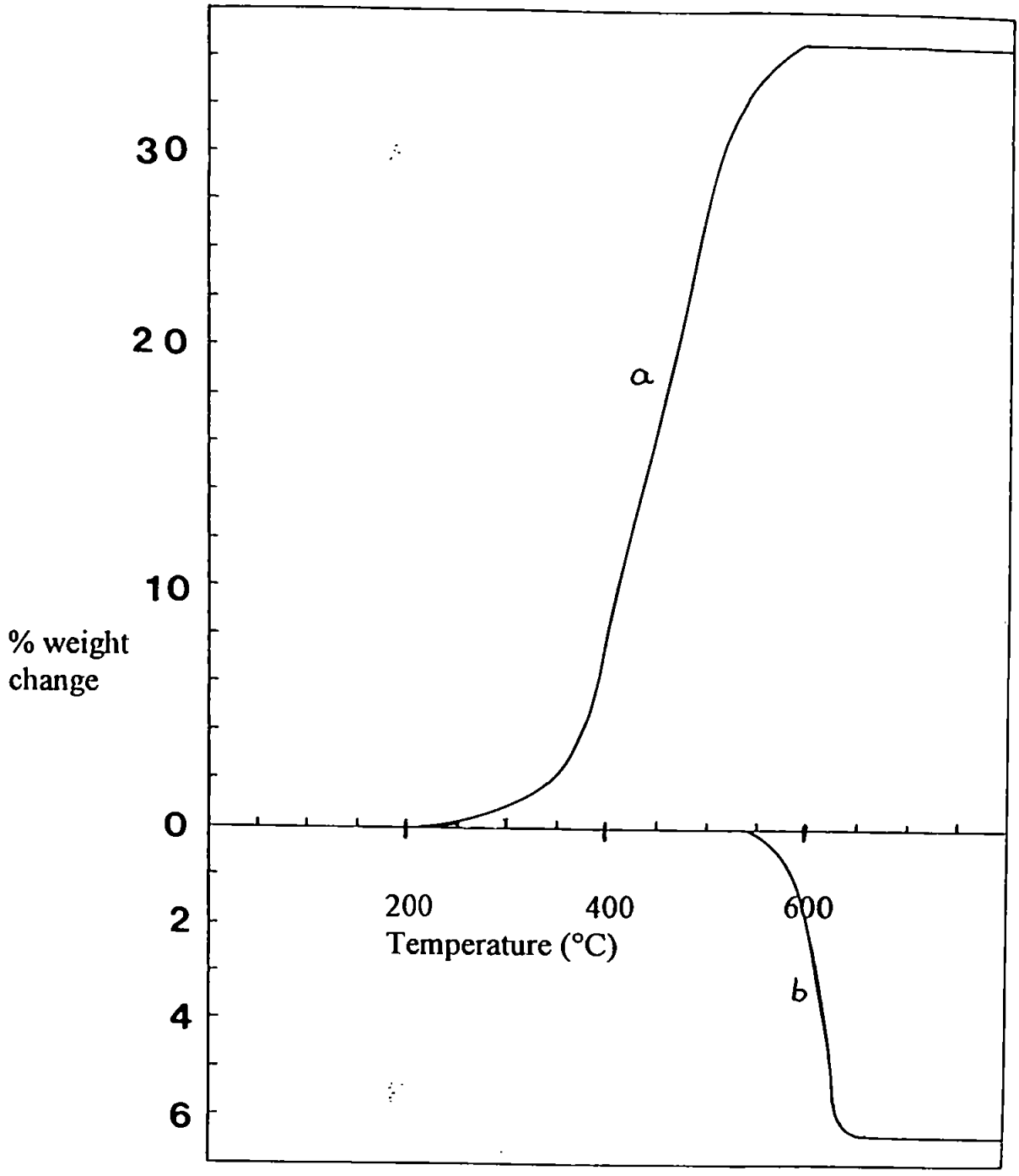

Figure 47
Iron nitride heated at 10 °C min^{-1} in (a) air showing oxidation, and (b) argon showing decomposition.

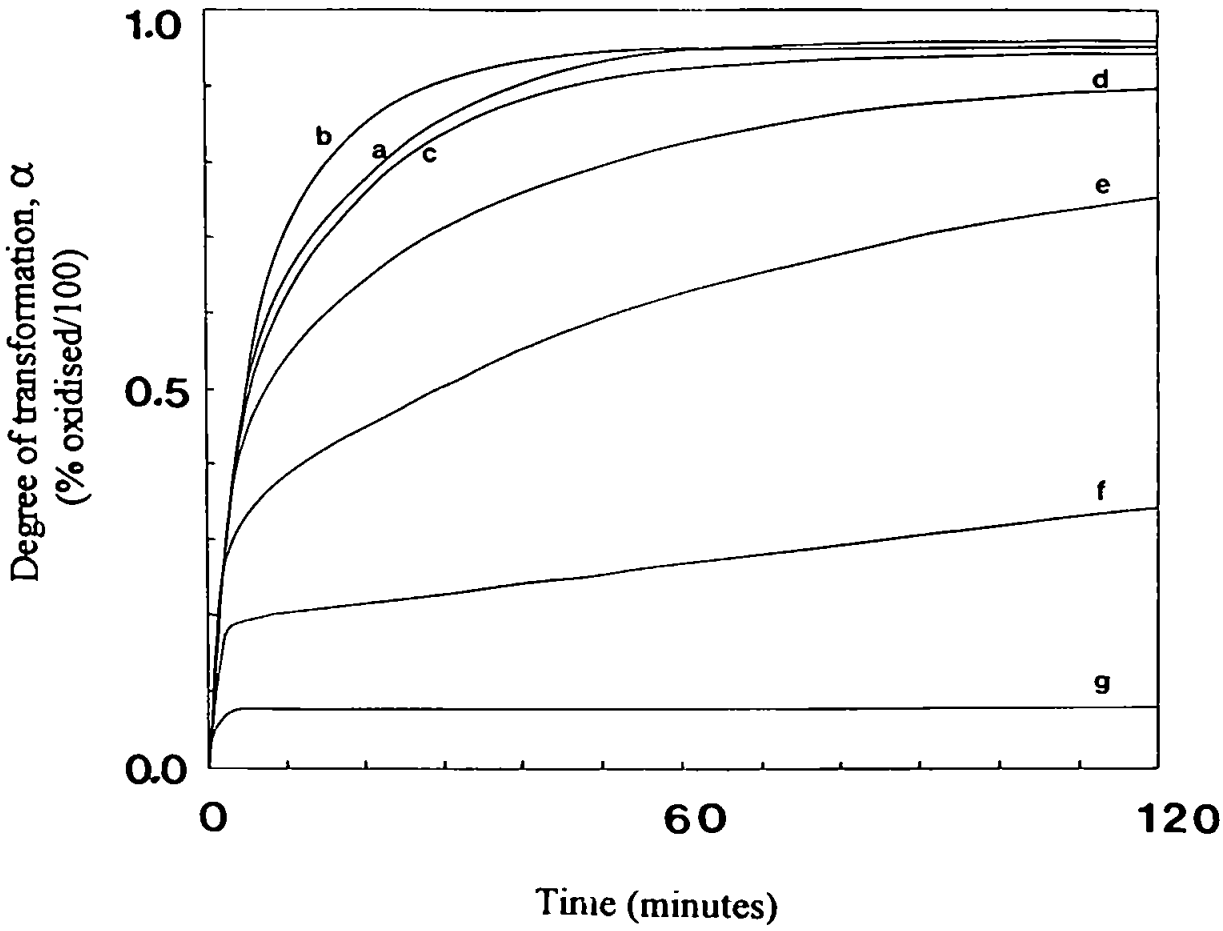

Figure 48

Isothermal TG curves for the oxidation of iron nitride in flowing air (300 ml min^{-1}) at a) 500 °C, b) 475 °C, c) 450 °C, d) 425 °C, e) 400 °C, f) 350 °C, g) 300 °C.

decompose to the metal. Oxidation of the metal at these temperatures would favour the formation of FeO and Fe_3O_4 (Tylecote and Mitchell (1960)). This would account for the presence of the lower oxide being formed during the dynamic oxidation where 25 % of the reaction occurred above 500 °C. Isothermal TG oxidations were not performed at temperatures above 500 °C, although samples were oxidised at 600 °C for x-ray and surface area purposes.

The kinetic plot (figure 49) shows that at 500 °C the two-thirds order plot is linear for the first half of the reaction, after which the plot deviates from the expected line. At lower temperatures the kinetic plots are inconclusive, neither the half order or two-thirds order kinetic plots are linear. The melting points of Fe_2O_3 and Fe_3O_4 being 1565 and 1534 °C respectively, it would be expected that the product would sinter by surface diffusion at temperatures above 330 °C and by crystal lattice diffusion above its Tammann temperature of 630 °C. Thus it is likely that the product sinters at temperatures below 500 °C but that this is not extensive enough to make the diffusion of oxygen through the product layer the rate determining step. The reaction is therefore under mixed control. Above 500 °C it would be expected that the decomposition of the nitride would further complicate the reaction kinetics. From the Arrhenius plot for the reaction (table 14 and figure 50) the activation energy for the reaction when carried out at temperatures below 500 °C was calculated to be 15.3 ± 0.2 kJ mol^{-1}.

The initial nitride has a specific surface area of 2.5 m^2g^{-1} and an average crystallite size of 0.33 μm. When 1 g of nitride (density 7.16 g cm^{-3}) is oxidised to oxide (density 5.22 g cm^{-3}) there is a 1.835-fold increase in volume. If the oxide forms a stable layer around the remaining nitride then the surface area change should be given by $S'/S = (1 + 0.835\alpha)^{2/3}$. The experimental surface area changes during oxidation are shown in figure 51.

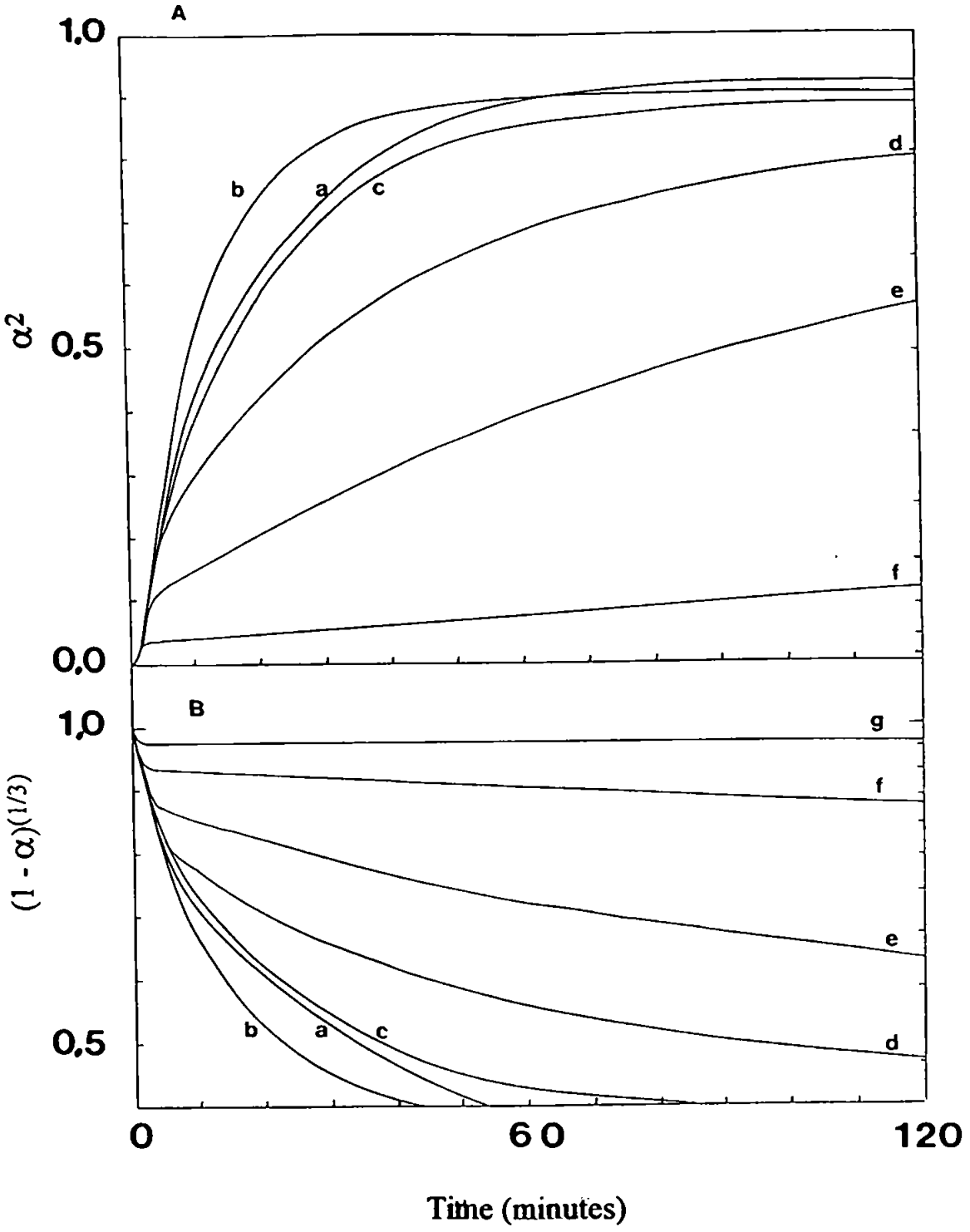

Figure 49
Half order (A) and two-thirds order (B) kinetic plots for the isothermal oxidation of iron nitride in air at a) 500 °C, b) 475 °C, c) 450 °C, d) 425 °C, e) 400 °C, f) 350 °C, g) 300 °C

Temperature, T		dα/dt	ln(dα/dt)	1/T
°C	K	x 10^{-3} sec^{-1}		x 10^{-3} K^{-1}
500	773	2.05	-6.19	1.29
475	748	2.17	-6.13	1.34
450	723	1.96	-6.23	1.38
425	698	1.80	-6.32	1.43
400	673	1.65	-6.40	1.49
350	623	1.26	-6.68	1.60
300	573	1.04	-6.87	1.75

Arrhenius plot
Gradient of slope = -1850 K
Correlation coefficient = -0.99

Table 14
Isothermal oxidation of iron nitride in air

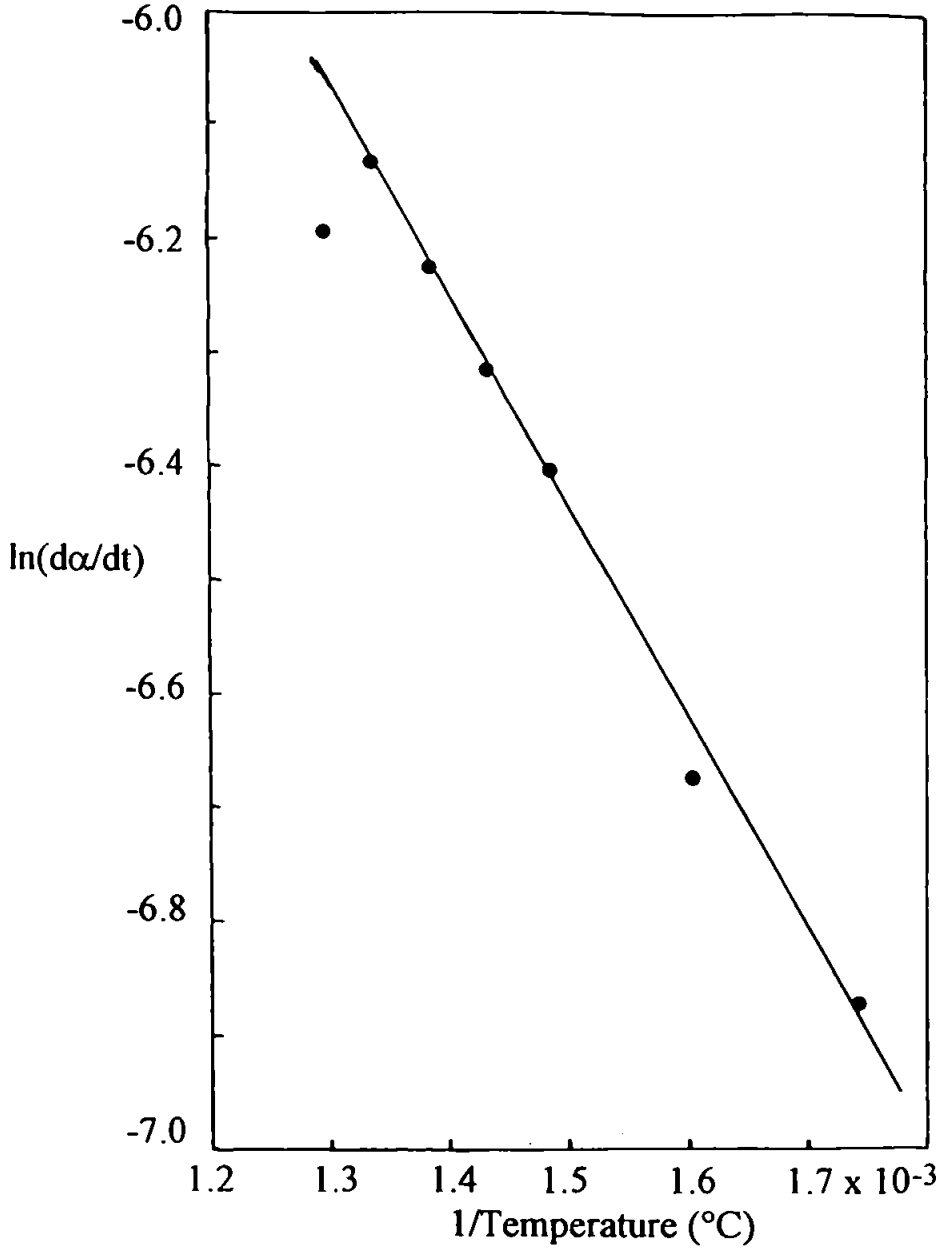

Figure 50
Arrhenius plot for the oxidation of iron nitride in air.

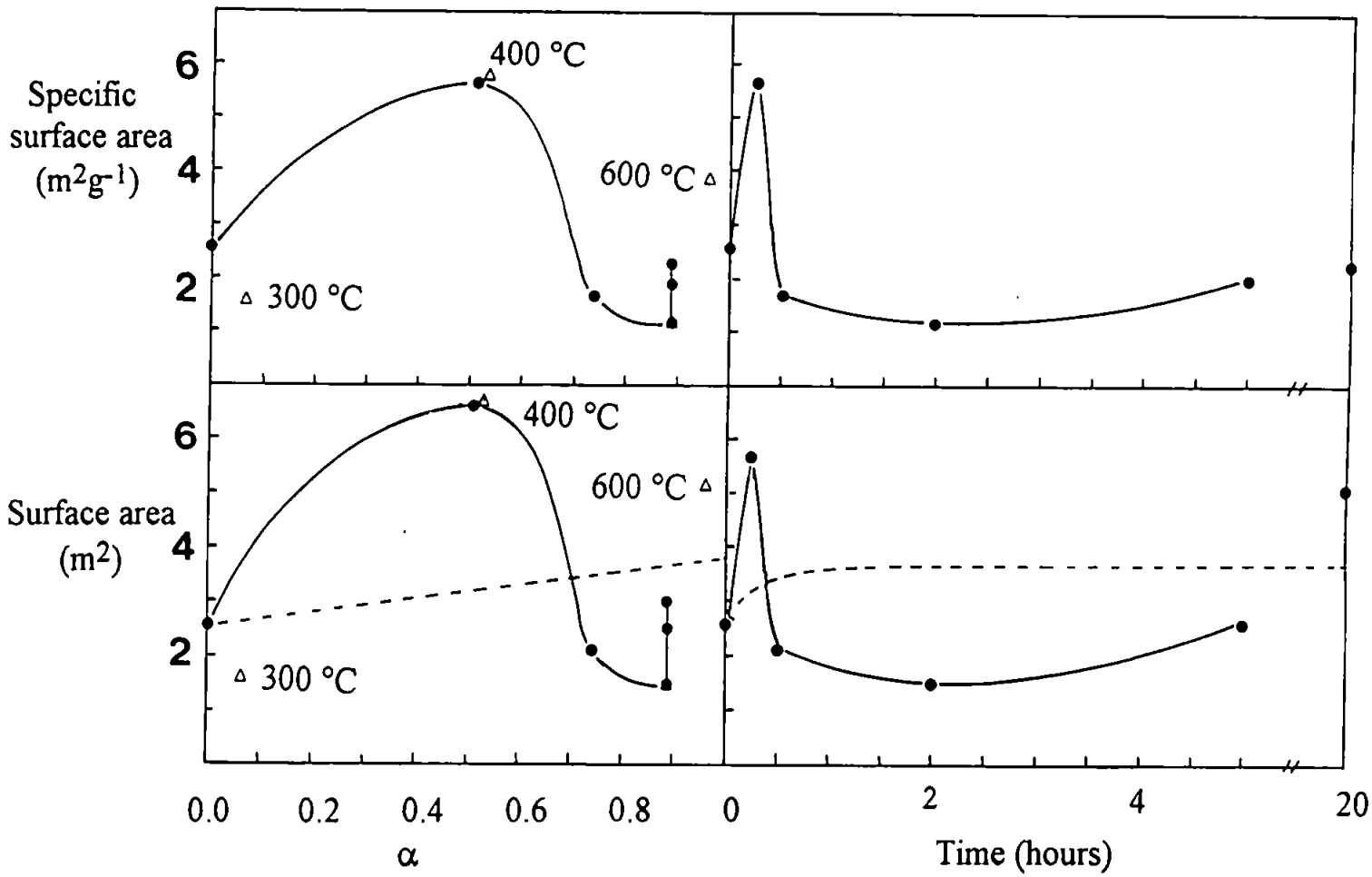

Figure 51

Specific surface area change (upper) during oxidation of iron nitride at 500 °C except where indicated, and (lower) surface area change of oxide produced from 1 g of iron nitride oxidised at 500 °C except where indicated. Theoretical surface area shown by broken line.

Theoretical surface area is shown by the broken line, assuming that there is no splitting or sintering of the oxide layers. Oxidation of the nitride at 500 °C shows that during the first half of the reaction the surface area increase is greater than that expected if the oxide is stable, indicating that the average crystallite size decreases and that the oxide layer is unstable. During the second half of the oxidation the surface area decreases so that at about three-quarters oxidation the surface area falls below that expected. This is due to the oxide sintering. On continued calcination there is a gradual increase in surface area, possibly due to the slow removal of remaining nitrogen and interconversion of the oxides. At 400 °C the surface area change is similar to that at 500 °C, but during the initial oxidation at 300 °C (6.7% after 2 hours) the surface area decreases below the theoretical surface area indicating that there may be some sintering of the nitride. At 600 °C the rapid oxidation of the nitride is accompanied by the decomposition to the metal and oxidation of the metal. Decomposition would be expected to destabilise the oxide produced thus the surface area remains greater than that expected from the oxidation after 2 hours.

Thus the nitride appeared to oxidise first to Fe_3O_4 which then sintered, this oxide was then slowly oxidised further to Fe_2O_3.

3.8 OXIDATION OF TANTALUM CARBIDE IN AIR

The tantalum carbide as supplied was stated as being TaC with a carbon content of 6.3 wt-% (corresponding to a formula of $TaC_{1.01}$). Dynamic oxidation of the carbide at 10 °C min^{-1} to 800 °C indicated that the oxidation began at 460 °C. The overall weight gain was 14 % (the theoretical weight gain for the oxidation of TaC was 14.4 %). X-ray diffraction studies of the carbide showed only the face centred cubic TaC (a = 4.4555 Å, JCPDS card 19-1292) phase as present in the initial carbide. The product was the pseudo-hexagonal pentoxide Ta_2O_5 (a = 3.62, c = 3.87 Å, JCPDS card 18-1304).

Isothermal oxidation curves are shown in figure 52. At low temperatures, below 650 °C, the oxidation showed unusual characteristics in that after the initial oxidation the reaction rate slowed before resuming. This may be due to a layer of oxide formed during the initial stages of oxidation which may form a temporary layer that hinders the reaction before spalling off. The large difference in density between the carbide (13.9 g cm^{-3}) and the oxide (8.2 g cm^{-3}) and the difference in crystal structure make it unlikely that the oxide can form stable layers around the remaining carbide as the oxide layer formed will be split open by new oxide expanding on formation before sintering. Tantalum carbide oxidised at 850 °C in an open furnace was observed to expand, filling the crucible and overflowing the sides of the crucible. Although the melting point of tantalum oxide is 1800 °C, and therefore the temperature at which sintering by surface diffusion can occur is 420 °C and by crystal lattice diffusion above its Tammann temperature of 760 °C, little coalescence of the oxide produced after 2 hours calcination at 850 °C was observed. At higher temperatures (884 °C) the reaction was almost completed within 10 minutes, however, continued calcination at this temperature resulted in weight loss, so that after 1 hour the final weight was less than that obtained at 650 °C. Alpher (1970) reports that at elevated

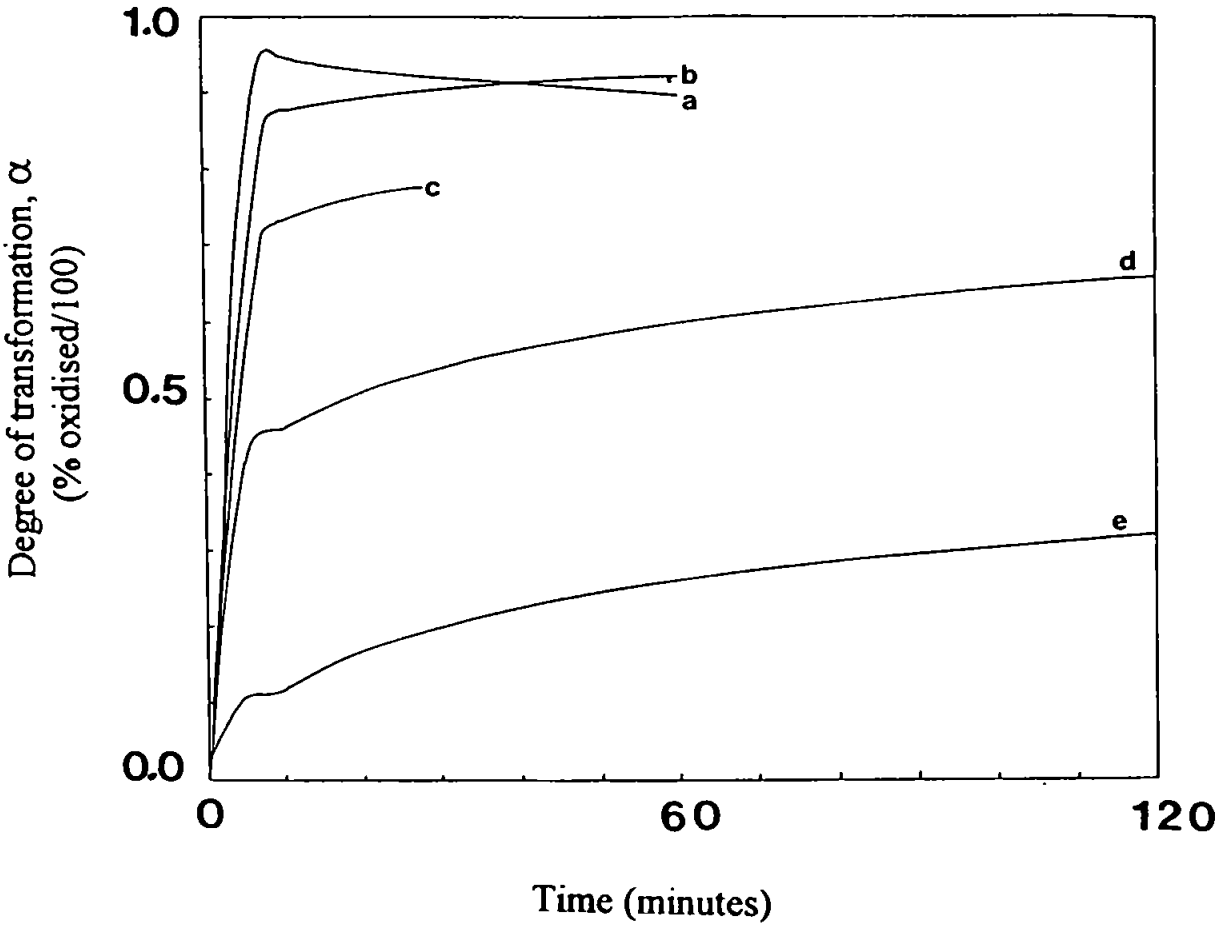

Figure 52
Isothermal TG curves for the oxidation of tantalum carbide in flowing air (300 ml min^{-1}) at a) 884 °C, b) 650 °C, c) 628 °C, d) 602 °C, e) 548 °C.

temperatures (above 1250 °C) the pentoxide may decompose to a mixture of the pentoxide and tantalum metal. This may explain the observed weight loss observed at 1000 °C, although x-ray analysis showed no other component. Thus any other constituent present in the product formed at 1000 °C must be in an amorphous state. From the Arrhenius plot (table 15 and figure 53) the activation energy was calculated to be 46.4 ± 0.5 kJ mol^{-1}.

The two-thirds order and half order plots for the reaction at temperatures below 650 °C are complicated by the anomaly in the oxidation curves (figure 54). At 884 °C the initial oxidation is best described by half order kinetics indicating that the reaction is controlled by the diffusion of oxygen through the oxide layer.

X-ray diffraction studies of the oxidation products showed that the only product formed at 800 °C and below was the pseudo-hexagonal δ-Ta_2O_5. There was no indication that any of the lower oxides (Ta_2O, TaO or TaO_2 or the high temperature α-Ta_2O_5) was formed at these temperatures.

Temperature, T		dα/dt	ln(dα/dt)	1/T
°C	K	min^{-1}		x 10^{-4} K^{-1}
884	1157	0.173	-1.749	8.64
650	923	0.133	-2.014	10.83
628	901	0.117	-2.140	11.09
602	875	0.100	-2.303	11.43
548	821	0.063	-2.763	12.18

Arrhenius plot
Gradient of slope = -2550 K
Correlation coefficient = -0.89

Table 15
Isothermal oxidation of tantalum carbide in air

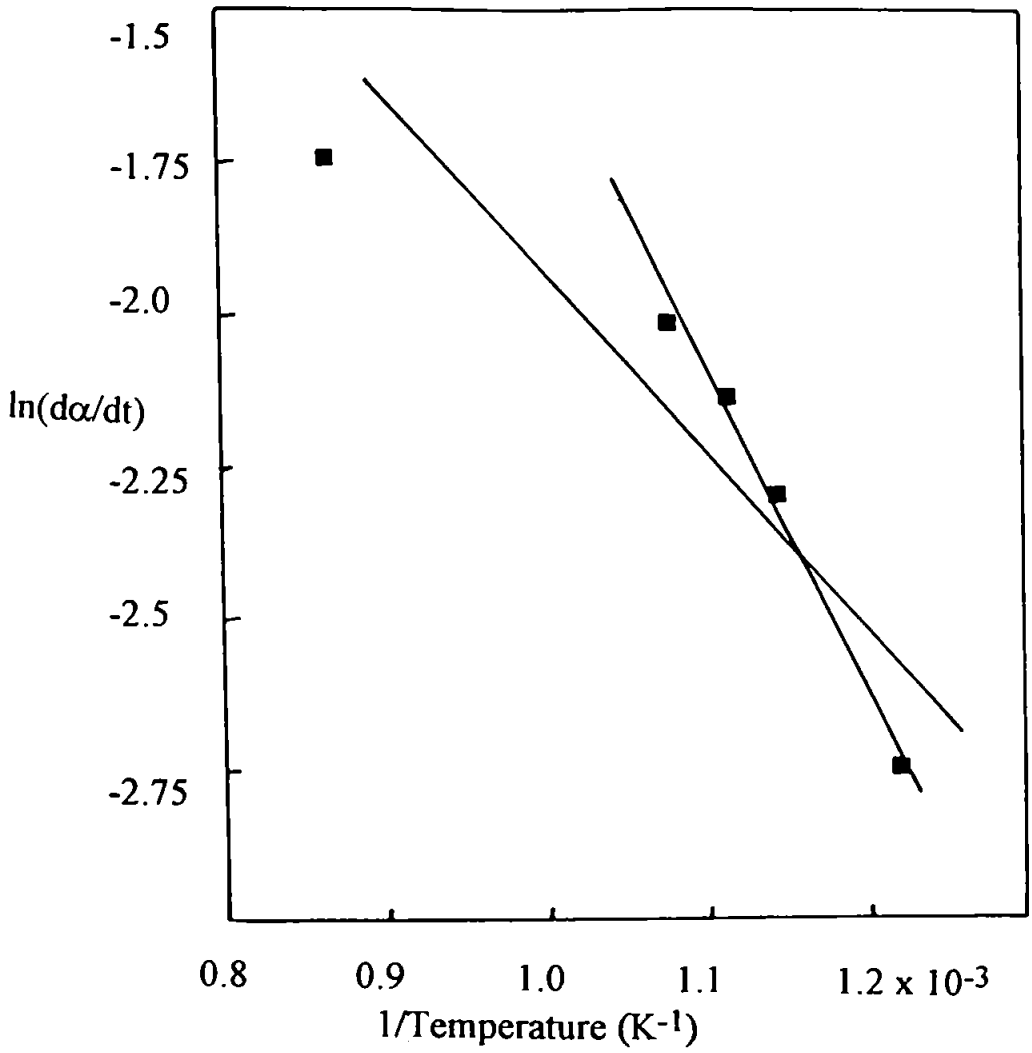

Figure 53
Arrhenius plot for oxidation of tantalum carbide in air.

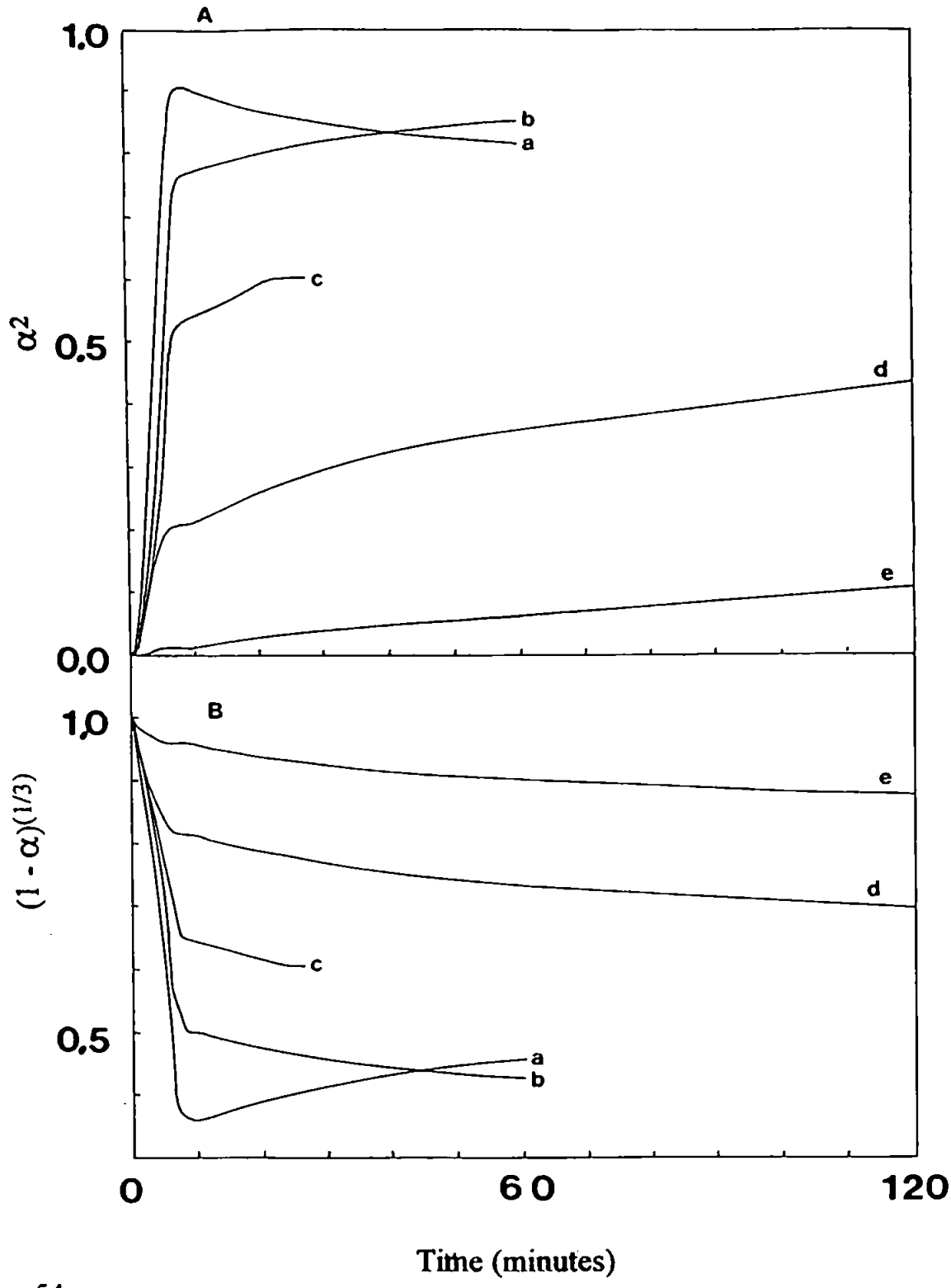

Figure 54
Half order (A) and two-thirds order (B) kinetic plots for the isothermal oxidation of tantalum carbide in air at a) 884 °C, b) 650 °C, c) 628 °C, d) 602 °C, e) 548 °C.

3.9 OXIDATION OF MANGANESE CARBIDE IN AIR

Manganese can form two carbides, Mn_5C_2 and Mn_3C. X-ray diffraction studies of the supplied material showed that the carbide was a mixture of monoclinic Mn_5C_2 (a = 11.66, b = 4.573, c = 5.086 Å, β = 97°75', JCPDS card 16-38) and another phase which was not listed in the JCPDS data file but was assumed to be Mn_3C. Oxidation of the carbide produced orthorhombic Mn_3O_4 (hausmannite, a = 9.404, b = 9.973, c = 8.536 Å, JCPDS card 24-734). Oxidation of the carbide in dynamic temperature conditions indicated that the final weight gain was 28.5 %, corresponding to a 50:50 weight mixture of the carbides. At temperatures above 900 °C Mn_3O_4 may decompose to MnO (Kubaschewski and Hopkins (1962)).

Isothermal oxidation curves are shown in figure 55. During the initial stages of oxidation the rate of reaction increased with temperature. Subsequently the oxidation slows down so that after 40 hours at 600 °C the reaction is 61 % complete compared with 42 % at 800 °C, suggesting that the reaction was impeded by the formation and sintering of the oxide. Since the Tammann temperature for the oxide is 720 °C sintering by both surface and crystal lattice diffusion is possible at 800 °C, which would stabilise the oxide layer and therefore inhibit the oxidation.

Mn_5C_2 has a monoclinic crystal structure and Mn_3O_4 has a tetragonal structure, which with the change in sample density (7.54 and 4.83 g cm^{-3} respectively) make it unlikely that the oxide layer would be compatible with the remaining carbide unless there was extensive sintering of the oxide at the temperature of the oxidation.

The specific surface area of the initial carbide was found to be 6.0 m^2g^{-1}, corresponding to an average crystallite size of 0.13 μm. The surface area of

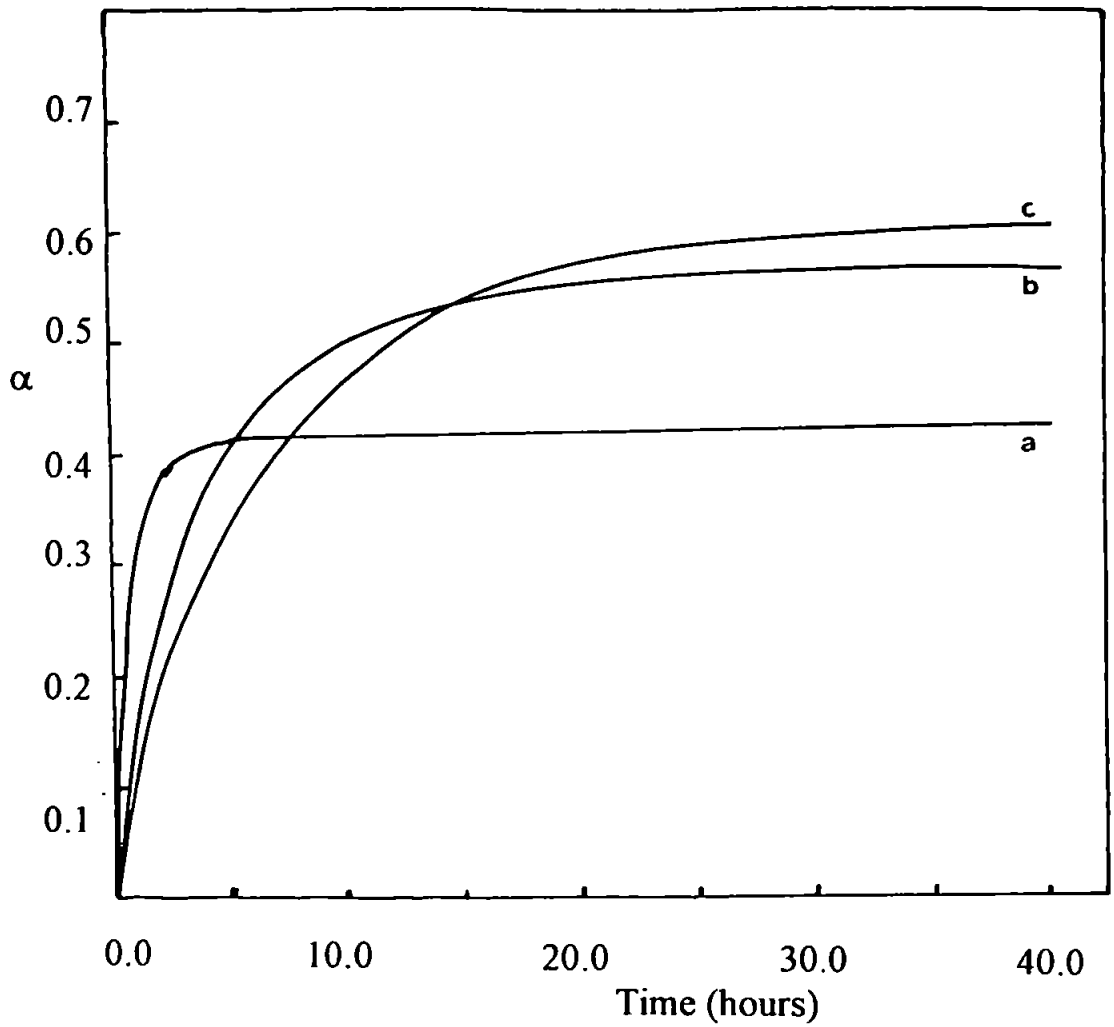

Figure 55

Isothermal TG curves for the oxidation of manganese carbide in flowing air (300 ml min^{-1}) at a) 800 °C, b) 700 °C, c) 600 °C.

the oxidation products are given in table 16. When 1 g of carbide is oxidised to 1.285 g of oxide there is a doubling of volume, assuming that there is no splitting or sintering of the oxide. The surface area change should be given $S'/S = (1 + 1\alpha)^{2/3}$. Figure 56 shows the change in specific surface area of the oxidation products (S), the change in surface area of the oxide (S') and the theoretical value of S' (indicated by broken line) for oxidation at 500 °C. If the experimental surface area value is greater than the theoretical then the oxide must split and or spall away from the reactant, if the experimental value is less then sintering must have occurred. As at all temperatures studied the values obtained experimentally were lower than the theoretical values, the oxide must have sintered.

The electron micrographs (plate 19) show that the original carbide consists of large crystals (approximately 50 μm diameter), the oxide formed and sintered at temperatures up to 800 °C retain a similar size distribution. As the surface area declined at 800 °C, pores must have closed. Only at 1000 °C is there any coalescence of the crystals to form larger particles.

Temperature °C	Calcining period hours	α	Specific Surface area m^2g^{-1}	Surface area of oxide m^2g^{-1}
Original material		0.00	6.0	
500	20	0.174	3.0	3.15
500	54	0.373	2.2	2.43
600	0.25	0.059	3.6	3.66
600	1	0.144	2.95	3.07
600	5	0.341	2.9	3.18
600	22	0.589	1.7	1.99
800	0.5	0.292	1.5	1.62
800	1	0.330	1.3	1.42
800	2.5	0.400	1.2	1.34
800	15	0.421	1.0	1.12

Table 16

Vaiation of specific surface area of manganese carbide and oxide products with temperature and oxidation period

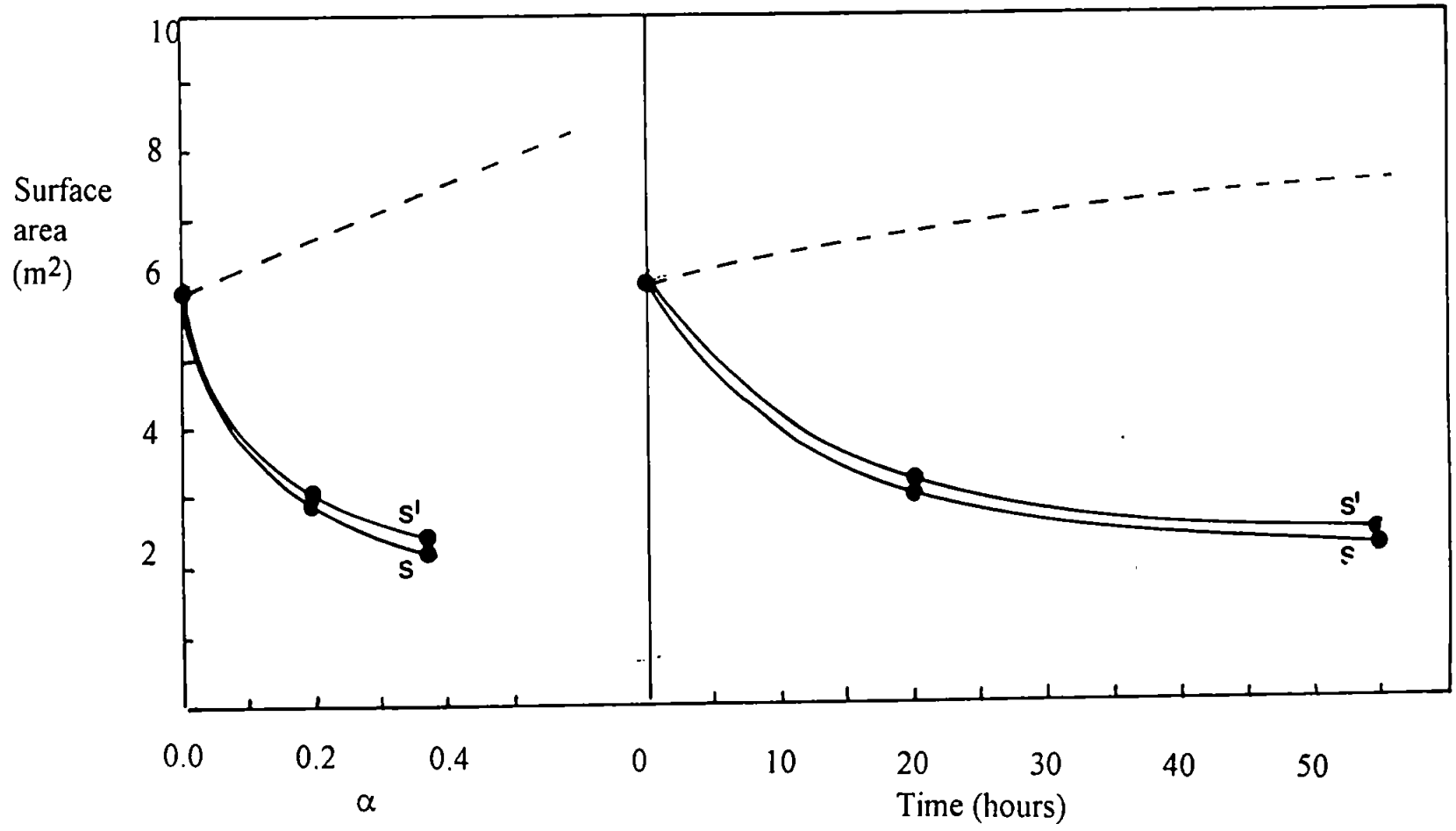

Figure 56
Specific surface area change (S) during oxidation of manganese carbide in air at 500 °C, and surface area (S') of oxide produced by the oxidation of 1 g of manganese carbide at 500 °C.
Theoretical surface area shown by broken line.

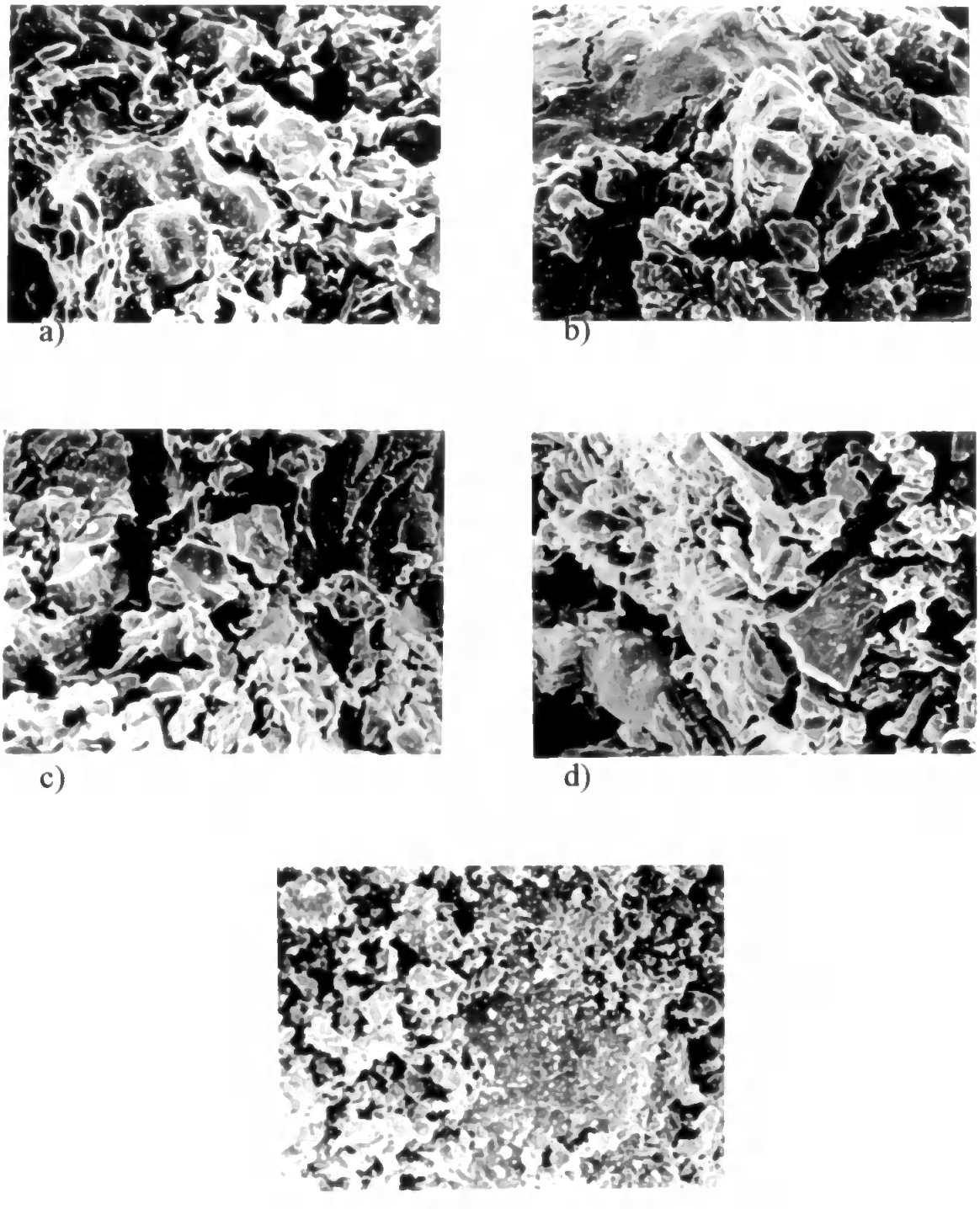

Plate 19

Manganese carbide (a) and its oxidation products when heated in air at

b) 600 °C for 22 hours
c) 700 °C for 41 hours
d) 800 °C for 15 hours
e) 1000 °C for 14 hours

3.10 EFFECT OF ADDITION OF CHROMIUM CARBIDE ON THE OXIDATION OF ZIRCONIUM CARBIDE IN AIR

It is known that the addition of chromium carbide improves the oxidation resistance of TiC-Co hard metals (Kubaschewski and Hopkins (1962) and Kieffer and Kölbl (1950)). The oxide scales formed are thinner, protective and more tenaciously adhering to the underlying unreacted material than when chromium carbide has not been added. Oxidation follows a parabolic (half order) mechanism, controlled by the diffusion of oxygen through the oxide layer.

As previously shown in this work, at 700 °C zirconium carbide was 94 % oxidised after 30 minutes, and chromium carbide was 25 % oxidised after 1 hour. When a 1:1 weight mixture of chromium and zirconium carbides was oxidised for 1 hour at 700 °C the zirconium carbide was only 84 % oxidised. The zirconium carbide was found to have a surface area of 0.59 m^2g^{-1} which when oxidised for 1 hour at 700 °C without chromium carbide increased to 5.3 m^2g^{-1}. If chromium carbide and its oxidation products had no effect on the oxidation of zirconium carbide then after 1 hour's oxidation at 700 °C of the mixture, a surface area of 2.5 m^2g^{-1} would be expected. The value found experimentally was 1.8 m^2g^{-1} indicating that the added chromium carbide had caused the oxidation products of the mixture to sinter. Thus the addition of chromium carbide had hindered the oxidation of zirconium carbide.

It is probable that it is the sintering of the chromium oxide produced by the oxidation of the carbide that hinders the oxidation of the zirconium carbide. It would therefore be expected that the addition of chromium carbide would have greatest effect on the oxidation of compounds that oxidise at temperatures equal to or higher than chromium carbide.

CHAPTER 4

RESULTS OF OXIDATIONS IN CARBON DIOXIDE

4.1 INTRODUCTION

Isothermal and dynamic thermogravimetric studies were made using a Stanton Redcroft Massflow Balance with between 100 and 200 mg samples and gas flow rates of 300 cm^3 min^{-1}. Samples to be studied isothermally were heated to the required temperature under an inert atmosphere of either argon or nitrogen. Once the sample temperature had stabilized carbon dioxide was admitted to the system.

From the TG curves, initial rate ($d\alpha/dt$) values were measured either within $\alpha = 0.05$ to 0.4 or within t = 5 to 15 minutes depending on the nature of the reaction, i.e. measurements were taken during the initial linear part of the reaction curve. Arrhenius plots, slope values and error limits were determined using the "Maths Powergraph" program running on a BBC microcomputer.

Larger samples for x-ray studies, BET studies and electron microscopy were heated and oxidised under similar conditions in a tube furnace.

All melting point temperatures and sample densities are quoted from Alfa (Johnson Matthey) Catalogue (1993), CRC Handbook of Chemistry and Physics 75th edition (1994) or from appropriate JCPDS file card.

4.2 OXIDATION OF CHROMIUM NITRIDE IN CARBON DIOXIDE

As has been previously shown in section 3.6 of this work, the chromium nitride as supplied consisted of 11.4 wt-% Cr_2N and 88.4 wt-% CrN. On heating the mixed nitride to temperatures above 900 °C in an inert atmosphere the nitrides decomposed to the metal.

Upon heating chromium nitride in carbon dioxide at 10 °C min^{-1}, the oxidation rate became appreciable at temperatures above 850 °C (figure 57). The final weight gain (16.7 %) was consistent with that obtained in air.

Isothermal oxidation of the nitride at 1000 °C showed that the nitride was 36 % oxidised after 2 hours and 87 % oxidised after 20 hours, compared with 74 % and 100 % respectively in air. As this temperature is above the temperature at which the nitride decomposes the oxidation must be accompanied by the simultaneous decomposition of the nitride.

X-ray diffraction analysis of the product produced after 2 hours at 1000 °C showed peaks due to cubic CrN (JCPDS card 11-65) and hexagonal Cr_2O_3 (JCPDS card 6-504), but no peaks due to the hexagonal sub-nitride Cr_2N (JCPDS card 1-1232 and 27-127). From this it can be deduced that under these conditions the sub-nitride is more readily oxidised than CrN. Although some of CrN may have decomposed to Cr_2N, the more rapid oxidation of the sub-nitride precludes any appreciable concentration of the sub-nitride from being established. Despite the fact that the sub-nitride is the more stable of the two nitrides when heated in an inert atmosphere at 1000 °C, after 20 hours oxidation in CO_2 there is no evidence for the sub-nitride in the x-ray trace.

At 1000 °C the rate determining step may be the decomposition of CrN to Cr_2N followed by the rapid oxidation of Cr_2N to Cr_2O_3 accounting for the

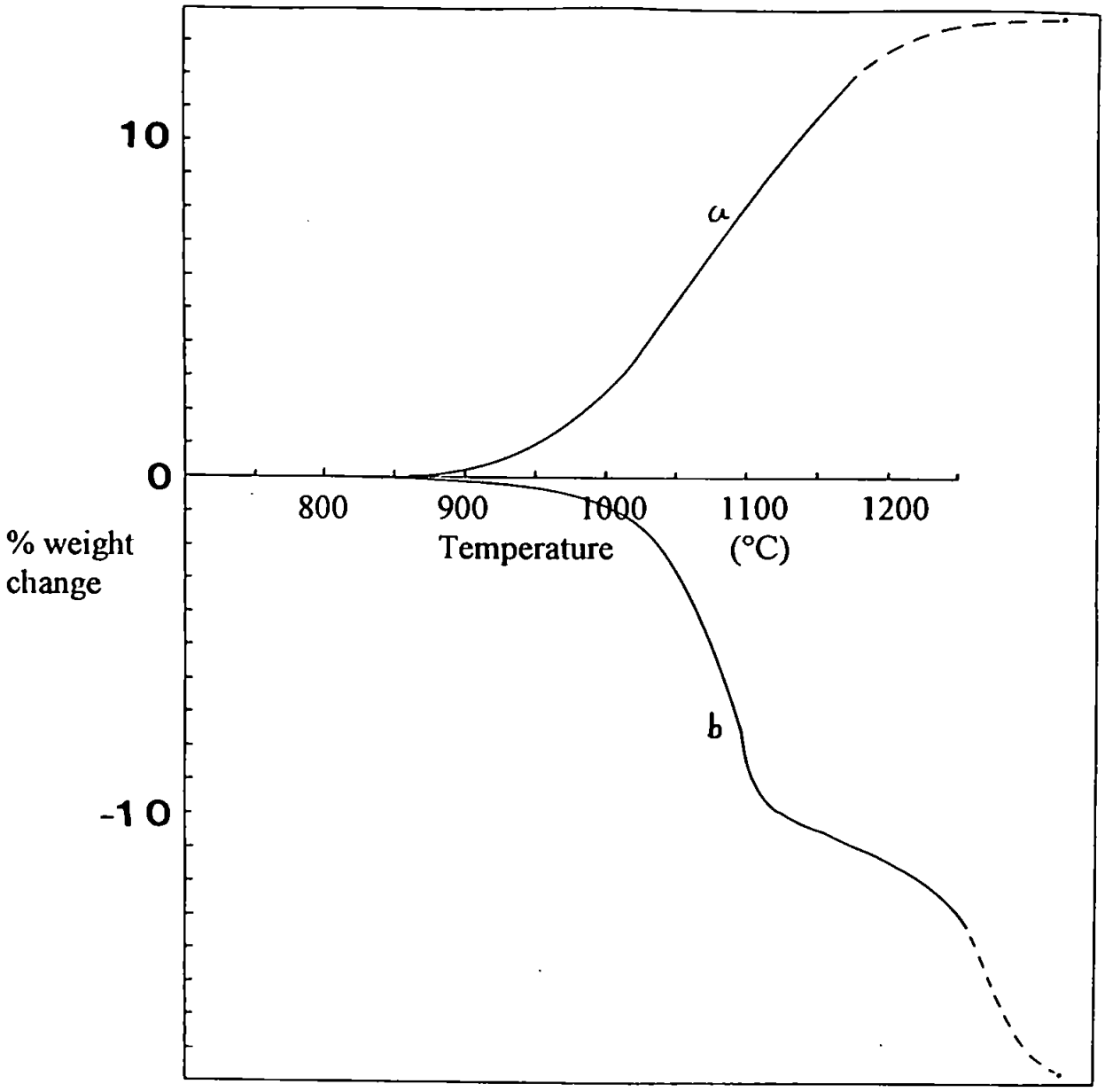

Figure 57
Chromium nitride heated at 10 °C min-1 in (a) carbon dioxide and (b) argon.

absence of Cr_2N in the x-ray traces. Alternatively CrN may be able to oxidise directly.

At no time was there any evidence of the deposition of free carbon. Above 800 °C any carbon that may be deposited would be oxidised in the Boudouard reaction (although at this temperature the reaction is slow)

$$C + CO_2 \rightarrow 2CO.$$

Therefore the oxidation may be represented by the equations

$$2Cr_2N + 6CO_2 \rightarrow 2Cr_2O_3 + N_2 + 6CO$$

$$4CrN \rightarrow 2Cr_2N + N_2$$

and/or

$$2CrN + 3CO_2 \rightarrow Cr_2O_3 + N_2 + 3CO.$$

Electron micrographs (plates 21 and 22) show that the products are, as with air oxidations, extensively sintered. The sintering of the oxide would hinder the further oxidation on the nitride.

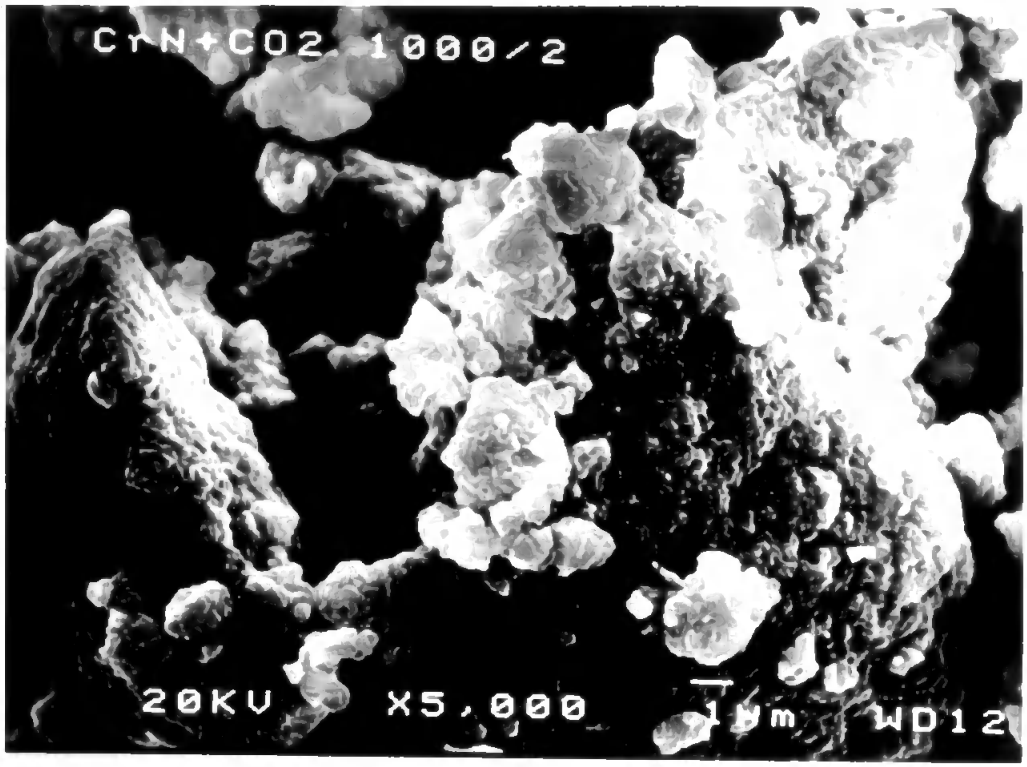

Plate 20
Chromium nitride oxidised for 2 hours at 1000 °C in carbon dioxide

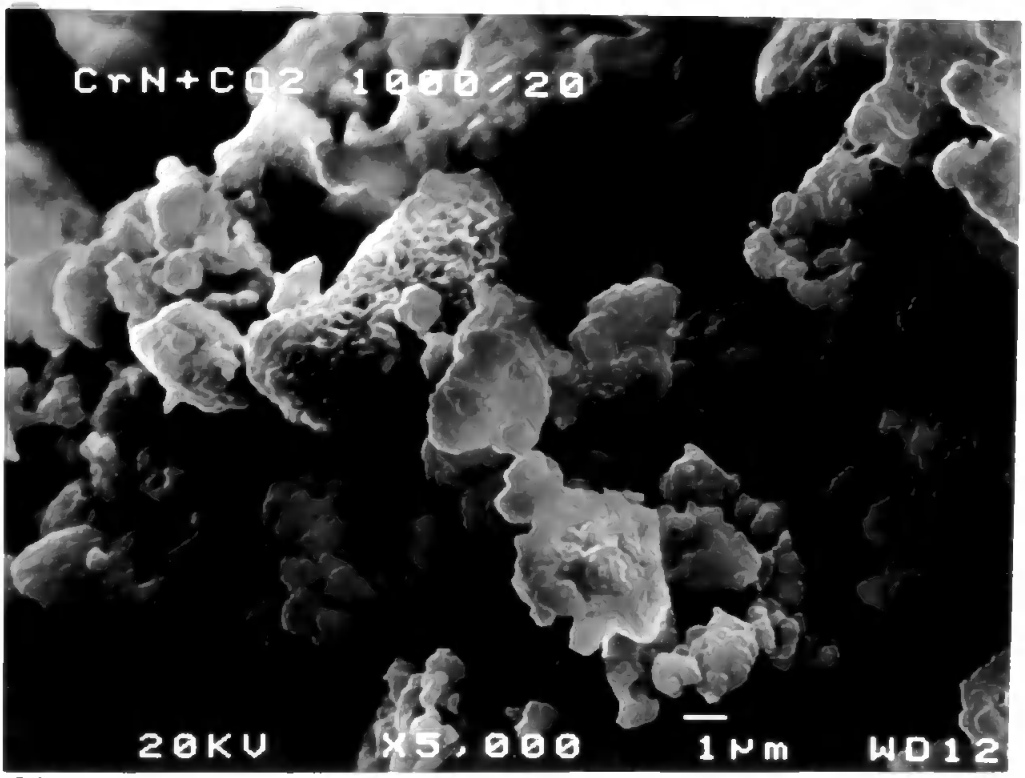

Plate 21
Chromium nitride oxidised for 20 hours at 1000 °C in carbon dioxide

4.3 OXIDATION OF IRON NITRIDE IN CARBON DIOXIDE

As has been shown previously in section 3.7 of this work, the iron nitride as supplied consisted of 90 wt-% Fe_4N and 10 wt-% Fe_2N which on oxidation in air formed 75 wt-% Fe_2O_3 and 25 wt-% Fe_3O_4. Dynamic heating of the nitride in argon resulted in decomposition of the nitride, with a 6.4 % weight loss.

On heating the nitride at 10 °C min^{-1} in carbon dioxide, oxidation began above 200 °C. The oxidation was not complete at 600 °C as in air oxidation, but only achieved constant weight after holding at 800 °C for a further 2 hours (figure 58). Thus, the reaction in carbon dioxide proceeded slower than in air. The final weight gain was 32.59 %, which is similar to that obtained in air (32.63 %).

After 90 minutes isothermal oxidation at 500 °C, constant weight was achieved (figure 59). X-ray diffraction analysis of the product produced after 2 hours oxidation in CO_2 at 500 °C indicated that the product was Fe_3O_4 (cubic magnetite, JCPDS card 19-629) with small quantities of unreacted nitride, but without any peaks due to Fe_2O_3 (hexagonal hæmatite, JCPDS card 24-72). Isothermal studies at lower temperatures (figure 60) showed that the reaction is hindered by the formation of the oxide, thus at 450 °C the reaction stops at $\alpha = 0.66$. As previously shown in this work Fe_3O_4 can sinter at 500 °C. The kinetic plot shows that at 500 °C the two-thirds order plot is linear for the first 20 minutes, before the plot deviates from the straight line indicating that the rate of reaction is initially controlled by the reaction occurring at the surface of a diminishing sphere before the product hinders the reaction. At 450 °C the reaction followed two-thirds order kinetics for the first 25 % and half order for the next 25 % before the reaction is stopped at $\alpha = 0.66$ by the oxide produced.

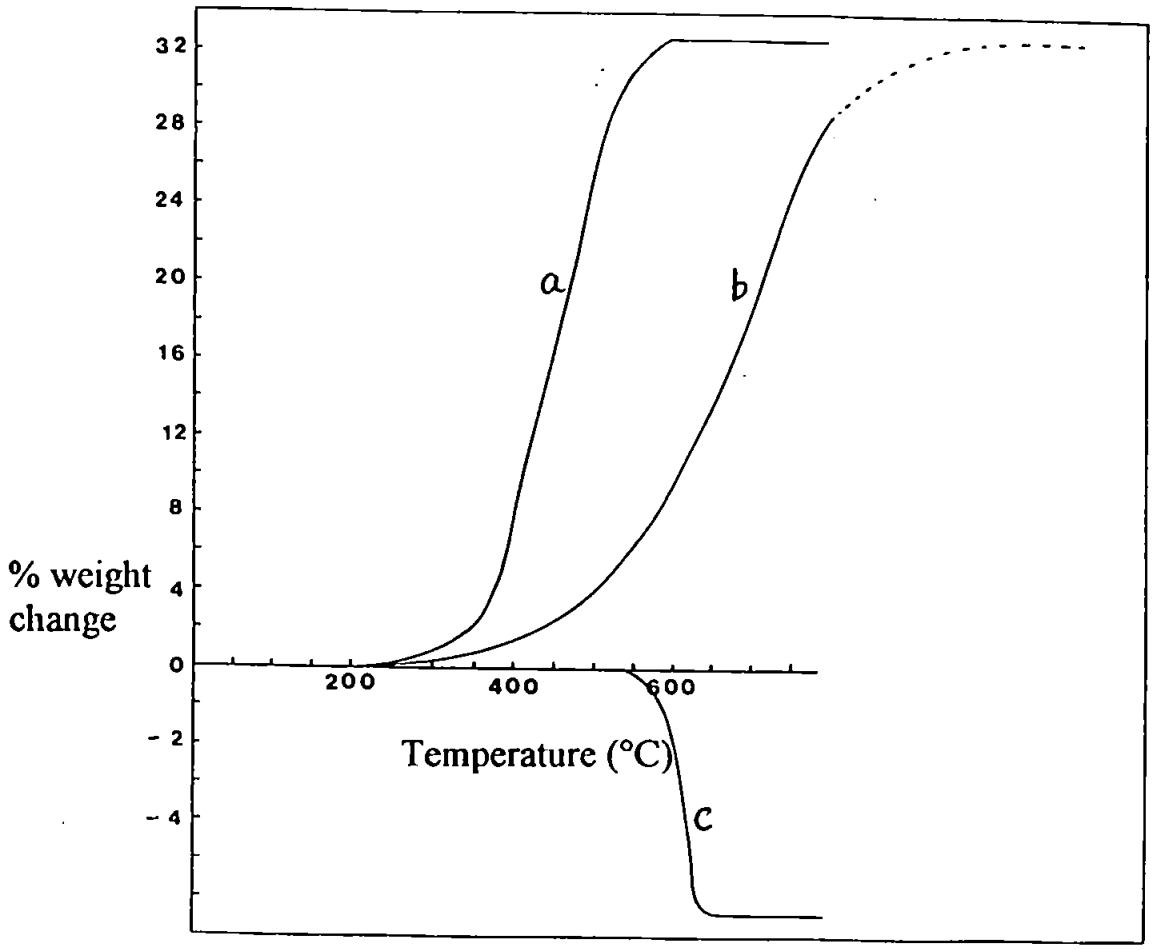

Figure 58
Iron nitride heated at 10 °C min-1 in (a) air (b) carbon dioxide and (c) argon.

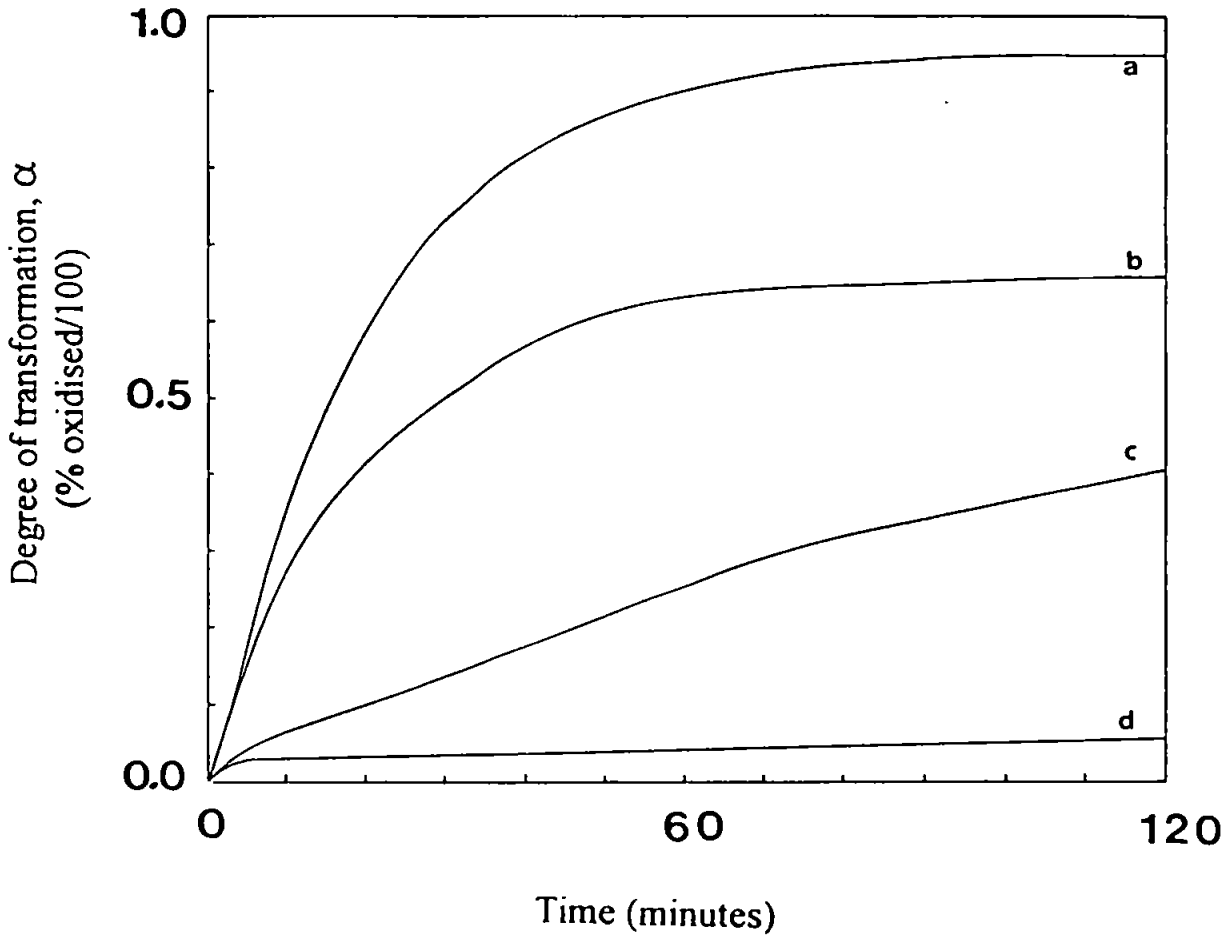

Figure 59

Isothermal TG curves for the oxidation of iron nitride in flowing carbon dioxide (300 ml min^{-1}) at a) 500 °C, b) 450 °C, c) 400 °C, d) 300 °C.

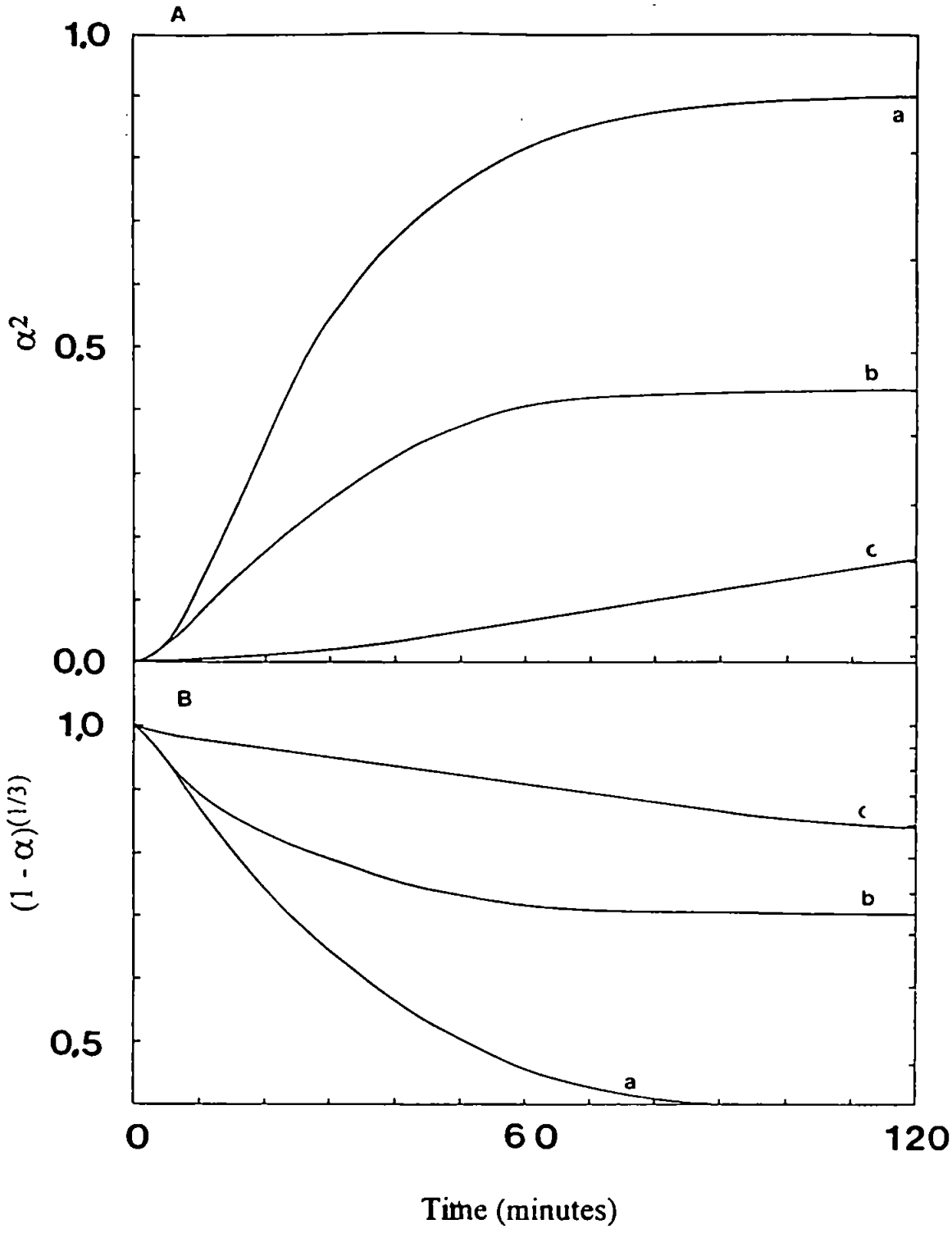

Figure 60
Half order (A) and two-thirds order (B) kinetic plots for the isothermal oxidation of iron nitride in carbon dioxide at a) 500 °C, b) 450 °C, c) 400 °C.

From the isothermal studies the initial gradients of the curves were determined, (table 17). From the Arrhenius plot (figure 61) the activation energy was calculated to be 22.7 ± 3 kJ mol^{-1} compared with 15.3 kJ mol^{-1} for the reaction in air.

From x-ray data already presented in this section, oxidation in carbon dioxide favours the formation of the lower oxide, Fe_3O_4, rather than the higher Fe_2O_3. There was no evidence for the deposition of carbon at 500 °C, although at this temperature any carbon that might be formed would be amorphous and therefore not detectable by x-ray diffraction. However, this mechanism would give rise to greater weight gains as any carbon deposited at 500 °C would not be oxidised in the Boudouard reaction. Therefore the overall reaction may be written as

$$6Fe_4N + 32CO_2 \rightarrow 8Fe_3O_4 + 3N_2 + 32CO$$

and

$$6Fe_2N + 16CO_2 \rightarrow 4Fe_3O_4 + 3N_2 + 16CO$$

Temperature, T		$d\alpha/dt$	$\ln(d\alpha/dt)$	$1/T$
^oC	K	min^{-1}		$x\ 10^{-3}\ K^{-1}$
500	773	0.0357	-3.332	1.294
450	723	0.0303	-3.496	1.383
400	673	0.0171	-4.069	1.485
300	573	0.0107	-4.533	1.745

Arrhenius plot
Gradient of slope = -2740 K
Correlation coefficient = -0.97

Table 17
Isothermal oxidation of iron nitride in carbon dioxide

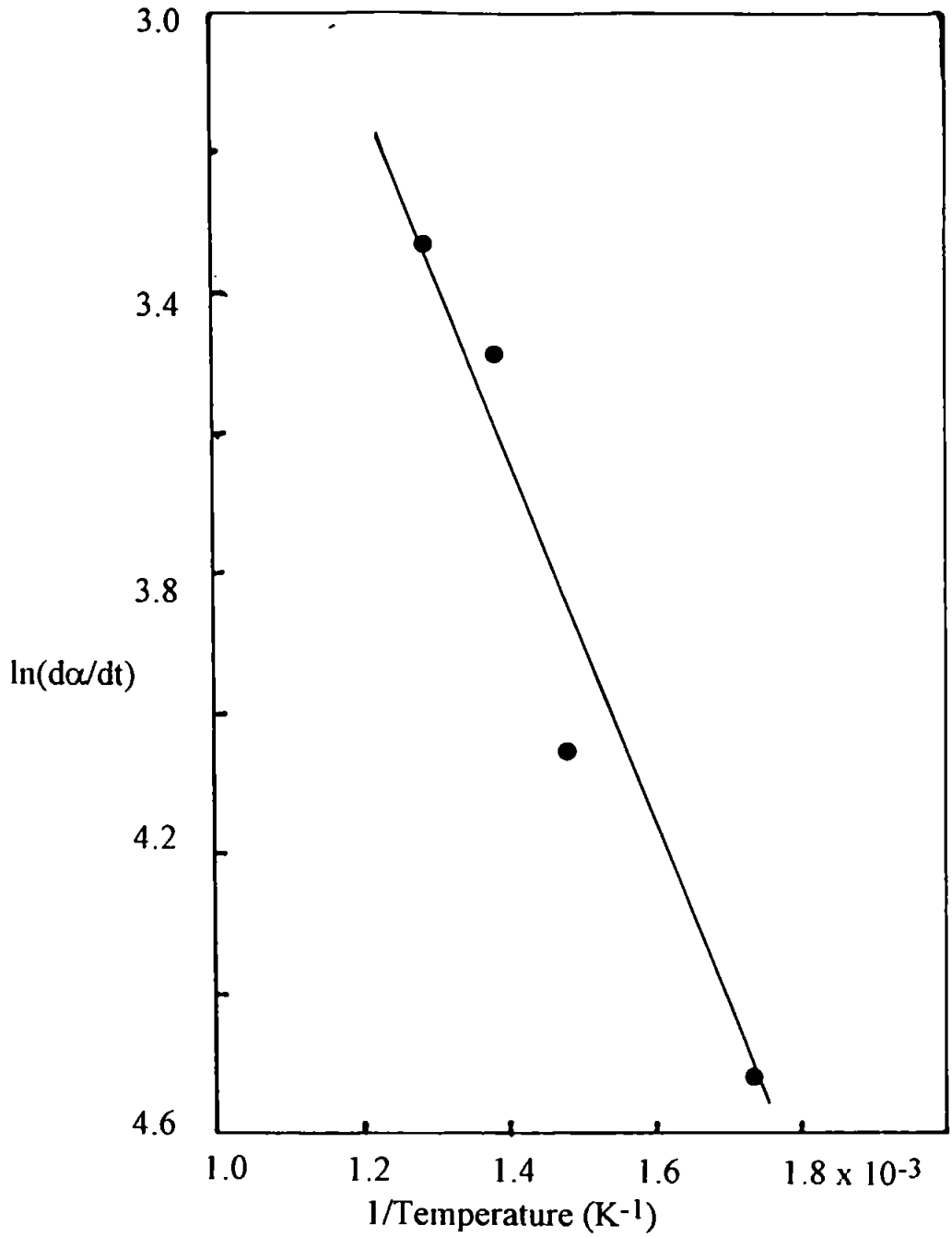

Figure 61
Arrhenius plot for the oxidation of iron nitride in carbon dioxide.

4.4 OXIDATION OF TITANIUM NITRIDE IN CARBON DIOXIDE

Titanium nitride undergoes oxidation at temperatures above 500 °C. Figure 62 shows the weight gain on heating the nitride in carbon dioxide at 10 °C min^{-1} to 1200 °C. The observed maximum weight gain was 30.9 % compared with the expected theoretical maximum of 29.1 %. X-ray analysis of the oxidation product showed the oxide to be TiO_2 (tetragonal rutile, JCPDS card 21-1276). No other species were detected.

The oxide when recovered from the furnace was observed to be pale orange in colour in contrast to the colour of TiO_2 which is usually white. Any carbon that may have been released as free carbon would be expected to be oxidised to carbon monoxide in the Boudouard reaction at temperatures above 800 °C. At temperatures below 800 °C any free carbon would colour the product a grey or black colour, not yellow or orange. Therefore the minor constituent could not be carbon. Rutile TiO_2 can lose oxygen at high temperatures, going from the fully oxidised state to a slightly reduced state. This is represented by $[Ti^{4+}_{1-x}Ti^{3+}_{x}O_{2-x/2}]$, the presence of Ti^{3+} giving a blue tinge to the oxide (Beals (1970)). This reduced form of titanium dioxide can be restored to the fully oxidised form on heating at 600 °C in an atmosphere containing oxygen (Alpher (1970)). The lower oxide TiO is yellow in colour (CRC Handbook of Chemistry and Physics (1994)). Peaks due to either of these lower oxides could not be detected in the x-ray diffraction trace when the oxide was analyzed. It would seem probable that the product is mainly titania with traces of TiO and possibly reduced TiO_2. The overall reaction is given by

$$2TiN + 4CO_2 \rightarrow 2TiO_2 + N_2 + 4CO$$

with some loss of oxygen.

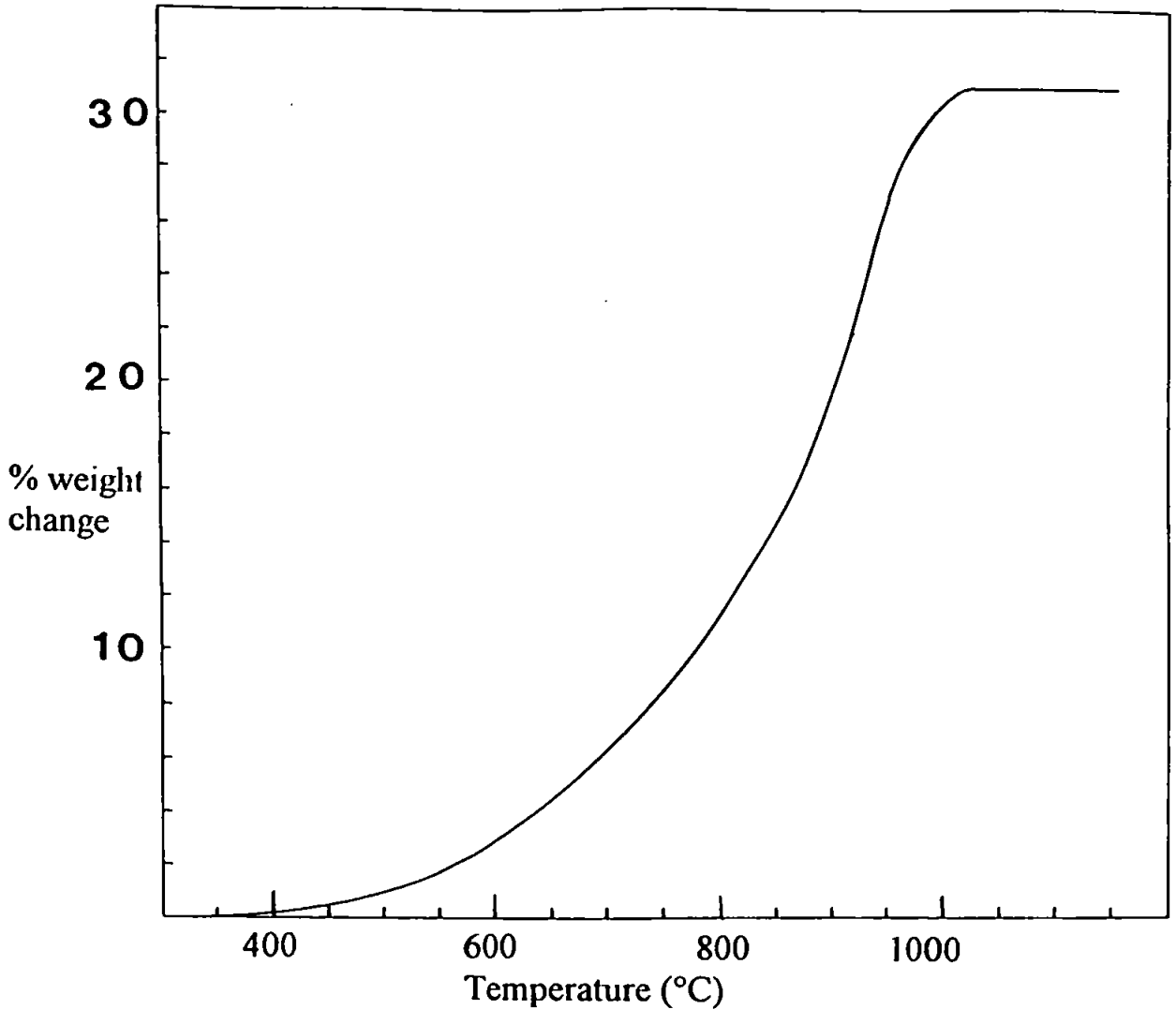

Figure 62
Titanium nitride heated at 10 °C min-1 in carbon dioxide.

CHAPTER 5

COMPARISONS AND CONCLUSIONS

5.1 INTRODUCTION

Table 18 summarises the transition metal nitrides and carbides studied along with the oxidation products detected and identified by x-ray diffractometry.

Figure 63 shows the standard free energies of formation, $\Delta G°_F$, of the nitrides and oxides of chromium, iron and titanium and also of carbon dioxide (Wick and Block (1963), Ali (1970), Glasson and Jayaweera (1968), JANAF (1965) and CRC Handbook (1994)). Application of Hess's law showed that the oxidation of these nitrides in carbon dioxide was thermodynamically possible at temperatures above 25 °C, as the sum of the standard free energies of the products was less than the sum of the standard free energies of the reactants.

The kinetics of the oxidation of the carbides and nitrides of titanium, zirconium and chromium together with the carbides of vanadium, niobium and tantalum and iron nitride in air have been studied. The oxidations of chromium, iron and titanium nitrides in carbon dioxide have also been studied. The activation energies of these reactions, calculated from the Arrhenius and Kissinger plots are summarised in table 19.

The activation energies determined in this work for the oxidation of titanium nitride, zirconium nitride and chromium carbide showed that those energies calculated from data obtained from DTA studies (Kissinger method) are considerably higher than those obtained from isothermal TG data (Arrhenius method). The activation energies calculated from isothermal oxidations was calculated from $d\alpha/dt$ values obtained at the start of the reaction whereas those from DTA studies are calculated from the DTA peak which occurs at higher values of α. Reed et al (1965) showed mathematically that the peak in the

Initial material	Oxide phases detected
Oxidation in air	
TiN (cubic)	TiO_2 (tetragonal - rutile).
TiC (cubic)	TiO_2 (tetragonal - rutile).
ZrN (cubic)	ZrO_2 (cubic) with increasing amounts of ZrO_2 (monoclinic - baddeleyite) above 600 °C.
ZrC (face centred cubic)	unidentified face centred cubic phase below 400 °C, with increasing amounts of ZrO_2 (cubic) between 400 and 600 °C and ZrO_2 (monoclinic - baddeleyite) above 600 °C.
V_4C_3 (cubic)	V_2O_5 (orthorhombic - shcherbinaite)
NbC (cubic)	β-Nb_2O_5 (monoclinic) although α-$Nb_{12}O_{29}$, β-$Nb_{12}O_{29}$ and $2(Nb_{47}O_{116})$ have very similar x-ray diffraction traces and could also be present.
Mixed CrN (cubic - carlsbergite) + Cr_2N (hexagonal)	Cr_2O_3 (rhombohedral - eskolaite)
Cr_3C_2 (orthorhombic)	Cr_2O_3 (rhombohedral - eskolaite)
Mixed Fe_4N (cubic) + Fe_2N (orthorhombic)	Fe_3O_4 (cubic - magnetite) + Fe_2O_3 (hexagonal - hæmatite)
TaC (face centred cubic)	Ta_2O_5 (pseudo-hexagonal)
Mn_5C_2 (monoclinic) + unidentified phase assummed to be Mn_3C	Mn_3O_4 (orthorhombic - hausmannite)

Mixed Cr_3C_2 (orthorhombic) + ZrC (face centred cubic)	Cr_2O_3 (rhombohedral - eskolaite) + ZrO_2 (cubic) with increasing amounts of ZrO_2 (monoclinic - baddeleyite) above 600 °C.
Oxidation in carbon dioxide	
Mixed CrN (cubic - carlsbergite) + Cr_2N (hexagonal)	Cr_2O_3 (rhombohedral - eskolaite)
Mixed Fe_4N (cubic) + Fe_2N (orthorhombic)	Fe_2O_3 (hexagonal - hæmatite) + Fe_3O_4 (cubic - magnetite)
TiN (cubic)	TiO_2 (tetragonal - rutile).

Table 18
Summary of starting materials and oxidation phases observed

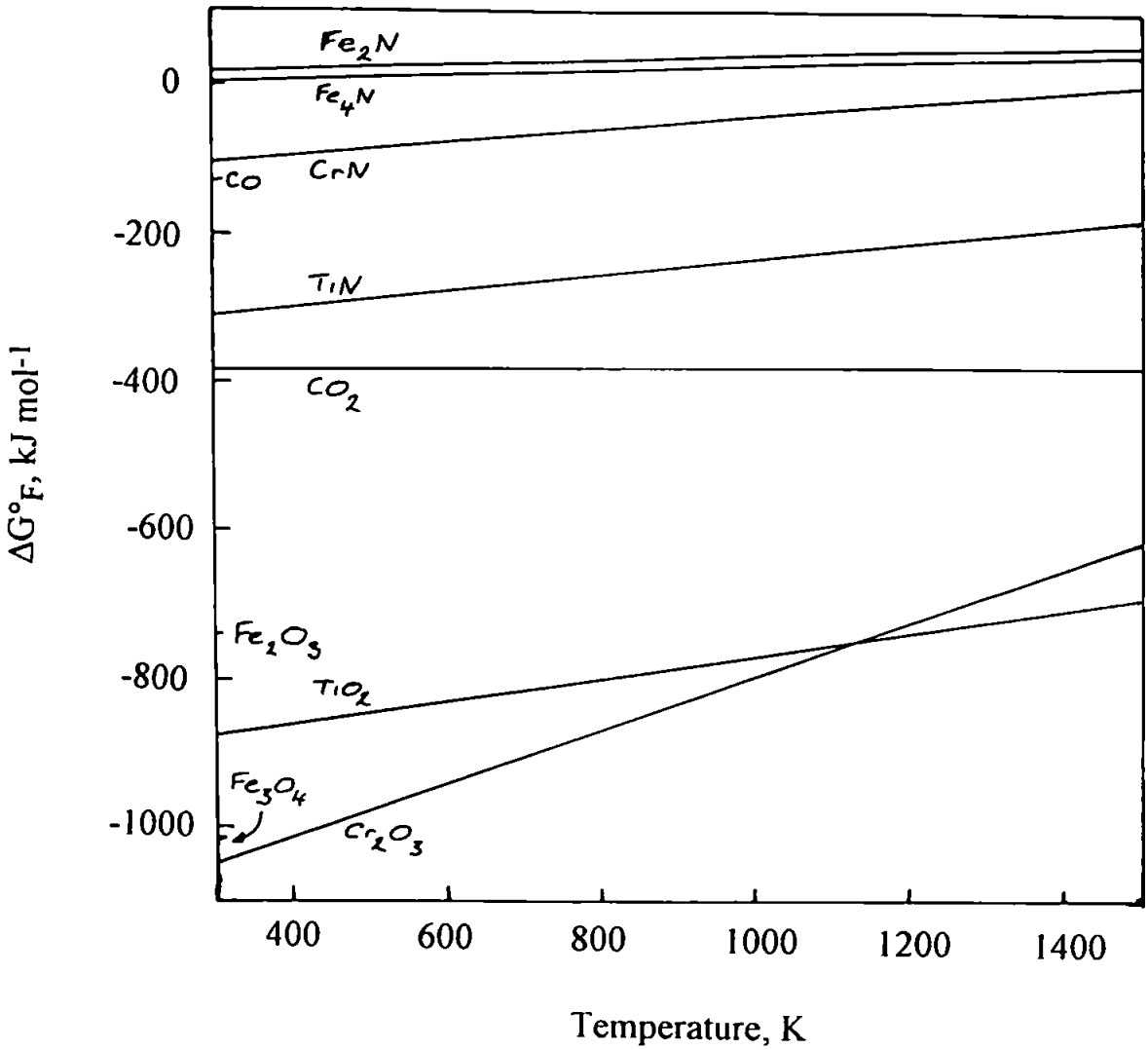

Figure 63
Standared free energy of formation of selected compounds

Compound	Activation energy, kJ mol^{-1}	
	Arrhenius method	Kissinger method
TiN	62.7 ±3	330. ±12
TiC	22.6 ±0.5	
ZrN	130. ±4	241. ±4
ZrC	14.6 ±0.3	
V_4C_3	76.8 ±20 [1]	
NbC	25.1 ±0.3 [1]	
CrN + Cr_2N	- -	
Cr_3C_2	83.1 ±3	269. ±3
Fe_2N + Fe_4N	15.3 ±0.2	
TaC	21.2 ±2 [2]	
Mn_5C_2 + MnC_3	- -	
Fe_2N + Fe_4N in CO_2	22.8 ±1	

[1] only selected data points used in determination of activation energy.
[2] 46.4 ±0.5 kJ mol^{-1} if 884°C data point omitted.

Table 19
Activation energies for the oxidation of selected transition metal nitrides and carbides determined by the Arrhenius and Kissinger methods

DTA trace does not always coincide with the maximum rate of reaction, thus indicating that the Kissinger method of determining activation energies is not valid in all circumstances. Benoit et al (1985) demonstrated that in order to obtain useful data from DTA studies it is necessary to show from isothermal studies that the reaction order is constant throughout the temperature range being studied. The Kissinger plots for the oxidations of titanium nitride and zirconium nitride (figures 15 and 26) have shown that at high heating rates the data points depart from the line of best fit obtained from data points at lower heating rates. In the oxidation of titanium nitride the Kissinger plot is further complicated by the DTA peak developing a shoulder at high heating rates. Thus although the carbides are less stable (having lower activation energies) the oxidation of the nitride is kinetically more favourable at higher temperatures.

5.2 COMPARISONS BETWEEN CARBIDES AND NITRIDES

The activation energies found for titanium carbide and zirconium carbide are considerably lower than their respective nitrides.

Titanium carbide could be oxidized at lower temperatures than the nitride, being approximately 20 % oxidized at 400 °C after 2 hours compared with the nitride which had to be oxidized at 500 °C, this corresponds with the higher activation energy determined for the oxidation of the nitride. At 1000 °C, however, the nitride was completely oxidized within 30 minutes but the carbide was only just completely oxidized after 2 hours.

Zirconium carbide was 40 % oxidized within 1 hour at 400 °C and completely oxidized within 1 hour at 700 °C compared with the nitride which was only 40 % oxidized within 1 hour at 600 °C, but like the carbide was completely oxidized within 1 hour at 700 °C.

Chromium carbide was approximately 50 % oxidized at 800 °C after 2 hours compared with the nitride which was only 18.5 % oxidized at that temperature after 20 hours.

Titanium, zirconium and chromium carbides oxidized at lower temperatures more easily than their nitrides. At the higher temperatures studied the nitride is oxidized quicker than the carbide, except chromium. The ability of the carbides to be oxidized at temperatures lower than the respective nitride is accounted for by the activation energies for the oxidation of the carbides being lower than for the respective nitride. At higher isothermal temperatures the nitrides of titanium and zirconium oxidized quicker than the carbide indicating that the pre-exponential factor, A, in the Arrhenius equation must be larger for the carbide than the nitride.

5.3 COMPARISONS WITHIN GROUP IVa

Titanium nitride and zirconium nitride are both cubic MN structures, where M = Ti or Zr, which on oxidation form MO_2. Titanium dioxide was found to have a tetragonal structure at all temperatures studied in this work and it would be expected for the oxide to be structurally incompatible with the remaining nitride and therefore spall off. Some sintering of the oxide would account for the hindered nature of the two-thirds order kinetics found for the oxidation of these compounds. Zirconium nitride formed the cubic form of the dioxide at temperatures up to 600 °C, and the monoclinic form of the dioxide at temperatures above (the high temperature tetragonal form was not found at the temperatures studied in this work). As previously indicated in chapter 3.3, the densities of the cubic nitride and oxide are similar and therefore it would be expected that the oxide produced at temperatures below 600 °C would be structurally compatible with the remaining nitride. The monoclinic form of the dioxide produced at temperatures above 600 °C, has a density significantly different from the nitride; thus it would be expected that the monoclinic form would be structurally incompatible with the remaining nitride and therefore split and spall off from the nitride. This would account for the oxidation following half order kinetics at temperatures up to 600 °C where the kinetics is determined by the diffusion of oxygen through a layer of oxide, and hindered two-thirds at temperatures above where the kinetics is determined by the oxidation of a decreasing sphere but hindered by a limited amount of oxide sintering. With both nitrides, the oxidation products offered little protection to further oxidation. The small amount of sintering of the products that can occur at the temperatures studied does not proceed fast enough to prevent the ingress of oxygen to the remaining nitride and hence prevent further oxidation.

Both carbides are also of the cubic MC structure, which on oxidation formed MO_2. Titanium carbide, like the nitride, formed an oxide that was

structurally incompatible with the remaining carbide. The reaction therefore followed two-thirds order kinetics, hindered by the limited sintering of the oxide. Zirconium carbide oxidation was complicated by the formation of an intermediate compound. Due to this the kinetic plots were indeterminate.

The activation energy for the oxidation of titanium nitride was found to be approximately half that of zirconium nitride, but the activation energy for the oxidation of zirconium carbide was found to be approximately two-thirds that of titanium carbide.

The isothermal TG curves showed that zirconium nitride and carbide oxidized at lower temperatures than titanium nitride or carbide.

5.4 COMPARISON WITHIN GROUP Va

During the course of this work difficulties were encountered with the determination of activation energies for the oxidation of the carbides of vanadium, niobium and tantalum. These included the low melting point and sublimation of vanadium pentoxide and the difficulty in maintaining isothermal conditions due to liberated energy in the oxidation reaction of niobium carbide. The activation energies found showed that the value for vanadium carbide is greater than that of both niobium and tantalum carbides. Tantalum carbide had a higher activation energy than niobium carbide.

Both vanadium and niobium carbides oxidized appreciably at 400 - 450 °C, but tantalum carbide oxidized at slightly higher temperatures (<500 °C). The melting points of both the carbide and oxides increase from vanadium (2810 and 690 °C respectively) to niobium (3500 and 1520 °C respectively) to tantalum (3880 and 1800 °C respectively), thus at the temperatures studied, the oxides were able to sinter by surface diffusion and possibly by crystal lattice diffusion (and in the case of vanadium oxide by melting). The oxides produced were therefore highly sintered and hindered the kinetics.

5.5 COMPARISON ACROSS FIRST TRANSITION SERIES

The activation energies found for the air oxidations of the carbides increases from 22.6 kJ mol^{-1} for TiC, 76.8 kJ mol^{-1} for V_4C_3 to 83.1 kJ mol^{-1} for Cr_3C_2. The minimum isothermal temperature at which oxidation was appreciable (>10 % after 2 hours) increased from 400 °C for TiC, 450 °C for V_4C_3, 600 °C for Cr_3C_2 to 600 °C for manganese carbide which oxidized very slowly. The increasing temperature at which oxidation is appreciable is in agreement with the increasing activation energies found for the reactions.

Titanium nitride oxidized appreciably (>10 % after 2 hours) at 500 °C, iron nitride oxidized appreciably at 300 °C but chromium nitride oxidized very slowly at 800 °C.

5.6 COMPARISON BETWEEN OXIDATION IN AIR AND CARBON DIOXIDE

The three nitrides studied in dynamic conditions oxidized in carbon dioxide at temperatures slightly higher than the oxidation in air. Chromium nitride began oxidising at 850 °C in carbon dioxide and at 750 °C in air.

Iron nitride began oxidising at 250 °C in both air and carbon dioxide, but in air the reaction proceeded more quickly so that the final weight gain had been achieved when the sample had been heated to 600 °C compared with carbon dioxide where the final weight gain was only achieved after prolonged heating at 900 °C. From isothermal studies the activation energy for the oxidation of iron nitride in carbon dioxide was found to be 22.8 kJ mol^{-1} and 15.3 kJ mol^{-1} in air. Iron nitride oxidized in carbon dioxide formed the lower oxide Fe_3O_4 whereas in air a mixed oxide was formed consisting of Fe_2O_3 + Fe_3O_4 in varying proportions.

Titanium nitride began oxidising in carbon dioxide and air at just over 400 °C. The TG traces for oxidation with the sample being heated at 10 °C min^{-1} in air and carbon dioxide are almost identical. The product from carbon dioxide oxidations showed a yellow colour indicating the presence of trace quantities of the lower oxide TiO as well as TiO_2. In air oxidations only TiO_2 was present in the high temperature products.

From these observations, the oxidation of these metal nitrides in carbon dioxide favours (where possible) the formation of lower oxides in greater quantities than in air oxidations. This is due to the lower oxidising power of carbon dioxide than air or oxygen. The activation energies for the oxidation of iron nitride is greater in carbon dioxide than in air as the overall reaction involves the reduction of carbon dioxide to the monoxide as well as the oxidation of the carbide.

5.7 CONCLUSIONS AND FUTURE WORK

5.7.1 RECENT RESEARCH

Recent research into the uses of transition metal nitrides, carbides and oxides (along with the borides and hydrides) as catalysts has indicated that these compounds are of industrial importance. The use of molybdenum oxicarbide as a catalyst for hydrocarbon isomerization has been reported by Ledoux et al (1995) and for the hydrotreatment of naptha and other hydrocarbon compounds important in the petrochemical industry by Liaw et al (1995) and Ramanathan and Oyama (1995). Dhandapani and Oyama (1995) have reported the use of these compounds as catalysts for the dehalogenation of chloro-fluoro-hydrocarbons (CFCs). CFCs have been used, until recently, as refrigerants in both domestic and commercial refrigeration units, as propellants in aerosol spray cans and as foaming agents in the production of foam thermal insulation material. The manufacture and use of CFCs is now strictly limited by the Montreal Protocol, as the daughter products formed by the breakdown of CFCs in the stratosphere are believed to be responsible for the depletion of stratospheric ozone. Stratospheric ozone, and the reactions that form ozone, absorbs ultra-violet radiation from the sun which would be harmful to life if they penetrated to ground level. A catalyst that can, at relatively low cost, be used to break down the CFCs recovered from decommissioned refrigeration units to harmless compounds is therefore of commercial importance.

Transition metal nitrides and carbides have interesting electrical, magnetic and optical properties. The changing electrical properties of tantalum oxynitride has been utilised by Ayerdi et al (1995) in high temperature strain gauges. Layered titanium nitride and tungsten is being investigated by Ruhl et al (1995) for applications in vertically integrated circuits. General electrical properties of nitrides, carbides, oxides and borides, some of which are semi-conductors or superconductors, have been studies by Wang et al (1995). The magnetic properties, along with the crystallographic properties, of finely divided iron

nitride has been studied by Kaczmarek (1995). The optical properties of titanium nitride and graphite coated Langmuir probes for space applications has been studied by Veszelei and Veszelei (1993). Kiuchi and Chayahara (1994) have studied the properties of titanium nitride as a transparent conductor with possible applications such as electrodes for liquid crystal displays and electrically heated glass.

Titanium nitride has been studied as a possible coating for replacement body parts such as artificial hips and knees where both biocompatibility combined with hard-wearing and inert characteristics are important (Narayan et al (1994)).

5.7.2 CONCLUSIONS

The transition metal nitrides and carbides studied in this work were used as supplied by the manufacturer. The surface chemistry was not studied by x-ray photo-electron spectroscopy (or at lower resolution, by SEM-energy dispersion x-ray micro-analysis) due to the lack of suitable equipment. Had suitable equipment been available it would have been possible to study whether the reactions occurred uniformally or in islands, whether there was any oxide covering present in the supplied material or any oxynitrides, oxycarbides or carbonates formed during the reactions. XRD studies did indicate some of the phases present in both starting reagents and oxidation products, however, x-rays will only be diffracted once crystallites present are above a critical size and thus will not be diffracted by amorphous phases or when the crystallites are below the critical size.

BET surface area studies were performed over the pressure range p/p_o = 0.0 to 0.3, and not over the full range p/p_o = 0.0 to 1.0 and thus it was not possible to include full isotherms which would have indicated the presence of porosity, which could have been further studied by mercury porosimetry. The BET

equipment could be used to determine the surface area of a sample with a surface area as low as 0.1 m^2g^{-1} for the older balance and considerably lower with the newer, more sensitive, balance. Theoretical surface areas were calculated which assumed that the material consisted of uniform spheres of uniform size, which whilst shown by SEM not to be the case, was useful when compared with the surface areas produced during oxidation studies. Surface area studies showed that during the first stages of oxidation the surface area increased and the average particle size decreased, indicating splitting of the remaining particle matrix.

The oxidation kinetics and rates were dependent on whether the oxide formed was structurally compatible with the remaining reactant and the ability of the oxide to sinter. Surface area determinations indicated whether the oxide formed spalled from the remaining particles or the extent of sintering. Those oxides that, due to change in crystal structure and volume changes, were not compatible with the remaining particles, offered less protection to further oxidation. Therefore the kinetic plots indicated the two-thirds order reaction kinetics expected for a reaction occurring at the surface of a sphere of diminishing radii. Half order kinetics indicates that the diffusion of oxygen through a layer of oxidation product limited the rate of the reaction. Due to the many variables within the reaction system (changing surface area, non-uniform particle size, surface chemistry, presence of impurities, presence of more than one oxide phase or oxynitride, oxycarbide or carbonate phase) the reaction kinetics do not fit a two-thirds or half order mechanism over all temperatures or at all stages of a reaction.

Sintering of the oxide may give some protection leading to hindered mechanisms. Sintering of the oxide is controlled by surface diffusion (promoting grain boundary penetration) at lower temperatures (above about 1/3 melting point in K). At higher temperatures (above about 1/2 melting point in

K - the Tammann temperature) sintering by crystal lattice diffusion can occur. Comparison of the oxidation of the metals and the metal nitrides has shown that sintering can be inhibited by the removal of nitrogen, but sometimes accelerated by the remaining metal (Ali (1970)).

Initial activation energies for oxidation in air, and for one case in carbon dioxide, were calculated from isothermal oxidations. The geometry of the sample crucible, the sample mass and how the sample is distributed within the sample container will affect the calculated energies. Similarly the activation energies calculated by this technique may not remain constant with temperature. Activation energies calculated by the Kissinger method, are calculated under dynamic temperature conditions and at α values greater than that used in the isothermal method. Thus the activation energies calculated by the two methods do not agree with each other. In this work it was found that the Kissinger method gave an activation energy considerably higher than that of the isothermal method (up to five times greater).

Both titanium nitride and carbide have cubic structures and oxidize to the tetragonal dioxide rutile TiO_2, at relatively low temperatures (400 - 600 °C). Due to the limitations stated above, no other phases were detected. The crystallites of dioxide split off from the remaining nitride or carbide before sintering can occur. SEM showed that at temperatures up to 800 °C, titanium nitride particles split open, greatly increasing the surface area and hence the oxide could not inhibit the reaction significantly. Only at temperatures above 900 °C did the oxide sinter, however, at these temperatures the reaction was completed within 30 minutes and sintering had little effect. Thus the reaction followed the expected two-thirds order mechanism, only deviating at $\alpha > 0.80$ at 900 °C. Titanium carbide, however, oxidised slower than the nitride and thus at temperatures above 800 °C sintering of the oxide did affect the reaction and hindered the reaction giving rise to deviations from the two-thirds order

mechanism. BET studies showed that for titanium carbide oxidation the total surface area reached its greatest value at 600 °C. For both compounds the Arrhenius plots indicated that the activation energies, as calculated from initial rates, were constant throughout the temperature range studied.

The oxidation of zirconium nitride is complicated by the formation of cubic zirconia (sometimes called 'amorphous' cubic) at temperatures below 600 °C and monoclinic above (tetragonal zirconia forms above 1200 °C), hence at temperatures below 600 °C the oxide is structurally compatible with the remaining reactant but above 600 °C the change in crystallite structure and the change in density causes the oxide to split and spall away from the remaining nitride. The Arrhenius plot shows that at temperatures above 640 °C the data points deviate from the straight line indicating that the activation energy, as calculated from initial rates, is not constant. Similarly the Kissinger plot shows deviation from the straight line at high heating rates. Zirconium carbide oxidation is further complicated by the formation of an intermediate that shares some of the crystal lattice planes with the carbide and is thus stabilised at low temperatures before both compounds are oxidized to the cubic or monoclinic (or tetragonal) dioxide. At high temperatures (above 600 °C) the weight gain shows a greater weight gain than expected which falls back to the expected weight. An intermediate compound is being formed which, however, could not be identified. The Arrhenius plot indicated that at the temperatures studied the initial rates activation energy remained constant.

Oxidation of vanadium carbide produced the orthorhombic pentoxide V_2O_5. The low melting point of the pentoxide (690 °C) resulted in extensive sintering. The sintering of the oxide inhibits the reaction, however, this was accompanied at temperatures above 600 °C by the sublimation of the oxide. Ali (1970) found that the maximum rate of oxidation of vanadium nitride occurred at 500 °C, and that the sintering of the oxide predominates over any splitting of

the remaining nitride. These results were confirmed by this work. The Arrhenius plot was not, at higher temperatures, conclusive due to erroneous weight readings caused by the sublimation of the oxide.

Niobium and tantalum carbides both oxidized to the pentoxide Nb_2O_5 and Ta_2O_5 respectively. The oxidation rate of niobium carbide was affected by the exothermic nature of the reaction. The self ignition of the starting material therefore gave rise to errors in determining the temperature of the reaction and thus points on the Arrhenius plot are scattered around the expected line at temperatures above 450 °C. Oxidation of both metal carbides was accompanied by large changes in density resulting in the oxide splitting away from the carbide although some sintering of the oxide partially inhibited the oxidation. The Arrhenius plot for the oxidation of tantalum carbide shows that at temperatures above 800 °C the activation energies calculated from initial rates changes. The TG curves show that at all temperatures studied a 'hiccup' occurs approximately 10 minutes after the reaction has started. At 884 °C the weight gain reached a value of 96 % of that expected then fell back to 90 %. No intermediate could be identified by the analytical techniques available.

The chromium nitrides (CrN and Cr_2N) were the most oxidation resistant of the nitrides studied, only being fully oxidized to the sesquioxide Cr_2O_3 at 1000 °C after 15 hours. The carbide is more reactive, being fully oxidized at 1000 °C within 6 hours. Extensive sintering is possible at 1000 °C, being above the Tammann temperature of the oxide, resulting in the kinetics of both reactions being impeded. Sintering of the oxide produced from the oxidation of the carbide was observed at 600 °C. The Arrhenius plot for the oxidation of chromium carbide, from initial rates, indicated that the activation energy is constant throughout the temperatures studied.

Iron nitride as supplied was a mixture of Fe_4N and Fe_2N, and oxidation of this mixture produced a mixture of Fe_2O_3 and Fe_4O_3. The kinetics plots show that the reaction is impeded at all temperatures studied, however, the Arrhenius plot shows that the activation energy calculated from initial rates remains constant throughout the temperature range studied. This work has shown that at higher temperatures the nitride can decompose to the metal. Oxidation of the metal would favour the production of the lower oxide Fe_3O_4 (Kubaschewski and Hopkins (1962)). Surface area studies of the oxidation products formed at 500 °C showed that during the first half of the reaction the surface area increased greatly indicating that the oxide was spalling away from the nitride and the average particle size decreased (see figure 51). During the third quarter of the reaction the surface area decreased due to sintering of the oxide. After the reaction had reached 89 % completion, the surface area once again increased indicating slow conversion of the lower oxide to the higher. This supports the proposed mechanism:

$$[Fe_2N + Fe_4N] \rightarrow (Fe) \rightarrow Fe_3O_4 \rightarrow Fe_2O_3$$

Surface area changes during the oxidation of manganese carbide showed extensive sintering of the oxide at the temperatures studied. The initial reaction rate increased with temperature, however, due to the extensive sintering of the oxide formed in the initial stages of oxidation the final weight gain and hence final percentage oxidized was inversely related to the temperature.

During the oxidation of the three carbides in carbon dioxide, the final weight gains indicated that free carbon had not been deposited. At temperatures above 800 °C it would be expected that the carbides could also be oxidized by a reaction similar to the Boudouard reaction:

$$MC + 2CO_2 \rightarrow MO + 3CO$$

or be reduced to the metal

$$MC + CO_2 \rightarrow M + 2CO$$

where M = transition metal, although the oxidation in carbon dioxide may favour the production of lower transition metal oxides than when oxidized in air.

Whilst transition metal nitrides and carbides are very hard materials that are widely used for their hardness, electrical properties and mechanical properties (Toth (1971)), many, as this work has shown, are easily oxidized at relatively low temperatures. It would be expected that those compounds with oxidation products that are structurally compatible with the remaining unoxidized material would have kinetics that are determined by the diffusion of oxidant gas through the oxidation products, however, if the oxidation product is not structurally compatible it would be expected that the product would spall away from the remaining unoxidized material and the kinetics determined by the chemical reaction. Oxidation products that sinter at the temperature of the oxidation may hinder further oxidation. From the compounds studied in this work, if the oxide layer is structurally compatible with the remaining reactant then the kinetics of the reaction is controlled by the diffusion of oxygen (or carbon dioxide) through the oxide layer. This results in half order type kinetics. If the oxide formed is not structurally compatible and does not sinter extensively at the temperature of the oxidation the reaction kinetics is controlled by the decreasing reactant particle size. This results in two-thirds order type kinetics. If the oxide sinters extensively at the temperature of the oxidation then the oxide layer is stabilised around the reactant particle hindering further oxidation of the reactant due to the increased difficulty for oxygen to diffuse through the oxide layer, resulting in hindered half order type kinetics.

In some of the reactions studied, intermediate compounds manifested themselves by the anomalous weight gains shown during the oxidation or, as in

the case of the oxidation of zirconium carbide, the formation of a stable intermediate with a "metallic" blue colour which was studied by x-ray diffractometry and identified as having a cubic structure but not listed in the JCPDS index. The intermediates formed, with the exception of that formed during the oxidation of zirconium carbide, could not be identified by the techniques used indicating that either they were not stable at room temperature or that they were amorphous (i.e. the phase was not able to form in a crystalline form that could be identified by x-ray powder diffractometry).

This work has shown that the nitrides and carbides of selected transition metals are oxidized relatively easily in air, when compared to the parent metal. Some of these compounds are also capable of being oxidized in carbon dioxide, without the apparent production of free carbon. The growing commercial importance of transition metal nitrides and carbides both in their traditional roles as hard materials for coatings on cutting tools and as catalysts, sensors and in electronic and optical applications require a greater knowledge of their characteristics. This work has shown that those studied are relatively easily oxidised, if only partially. Only those oxides that sintered extensively were able to prevent the complete oxidation. This work has shown that three of the carbides can be oxidised in carbon dioxide and are thus likely to be oxidised in more oxidising gases such as the oxides of sulphur or the oxides of nitrogen.

5.7.3 FUTURE WORK

Pollution by the oxides of nitrogen and sulphur are of significant environmental importance. Further studies may show that transition metal nitrides and carbides are able to catalyse the reduction of the oxides of nitrogen or sulphur, to less harmful compounds thus replacing the expensive catalysts (containing platinum, palladium and rhodium metals) presently used. In this work it has been shown that some transition metal nitrides and carbides can be oxidized in carbon dioxide at temperatures slightly higher than the oxidation in air. It is

possible that some of these transition metal nitrides and carbides may also be oxidized by oxidizing gases such as the oxides of nitrogen or sulpher. The possible catalytic properties of these compounds may thus be impaired if they oxidize at the temperature of the reaction that is to be catalysed.

The catalytic properties of a catalyst depends, inter alia, on the physical properties of its surface. Further studies of the surface area and porosity of these transition metal nitrides and carbides by techniques such as chemisorption, BET surface area determinations and mercury porosimetry will yield further information concerning the physical nature of the surfaces. Similar studies of the changes in these properties during the oxidation of transition metal nitrides and carbides in air, carbon dioxide and other oxidizing gases and during any sintering of either the original material or of oxide product are required.

Investigation of the chemical properties of the surface of these transition metal nitrides and carbides by such techniques as x-ray photo-electron spectroscopy or Auger spectroscopy would give further insights as to the reaction mechanism of the oxidation. For example indicating whether the reaction occurs at localised sites on the surface or over the whole surface simultaneously, and the effect of impurities within the material.

The ability of an oxidizing gas to diffuse through an oxide layer will also be dependent on the partial pressure of the oxidant, and therefore further studies of the oxidation under controlled partial pressures are required to gain further insights in to the mechanisms involved.

It has been shown in this work that during the oxidation of several, if not all, of the transition metal nitrides and carbides studied, intermediate compounds are formed before the final oxide. Further studies of these intermediates by

techniques such as those referred to above would indicate the composition of these intermediate compounds and whether it is possible to crystallize the intermediate compounds and characterise them further as, like the parent compound, they may have interesting electrical, optical, magnetic and chemical properties.

REFERENCES

Adams, K.E.: PhD Thesis, C.N.A.A., Plymouth Polytechnic, 1988.

Ali, I.: PhD Thesis, C.N.A.A., Plymouth Polytechnic, 1970.

Alpher, A.M.: High Temperature Oxides Part 2, Academic Press, London, 1970.

Arbuzov, M.P., Golub, S.Ya. and Khaenko, B.V.: Izv. Akad. Nauk. SSSR. Neorg. Mater, 1977, 13(10), 1434.

van Arkel, A.E.: Molecules and Crystals, Butterworths, London, 1956.

Askarova, L.K. and Zhilyaev, V.A.: Z. Neorganicheskoi Khimii, 1994, 39(5), 743.

ASTM Standard E 698-79(1984): Test Method for Arrhenius Kinetic Constants for Thermally Unstable Materials, American Society for Testing and Materials Standards, Volume 14 part 2, ASTM, Philadelphia, 1984.

Ayerdi, i., Castano, E., Garciaalonso, A. and Gracia, F.J.: sensors and Actuators A-Physical, 1995, 46(1-3), 179.

Backovic, N., Weatherly, G.C. an Elder, J.E.: Canad. Metallurgical Quart., 1994, 33(1), 67.

Bamberger, C.E., Angelini, P. and Nolan, T.A.: J. Amer. Ceram. Soc, 1989, 72(4), 587.

Banerjee, P.K., Kim, J.S. and Mitra, S.S.: Thin Solid Films, 1991, 200(2), 341.

Bargeron, C.B., Benson, R.C., Jette, A.N. and Phillips, T.E.: J. Amer., Ceram. Soc., 1993a, 76(4), 1040.

Bargeron, C.B., Benson, R.C., Newman, R.W., Jette, A.N. and Phillips, T.E.: John Hopkins Apl. Tech. Digest, 1993b, 14(1), 29.

Baughan, E.C.: Trans. Farad. Soc., 1959, 55, 2025.

Beals, M.D.: in High Temperature Oxides Part 2: Ed. Alper, A.M., Academic Press, London, 1970

Benoit, P.M.D., Ferrillo, R.G. and Granzow, A.H.: J. Therm. Anal., 1985, 30, 869.

Bilz, H.: Z. Phys., 1958, 153, 338.

Blazec, A.: Thermal Analysis, Van Nostrand Reinhold, 1973.

de Boer, J.H.: Adv. Catalysis, 1956, 8, 18.

Bolgar, A.S., Litvinenko, V.F., Kizhikina, L.A., Timofeeva, I.I. and Kulik, O.P.: Porosh Metal., 1976, 11, 48.

Boudouard, O.: Ann. Chim. Phys., 1901, 24, 5

Bradshaw, W.G. and Matthews, C.O.: Properties of Refractory Materials; Collected Data and References, IMSD-2466, 1958.

Brager, A.: Acta Physicochim. URSS, 1939a, 10, 593.

Brager, A.: Acta Physicochim. URSS, 1939b, 11, 617.

Brauer, G. and Schnell, W.D.: J. Less Common Metals, 1964, 6(4), 326.

Bronoel, G., Museux, E., Leclercq, G, Leclercq, L. and Tassin, N.: Electrochimica Acta, 1991, 36(10), 1543.

Brown, B.R.: in Comprehensive Treatise on Inorganic and Theoretical Chemistry, Supplement to Vol.8, part 1, Longmans, London, 1964.

Brunauer, S., Demming, L.S., Demming, W.S. and Teller, E.: J. Amer. Chem. Soc., 1940, 62, 1723.

Brunauer, S., Emmett, P.H. and Teller, E.: J. Amer. Chem. Soc., 1938, 60, 309.

Cadoff, L. and Nielson, J.P.: J. Metals, 1953, 5, 248.

Calka, A.: Appl. Phys. Letters, 1991, 59(13), 1568.

Caillet, M., Ayedi, H.F. and Besson, J.: J. Less-Common Metals, 1977, 51(2), 305.

Carter, R.E.: J. Chem. Phys., 1961, 35, 1137.

Choi, J.G., Choi, D. and Thompson, L.T.: J. Materials Research, 1992, 7(2), 374.

Clarke, J. and Jack, K.H.: Chemy. Ind., 1951, 1004.

Coble, R.L.: Sintering and Related Phenomena, Materials Science research Vol 6, Ed. Kuczynski, Plenum Press, 1973.

Colombier, C. and Lux, B.: J. Materials Sci., 1989, 24(2), 462.

Cooper, J.R and Hansler, R.L.: J. Chem. Phys., 1963, 39, 248

Cotton, F.A. and Wilkinson, G.: Basic Inorganic Chemistry, 2nd Ed, John Wiley and Sons, London, 1976.

Courtright, E.L., Prater, J.T., Holcomb, G.R., StPierre, G.R. and Rapp, R.A.: Oxid. of Metals, 1991, 36(5-6), 423.

Coyne, H.J. Jr. and Tauber, R.N.: J. Appl. Phys., 1968, 39(12), 5585.

Cranston, R.W. and Inkley, F.A.: Advances in Catalysis, 1957, 9, 143.

CRC Handbook of Chemistry and Physics 75rd ed., CRC Press, London, 1994.

Croato, U., Genta, V. and Maltese, P.: Gazz. Chim. Ital., 1951, 81, 827.

Currie, A.L. and Howard, K.E.: J. Materials Sci., 1992, 27(10), 2739.

Denker, S.P.: J. Less-Common Metals, 1968, 14(1), 1.

Desmaison, J.G., Billy, M. and Smeltzer, W.W.: React. Solids (Proc. of 8th Inter. Conf.), 1977, 107.

Dhandapani, B. and Oyama, S.T.: Catalysis Letters, 1995, 35(3-4), 353.

Dubinin, M.M.: Chem. Rev., 1960, 2, 18.

Duwez, P. and Odell, F.: J. Electrochem. Soc., 1950, 97, 299.

Egorova, L.A., Klimentenko, O.P. and Kozik, V.V.: Inrg. Materials, 1992, 28(9), 1630.

Elger, G.W., Traut, D.E., Slavens, G.J. and Gerdemann, S.J.: Mett. Trans. B., 1989, 20(4), 493.

Epelbaum, V.A. and Ormont, B.F.: J. Phys. Chem. USSR., 1946, 20, 459.

Epelbaum, V.A. and Ormont, B.F.: J. Phys. Chem. USSR., 1947, 21, 3.

Frad, W.A.: Adv. Inorg. Chem. and Radiochem., 1968, 11, 153.

Franck, M., Blanpain, B., Oberlander, B.C., Celis, J.P. and Roos, J.R.: Solar Energy Materials and Solar Cells, 1993, 31(3), 401.

Freundlich, H.M.F.: Kappilarchemie, Leipzig, 1909.

Fridlender, B.A., Neshpor, V.S., Eron'yan, M.A. and Petrov, A.V.: Teplofizika Vysokikh Temperatur, 1977, 15(4), 779 (English translation p. 657).

Funakubo, H., Mizutani, N. and Tatsuno, T.: J. Materials Sci., 1993, 28(4), 994.

Garvie, R.C.: in High Temperature Oxides, Volume 5 Part 2, Ed. Alper, A.M., Academic Press, London, 1970.

Gaydon, F.P.: Vacuum, 1967, 17(6), 325.

Georgson, M., Roos, A. and Ribbing, C.G.: J. Vacuum Sci. and Tech. A., 1991, 9(4), 2191.

Glasson, D.R.: J. Chem. Soc., 1956, 1506.

Glasson, D.R.: J. Appl. Chem., 1956a, 8, 793.

Glasson, D.R.: J. Appl. Chem., 1956b, 8, 798.

Glasson, D.R.: J. Appl. Chem., 1960, 10, 38.

Glasson, D.R.: J. Appl. Chem., 1961a, 11, 24.

Glasson, D.R.: J. Appl. Chem., 1961b, 11, 201.

Glasson, D.R.: J. Appl. Chem., 1963a, 13, 111.

Glasson, D.R.: J. Appl. Chem., 1963b, 13, 119.

Glasson, D.R.: J. Appl. Chem., 1967, 17, 91.

Glasson, D.R. and Jayaweera, S.A.A.: J. Appl. Chem., 1968, 18, 65.

Glasson, D.R. and Jayaweera, S.A.A.: J. Appl. Chem., 1969, 19, 182.

Glasson, D.R. and Jones, J.A.: J. Appl. Chem., 1969a, 19, 125.

Glasson, D.R. and Jones, J.A.: J. Appl. Chem., 1969b, 19, 137.

Glasson, D.R. and Linstead-Smith, D.E.B.: Progress in Vacuum Microbalance Techniques Vol. 2, Heyden, 1973.

Glasson, D.R. and Sheppard, M.A.: J. Appl. Chem., 1968, 18, 327.

Goldstein, J.I., Newberry, D.E., Echlin, P., Joy, D.C., Fiori, C. and Lifshin, E.: Scanning Electron Microscopy and X-ray Micro-analysis. Plenum Press, 1981.

Golovko, E.I., Voitovich, V.B., Sereda, N.N. and Beloborodov, L.N.: Soviet Powder Metallurgy and Metal Ceramics, 1990, 29(4), 332.

Goodenough, J.B.: Phys. Rev., 1960a, 117, 1442.

Goodenough, J.B.: Phys. Rev., 1960b, 120, 67.

Goodenough, J.B.: Magnetism and the Chemical Bond, Wiler-Interscience, New York, 1963.

Gorbach, V.G., Meshashti, S. and Moskalenko, Y.N.: Soviet Powder Metallurgy and Metal Ceram., 1991, 30(4), 283.

Gregg, S.J.: The Surface Chemistry of Solids, Chapman and Hall, London, 1961.

Gregg, S.J. and Sing, K.S.W.: Adsorption, Surface area and Porosity, Academic Press, London, 1967.

Guilland, C. and Wyart, J.: J. Rech. Cent. Natn., Rech. Scient., 1947, 3, 123

Hägg, G.: Z. Phys. Chem., 1930, B7, 339.

Hägg, G.: Z. Phys. Chem., Abt, 1931a, B12, 33.

Hägg, G.: Metallwirt., 1931b, 10, 387.

Hägg, G.: Iva, 1953, 24, 345.

Hahn, H.: Z. Anorg. Chem., 1949, 258, 58.

Hannay, N.B.: Solid State Chemistry, Prentice-Hall, London, 1967.

Hara,T., Tani, K., Inoue, K., Nakamura, S. and Murai, T.: Appl. Phys. Letters, 1990, 57(16), 1660.

Hedge, R.I., Fiordalice, R.W. and Tobin, P.J.: Appl. Phys. Letters, 1993, 62(19), 2326.

Hennessey, T.P. and Morral, J.E.: Oxid. of Metals, 1992, 38(1-2), 163.

Huand, J.S.: Nuclear Instr. and Methods in Phys. Research B., 1991, 59(Jul), 651.

Hume-Rothery, W.: Ann. Rept. Prog. Chem., 1949, 46, 42.

Hume-Rothery, W.: Phil. Mag., 1953, 44, 1154.

Ibidunni, A.O.: Oxid. Metals, 1993, 40(1-2), 5.

Ibidunni, A.O., Masaitis, R.L., Opila, R.L., Davenport, A.J., Isaacs, H.S. and Taylor, J.A.: Surface and Intrface analysis, 1993, 20(7), 559.

Ignatev, A.S., Petrova, A.G. and Ryabov, Y.E.: Pisma V Z. Tekhnicheskoi Fizik, 1992, 18(10), 67.

Jack, K.H.: Proc. Roy. Soc. (A), 1948, 195, 41.

Jaggers, C.H., Michaels, J.N. and Stacy, A.M.: Chem. of Materials, 1990, 2, 150.

JANAF Thermochemical Tables, Clearinghouse for Federal Scientific Scientific and Technical Information, PB 168 370, 1965

Jayaweera, S.A.A.: PhD Thesis, London Univ., 1969.

Jentzsch, W.D. and Boehmer, S.: Neue Huette, 1979, 24(7), 249.

Jervis, T.R. and Zocco, T.G.: Materials Letters, 1990, 9(4), 147.

Jiang, C.C., Goto, T. and Hirai, T.: J. Materials Sci., 1990, 25(2a), 1086.

Jimenez, C., Perriere, J., Palacio, C., Enard, J.P. and Albella, J.M.: Thin Solid Films, 1993, 228(1-2), 247.

Johnson, W.B., Nagelberg, A.S. and Breval, E.: J. Amer. Ceramic Soc., 1991, 74(9), 2093.

Joint Committee for Powder Diffraction Standards file, 1967 et seq.

Juza, R., Anschutz, E. and Puff, H.: Angew. Chem., 1959, 71, 161.

Kaczmarek, W.A.: Scripta Metallurgica et Materialia, 1995, 33(10-11), 1687.

Kaizuka, T., Shinriki, H., Takeyasu, N. and Ohta, T.: Jap. J. Appl. Phys. Part 1., 1994, 33(18), 470.

Katsura, M.: J. Alloys and Compounds, 1992, 182(1), 91.

Kawaguchi, K. and Sohma, M.: Jap. J. Appl. Phys. 2, 1991, 30(12B).

Keattch, D.J. and Dollimore, D.: An Introduction to Thermogravimetry 2nd Ed. Heyden Press, London, 1975.

Kelly, A. and Groves, G.W.: Crystallography and Crystal Defects. Longmans, London, 1973.

Kieffer, R. and Benesovsky, F.: Encyclopedia of Chemical Technology, 2nd ed., Vol. 4, Wiley Interscience, New York, 1964a.

Kieffer, R. and Benesovsky, F.: Encyclopedia of Chemical Technology, 2nd ed., Vol. 13, Wiley Interscience, New York, 1964b.

Kieffer, R. and Kölbl, F.: Z. Anorg. Chem., 1950, 262, 229.

Kieffer, R., Schwarzkopf, P. with Benesovsky, F. and Leszynski, W.: Hartstoffe und Hartmetalle, Springer, Vienna 1953.

Kiessling, R.: Acta,. Chem. Scand., 1950, 4, 209.

Kiessling, R.: Met. Rev., 1957, 2(5), 77.

Kiffer, A.D.: WADD T.R.6 0-52; Defense Doc. Centre No AD-238-061, 1960.

Kingery, W.D.: J. Am. Ceram. Soc., 1955, 38, 3.

Kingery, W.D.: Introduction to Ceramics, Wiley, London, 1960.

Kissinger, H.E.: J. Research of the Nat. Bureau of Standards, 1956, 57, 217.

Kissinger, H.E.: Anal. Chem, 1957, 29, 1702.

Kiuchi, I., Fujii, K., Miyamura, H., Kadono, K., Satou, M. and Fujimoto, F.: Nuclear inst. and Methods in Phys. Research B, 1989, 37(Feb), 701.

Kiuchi, M. and Chayahara, A.: Appl. Phys. Letters, 1994, 64(8), 1048.

Klug, H.P and Alexander, L.E.: R-ray Diffraction Procedures, Wiley, London, 1954.

Kobayashi, H., Shimosaka, K. and Mitamura, T.: Nippon Seramikkusu Kyokai Gakujutsu Ronbunshi (J. Ceram. Soc. Jap.), 1992, 100(11), 1338.

Kobayashi, H., Shimosaka, K., Kamiyama, Y. and Mitamura, T.: Nippon Seramikkusu Kyokai Gakujutsu Ronbunshi (J. Ceram. Soc. Jap.), 1993, 101(3), 342.

Kochergina, A.A. and Fedoseev, D.V.: Inorg. Materials, 1990, 26(3), 549.

Konuma, M. and Matsumoto, O.: J Less-Common Metals, 1977, 55(1), 97.

Kosolapova, T. Ya.: Carbides; Properties, production and applications. Plenum Press, New York and London, 1971.

Krysmann, W. and Schroter, WE.: Materialwissenschaft und Werkstofftechnik, 1992, 23(11), 385.

Kubaschewski, O. and Hopkins, B.E.: Oxidation of Metals and Alloys (2nd Ed). Butterworths, London, 1962.

Kume, K. and Yamagish, H.: J. Phys. Soc. Jap., 1964, 19, 414.

Lakhtin, Y.M., Kogan, Y.D. and Shaposhnikov, V.N.: Elektron. Obrab. Mater., 1978, 5, 9.

Lakhtin, Y.M., Kogan, Y.D., Borovskaya, T.M. and Solodkin, G.A.: Izv. Akad. Nauk. SSSR. Met., 1979, 4, 176.

Langmuir, I.: J. Amer. Chem. Soc., 1916, 38, 2221.

Leclercq, L., Provost, M., Pastor, H., Grimblot, J., Hardy, A.M., Grengembre, L. and Leclercq, G.: J. Catalysis, 1989, 117(2), 371.

Ledoux, M.J., Phamhuu, C., Delporte, P., Blekkan, E.A., York, A.P.E., Derouane, E.G. and Fonseca, A.: Studies in Surface Sci. and Catalysis, 1995, 92, 81.

Lefort, P., Desmaison, J. and Billy, M.: C.R. Acad. Sc. Paris., 1977, 285(11), 361.

Lefort, P., Desmaison, J. and Billy, M..: C.R. Acad. Sc. Paris., 1978, 286(13), 361.

Lefort, P., Desmaison, J. and Billy, M..: C.R. Hebd. Seances, Acad, Sci. C 1979a, 289(10), 271.

Lefort, P., Desmaison, J. and Billy, M.: Oxid. of Metals., 1979b, 13(3), 203.

Liaw, S.J., Raje, A., Bi, X.X., Eklund, P.C., Graham, U.M. and Davis, B. H.: Energy and Fuels, 1995, 95, 921.

Lipson, H. and Steeple, H.: Interpretation of X-ray Powder Diffraction Pattens. MacMillan, London, 1970.

Litinenko, V.F., Bolgar, A.S., Kas'yan, V.I., Shvedova, L.K. and Timofeeva, I.I.: Porosh. Mettal. Kiev, SSSR, 1980, 2, 46.

Liu, B.X and Cheng, X.Y.: J. Phys. Condensed Matter, 1992, 4(16).

Louw, C.W., Strydom, I.L., Vandenheever, K. and Vanstaden, M.J.: Surf. and Coatings Tech., 1991, 49(1-3), 348.

Lowell, S.: Introduction to Powder Surface Area. Wiley, 1979.

Lyubimov, V.D., Timoshchuk, T.A. and Kalacheva, M.V.: Russ. Mettallurgy USSR, 1992, 3, 12.

MacInnes, A.N., Barron, A.R., Li, J.X. and Gilbert, T.R.: J. Amer. Ceram. Soc., 1991, 74(11), 2928.

Massiani, Y., Medjahed, A. and Picq, G.: Thin Solid Films, 1992, 207(1-2), 109.

Matsumura, Y., Chujo, T., Uchida, H and Uchida, H.H.: Surf. and Coatings Tech., 1993, 60(1-3), 489.

Mellor, J.W.: Comprehensive Treatise on Inorganic and Theoretical Chemistry, Vol 8, Longmans, London, 1927 (also 1969 edition).

Meerson, G.A.: in A Consise Chemical Encyclopedia, Vol. 3, Izd. "Sovetskaya Entsiklopediya", 1964.

Michalski, J. and Wierzchon, T.: J. Materials Sci. Letters, 1989,8(7), 779.

Miki, M., Ymasaki, T. and Ogino, Y.: Materials Transac., 1992, 33(9), 839.

Min, Z., Li, W.Z. and Li, H.D.: Nucl. Instrum. and Methods in Phys. Research B, 1991, 59(July), 1358.

Mitchell, D.R.G., and Stott, F.H.: Corrosion Sci., 1992, 33(7), 1083.

Moers, K.: Z. Anorg. Allg. Chem, 1931, 198, 243.

Moissan, H.: Compt. Rend., 1895, 120, 290.

Moissan, H.: Compt. Rend., 1897, 125, 839.

Montero, I., Jimenez, C., Albella, J.M. and Perrier, J.: Surf. and Interface Anal., 1993, 20(6), 503.

Moon, J., Ito, T., Ma, J.S. and Hiraki, A.: J. Crystal Growth, 1991, 115(1-4), 589.

Moore, C.H.: Ceramic Age, 1948, 52, 281.

Mott, N.F.: Nuovo. Cim., 1958, 7(10), Suppl. 312.

Nakagawa, Y., Ohtani, S., Nakata, T, Mikoda, M. and Takagi, T.: Nuclear Instr. and Methods in Phys. Research Section B, 1993, 80-1(Jun), 1402.

Narayan, J., Fan, W.D., Narayan, R.J., Tiwari, P. and Stradelmaier, H.H.: Material Sci. and Engin. B-Solid State Materials for Advanced Techn., 1994, 25(1), 5.

Nemchenko, V.F., L'vov, S.M. and Samsanov, G.V.: Ukr. Fiz. Zh., 1962, 7, 331.

Neshpor, V.S.: Refractory Transitional Metal Compounds, Ed. Samsanov, G.V., Academic Press, New York, 1964.

Norris, A.C., Pope, M.I., Selwood, M. and Judd, M.D.: Thermal Anal. 1, Proceedings Fourth ICTA, Budapest, 1974.

Norton, J.T. and Lewis, R.K.: Adv. Met. Research Corp., N63-18389, 1963.

Oberlander, B.C., Franck, M., Celis, J.P. and Roos, J.R.: Surf. and Coatings Tech., 1994, 64(1), 25.

Okada, S. and Atoda, T.: Yogyo Kyokaishi, 1980, 88(5), 242.

Omura, Y., Inokawa, H. and Izumi, K.: J. Materials Research, 1991, 6(6), 1238.

Oyama, S.T.: Catalysts Today, 1992, 15(2), 179.

Partch, R.E., Xie, Y.M., Oyama, S.T. and Matijevic, E.: J. Materials Research, 1993, 8(8), 2014.

Padilla, M.H., Rapp, R.A. and Stewart, H.A.: Forest Products J., 1991, 41(10), 31.

Pauling, L.: Phy. Rev., 1938, 54, 899.

Pauling, L.: The Nature of the Chemical Bond, 2nd Ed, 1940, (3rd Ed, 1960), Ithaca, New York: Cornell Univ. Press.

Pauling, L.: J. Am. Chem. Soc., 1947, 69, 542.

Pauling, L.: J. Chem. Soc., 1948, 1461

Pauling, L.: Proc. Roy. Soc.(A), 1949, 196, 343.

Pauling, L. and Ewing, F.J.: Rev. Mod. Phy., 1948, 20, 112.

Pilyankevich, A.N., Sinel'nikova, V.S., Strashinskaya, L.V., Shaposhnikova, T.I. and Golub, S.Ya.: Poroshk Metall, 1977, 10, 768

Polanyi, M.: Verh. Dtsh. Physik Ges., 1914, 16, 1012.

Pope, M.I. and Judd, M.D.: Differential Thermal Analysis, Heyden Press, London, 1977.

Precht, W. and Hollox, G.E.: J. Cryst. Growth, 1968, 3/4, 818.

Prosvirin, B.I.: Vest. Mettoprom. 1937, 17(12), 102.

Pugach, E.A., Lavrinenko, L.N. and Filipchenko, S.I.: Soviet Powder Metallurgy and Metal Ceramics, 1991, 29(5), 392.

Ramanathan, S. and Oyama, S.T.: J. Phys. Chem., 1995, 99(44), 16365.

Rao, G.A.R. and Venugopal, V.: J. Alloys and Compounds, 1994, 206(2), 237.

Reed, R.L., Gottfried, B.S. and Weber, L.: Ind. Eng. Chem. Fundamentals, 1965, 4, 38.

Ribeiro, F.H., Betta, R.A.D., Guskey, G.J and Boudart, M.: Chem. of Materials, 1991, 3(5), 805.

Richter, R., Kupfer, H., Giegengack, H., Schaarschmidt, G, Scholze, F., Elstner, F. and Hecht, G.: Surf. and Coatings Tech., 1992, 54(1-3), 338.

Rudy, E., Harmon, D.P. and Bruki, C.E.: Air Force Material Lab., Research and Tech. Div., AFML-TR-65-2, 1965, 2(1).

Ruhl, G., Froschle, B., Ramm, P., Intemann, A. and Palmer, J.: Appl. Surdace Sci., 1995, 91(1-4), 382.

Rundle, R.E.: Acta Cryst., 1948, 1, 180.

Saha, N.C. and Tompkins, H.G.: J. Appl. Phys., 1992, 72(7), 3072.

Sakka, Y., Ohno, S. and Uda, M.: J. Amer. Ceram. Soc., 1992, 75(1), 244.

Samsanov, G.V.: Dolk. Akad. Nauk. SSSR., 1953, 93, 689.

Samsanov, G.V.: Izg. Sek. Fiz. Khim. Anal., 1956a, 26, 716.

Samsanov, G.V.: Zh. Takh. Fiz., 1956b, 1, 695.

Samsanov, G.V.: Ukr. Khim. Zh., 1956, 23, 287.

Samsanov, G.V.: Handbook of High Temperature Materials, No. 2, Properties Index, Plenum Press, New York, 1964.

Samsanov, G.V.: Poroshkovaya Met., 1965a, 1, 98.

Samsanov, G.V.: Ukr. Khim. Zh., 1965b, 31(10), 1005.

Samsonov, G.V. and Golubeva, N.K.: J. Phys. Chem., Moscow, 1956, 30, 1258.

Samsanov, G.V. and Neshpor, V.S.: Dokl. Akad. Nauk. SSSR., 1958, 122,1021.

Samsanov, G.V. and Neshpor, V.S.: Powder Metallurgy and Strength of Materials, Vol 7, Izdvo Akad. Nauk. SSSR., Kiev, 1959.

Samsanov, G.V., Verkhoglyadova, T.S. and Dubovik, T.V.: Porosh Metal. Akad. Nauk. Ukr. SSSR., 1961, 1(4), 9.

Santoro, G. and Dolloff, R.T.: J. Appl. Phys., 1968, 39, 2293.

Sarkisov, E.S.: Zh. Fiz. Khim., 1954, 28, 625.

Sawarda, Y. and Hashimoto, A.: Thermochimica Acta, 1994, 231(Jan), 307.

Schaffer, P.T.B. and Samsanov, G.V.: High Temperature Materials, Handbooks 1 and 2, Plenum, New York, 1964.

Schwarzkopf, P.: Powder Met. Bull., 1950, 5, 68.

Schwarzkopf, P. and Kieffer, R.: Refractory Hard Metals: Borides, Carbides, Nitrides amd Silicides, MacMillan, New York, 1953.

Seith, W. and Kubaschewski, O.: Z. Electrochem., 1935, 41, 551.

Selvam, P., Viswanathan, B. and Srinivasan, V.: J. Less-Common Metals, 1990, 161(1), 77.

Sharp, J.H.: in 'Differential Thermal Analysis', Ed. Mackenzie, Academic Press, 1972.

Shimada, S., Inagaki, M. and Matsui, K.: J. Amer. Ceramic Soc., 1992, 75(10), 2671.

Shimer, P.W.: Proc. Roy. Soc., 1887, 42, 89.

Shorter Oxford Dictionary, Oxford University Press, Oxford, 1993.

Shulishova, O.I.: High Temperature Cermet Materials, Izd. Akad. Nauk. SSSR., Kiev, 1962.

Singer, I.L., Fayeulle, S. and Ehni, P.D.: Wear, 1991, 149(1-2), 375.

Stademmaiser, H.H. and Tong, S.Y.: Z. Mettalk., 1961, 52, 477.

Steinmann, P.A. and Hintermann, H.E.: J. Vac. Sci. Technol. A, 1985, 3(6), 2394.

Stolten, H., Spencer, P. and Neuschutz, D.: J. de Chimie Phys. et de Physico-chim. Biol., 1993, 90(2), 209.

Storms, E.K.: The Refractory Carbides, Academic Press, London, 1967.

Stott, F.H. and Mitchell, D.R.G.: Materials at High Temperature, 1991, 9(4), 185.

Stout, G.H. and Jenson, L.H.: X-ray stucture Determination: A Practical Guide. MacMillan, London, 1968.

Straumanis, M.E., Fraunce, A.A. and James, W.J.: Acta Met., 1967, 15(1), 65.

Sugimoto, A., Sano, T. and Kaneko, Y.: Nippon Kagaku Kaishi, 1994, 2, 126.

Sun, Y. and Bell, T.: Wear, 1993, 166(1), 119.

Sutherland, J.W.: in 'Porous Carbon Solids'. (Ed) R.I. Bond. Academic Press, 1967.

Szekely, J., Evans, J.W. and Sohn, H.Y.: Gas Solid Reactions, Academic Press, London, 1976

Thorne, K., Ting, S.J., Chu, C.J., Mackenzie, J.D., Getman, T.D. and Hawthorne, M.F.: J. Materials Sci., 1992, 27(16), 4406.

Tobin, J.M. and Fleischer, L.R.: Westinghouse Electric Co., Pittsburgh Pa., Astronuclear Lab. Tech. Rep. AF 33 (615) 3982; AFML-TR-67-137, Part 1 and 2 (1967); Defense Doc. Centre No. AD-663-248 (1968).

Tompkins, H.G.: J. Appl. Phys., 1991, 70(7), 3876.

Tompkins, H.G.: J. Appl. Phys., 1992, 71(2), 980.

Toth, L.E.: Transitional Metal Carbides and Nitrides, Academic Press, London, 1971.

Tylecote, R.F. and Mitchell, T.E.: J. Iron St. Inst, 1960, 196, 445.

Ubbelohde, A.R.: Trans. Farad. Soc., 1932, 28, 275.

Ubbelohde, A.R.: Proc. Roy. Soc. (A), 1937, 159, 295.

Umanskii, Ya.S.: Izv. Sek. Fiz. Khim. Anal., 1943, 16, 127.

Voitovich, R.F. and Golovko, E.I.: Russ. J. Phys. Chem., 1980, 54(6), 817.

Veszelei, M. and Veszelei, E.: Thin Solid Films, 1993, 236(1-2), 46.

Voitovich, V.B. and Laverenko, V.A.: Soviet Powder Metallurgy and Metal Ceramics, 1991, 30(11), 927.

Wakamatsu, Y., Izumida, M., Shimozaki, T. and Onishi, M.: J. Jap. Inst. Metals, 1993, 57(5), 538.

Waldron, M.B. and Daniell, B.L.: Sintering, Heyden, 1978.

Wang, C.C., Akbar, S.A., Chen, W. and Patton, V.D.: J. Material Sci., 1995, 50(3), 265.

Wendlandt, W.W.: Thermal Analysis 3rd Ed, Wiley and Sons, New York, 1986.

Whittemore, O.J.: The Trend in Engr. (Univ. Washington), 1968, 20(2), 28.

Wicks, C.E. and Block, F.E.: Thermodynamic Properties of 65 Elements - Their Oxides, Halides, Carbides and Nitrides, US Bureau of Mines Bulletin 605, 1963.

Williams, W.S.: Phys. Rev., 1964, A135, 505.

Wittmer, M., Noser, J. and Melchior, H.: J. Appl. Phys., 1981, 52(11), 6659 - 6664.

Won, C.W. and Chun, B.S.: J. Materials research, 1993, 8(10), 2702.

Yoshida, T., Kawasaki, A., Nakagawa, K. and Akashi, K.: J. Materials Sci., 1979, 14, 1624.

Zhang, Y.C. and Schleich, D.M.: J. Solid State Shem., 1994, 110(2), 270.

Zhao, G.Y., Revankar, V.V.S. and Hlavacek, V.: J. Less-common Metals, 1990, 163(2), 269.

Zhou, X., Dong, H.K. and Li, H.D.: Vacuum, 1989, 39(2-4), 307.

APPENDIX 1

Paper reprinted from Thermochimica Acta, 1986, 103(1), 193 - 199

Thermochimica Acta, 103 (1986) 193–199
Elsevier Science Publishers B.V., Amsterdam — Printed in The Netherlands

OXIDATION OF CHROMIUM CARBIDE

JEREMY N. CLARK[1], DOUGLAS R. GLASSON[1] and S. AMARASIRI A. JAYAWEERA[2]

[1]John Graymore Chemistry Laboratories, Department of Environmental Sciences, Plymouth Polytechnic, Plymouth, PL4 8AA, Devon, England, U.K.

[2]Department of Chemistry, Teesside Polytechnic, Middlesbrough, TS1 3BA, Cleveland, England, U.K.

ABSTRACT

The oxidation of chromium carbide has been studied gravimetrically. Products of reaction have been examined by gas sorption analysis and X-ray diffraction. Changes in phase composition, crystallinity and crystallite size are correlated with the reaction conditions.

Chromium carbide, Cr_3C_2, differs from most of the transitional metal carbides in that it forms stable films of metal oxide (Cr_2O_3) around the remaining carbide particles, inhibiting further oxidation. Thus chromium carbide additive inhibits oxidation of interstitial zirconium carbide, ZrC, by forming some chromic oxide which stabilises the zirconia (ZrO_2) layer around the remaining carbide crystallites.

INTRODUCTION

Transitional metal carbides (ref.1) are generally refractory materials in which high melting points (above 3000 °C) is accompanied by high degree of hardness (Mohs scale 8-9). Many of them are interstitial compounds, MC, (M = metal) with cubic (NaCl-type) structures analogous to the corresponding refractory hard metal nitrides (ref. 2), MN. Metals with up to 5 electrons in the d-shell form less stable d^0 and more stable d^5 configurations. Where the d^0 and d^5 stable configurations can vary widely, as in TiC or ZrC, there is only one carbide and it has a wide range of homogeneity. Larger numbers of carbide phases with narrower homogeneity ranges are formed as d^5 becomes the more probable configuration. Thus chromium forms 3 phases with high metal content, $Cr_{23}C_6$, Cr_7C_3 and Cr_3C_2.

Both transitional metal nitrides and carbides suffer from the disadvantage of atmospheric oxidation becoming appreciable at low temperatures (above about 500-700 °C) compared with their melting points. Earlier research on the oxidation of titanium and zirconium nitrides (ref. 3) has shown that the titanium and zirconium dioxide coatings are incompatible with the remaining nitrides and break away in finely-divided form. The oxidation of titanium carbide (ref. 4) suggests a similar behaviour.

In the present research, oxidation of chromium carbide has been studied

0040-6031/86/$03.50

gravimetrically. The surface area and porosity of the products have been examined by gravimetric nitrogen gas sorption, using a vacuum microbalance. Further information on changes in phase composition, crystallinity and particle size has been obtained by X-ray diffraction, so that the compatibility and stability of the chromium oxide coating can be ascertained. The behaviour of zirconium carbide on oxidation has been determined similarly and the possibility has been examined of chromium carbide additive forming oxide to stabilise the zirconia layer and thus inhibit oxidation.

EXPERIMENTAL

Thermogravimetric studies of the atmospheric oxidation of chromium carbide, Cr_3C_2, and zirconium carbide, ZrC, were made using a Stanton-Redcroft STA 781 thermal analyser. Larger samples (1 g) of the carbides were oxidised for various times at each of a number of fixed temperatures in air in a furnace.

The specific surface areas, S, of the cooled samples were determined by a gravimetric BET method (ref. 6) with nitrogen at -196 °C as the adsorbate on a CI Electronics mark 2C vacuum microbalance with μg to mg sensitivity, using samples of 0.2 g. The adsorption isotherms also indicated any porosity present (from hysteresis) and pore size ranges. Average crystallite sizes were deduced from the specific surfaces of the less porous materials. The metal oxides formed were identified by X-ray diffractometry.

RESULTS AND DISCUSSION

Chromium carbide oxidation

TG and X-ray diffraction data indicate that the initial carbide was Cr_3C_2 which oxidised to Cr_2O_3. The specific surface, S, of the initial chromium carbide was 0.42 m^2g^{-1}, (average crystallite size 2.1 μm). The chromium carbide slowly oxidised in air at 600 °C, being 22 % oxidised in 79 h, but there was no increase in the specific surface (cf. Fig. 1), so that the oxide did not scale off the remaining carbide. The final specific surface was only 0.39 m^2g^{-1}. After allowing for the 5.9 % weight increase on oxidation, the initial 1 g sample had only changed its total surface area, S', from 0.42 m^2 to 0.39 x 1.059 = 0.41 m^2.

Theoretically the change in volume on oxidation of 1 g Cr_3C_2 (X-ray density, D_x = 6.68) to 1.267 g Cr_2O_3 (D_x = 5.23) should be from 0.150 to 0.242 cm^2, representing a 0.615-fold increase. Thus if the oxide forms a stable layer around each carbide crystallite, the surface area change should be given by $S'/S = (1 + 0.615x)^{2/3}$, where x = fraction of carbide oxidised (ref. 7). For 22 % oxidation, the surface area of the initial Cr_3C_2 of 0.42 m^2 should increase to 0.46 m^2. Since the experimental result of 0.41 m^2 is slightly less, a small amount of oxide sintering must have occurred, coalescing some of the particles.

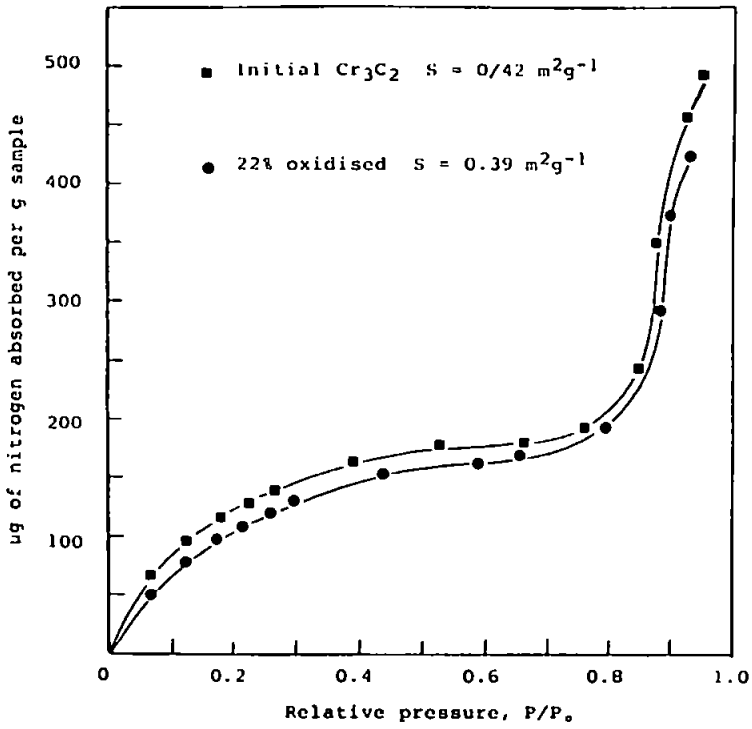

Fig. 1. Nitrogen adsorption isotherms at -196 °C on chromium carbide.

A limited amount of sintering of Cr_2O_3 by surface diffusion is possible, since 600 °C (873 K) is about one third of the melting point of Cr_2O_3 (2400 °C, 2673 K) in K. Sintering by crystal lattice diffusion also becomes appreciable above half the melting point in K (1064 °C, 1337 K). Therefore at higher temperatures, where oxidation to Cr_2O_3 is complete, the oxide product sinters more extensively and consolidates. There is certainly no scaling off (or spalling) of the oxide from the carbide surface even at 600 °C, in sharp contrast to the behaviour of zirconium carbide on oxidation.

Zirconium carbide oxidation

The initial specific surface area of the zirconium carbide was 0.59 m^2g^{-1} (average crystallite size 1.5 µm). Atmospheric oxidation became appreciable above 400 °C, (22 % oxidised in 1 h at 400 °C and complete in 1 h above 500 °C). Although there was no change in the surface area at 400 °C, there were considerable changes at the higher temperatures, as illustrated in Fig. 2 for the samples oxidised isothermally for 1 h. The maximum increase in surface area is given at 500 °C, i.e., from 0.6 to 15.2 m^2g^{-1}. The smaller increases in the

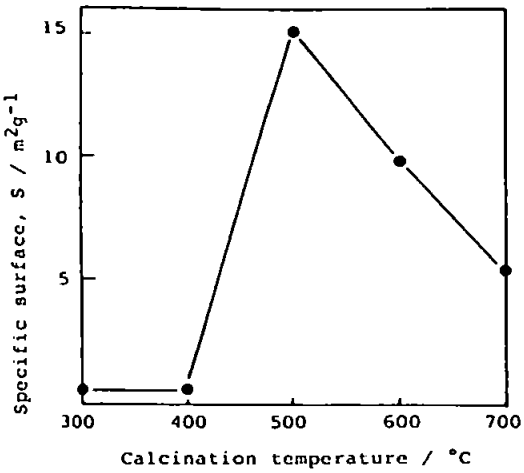

Fig. 2. Oxidation of zirconium carbide in air at different temperatures for 1 h.

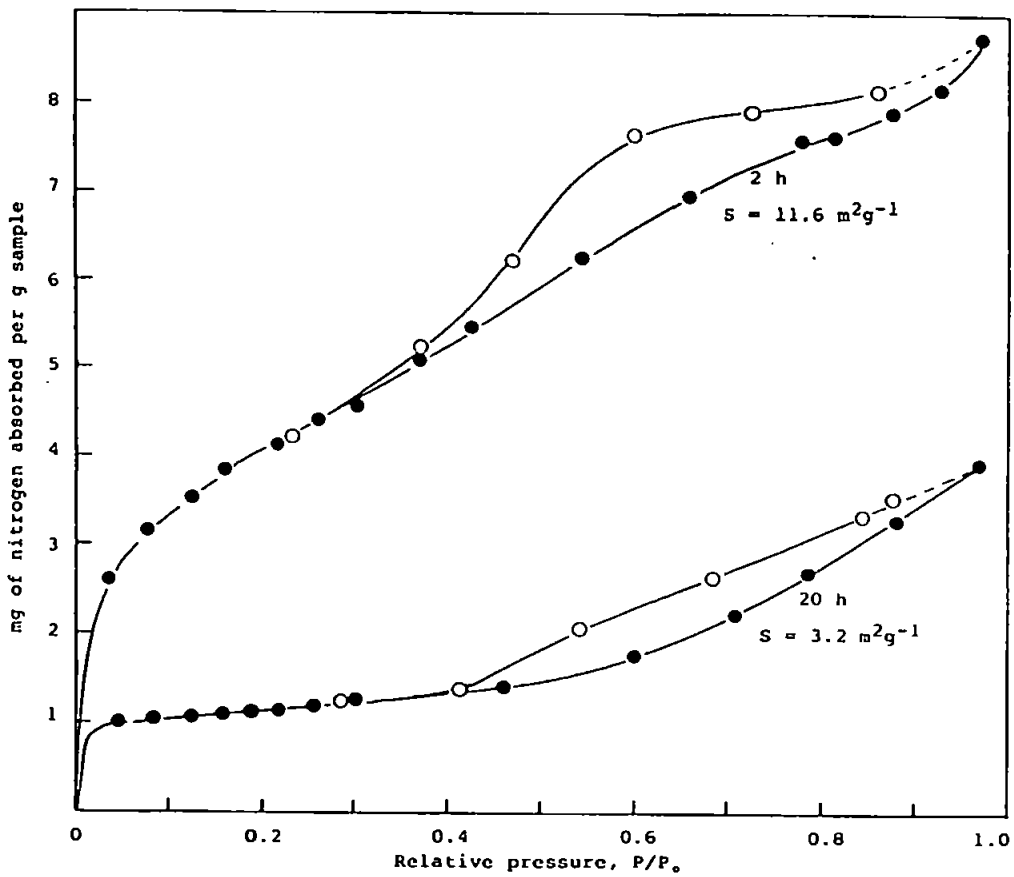

Fig. 3.a. Nitrogen adsorption isotherms at -196 °C on ZrC oxidised at 500 °C.

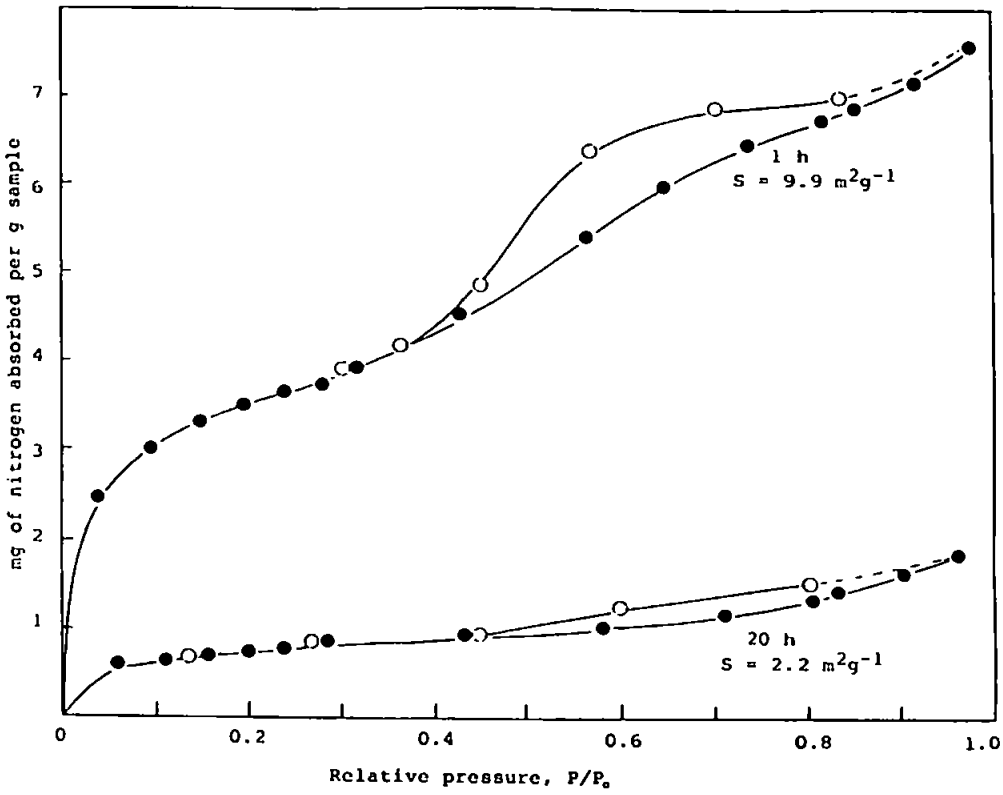

Fig. 3.b. Nitrogen adsorption isotherms at -196 °C on ZrC oxidised at 600 °C.

surface area at 600 and 700 °C are ascribed to more sintering of the newly-formed zirconia. This is evidenced further by comparing the surface areas and porosity of the zirconia products on further calcination at 500 and 600 °C in Fig. 3.a. and b. The surface areas and porosity both decrease on heating for 20 h. The hysteresis loops indicate full ranges of mesoporosity (2-50 nm pore diameters, corresponding to relative pressure ranges of 0.38-0.96 in the Kelvin equation) with some loss of the smallest pores and general diminution in the pore volume (from decreasing size of the hysteresis loops) after 20 h.

Effect of chromium carbide on the oxidation of zirconium carbide

The zirconia formed at 700 °C from 1h oxidation of zirconium carbide still retains some mesoporosity, even though its surface area is only 5.3 m^2g^{-1} (Fig. 4). It is known that the addition of chromium carbide improves the oxidation resistance of TiC-Co hard metals (where the % Co may be up to 18 %). The scales formed are thinner, protective and tenaceously adhering; a parabolic oxidation rate is given in contrast to linear rates where the scales spall off (ref. 4 and

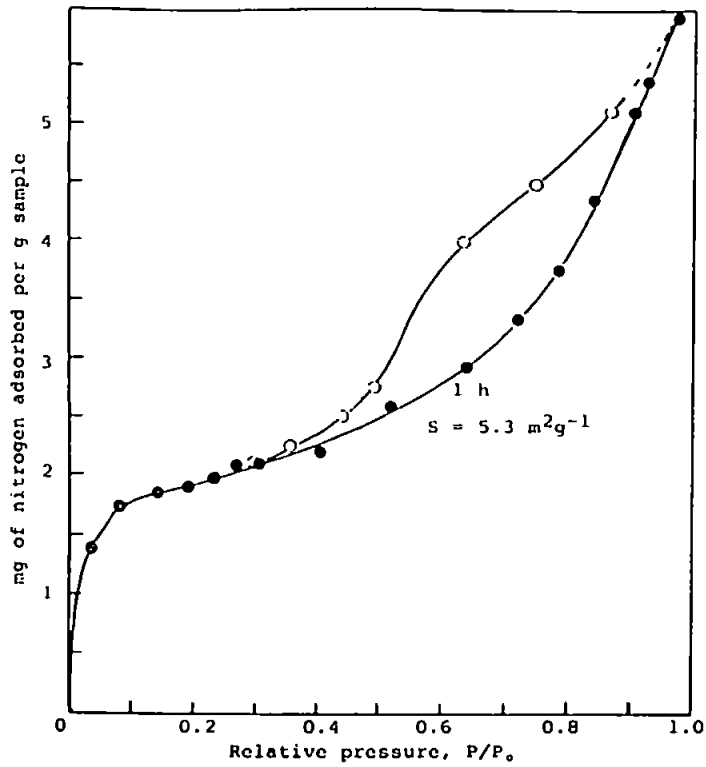

Fig. 4. Nitrogen adsorption isotherms at -196 °C on ZrC oxidised at 700 °C.

5). By analogy the oxidation of zirconium carbide was expected to be inhibited by the addition of chromium carbide. This was investigated as follows.

An approximately 1:1 mixture (by weight) of ZrC and Cr_3C_2 was investigated by thermogravimetry. At 700 °C, isothermal TG in air showed that less than 84 % of the ZrC was oxidised in 1 h, compared with almost complete (94 %) oxidation of ZrC in ¼ h when Cr_3C_2 is absent. Comparison with the TG curves for the separate oxidations in air of the ZrC and Cr_3C_2 at a heating rate of 10 °C min^{-1} showed that ZrC oxidised mainly at 400 - 650 °C and Cr_3C_2 at 650 - 1200 °C. Thus the Cr_3C_2 inhibits oxidation of the ZrC even when only a small amount of it is oxidised to Cr_2O_3. The Cr_2O_3 evidently promotes the sintering of the newly-formed zirconia, giving a more stable oxide layer around the remaining ZrC and this is confirmed by the specific surface area of the 1 h oxidised product being only 1.8 m^{2}g^{-1} instead of 2.5 m^{2}g^{-1} if the chromium carbide had been ineffective.

ACKNOWLEDGEMENTS

The authors wish to thank Mr. R.R. Willmers of the British Steel Corporation (Teesside Laboratories) for his collaboration and the Science and Engineering

Research Council for research grants.

REFERENCES

1 D.R. Glasson and J.A. Jones, J. appl. Chem., 19 (1969) 125-37
2 D.R. Glasson and S.A.A. Jayaweera, J. appl. Chem., 18 (1968) 65-77
3 D.R. Glasson and S.A.A. Jayaweera, J. appl. Chem., 19 (1969) 182-4
4 O. Kubaschewski and B.E. Hopkins, Oxidation of metals and alloys, 2nd Edn., Butterworths, London, 1962, pp. 262-5
5 R. Kieffer and F. Kölbl, Z. anorg. Chem., 262 (1950) 229
6 D.R. Glasson, J. chem. Soc., (1956) 1506-10
7 D.R. Glasson, J. appl. Chem., 8 (1958) 798-803

APPENDIX 2

Paper reprinted from Revue de Chimie Minérale, 1987, 24(6), 654 - 666

Revue de Chimie minérale,
t. 24, 1987, p. 654

The oxidation of some transition metal nitrides and carbides

by

J. N. CLARK (*), D. R. GLASSON (*) and S. A. A. JAYAWEERA (**)

(*) Department of Environmental Sciences,
Plymouth Polytechnic,
Plymouth PL4 8AA,
UK.

(**) Department of Chemistry,
Teesside Polytechnic,
Middlesbrough TS1 3BA.

ABSTRACT. — The use of transition metal nitrides and carbides as refractory materials is limited by their temperatures of oxidation (400-1,000°C). The oxidations are affected by the stability of the oxide product layer and the formation of protective coatings.

The reactivity of nitrides and carbides of titanium, zirconium and chromium towards air and carbon dioxide at different temperatures has been investigated. Products have been examined by *x*-ray diffraction for phase composition, by gravimetric nitrogen gas sorption for surface area, and by scanning electron microcospy for particle size.

Results indicate that the oxides of titanium and zirconium did not form protective layers on the remaining carbides or nitrides at lower temperatures and thus did not inhibit the oxidation. At higher temperatures, the oxidations were rapid and were largely complete before the oxide layers sinter to an appreciable extent. In contrast, chromium oxide, Cr_2O_3, formed protective layers and inhibited further reaction. Thus the nature of the oxide layers is similar to those formed during oxidation of the metals.

RÉSUMÉ. — L'emploi de nitrures et de carbures de métaux de transition est limité par leurs températures d'oxydation (400-1 000°C). Les oxydations sont affectées par la formation de couches d'oxyde protectrices et par la stabilité de ces dernières.

Le comportement de nitrures et de carbures de Ti, Zr et Cr à l'air et dans CO_2 a été étudié à différentes températures. Les produits ont été examinés aux rayons X, par gravimétrie d'adsorption d'azote pour déterminer l'aire de surface, et par microscopie électronique de balayage pour déterminer les dimensions des particules.

Il apparaît que les oxydes de Ti et Zr ne constituent pas de couches protectrices sur les carbures et nitrures aux températures relativement basses; ils ne limitent donc pas l'oxydation. A des températures plus élevées, l'oxydation est rapide et complète avant formation de

(*) Présenté aux Journées d'Études sur les Nitrures « JENI VII », Rennes, 14-15 septembre 1987.

REVUE DE CHIMIE MINÉRALE. 0035-1032/87/6 654 13/$3.30/© Gauthier-Villars

couches protectrices. En revanche, l'oxyde Cr_2O_3 donne des couches compactes ce qui limite l'oxydation du nitrure et du carbure de Cr. Ainsi, la nature des couches d'oxydes est similaire à celles formées lors de l'oxydation des métaux.

INTRODUCTION

The more extensive use of metals and refractories at higher temperatures has increased the industrial importance of transition metal nitrides and carbides. They are refractory materials with high melting points, usually above 2,000°C, and high degrees of hardness (about 8 to 9 on Mohs scale); hence they are termed refractory hard metals.

The refractory hard metals are oxidised in air at low temperatures (400-1,000°C) compared with their melting points. In the oxidations, the nitrogen and carbon are replaced by oxygen, but if the metal oxide layers formed on the surface are compatible with the remaining metal nitride or carbide, they would inhibit further oxidation. Above certain temperatures, the stability of the oxide layers is increased by sintering.

To investigate the oxidation kinetics and the effect of the oxide products, in the present research samples of transition metal nitrides and carbides have been oxidised in air at a series of temperatures. Variations in composition between the residues have been checked by X-ray diffractometry. Changes in surface area, average crystallite and aggregate sizes have been determined by examining some of the residues by gravimetric B.E.T. nitrogen gas sorption and electron microscopy.

Thermal analysis studies on the oxidation of titanium nitride were described at the last nitride symposium (1984). Further information has been obtained on the oxidation of this nitride and comparison made with the oxidation of zirconium nitride and titanium and zirconium carbides.

EXPERIMENTAL

Thermogravimetric studies of the atmospheric oxidation of the nitrides and carbides were made, using a Stanton-Redcroft Mass-flow balance MF-H 5 and an STA 781 thermal analyser. Larger samples (1 g) were oxidised for various times at each of a number of fixed temperatures in air in an electrical furnace.

The specific surface areas, S, of the cooled samples were determined by a gravimetric B.E.T. method [1] with nitrogen at −196°C as the adsorbate on a CI Electronics mark 2C Microforce balance with μg to mg sensitivity, using samples of 0.2 g. The adsorption isotherms also indicated any porosity present (from hysteresis) and pore size ranges. Average

crystallite sizes were deduced from the specific surfaces of the less porous materials. The metal oxides formed were identified by X-ray diffractometry and their microstructures were examined by scanning electron microscopy.

RESULTS AND DISCUSSION

Crystal structures of the oxidation products

X-ray diffraction results indicate that titanium nitride, TiN, and titanium carbide, TiC, both have cubic-F type lattices. They generally oxidise to rutile, TiO_2, which has a tetragonal lattice. The diffractometer traces give no direct indications of any oxynitrides being formed in the earlier stages of the titanium nitride oxidations at temperatures between 400-1,000°C. However, the titanium dioxide X-ray patterns are given only after about a quarter of the total weight increases are recorded at 600°C, but rutile patterns are detected after only 7% oxidation at 500°C. The longer calcination time at the lower temperature evidently permits crystallisation of the rutile, while at higher temperatures TiN has a limited solubility in TiO which is a possible intermediate. The lattice constant of TiN can remain unchanged from TiN to $TiN_{0.6}O_{0.4}$ when the binary compounds are sintered at 1,700°C and this may retard the crystallisation at higher temperatures. Likewise, the diffractometer traces give no indications of oxycarbides being formed in the oxidation of titanium carbide.

Zirconium nitride and carbide also have cubic-F type lattices and oxidise to cubic zirconia, ZrO_2, at lower temperatures of 400-600°C. In the earlier stages (22%) of the slow ZrC oxidation at 400°C (Fig. 1) X-ray traces show an intermediate, possibly ZrO or an oxycarbide, with a cubic-F lattice in which the (111) spacing is topotactically produced from the (200) spacing of the cubic-F ZrC lattice. This intermediate has almost disappeared in the 84% oxidation at 500°C when the oxide product is almost entirely cubic ZrO_2. Oxidation at temperatures above 600°C and up to 1,000°C gives increasing amounts of monoclinic ZrO_2. The 1.80 and 1.53 Å spacings of the cubic form evidently become the 1.81 and 1.54 Å spacings of the monoclinic form. At the highest temperatures, particularly over 1,200°C, tetragonal ZrO_2 is formed.

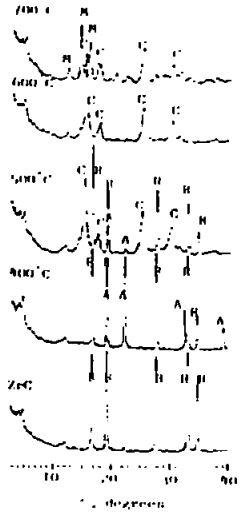

Fig. 1. — X-ray diffraction traces of isothermal oxidation products of ZrC.

Kinetics of oxidation

TG curves for the oxidation of titanium nitride are shown in Figure 2. In flowing air, i. e., dynamic conditions, on a mass-flow balance, oxidation is complete within 2 hours at temperatures above 755°C. In static conditions, on the thermal analyser, oxidation is somewhat slower as illustrated by the curves at 718 and 800°C being somewhat lower than those at 700 and 755°C respectively. Nevertheless, oxidation is complete within a half hour at 900°C and a quarter hour at 1,000°C.

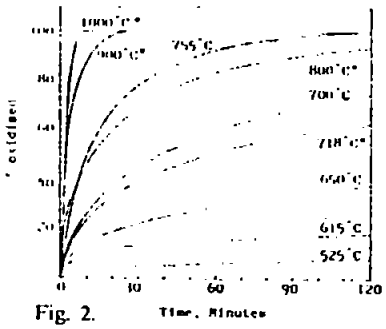

Fig. 2.

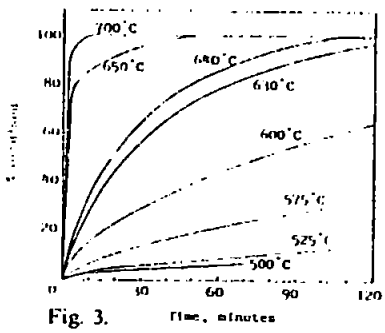

Fig. 3.

Fig. 2. — Isothermal oxidation of TiN at different temperatures in flowing air (* indicates static air).

Fig. 3. — Isothermal oxidation of ZrN at different temperatures in flowing air.

The TG curves in Figure 3 show that zirconium nitride oxidises more readily than titanium nitride. The particle sizes of the initial nitrides are similar, but oxidation of the zirconium nitride is complete within a quarter hour at 700°C, compared with 1,000°C required by the titanium nitride.

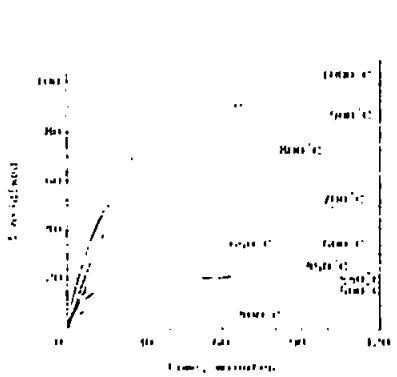

Fig. 4.

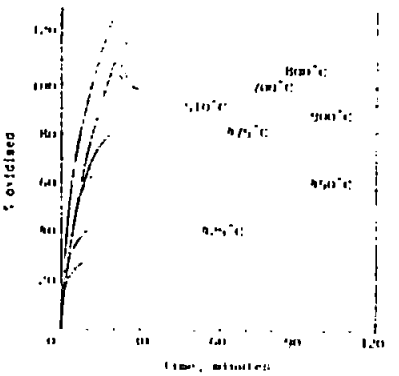

Fig. 5.

Fig. 4. – Isothermal oxidation of TiC at different temperatures in flowing air.
Fig. 5. – Isothermal oxidation of ZrC at different temperatures in flowing air.

The TG curves in Figure 4 show that the titanium carbide oxidises less readily than the nitride, requiring 2 hours for complete oxidation at 1,000°C. However, zirconium carbide (Fig. 5) oxidises more readily than the nitride, being almost completely oxidised in one hour at 500°C compared with only 6% oxidation of the nitride at this temperature (Fig. 3).

The kinetics of the oxidations indicate that the oxide products impede the reactions. Ideally the nitride or carbide should oxidise at an interface proceeding linearly inwards from the outside of each particle, resulting in two-thirds order kinetics, i.e., plots of the cube root of the weight of remaining nitride or carbide, fraction unoxidised, should be linear with time. Figure 6 for titanium nitride oxidation shows that this is achieved only at the lowest oxidation temperatures, ca. 650°C, but at higher temperatures the oxidation is much slower than expected. Thus the reactions are impeded by the layers of oxide product around the remaining nitride particles.

Therefore the oxygen from the surrounding air has to diffuse through the oxide layers and the gaseous products also have to diffuse to escape. If the reactions were diffusion controlled the oxidations would be parabolic, i.e., plots of % oxidised squared against time should be linear. However, in Figure 6, these plots are still non-linear with the oxidation rates still too low. Similar behaviour is shown with the other nitride and

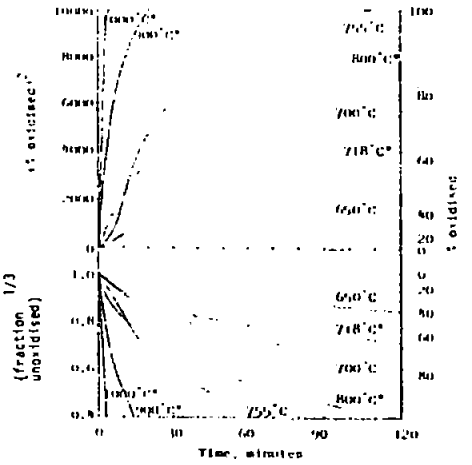

Fig. 6.

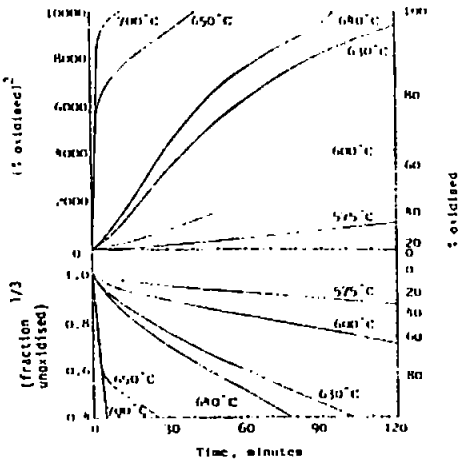

Fig. 7.

Fig. 6. – Kinetic half order and two-thirds order plots of TiN oxidations.
Fig. 7. – Kinetic half order and two-thirds order plots of ZrN oxidations.

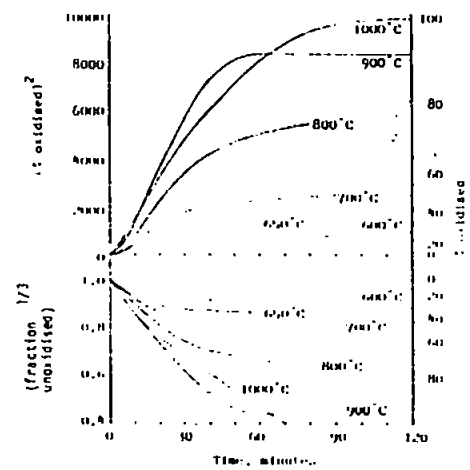

Fig. 8.

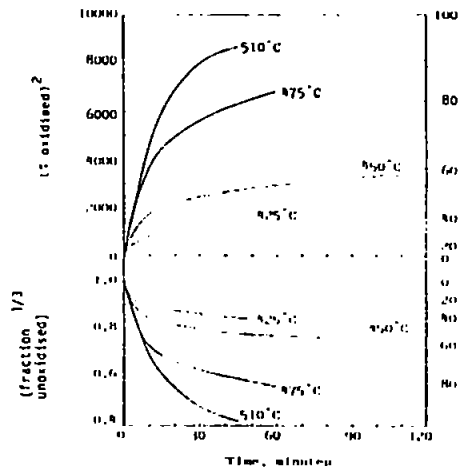

Fig. 9.

Fig. 8. – Kinetic half order and two-thirds order plots of TiC oxidations.
Fig. 9. – Kinetic half order and two-thirds order plots of ZrC oxidations.

carbides in Figures 7, 8 and 9. Further impedence could be caused by the sintering of the oxide layers above certain temperatures. This has been investigated by measurements of surface area and electron-microscopy.

Changes in surface area and crystallite sizes during oxidation

Earlier research on the oxidation of titanium nitride showed that crystallites of rutile, TiO_2, split off from the remaining nitride before they sinter [2]. Thus at 600°C the surface area increases during the first half of the oxidation and there is a maximum increase in the number of crystallites of about 20-fold. The crystallite splitting results mainly from the changes in type of crystal structure (cubic-F type to tetragonal) and a volume increase (0.630 of the original volume) as the nitride is converted to the less dense oxide. The splitting apparently facilitates release of nitrogen, since the material ultimately (after 200 hours) reaches constant weight corresponding to complete conversion of the nitride to titania, TiO_2. There is a limited amount of sintering of the oxide product by surface diffusion, since 600°C or 873 K is above one-third of the melting point of TiO_2 in K and thus the surface area decreases somewhat in the later stages of oxidation. Samples oxidised above 800°C sinter more extensively since this is above the Tammann temperature of TiO_2 (half m.p. in K) when sintering by crystal lattice diffusion becomes possible. Indeed at 1,000°C the oxide consolidates in 2 hours.

The titania formed from the oxidation of the carbide exhibits similar sintering behaviour. Only 25% of the carbide, TiC, oxidises at 600°C in 1 hour when the surface area increases from 0.8 to $1.8\,m^2\,g^{-1}$, but this represents formation of oxide of specific surface area about $4\,m^2\,g^{-1}$. In comparison at 800°C, there is about 75% oxidation in 1 hour, but the surface area only increases to $1\,m^2\,g^{-1}$, representing formation of oxide of specific surface of only $0.7\,m^2\,g^{-1}$. This again indicates extensive sintering of titania at 800°C, when sintering by crystal lattice diffusion is possible. Likewise, the sintering is excessive at 1,000°C, which considerably impedes the oxidation (Fig. 4) so that its rate is only about the same as that at 900°C.

The zirconias formed from the oxidation of the nitride and carbide do not sinter so readily, since zirconia has a Tammann temperature of 1,220°C, much higher than that of titania of 780°C. Thus in earlier researches [2 and 3] the authors found that the oxidation products had specific surfaces of up to $15\,m^2\,g^{-1}$, correspondingly higher than the titanias. The average crystallite sizes indicated that most of the submicron titania crystallites sintered to above micron size at temperatures above 800°C compared with 1,200°C for the zirconia. These findings were confirmed by scanning electron microscopy (Plates 1 to 5).

In Plate 1, crystals of the original titanium nitride (*a*) and the oxidation products at lower temperatures, viz., (*b*) 518°C and (*c*) 690°C, were mainly angular in appearance, but those above 800°C, (*d*) to (*f*) showed some rounding at the edges, indicating more extensive sintering of titania above its Tammann temperature. Titania formed by oxidation of titanium carbide showed similar sintering behaviour (Plate 2). The powdered material began to consolidate into lumps at temperatures above 800°C, especially where the powder had been in contact with the lower part of the crucible to produce a visibly smooth surface, the microstructure of which is shown in (*d*) and (*e*) compared with that of the rougher surface of the lump (*f*) which had not been in contact with the crucible. Nevertheless, all products obtained at temperatures above 800°C show some rounding of the particles.

Electron micrographs for the oxidation of zirconium nitride also show angular crystals at lower temperatures (Plate 3), but the zirconia particles become less angular above 1,000°C and especially at 1,300°C (Plate 4). There are similar findings for the oxidation of zirconium carbide (Plate 5), where again the initial zirconium carbide crystals and the lower temperature oxidation products (*a*) to (*d*) are mainly angular, but there is rounding of particles caused by sintering at temperatures above 1,000°C, (*e*) and (*f*).

Results generally indicate that the titania and zirconia do not form very protective layers on the remaining nitrides and carbides and only inhibit the oxidations to a limited extent. In contrast, chromium oxide, Cr_2O_3, from the oxidation of the nitride or carbide [3] forms protective layers which considerably inhibit further reaction. Thus the nature of the oxide layers from the refractory hard metals is similar to those which the authors found were formed during oxidation of the metals themselves.

Acknowledgements. – The authors wish to thank Mr. R. R. Willmers of the British Steel Corporation (Teesside Laboratories) for his collaboration and the Science and Engineering Research Council for research grants.

REFERENCES

[1] D. R. Glasson, *J. chem. Soc.*, 1956, p. 1506-1510.
[2] D. R. Glasson and S. A. A. Jayaweera, *J. appl. Chem. Lond.*, 1969, **19**, p. 182-184.
[3] J. N. Clark, D. R. Glasson and S. A. A. Jayaweera, *Thermochimica Acta*, 1986, **103**, p. 193-199.

(Received October 30, 1987.)

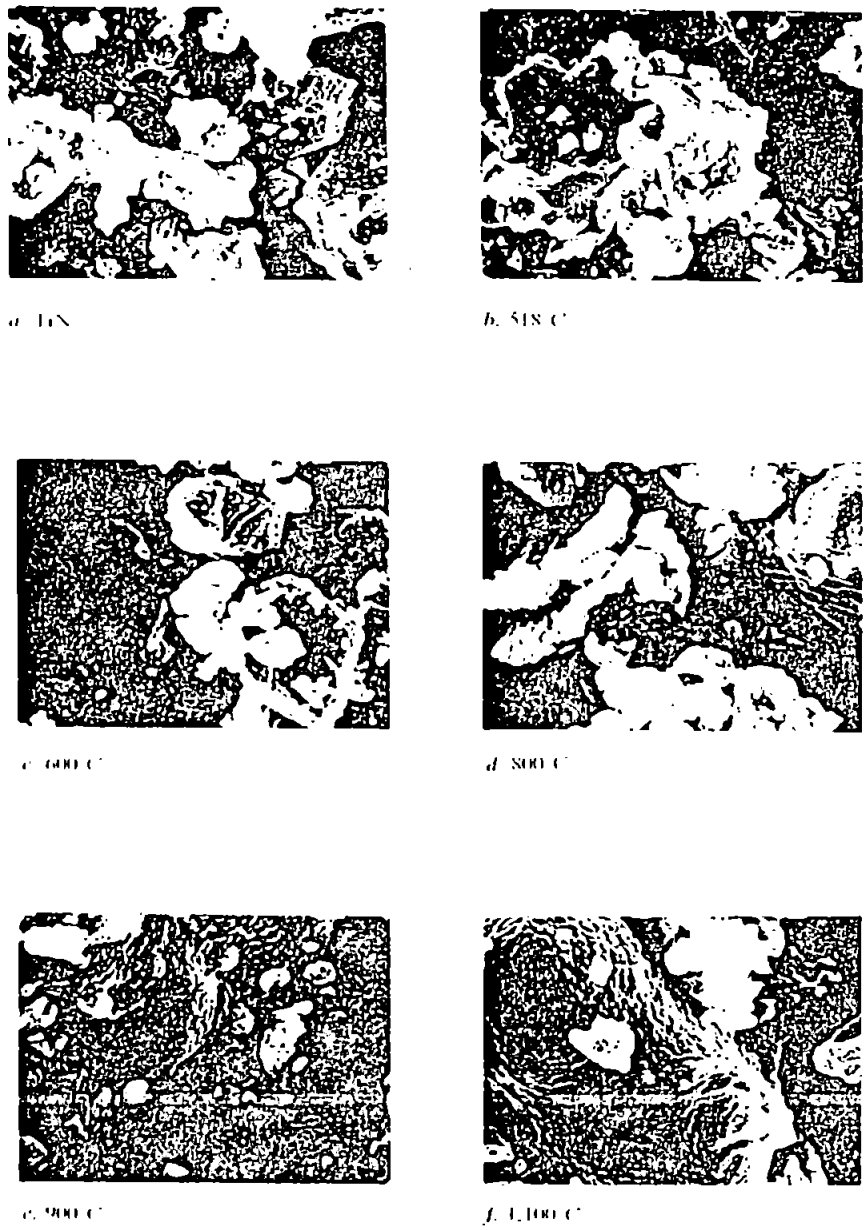

a, TiN; *b*, 518 °C; *c*, 600 °C; *d*, 800 °C; *e*, 900 °C; *f*, 1,100 °C

Plate 1 Scanning electron micrographs of TiN and its oxidation product

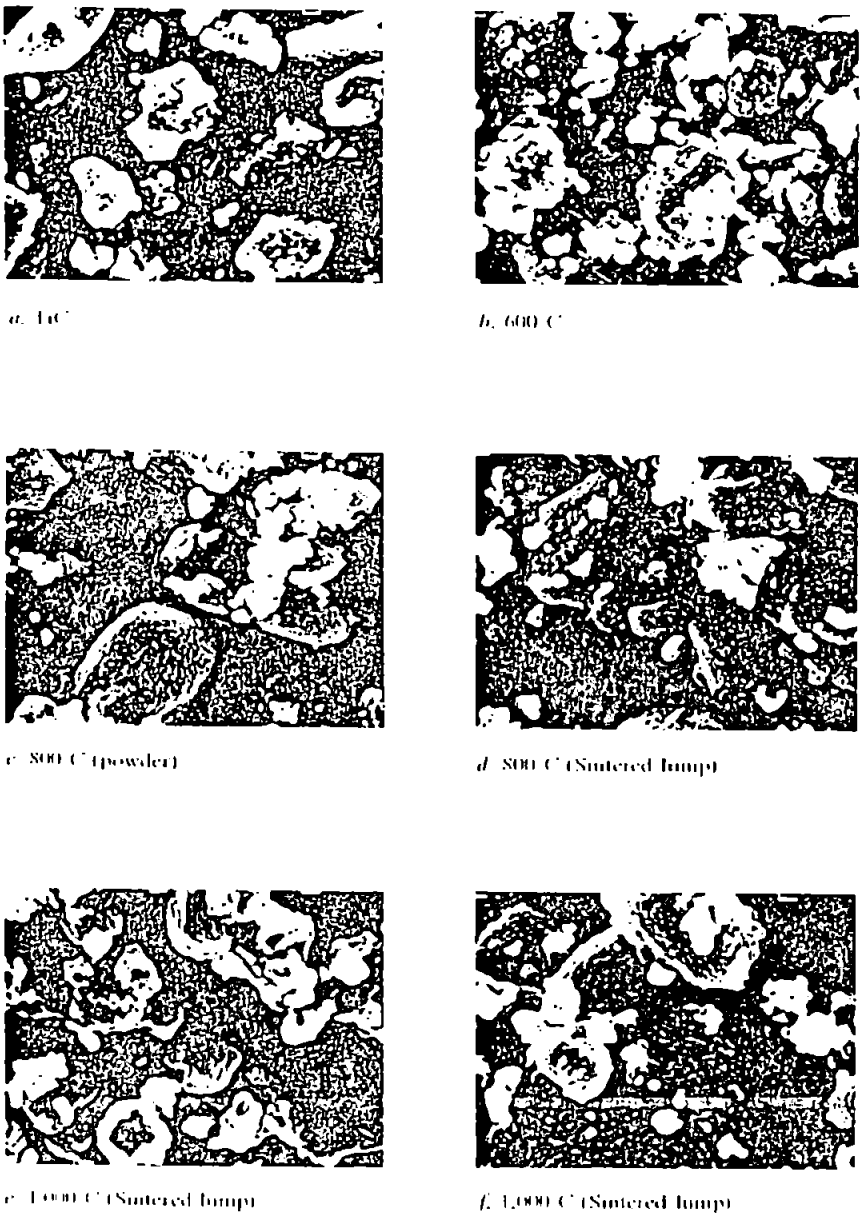

a, TiC *b*, 600 °C

c, 800 °C (powder) *d*, 800 °C (Sintered lump)

e, 1000 °C (Sintered lump) *f*, 1,000 °C (Sintered lump)

10 μm

Plate 1 Scanning electron micrographs of TiC and its oxidation products

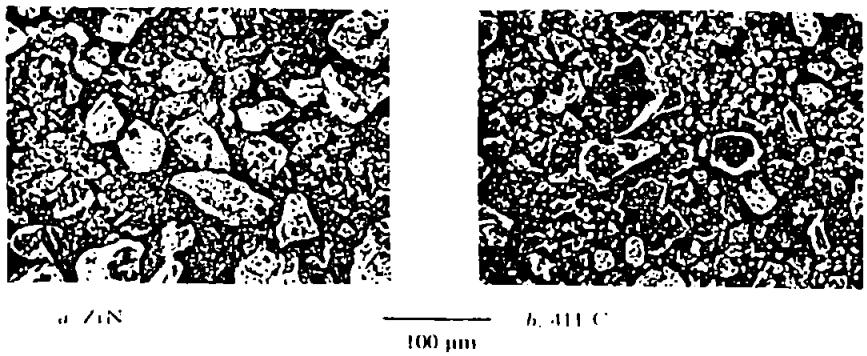

a, ZrN — b, 411 °C

100 μm

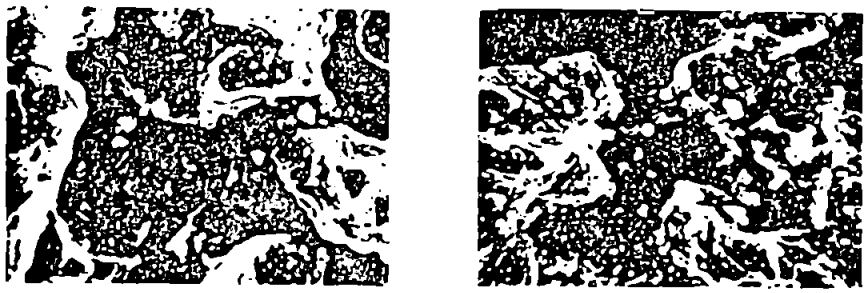

c, ZrN — d, 411 °C

e, 480 °C

10 μm

PLATE 3 Scanning electron micrographs of ZrN and its oxidation products

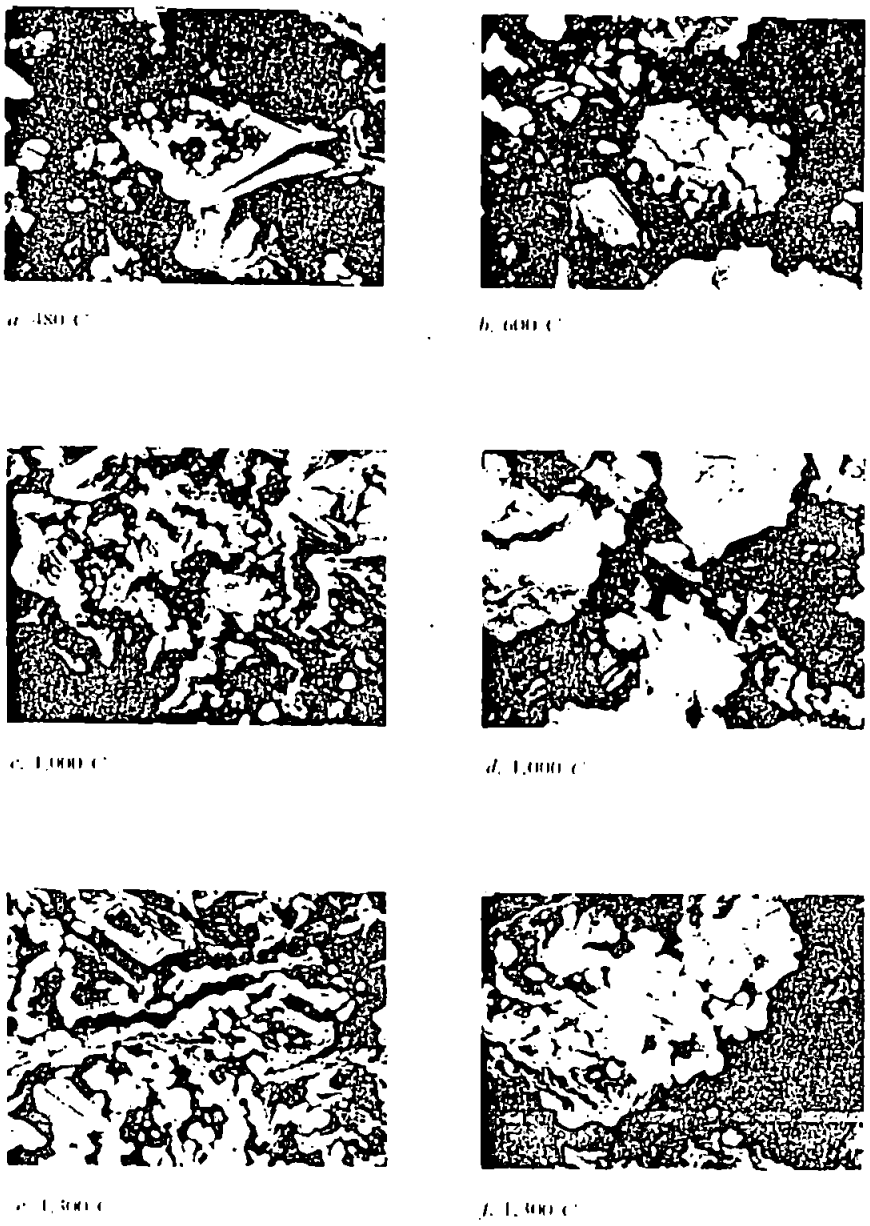

a, 480 °C; *b*, 600 °C; *c*, 1 000 °C; *d*, 1 000 °C; *e*, 1 300 °C; *f*, 1 300 °C

10 μm

Plate 1 Scanning electron micrographs of oxidation products of ZrN

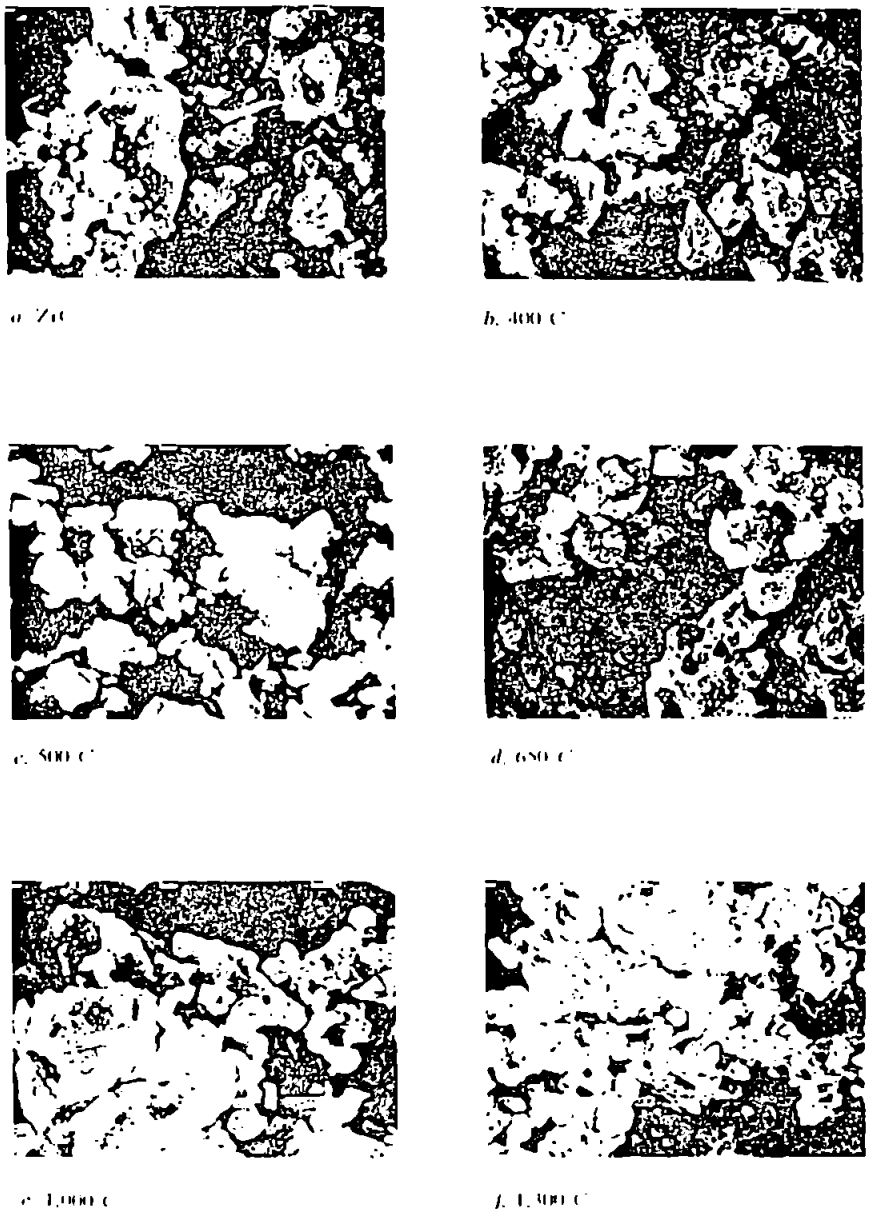

Plate 2 Scanning electron micrographs of ZrC and its oxidation products

And finally,

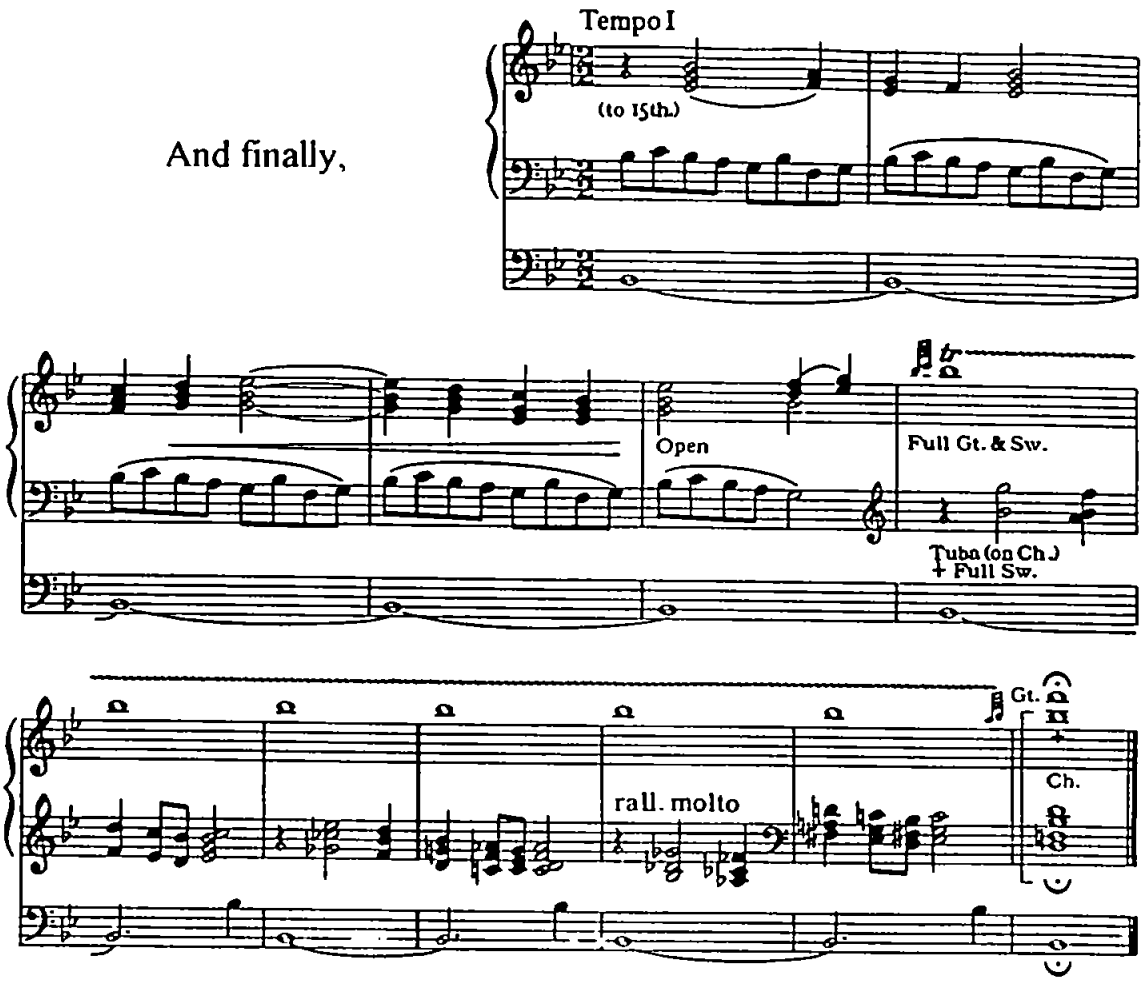

Extract from "Sortie" from Seven Sketches for Organ by Percy Whitlock, reproduced by permission of Oxford University Press.